UNIVERSITY OF BIRMINGHAM

Operation, characterisation & physical modelling of unflattened medical linear accelerator beams and their application to radiotherapy treatment planning.

by

Jason Cashmore

A thesis submitted to the
University of Birmingham
for the degree of
DOCTOR OF PHILOSOPHY

School of Physics and Astronomy
University of Birmingham
July 2013

ABSTRACT

The flattening filter is a conical shaped piece of metal sitting within the treatment head of a linear accelerator, used to produce a flat, uniform beam of X-rays from the forward-peaked distribution exiting the target. Despite their routine use since the introduction of the linac in the 1950's, however, there are still several unresolved issues surrounding their use. The photon scatter and electron contamination introduced by modifying the fluence are difficult to model, as is the variation in energy spectrum caused by differential absorption across the field. Leakage radiation also causes increased whole body doses to the patient, and the filter itself causes acts as an amplifier for beam bending and steering issues.

With advances in tumour imaging, dose optimisation and in-room image-guidance it is now possible to locate a tumour accurately in space and to design radiation fields to conform to its shape, avoiding adjacent normal and critical tissues. This *active production* of non-flat fields means that the prerequisite for flat fields no longer exists, and the filter is potentially no longer a necessary component.

This thesis reports on research to produce a filter-free linear accelerator, from basic operation and optimisation, dosimetric characterisation and beam modelling, through to treatment planning and dose delivery. FFF beams have been shown reduce many of the problems seen with the current generation of linear accelerators, producing beams that are inherently more stable, simple to model and with reduced patient leakage (leading to reduced secondary cancers). The increase in dose rate also translates into shorter treatment times for many treatments, aiding patient comfort and reducing problems associated with intra-fraction motion.

ACKNOWLEDGEMENTS

A number of people have been of great help, assistance and inspiration during the course of this research.

I would like to thank Prof. Stuart Green and Prof. Alun Beddoe in their roles as both supervisors and mentors for their guidance along the way, and for keeping me focussed and on track. Within the department at UHB I would also like to acknowledge the work of Dr. Mark Ramtohul, who has worked on a number of aspects of FFF radiotherapy, often at very unsociable hours, and also Dr. Geoff Heyes for assistance with SRS measurements.

In hindsight, removal of the flattening filter is an obvious step to make, and the idea of the FFF linac is now firmly established within the radiotherapy community, but this was not always so... I would like to thank staff at Elekta, not just for supporting this work, but also for believing it *could* work. Particular thanks must go to Kevin Brown, Dr. Leonard Wee, and Neil Harvey in this respect.

And finally, to my family, for putting up with so many late nights, weekends and time spent away from home. I couldn't do it without you.

CONTENTS

LIST OF FIGURES

LIST OF TABLES

ACRONYMS

3D-CRT	Three-dimensional conformal radiotherapy
ART	Adaptive radiotherapy
AVM	Ateriovenous malformation
Bf	Bending fine
CAX	Central axis
CEE	Collimator exchange effect
CI	Conformity index
CNS	Central nervous system
CT	Computed tomography
CTV	Clinical target volume
DD	Depth dose
Dmax	Depth of dose maximum
DVH	Dose volume histogram
EPID	Electronic portal imaging device
ESTRO	European society for radiotherapy and oncology
EUD	Equivalent uniform dose
FF	Flattening filter
FFF	Flattening filter free
FiF	Field in field
GTV	Gross tumour volume
H&N	Head and neck
HI	Homogeneity index

IAEA	International Atomic Energy Agency
ICRU	International Commission on Radiological Units and Measurements
IEC	International Electrotechnical Commission
IGRT	Image-guided radiotherapy
IMAT	Intensity-modulated arc therapy
IMRT	Intensity-modulated radiotherapy
kV	Kilovoltage
MC	Monte Carlo
MLC	Multi-leaf collimator
MRI	Magnetic resonance imaging
MU	Monitor units
MV	Megavoltage
NACP	Nordic Association for Clinical Physics
NTCP	Normal tissue complication probability
OAR	Organ at risk
PRF	Pulse repetition frequency
PRV	Planning organ at risk volume
PTV	Planning target volume
QA	Quality assurance
QI	Quality index
RF	Radiofrequency
RSD	Relative surface dose
SABR	Stereotactic ablative radiotherapy
SBRT	Stereotactic body radiotherapy
SCD	Source to chamber distance
SPECT	Single photon emission computed tomography

SRS	Stereotactic radiosurgery
SSD	Source to surface distance
TBI	Total body irradiation
TCP	Tumour control probability
TLD	Thermoluminescent dosimeter
TPR	Tissue phantom ratio
TPS	Treatment planning system
UHB	University Hospital Birmingham
VMAT	Volumetric modulated arc therapy
VSM	Virtual source model

CHAPTER 1

AN INTRODUCTION TO CANCER AND RADIOTHERAPY

This chapter introduces the basics of cancer biology, the causes of cancer and its subsequent treatment, focussing specifically on radiotherapy treatments. The concepts of linear accelerator function and treatment planning are also introduced, as is the rationale for flattening filter removal and its consequences.

1.1 Cancer

1.1.1 Cancer biology

Cell multiplication (*proliferation*) is a normal physiological process that occurs in almost all tissues. Normally the balance between proliferation and cell death is tightly regulated to ensure the integrity of organs and tissues, but mutations in DNA can disrupt these processes leading to cancer. Cancer therefore refers to a group of

diseases characterized by uncontrolled cell division leading to growth of abnormal tissue.

The uncontrolled and often rapid proliferation of cells can lead to either a *benign* tumour or a *malignant* tumour (cancer). Benign tumours do not spread to other parts of the body or invade other tissues, and they are rarely life threatening. Malignant tumours, on the other hand, can invade other organs, spreading to distant locations in the body via the lymphatic system or the bloodstream and becoming life threatening.

1.1.2 Cancer incidence & causes of cancer

There are more than 200 types of human cancer, each with different causes, symptoms and treatments. In 2009 there were 264,700 newly diagnosed cases of malignant cancer registered in England. Of this total, 134,700 cancers were in males and 130,000 for females, with four types of cancer accounting for over half of all new cases (figure 1.1a).

Cancers are predominantly an environmental disease with 90-95% of cases being attributed to lifestyle factors, and 5-10% due to genetics (Anand *et al* 2008). Common environmental factors leading to cancer death are shown in the figure 1.1b.

Some slow-growing cancers are particularly common with post-mortem studies in Europe and Asia showing that up to 36% of people have undiagnosed thyroid cancer at the time of their deaths, and that 80% of men develop prostate cancer by age 80 (Fraumeni *et al* 2006, Bostwick *et al* 2007). These cancers are often very small and tend to be diseases people die *with* rather than *of*.

While cancer can affect people of all ages the overall *risk* of developing cancer generally increases with age, at least up to age 80-85 yr. In 2007, cancer caused about

13% of all human deaths worldwide (7.9 million). These rates are rising as more people live to an old age and as lifestyle changes occur in the developing world.

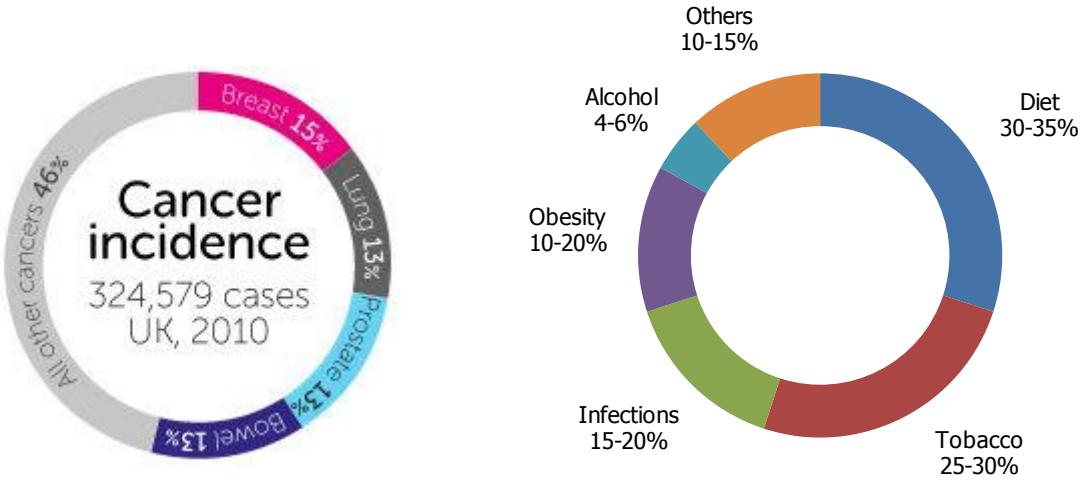

Figure 1.1. (a) Cancer incidence figures in the UK for 2010 (accessed May 2013 at http://www.cancerresearchuk.org), (b) Causes of cancer, modified from Anand (2008)

1.1.3 Types of cancer

Cancers originate from a single cell; hence cancers can be classified by the type of cell in which it originates and by the location of the cell.

Carcinoma: Cancers originating from epithelial cells. This group includes many of the most common cancers and include nearly all those developing in the breast, prostate, lung, pancreas and colon. Adult cancers usually form in epithelial tissues.

Sarcoma: Cancers arising from connective tissue (i.e. bone and muscle).

Lymphoma and leukemia: These two classes of cancer arise from haematopoietic (blood-forming) cells that leave the marrow and tend to mature in the lymph nodes (lymphatic tissue) and blood (bone marrow stem cells), respectively.

Teratoma/Germ cell tumour: Begins within germ cells most often in the testicles or the ovaries (seminoma and dysgerminoma) respectively

Blastoma: Cancers derived from immature "precursor" cells or embryonic tissue, these are most common in children.

Melanoma arises in melanocytes, normally those in the skin.

1.1.4 Cancer staging and treatment

The stage of a cancer is a description of how far a cancer has spread within a patient's body, taking into account the size of a tumour, how deeply it has penetrated, how many lymph nodes it has spread to (if any), and whether it has spread to distant organs (metastasis).

The TNM staging system is used for solid tumours, and is an acronym for the words "Tumour", "Nodes", and "Metastases". For example, a T1N2M0 cancer would be a cancer with a T1 tumour, N2 involvement of the lymph nodes, and no metastases.

Staging of cancer is critical because the stage at diagnosis is the most powerful predictor of survival, and treatments are often changed based on the stage. Thus, incorrect staging can lead to improper treatment. Staging can also be used to identify any clinical trials that may be suitable for a particular patient.

Cancer staging can be subdivided into a *clinical* stage and a *pathologic* stage, denoted by a small "c" or "p" before the stage (e.g. cT1N1M0 or pT2N0). The c-prefix is implicit in absence of the p-prefix. Clinical stage is based on all of the available information obtained before a surgery to remove the tumour, therefore it may include information about the tumour obtained by physical examination or radiological examination. Pathologic stage adds in additional information gained by microscopic

examination of the tumour by a pathologist. Since they use different information, clinical stage and pathologic stage are often different.

Metastatic tumours are very common in the late stages of cancer and may spread via the blood, the lymphatic system, or both. The most common places for metastases to occur are the lungs, liver, brain, and the bones.

When tumour cells metastasize, the new tumour is called a *secondary* or *metastatic* tumour, and its cells are like those in the original tumour. This means, for example, that, if breast cancer metastasizes to the lungs, the secondary tumour is made up of abnormal breast cells, not of abnormal lung cells.

Tumour *grading* is different to staging in that it describes how abnormal the tumour cells look under microscopic examination. Tumours are usually graded from 1 to 4 depending on the amount of abnormality, with grade 1 being 'well-differentiated' i.e. the tumour cells are organised in a similar way to normal cells, and grade 4 being 'undifferentiated', i.e. cells are abnormal in nature, lacking normal tissue structures. Higher grades of tumour tend to grow and spread more rapidly than lower grades, so generally indicate a worse prognosis.

When given, treatment can involve surgery, chemotherapy, radiotherapy and targeted therapies (using hormonal and biological agents). Conventional surgery is the treatment of first choice for most solid tumours but in practice most patients will receive a combination of treatments, the exact nature of which depends on the type of cancer, its location and grade, and also on the stage of the disease, as well as the general state of a person's health.

Most cancers are suspected by initial signs or symptoms (or through screening) but the definitive diagnosis of most malignancies must be confirmed by histological examination of the cancerous cells by a pathologist.

The tissue diagnosis indicates the type of cell that is proliferating, its histological grade, genetic abnormalities, and other features of the tumour. Together, this information is useful to evaluate the prognosis of the patient and to choose the best course of treatment.

1.2 Radiotherapy

1.2.1 Background

High energy radiation from X-rays and particles (electrons, protons and heavy ions) damage living cells and can be used to target tumours. Radiotherapy is simply the use of radiation to treat illness and is one of the most effective ways of treating cancer. Shortly after their discovery in 1895 by Roentgen, X-rays were being used to treat breast cancer patients. Since then they have taken on a routine role in the investigation, diagnosis and treatment of disease and 40-50% of people with cancer will now have radiotherapy as part of their treatment.

It has been estimated that the addition of radiotherapy to cancer treatment improves 5 year survival by 16% (Barton *et al* 1995). In comparison the 5 year survival contribution from chemotherapy drugs is estimated at 2% (Morgan *et al* 2004), making radiotherapy second only to surgery in its effectiveness.

Radiotherapy can be given by:-

1. **External beam radiotherapy** (teletherapy): radiation is delivered from an external source outside of the patient using x-rays, gamma rays or high energy particles (tele = Greek for far away)
2. **Brachytherapy**: dose is delivered from radioactive sources implanted in the patient close to or inside the target (brachys = Greek for short distance)

3 **Unsealed source therapy**: a radioactive substance is swallowed or injected to irradiate internally

Here we are concerned with external beam radiotherapy which currently constitutes approx. 90% of radiotherapy treatments.

1.2.2 Rationale for radiotherapy and the need for accuracy

Radiotherapy relies on the delivery of therapeutic doses of radiation to the tumour volume whilst minimising the dose to surrounding normal tissues. In order to maintain a high 'tumour control probability' (TCP) we must deliver as much dose as possible to the target in order to kill all of the viable cancer cells.

In doing this we also damage surrounding normal tissues and this dose must be minimised to give a low 'normal tissue complication probability' (NTCP) [see figure 1.2]. As with most treatments, radiotherapy therefore treads a fine line between cure and complication.

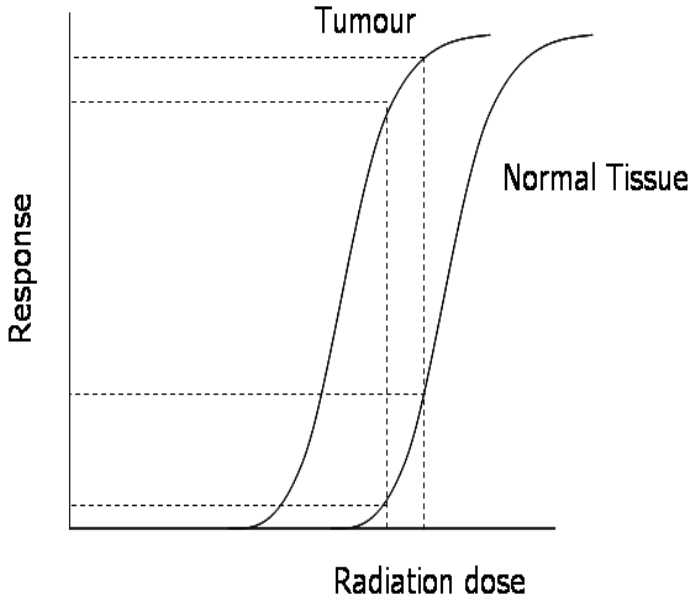

Figure 1.2. Generalised dose-response curve for tumour and normal tissues. In this case a small change in dose has a much greater effect on the normal tissue than on the tumour itself.

In practice a dose must be chosen that gives acceptable complication levels, accepting the level of cure possible.

Due to the gradient of the respective curves at the prescription dose level, any uncertainty in dose means that the response can be greater in the normal tissues than for the tumour (see figure 1.2), highlighting the need for greater accuracy in the delivery and reporting of radiotherapy doses. In practice a dose must be chosen that gives acceptable complication rates for a given level of cure.

The radiation dose delivered to the target and surrounding tissues is one of the major predictors of radiotherapy treatment outcome. It is generally assumed that the dose must be delivered within an uncertainty of less than ± 3.5% of the prescribed dose to ensure the treatment aims are met (IAEA TecDoc 734, 1994). In clinical situations this is realistically 5-8% (Svensson H, 1984), with 'best practice' currently being around 5% (table 1.1).

Table 1.1. Uncertainties in 'best practice' radiotherapy dose delivery (95% 2SD). (Knoos and McClean, 2007).

1	Dose at calibration point	1.5%
2	Dose at other points	1.1%
3	Patient data	1.5%
4	Dose-calculation	3.0%
5	Set-up	2.5%
6	Beam monitor stability	1.0%
7	Beam flatness/symmetry	1.5%
	Total	**5.0%**

Normal tissues usually have superior repair mechanisms than tumour cells for low doses, therefore to further reduce toxicity the total dose is split into small fractions of typically ~2Gy. Delivery of dose over a long period in this way

(fractionation) rather than in a single dose requires the patient to be repeatedly irradiated in the same position and it is vital that each fraction is delivered according to plan each day, so the treatment positioning must be stable and reproducible.

1.2.3 The treatment planning process

The patient pathway through the treatment process (figure 1.3) generally begins with the patient either presenting to a GP with non-specific symptoms, or though a screening process (e.g. mammography). Since there are no symptoms unique to cancer further tests are required, and if cancer is suspected then referral is made to an oncologist. Once a definitive diagnosis of cancer is confirmed (by tumour biopsy) the patient will then go on to the staging process. Treatment outcomes are very closely related to the disease stage, and categorising patients in this way leads to a good estimation of prognosis and to an appropriate course of treatment. At this stage the performance status of the patient and individual wishes are also an important factor in any decision to treat.

Depending on these assessments the first choice to be made is whether the treatment will be radical (of curative intent) or palliative (for symptom relief). Decisions can then be made regarding the treatment mode (e.g. surgery, radiotherapy).

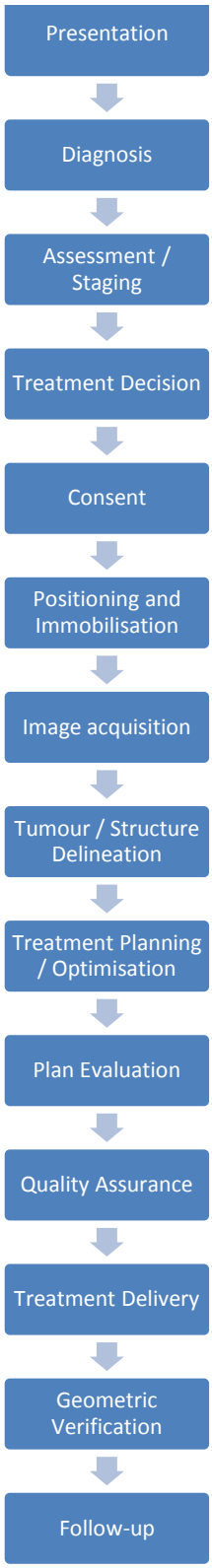

Figure 1.3. Basic stages in the radiotherapy treatment process.

Once a decision is made to deliver radiotherapy a series of further imaging studies (such as MRI, SPECT, ultrasound etc.) may be undertaken to localise the tumour within the body, and to define a target volume and shape. To allow accurate and reproducible delivery on a daily basis it is usually necessary to immobilise the patient in some way and this should be achieved before any further imaging is performed. Depending on the complexity of the plan a simple outline of the patient may be sufficient, but generally a CT scan of the region is obtained to allow accurate delineation of the target region(s) and any surrounding critical structures.

Historically, beam placement was often carried out using a dedicated unit known as a *simulator*, a low-energy unit designed to accurately mimic the mechanical movements of the treatment machine. Treatment areas are targeted using diagnostic energy X-rays, with borders being marked according to anatomical boundaries.

It is now more usual for the patient to receive a CT scan before treatment and to use *virtual* simulation. A virtual simulator is a software package designed to allow the reconstruction of imaging data to aid visualisation and allow the creation of 3D treatment volumes and delineation of organs at risk (figure 1.4).

Treatment planning is performed using specialised software capable of calculating dose within a specified volume. The complexity of the dose calculations has increased over time, from simple 2D calculations using lookup tables to sophisticated 3D algorithms and Monte Carlo. Most planning systems now use beam algorithms based on splitting the dose into primary and scatter components which utilise machine- and energy-specific beam models. These algorithms in turn require CT information for accurate dose calculation, as these images provide accurate electron density (and hence attenuation) information.

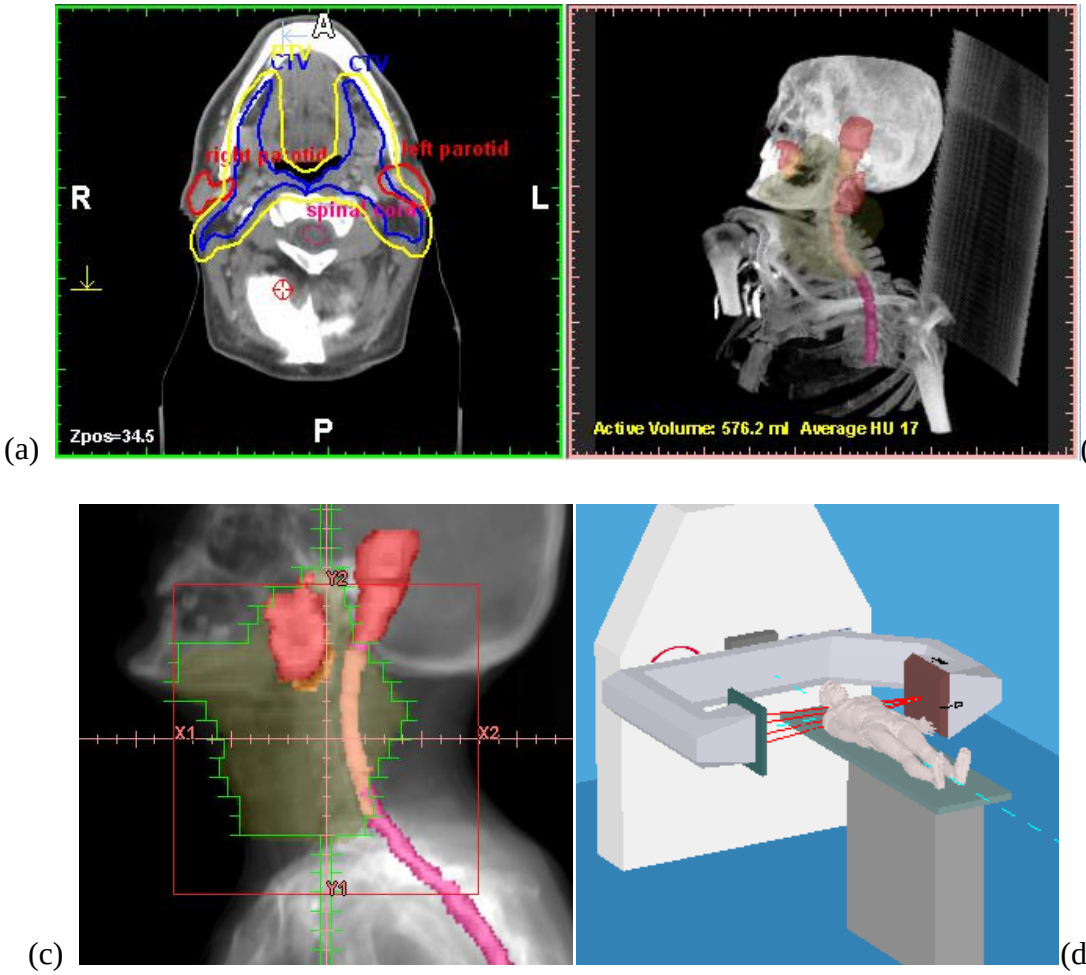

Figure 1.4. Virtual simulation of an oropharangeal carcinoma. (a) Coronal CT slice with target and normal structures outlined, (b) 3D reconstruction of the CT data showing the internal position of target and critical structures, (c) custom shielding using an MLC and (d) 3D representation of the treatment machine.

When CT information is available it is usual to outline the treatment area and normal structures. As not all of the tumour may be visible on a CT image it often beneficial to include further imaging (e.g. PET and MRI) to aid this process. To account for microscopic spread of the cancer, and any movement (e.g. due to respiration or rectum/bladder filling) further volumes must also be added. These are discussed in further detail in chapter 5 and Appendix B.

Patient specific planning is usually based on a 'class solution' for the site in question. This usually specifies a standard initial setup including the number of

beams, their arrangement around the patient, and any particular weighting parameters. By changing each these parameters the planner will attempt to deliver the prescribed dose to the tumour (within -5% and +7% [ICRU 50, 1993 and ICRU 62, 1999]) whilst minimising the dose to surrounding normal tissues and critical structures. This equates to aiming for a high TCP and low NTCP. Treatment planning is always limited by normal tissue tolerance, and if a level of normal tissue sparing cannot be achieved then target coverage may be sacrificed. To help shape the high dose region and to shield critical structures, beam shaping devices such as wedges and customised shielding blocks may be used.

An alternative to the physical manufacture of custom shaped blocks is the use multi-leaf collimators (MLCs), which are individual leaves of tungsten that can be moved into the beam under computer control (figure 1.4c).

Once a plan is ready it must be evaluated by an oncologist and receive further checks by dosimetry staff before it can be transferred electronically to the patient management system. This software acts as a booking system and a 'record and verify' system, controlling the treatment machine and logging radiation delivery. Before treatment can begin the beam positioning must be verified relative to internal patient anatomy either by 2D transmission (portal) imaging or by use of 3D cone-beam (CT) imaging. Any discrepancies in position are evaluated and can result in a positional correction or, if the difference is too large, repeat imaging/planning. Imaging will also occur at additional points as the treatment progresses to ensure consistency, and to monitor any changes in patient anatomy (e.g. due to weight loss or tumour shrinkage). If changes occur that are likely to affect the delivery of the intended plan then action must be taken to modify the treatment to compensate. These are the basic concepts of image-guided radiotherapy (IGRT) and adaptive radiotherapy (ART).

1.3 Radiotherapy treatment machines

Figure 1.5 shows the depth dose characteristics for several x-ray beam energies. To treat deep seated tumours without exceeding tolerance doses to the skin multiple (converging) high energy beams are required and it can be seen that the relative dose at depth increases with increasing beam energy. High energy beams also allow a certain amount of 'skin-sparing' due to the dose build-up effect which is clinically important since all of the beams in external radiotherapy enter through the skin.

Initial experiences with radiotherapy were hampered by the limited energy of x-ray generators. These were useful for treating skin lesions, but for deep seated tumours they were of insufficient energy to deliver high enough doses to the tumour without exceeding tolerance doses to the skin. Advances in radiotherapy technology were therefore initially centred on producing ever increasing beam energies to maximise dose at depth and improve skin-sparing. The first sources used for external beam radiotherapy were gas filled x-ray tubes, but these were quickly followed by the vacuum tube in 1913, operating at up to 140kVp. Subsequent designs allowed x-ray generation at up to 400kV but were still 'soft' with the maximum dose being delivered at the skin surface, limiting the dose that could be safely applied to the tumour. Emphasis then shifted to gamma emitting radionuclides with the introduction of the 'radium cannon' in 1912, but due to the high costs and limited availability of ^{226}Ra, production was soon stopped. In the early 1930s work began on the use of resonant transformers which could obtain peak voltages of 1-2MV but, again, this technology was soon superseded by the introduction of the Van de Graff machine (the first of which treated patients in Boston in 1937). By 1946 commercial production of these units had started, with 40 accelerators being built before 1959 (12 of which were still operating in 1983). However, these units tended to be large, un-manoeuvrable and very expensive.

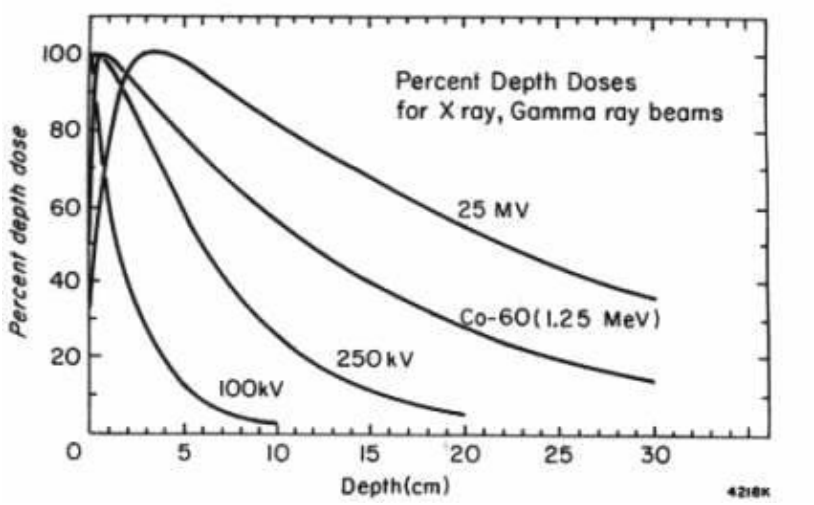

Figure 1.5. Depth dose characteristics of x-ray beams. Increasing the energy of the photon beam raises dose at depth relative to the surface and also allows some skin-sparing due to the buildup effect.

For these reasons the emphasis shifted back to radionuclide units, but now concentrating on ^{60}Co sources, the first three of which were produced in 1952 and installed in Canada and the USA. Each source contained several kilocuries of ^{60}Co, emitting gamma rays with energies of 1.17 and 1.33MeV (mean 1.25MeV). The depth dose curve for ^{60}Co has its peak at 5mm below the skin surface allowing some skin-sparing (figure 1.5).

At the same time further increases in photon energy were made possible by the introduction of the betatron, with the first patient treatment in 1949 with x-rays generated from 20MeV electrons (USA). Betatrons played a significant role in the development of radiation therapy since the increased energy provided greater skin-sparing, higher depth doses and produced less side scatter than beams from radioisotope sources or x-ray tubes. The major disadvantages were their weight, low beam intensity (approx. 40cGy/min) and small field size (12.5 x 12.5cm^2).

Table 1.2. Summary of external beam radiotherapy (EBT) treatment approaches.

Superficial X-Rays	40 to 120kVp
Orthovoltage X-Rays	150 to 400kVp
Telecurie units	^{137}Cs and ^{60}Co
Megavoltage X-Rays	Linear accelerators (MV)
Electrons	Linear accelerators (MeV)
Heavy charged particles	Protons, C, Ar, … (MeV to GeV)
Others	Neutrons, pions

RF linear accelerators were made possible by the advances made during World War II in the construction of magnetrons for radar. In England the first travelling-wave linear accelerator (using microwave generators for electron acceleration) was demonstrated in 1946 by DW Fry. In contrast to betatrons the RF accelerator can deliver dose-rates of 400cGy/min with field sizes of 40x40cm. The first of these was installed at the Hammersmith Hospital in 1952. The first patient was treated in 1953 (figure 1.6) and the last in 1969. Table 1.2 summarises the different treatment approaches and energies associated with external beam radiotherapy.

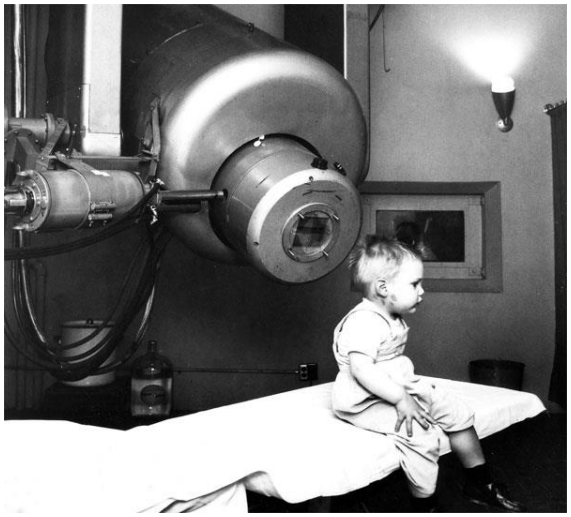

Figure 1.6.Historical image showing Gordon Isaacs, the first patient treated on the Stanford linear accelerator (1956). (http://news.stanford.edu/news/2007/april18/med-accelerator-041807.html)

1.3.1 The linear accelerator

The modern medical linear accelerator (linac) is a machine used to treat cancer in patients by irradiating the tumour with high energy X-rays or electrons. Although many types of linear accelerator are available for medical use they generally all consist of a standard subset of components as illustrated in the block diagram of figure 1.7 below.

The main beam forming components of a modern linac can be grouped into six categories (Podgorsak 2005):

1 Injection system
2 RF power generation
3 Accelerating waveguide
4 Beam transport
5 Beam collimation and monitoring
6 Auxiliary systems (e.g. cooling, vacuum)

1.3.1.1 Accelerating structure

Electromagnetic waves travel at the speed of light in free air, but when confined within a suitably designed waveguide this speed can be reduced. An RF field can therefore be used to accelerate electrons provided that the waveguide is designed so that at each point along its length the propagation speed matches that of the electrons.

The waveguide itself is a cylindrical tube with a series of circular cavities designed so that the speed of propagation of the microwaves used for acceleration increases in the first part of the structure and reaches almost the speed of light for the

remainder. Bunches of electrons from the gun are injected into the waveguide to coincide with pulses from the microwave source, and are accelerated down the tube by riding the wave as it increases in speed.

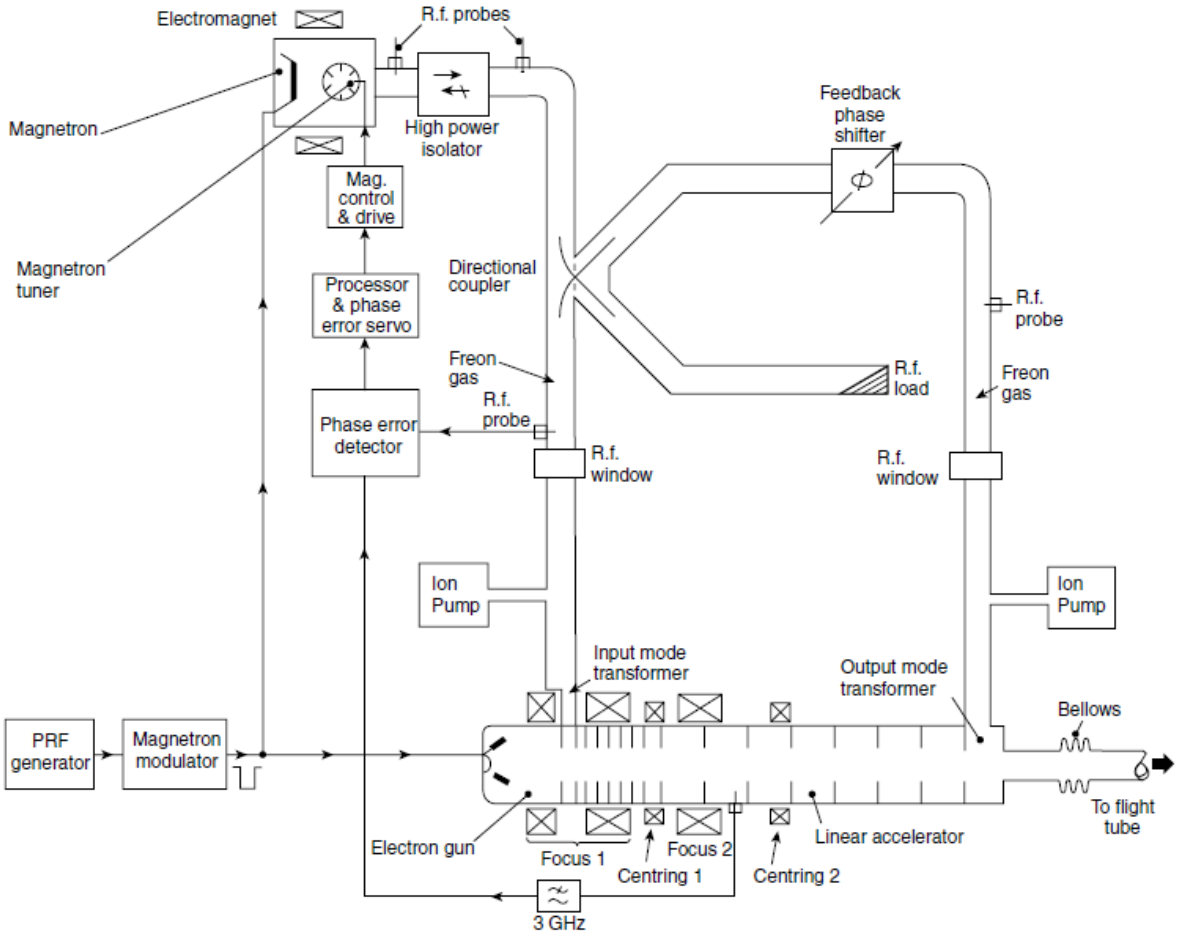

Figure 1.7. Block diagram of an Elekta linac.

The RF power source for microwave generation is either a **magnetron** (an RF oscillator) or **klystron** (an RF amplifier) operating in the 2-10MW range, with the power of the source defining the maximum energy of the accelerator.

Power is supplied to the microwave source by high voltage pulses from a **modulator**. Microwaves are then transported to the accelerator through rectangular waveguides pressurised with SF_6 to prevent electrical breakdowns.

The **automatic frequency control (AFC)** system constantly monitors the

frequency within the accelerator, tuning the magnetron for optimum output.

There are two distinct types of accelerator waveguides: the travelling wave (wave is propagated along the accelerator axis, used by Elekta) and standing wave (where the wave is stationary, used by Varian, Siemens). Both systems inject electrons into the accelerator waveguide in phase with the RF power. Electrons enter an initial **buncher section** (typically 30cm long) where they increase in speed until close to the speed of light. After this section the irises have a constant spacing and energy gains result in a relativistic mass increase.

The pulsed electron beam is provided by a heated tungsten wire, the **electron gun**, the temperature of which can be used to control the energy and dose rate of the accelerator.

The **vacuum system** provides the low pressures needed for the electron gun, accelerator waveguide and bending system. Without this the gun would quickly burn out, and the electrons would quickly disperse due to collisions with air molecules.

Since mutual repulsion of electrons in the guide causes the beam to diverge, a system of **focussing and steering coils** are used along the waveguide to focus and centre the beam. Most of these currents are set during installation, but a set of coils mounted near the end of the structure (2R and 2T) are under servo control to adjust beam steering during operation.

Accelerating structures tend to be too long to mount vertically on the accelerator gantry, so it is necessary to bend the beam through approx. 90° towards the patient. This is achieved using a **bending magnet**. For a usable clinical beam it is necessary for the electron beam to enter the treatment head at the correct angle and energy and to provide a small focal spot, a fairly simple task if the beam is mono-energetic. Since it is difficult to control the energy spread, an achromatic bending system is generally used, which will ensure that electrons of different energies exit the bending system at

the same point and in the same direction regardless of their initial energy. In an Elekta linac this is achieved with a slalom bending system.

1.3.1.2 Treatment head

MV X-rays are generated by high energy electrons striking a high Z metal **target** (figure 1.8). These electrons undergo rapid deceleration resulting in x-ray formation. X-ray production at high energies tends to be along the direction of travel of the incident electrons so the x-rays pass *through* the target. Megavoltage accelerators therefore use *transmission* targets.

Since the efficiency of bremsstrahlung production is low the target needs to be water cooled. The **cooling system** acts to both remove heat from the accelerator components, and to maintain an even operating temperature to maintain stability for any components sensitive to temperature change (such as the accelerator waveguide).

The photon beam then passes through a **primary collimator** which has a circular aperture and sets an initial limitation on the beam size and shape.

The problem with high-energy x-ray production by bremsstrahlung processes is that photons are emitted within a relatively narrow cone, and this cone becomes narrower with increasing energy. The 'ideal' x-ray distribution on leaving the target is an even intensity spread across the width of the beam, resulting in the uniform irradiation of a target volume in a patient. Since x-ray production is predominantly in the forward direction this results in an x-ray intensity lobe that is peaked in this direction so to avoid delivering a higher dose on the central axis a beam **'flattening filter'** is used.

The flattening filter itself is an energy specific, conical shaped piece of metal. This preferentially absorbs x-rays on the central axis (CAX) providing a more uniform

intensity across the beam.

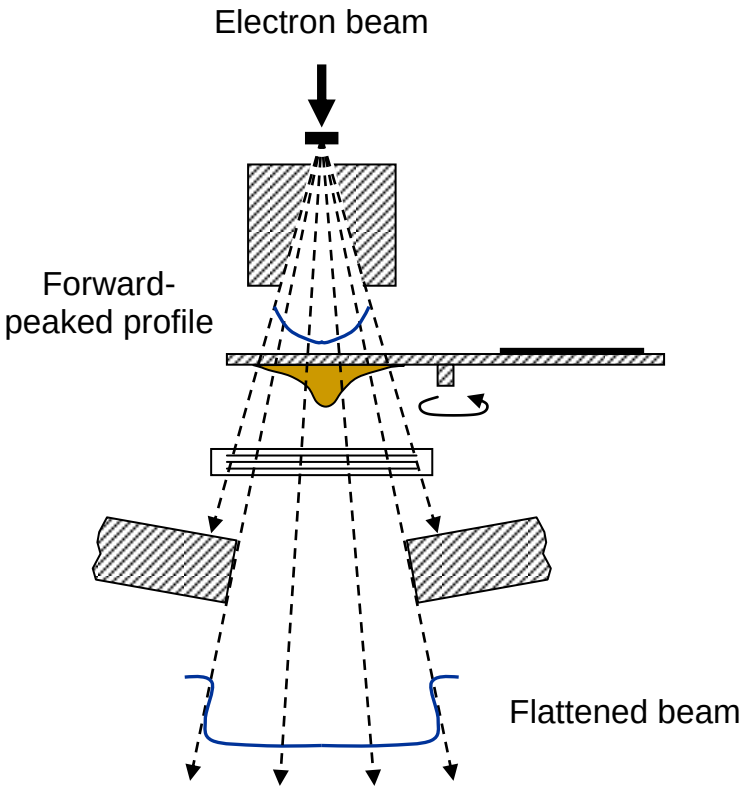

Figure 1.8. The flattening filter acts to produce a 'flat' radiation beam from the forward-peaked bremsstrahlung dose produced by the target.

As the beam passes through there is an inevitable change in the energy spectrum. The materials used to manufacture the flattening filter vary, but in general high atomic number such as lead are avoided and metals like aluminium, copper and steel are used. Since the shape of the peak is energy dependant a different flattening filter (or combination of filters) is required for each photon energy used.

Modern accelerators are generally capable of operating at several x-ray and electron energies so various filters are necessary, and are located on a rotating carriage (the **carousel**) in the treatment head (figure 1.9).

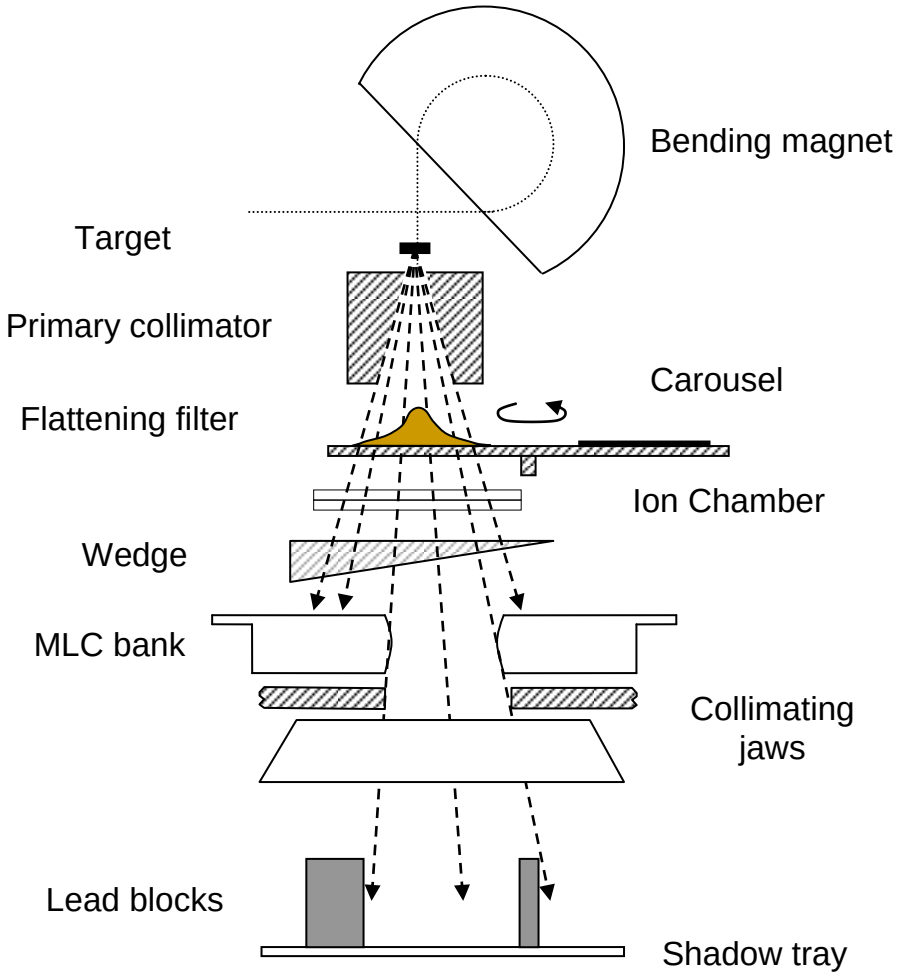

Figure 1.9. Simplified view of the linac head (Elekta design).

Below the flattening filter is a system of ionisation chambers to measure radiation dose and to maintain beam stability. A set of **secondary collimators** (jaws) then exists to shape the radiation to the desired (rectangular) field size. Further collimation can be provided either by lead blocks or by **multi-leaf collimators (MLC)** or lead blocks mounted on a *shadow tray* (figure 1,9).

1.3.1.3 Beam monitoring and control

A transmission ionisation chamber is mounted in the treatment head just below the flattening filter to monitor and control dose delivery. The unit consists of a series of

parallel plate chambers sandwiched together, each divided in separate zones (figure 1.10). The use of two chambers ensures dual dosimetry in case of a failure in one of the units.

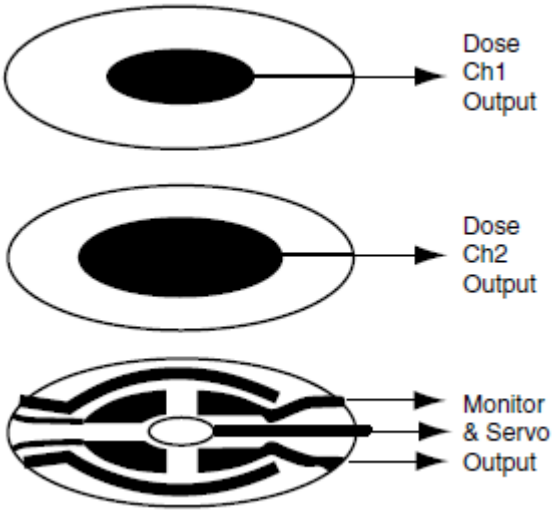

Figure 1.10. Exploded diagram of a transmission ionisation chamber, as used by Elekta.

The currents in the steering coils at the gun end of the waveguide, the focussing coils, and the bending magnet are run from stabilised power supplies at predetermined values depending on the beam energy.

Currents in the target end steering coils are under servo control by signals from the monitor chamber. With the beam on information from the chamber is used to regulate the position of the focal spot which must be closely monitored to maintain a flat, uniform beam. The chambers monitor the beam energy, dose rate and beam uniformity, symmetry and flatness. An imbalance in any of the signals from paired chambers can be used to actively servo the electron gun and beam steering magnets (2R and 2T) to maintain correct running conditions.

The treatment head and gantry itself are capable of 360° rotation around a single reference point. The intercept of the beam central axis with the gantry, collimator and couch rotation axes is known as the **isocentre** (figure 1.11). This is ideally a single point in space, but due to the weight of the gantry arm and the torque exerted by the

treatment head, the isocentre is realistically confined to a sphere with a diameter of approx. 1mm (see section 8.3.4). The idea then is to place the tumour at the isocentre position so that beams can be directed into the patient from various angles without having to enter the room or move the patient between fields. As the gantry rotates the accelerator waveguide and bending system move through the Earth's magnetic field which, while small in strength, is strong enough to move the beam away from its correct trajectory. The currents in the steering magnets 2R and 2T therefore need to vary with gantry angle, and are controlled by **look-up tables**. The 'aim' value is updated with gantry angle, and the servos will operate around this value to maintain beam steering.

The linac is constantly monitored by a digital **control system** to ensure correct performance and the safe, accurate delivery of the radiation dose to the patient. Any deviations from intended performance can give rise to a series of fault warnings which can halt or terminate the beam depending on severity.

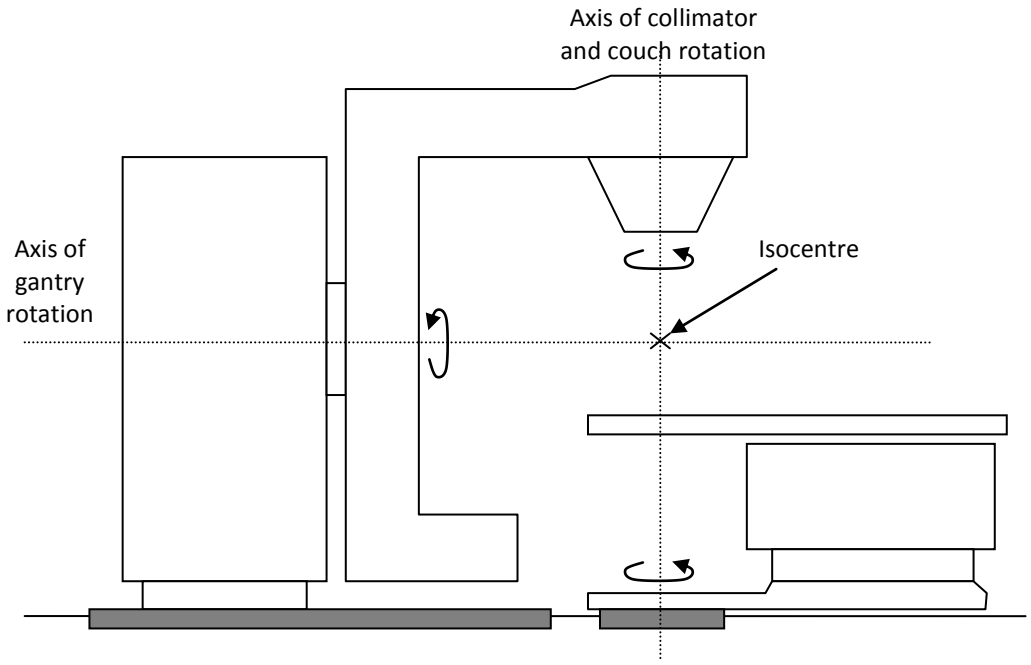

Figure 1.11. Diagram to illustrate the concept of the treatment isocentre.

These interlocks are in place to ensure the performance and safety of the linac in delivering the correct dose to the patient.

1.4 Rationale for flattening filter free

Beam flatteners have been regarded as an essential component since the introduction of linear accelerators in the 1950's. However, despite their longstanding use there are still a number of unresolved issues regarding their use.

In order to produce this flat radiation beam it is necessary to remove a large proportion of the beam intensity (see figure 1.12), and this radiation is converted to scatter with the flattening filter acting as a secondary source of radiation (for both photons and electrons). The photon head scatter and electron contamination produced by the flattening filter are still the subject of much research and are still not modelled accurately within most radiotherapy treatment planning systems.

Monte Carlo studies have shown that the flattening filter is responsible for the majority of scatter produced in the treatment head (Petti *et al* 1983, Zhu and Bjarngard 1995).

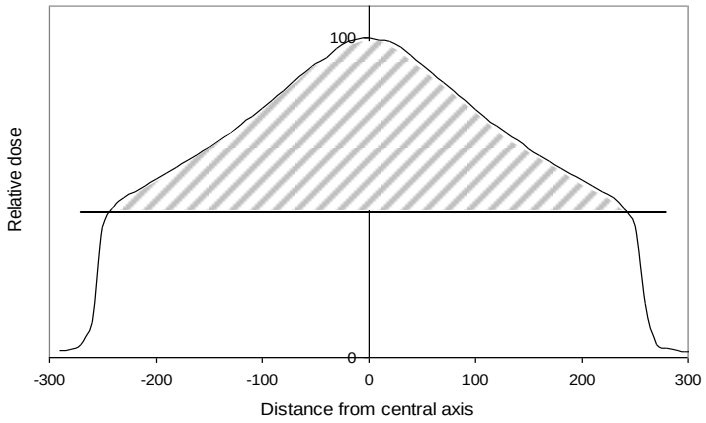

Figure 1.12. The flattening filter removes a large proportion of the beam shown, reducing the central axis dose to approx. 50% of its initial value (at 6MV).

It is estimated that extra-focal radiation contributes 11-16% of the photon fluence at the isocentre and that roughly 70% of this comes from the flattening filter (Liu *et al* 1997, Petti *et al* 1983); exact figures are energy and vendor specific. The filter also acts as the main source of electron contamination (which is also very difficult to model) (Nilsson and Brahme 1986, Hounsell and Wilkinson 1999, Klein and Esthappan 2003). Leakage radiation from the head also delivers a whole-body dose to the patient necessitating the use of considerable amounts of shielding around the head of the machine to reduce this.

The primary function of the flattening filter is to provide a flat radiation beam. However, due to the effects of scatter within the patient and changing beam spectrum it is not possible to create a beam with a 'flat' profile at all tissue depths, and flattening filters are generally designed to produce a flat profile at only one given depth (usually 10cm). Nearer the surface the beam will have 'ears', and at greater depth will be more curved (figure 1.13). The flattening filter therefore only produces a beam of 'nominal' flatness.

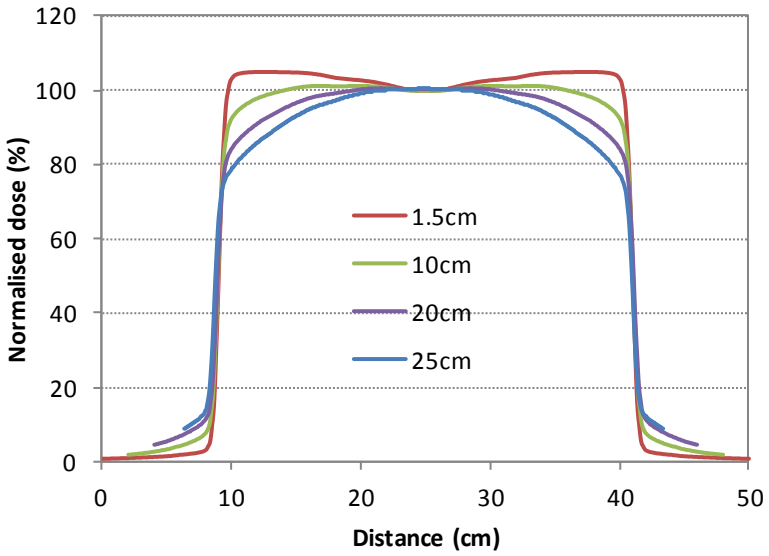

Figure 1.13. Change in beams profile with depth. Normalised to 100% on the central axis and scaled to remove divergence. Note the change in beam profile towards the edge of the beam with increasing depth.

In producing a flat beam the filter therefore causes a series of problems, such as:-

- Decreased primary beam intensity, leading to reduced dose rate
- Differential absorption across the field (changes in beam spectrum) causing problems for dose calculation and beam modelling
- The need for the introduction of "horns" in the particle fluence to compensate for this angular variation of the spectrum
- The creation of a significant source of extra-focal scattered radiation within the beam
- Electron contamination in the primary beam
- Increased leakage radiation from the treatment head
- Amplification of beam steering errors necessitating active beam monitoring and servo control

The problem with unflattened beams of course has always been utilising the forward peak in the dose distribution. Historically, radiotherapy has been based on the delivery of flat (or wedged) beams to treat 'box-like' volumes to a uniform dose. Modern imaging techniques and advances in computer hardware/software now allow a much more detailed view of the patient anatomy necessitating the use of intensity modulation within each field. Modern radiotherapy therefore relies less and less on flat radiation fields and more on the routine use of fluence modifying devices and techniques. At the extreme end of this is intensity-modulated radiotherapy (IMRT) (Appendix A). In these circumstances it is likely that the flattener isn't actually necessary as all modulation could be performed by the MLC (see figure 1.14). If the initial field shape can be taken into account in the segmentation process the filter might not be necessary at all.

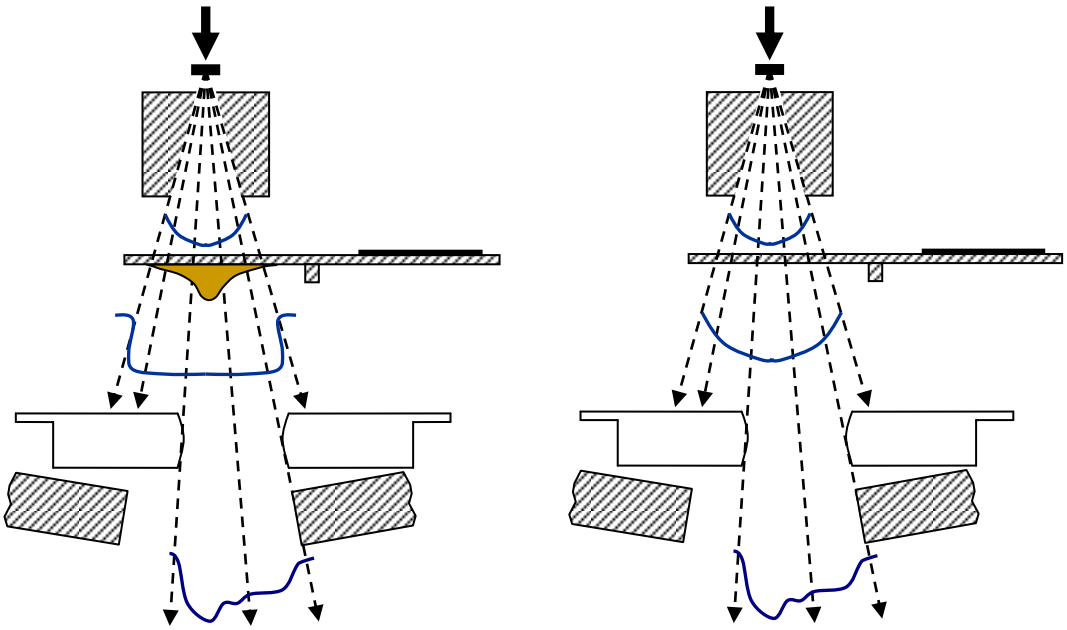

Figure 1.14. The IMRT process relies on the MLC leaves to modulate the 'flat' beam to produce the photon fluence necessary. It is possible that an initially flat beam is not required (a) and that all modulation necessary can be performed by the MLCs (b).

The study of unflattened beams has come to be known by the acronym FFF, for flattening-filter-free. FFF beams were first studied by O'Brien et al (1991) who studied their use on a Therac-6 linear accelerator with the intention of increasing the dose rate to reduce treatment times for intracranial stereotactic treatments. At this time there was already an accelerator operating without a flattening filter, the Racetrack Mictrotron MM50 (Brahme *et al* 1980, Karlsson *et al* 1993) which utilised a scanning electron beam incident on the target to buildup dose in the patient in a similar manner to spot-scanning proton beams.

In recent years the flattening filter free linac has gained popularity, with a significant number of articles on the subject appearing in the literature, and reference is made to these throughout this work. At the beginning of this research project a small number of research articles had been published on the dosimetric properties of FFF beams from Varian accelerators, but as yet nothing regarding the Elekta linac

(Fu *et al* 2004, Titt *et al* 2006a & b, Vassiliev *et al* 2006a & b, Mesbahi 2007, Ponisch *et al* (2006) and Zhu *et al* (2006)).

1.5 Scope of work

Flattening filter removal could aid treatment accuracy by reducing some of the sources of uncertainty in beam modelling and dose calculation, helping to reduce variations in beam symmetry and uncertainties in relative dose calculation (2, 4 and 6 in table 1.1). In reality some of these uncertainties are linked (2&7, 1&6).

Specifically, removal of the flattening filter from the beam line should lead to:-

- Increased dose rate
- Greatly reduced head scatter
  - → More accurate dosimetry
  - → Less leakage (whole-body) radiation
  - → Tighter beam penumbra
- Greater beam stability
- Reduced range of output and wedge factors
- Simplified beam spectrum variations
- More consistent profile with depth
- Better imaging due to increased low energy x-ray component

This thesis explores the factors which affect radiotherapy treatments when the flattening filter is removed, following the chain of events necessary to bring the FFF linac to clinical use, from dosimetric characterisation and machine operation through to beam modelling, treatment planning and quality assurance.

Efforts have been concentrated on the use of a 6 MV X-ray FFF beam from an Elekta Precise linear accelerator as this now seems to be the standard beam energy used by most radiotherapy departments for modulated techniques, but some 10MV data is also presented.

A significant proportion of results reported in the work are based on relative, rather than absolute measurements. Where appropriate, uncertainties have been included in text, tables and figures. Where uncertainties have not been specified in figures it can be assumed that error bars are within the bounds indicated by the marker points.

CHAPTER 2

LINAC SETUP AND DOSIMETRIC CHARACTERISATION

In this chapter the technical details of machine setup and characterisation will be discussed. This begins with a description of the filter removal process and the changes in machine operation caused by its removal. Following on from this the basic beam characteristics are described and their possible advantages in radiotherapy discussed. Sections of this chapter have been published in a paper by the author in *Physics in Medicine and Biology* (Cashmore J, 2008).

2.1 Linac setup

As discussed in the previous chapter, the flattening filter is mounted at the secondary filter-stage on a five-position rotating carrier (the carousel) in the treatment head of the machine (figure 2.1). At this stage a low energy Elekta Precise linear accelerator located at University Hospital Coventry (Arden Cancer Centre) was being used for

measurements. This linac was fitted with a standard 80 leaf MLC (MLCi), and operated at 6MV in photon mode and 10MeV in electron mode. Only two of these ports in the carousel are used clinically, one for the 6MV flattening filter and the other for the 10MeV electron scatter foil. This leaves three ports free, and within the machine's service mode it is a simple matter to rotate the filter out of the beam line to an 'open' port position. In practice these unused ports are not open, but contain a 'blanking plate' of 2mm aluminium. Initial experiments were carried out using the standard clinical beam setup with the carousel rotated to one of these 'open' ports to remove the influence of the flattening filter from the beam. This beam (exiting through the 2mm Al plate) was then used to investigate the basic operational characteristics of the unflattened beam.

Figure 2.1. The carousel ("egg-poacher") in the treatment head

As stated, filter removal is a simple process, but once it became apparent that further investigation was warranted it became necessary to consider changing the running parameters of the beam. This could potentially impact on clinical delivery if not corrected between research and treatment, so Elekta Ltd were approached to obtain a licence for an *additional* beam energy for research purposes. It is not

possible to have identical energies on the linac so a 10MV licence was obtained for research use. All energy specific beam parameters pertaining to 6MV were copied to this new energy and the gun servo, steering currents, beam hump and uniformity reset to allow the beam to run. The '10MV' research beam was inaccessible for clinical use and could not be accessed by the record and verify system, Mosaiq.

The beam essentially remains unaffected up until the point where it would normally strike the flattening filter; hence the vast majority of operational parameters remain unchanged. Issues only start to arise when the unflattened beam reaches the ionisation chamber; not only does this monitor the dose delivered but also acts to servo the radial and tangential steering currents (2R and 2T on Elekta machines) to maintain a symmetrical beam. The difference between the inner and outer plates (hump error) is also used to control the gun current and hence maintain beam energy.

It is expected that filter removal will cause changes in dose rate, energy spectrum and scatter conditions in the head. There are therefore several fundamental questions to ask of machine performance/operation when removing the flattening filter:-

1. How does the increased dose rate/dose per pulse affect dosimetry?
2. Can the gun servo be reset and still function to control the beam energy?
3. Can the steering servos be reset to allow operation around their new operating values?
4. How does filter removal affect beam energy and energy spectrum?
5. What the dosimetric characteristics of these beams?

2.2 Dosimetric characteristics

The following sections give details of the measurements taken in order to characterise the dosimetric changes to the beam caused by filter removal.

2.2.1 Dose rate

Flattening filters have a conical shape and are made from medium to high atomic number materials. Since they can be several centimetres thick on the central axis the dose rate is severely affected by its presence. The first (and most obvious) consequence of running the linac with no flattening filter is the huge increase in observed dose rate. For the beam in its current state, running both beams at peak dose rate and taking measurements at d_{max} (15mm) with a Farmer chamber, the dose rate was seen to rise by an average of 2.3 times for an open beam, and by 1.9 times for the wedged beam. The lower value seen for the wedged beams is due to increased absorption (lower wedge transmission factor) in the physical wedge due to the change in energy spectrum. Due to hardware limitations in the Elekta *Desktop* software (v. 5.02) it is not possible to run the linac at full dose rate (capped at 1200 MU per minute [12Gy/min under reference conditions). This increase in dose rate could clearly be a useful factor in many treatments (e.g. respiratory gated breathing and stereotactic radiosurgery [SRS]). In practice the dose rate was higher than necessary, so the pulse repetition frequency (PRF) was lowered (from 400 to 200) to regain a 'normal' dose rate.

A range of dose rates for FFF beams have been reported in the literature (Vassiliev *et al* 2006, Kragl *et al* 2009, Cashmore 2008, Fu *et al* 2004 1.92. O'Brien *et al* 1991). To some extent these are influenced by the calibration of the beam and to hardware limitations of each accelerator. Factors of 2 are common at 6MV and a dose rate of approx. 1200 MU/min is anticipated in a clinically released product.

Measurements were also performed to assess the linearity and reproducibility of dose delivery (figure 2.2), confirming that the internal ion chambers respond well to the higher dose rate and that doses delivered are accurate (<1% error) down to 2mu.

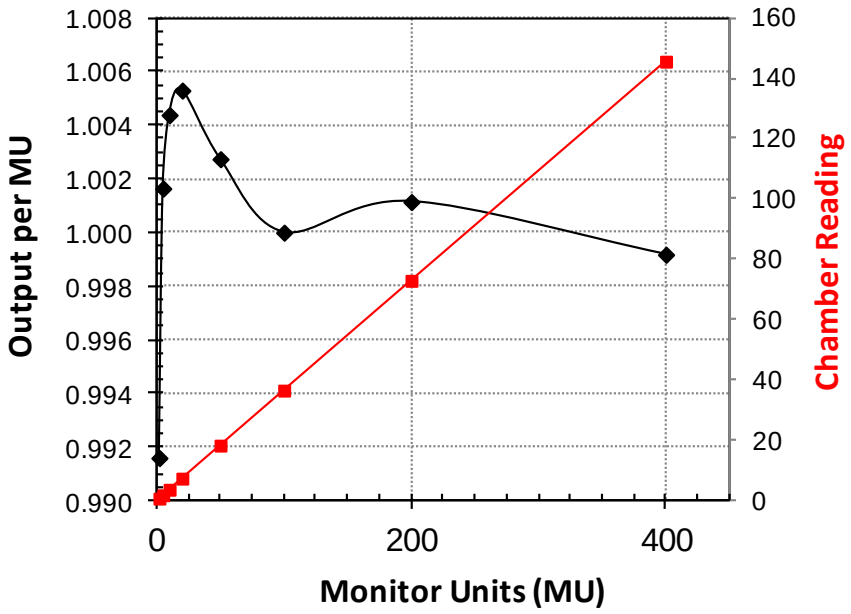

Figure 2.2. Dose linearity as a function of monitor units (MU) delivered, and the output per MU normalised to the dose recorded for 100MU.

2.2.2 Dose per pulse

As the electrons are accelerated in bunches, the radiation is delivered in discrete pulses of radiation. The increase in dose rate observed with filter removal is therefore due to an increase in dose-per-pulse. This effectively stays constant, and the dose rate is then changed by changing the pulse repetition frequency (PRF). Although the dose rate can be lowered back to the original level if required this increase in dose-per-pulse will remain and is likely to affect the rate of ion recombination in ionisation chambers.

Even though the dose-per-pulse of the beam is 'fixed' it can in fact be varied by changing the source to chamber distance (SCD). Figure 2.3 shows the dose-per-pulse

dependence of a NE2571 Farmer chamber in the FFF beam; the curves are normalized at 100cm SSD for a 10x10cm² field. The dose-per-pulse will affect the response of the chamber, but the two curves overlie each other indicating that these corrections should hold even at these high dose rates. The characteristics of ionisation chambers to pulsed radiation beams has been well reported (Derikum and Roos 1993, Bruggmoser *et al* 2007) and extended to include FFF beams by Lang et al (Lang *et al* 2012a).

Finally, it should be noted that in the current software version (Release 5) the machine cannot be calibrated to give 1mu = 1cGy under standard conditions due to a software limitation on the range of 'Dose Reference' values.

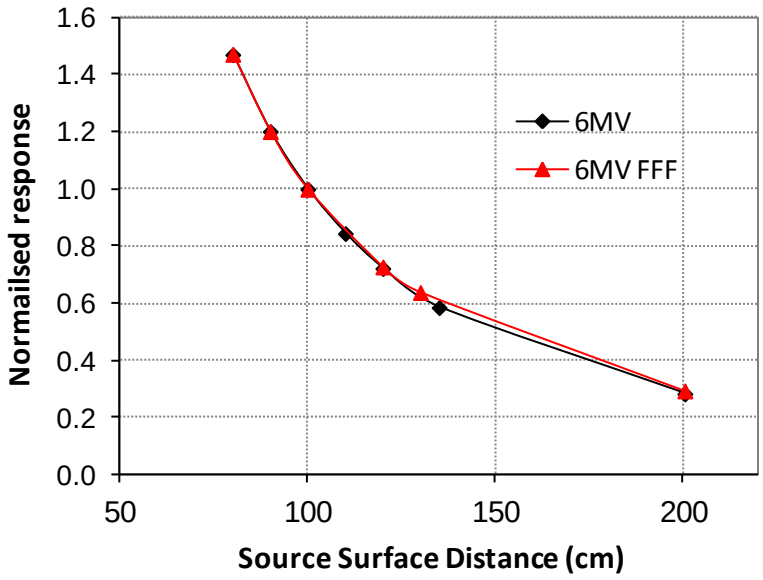

Figure 2.3. Dose per pulse dependence of a NE2571 Farmer type chamber.

2.2.3 Head scatter (Sc)

A reduction in head scatter (Sc) is expected with filter removal as the FF is the major source of scatter (Petti *et al* 1983, Zhu and Bjanrngard 1995), and a reduction in Sc could be very beneficial in many ways. Figure 2.4 shows head scatter measurements as a function of field size made using a Perspex mini-phantom (90cm SSD, 10cm

deep) relative to a 10x10cm² field. A significant decrease is seen in the range of readings compared to the flattened field with a variation of only 3% over the entire range 4x4 to 40x40cm² compared to a 9% variation with the filter in place. This is a reduction of approximately a factor of 3, and matches well with other reported data (Zhu *et al* 2006). Modelling of scatter with variations in field size and shape are very important, especially for IMRT (see section 6.1). The flattening filter is the dominant source of these variations so filter removal could have several favourable consequences for the dosimetry of small field and IMRT beams where errors in the calculation of head scatter lead to errors in monitor unit calculation.

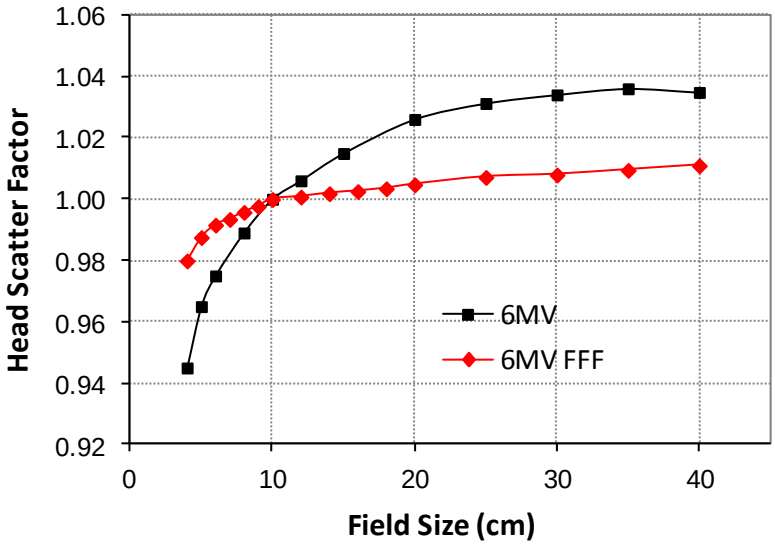

Figure 2.4. Head scatter measured using a Perspex mini-phantom (normalized to a 10x10cm² field).

2.2.4 Total scatter (Sc,p)

Total scatter factors measured at 100cm SSD, d_{max} (Figure 2.5) also show a reduced range when plotted against equivalent square with a significant reduction at large field sizes. Sc and Sc,p fall rapidly at small field sizes due to source occlusion. The reduction in the range of readings for both parameters should aid dosimetry for small-field beams and those measured under non-equilibrium conditions.

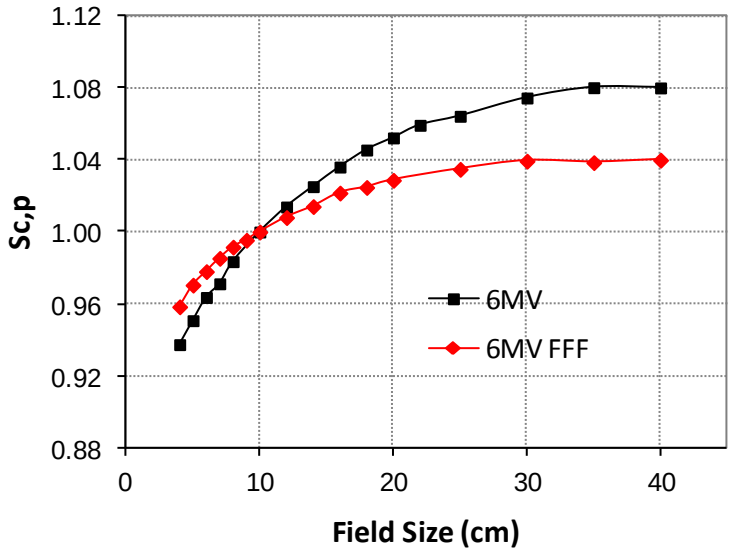

Figure 2.5. Variation of total scatter factor measured at 100cm SSD, d_{max} and normalized to a 10x10cm² field.

The ratio of 40x40 to 4x4cm² readings is 1.15 for the flattened beam and 1.08 for the filterless beam, i.e. half the variation in total scatter factor. Similar results have been shown by Ponisch *et al* (2006).

2.2.5 Collimator exchange effect

This reduction in scatter should also lead to a reduction in the Collimator Exchange Effect (CEE) – the variation in output seen for same size rectangular fields depending on which set of jaws (upper or lower) defines the larger dimension. Measurements of this effect were made by sequentially fixing the X and Y jaw at 4cm and varying the other jaw dimension from 4 to 40cm (as recommended in ESTRO Booklet 6, Mijnheer *et al* 2001). The magnitude of the effect is on average 1.6% for standard operation and 0.6% with the filter removed (figure 2.6). These figures reflect the two thirds reduction of head scatter observed in figure 2.5.

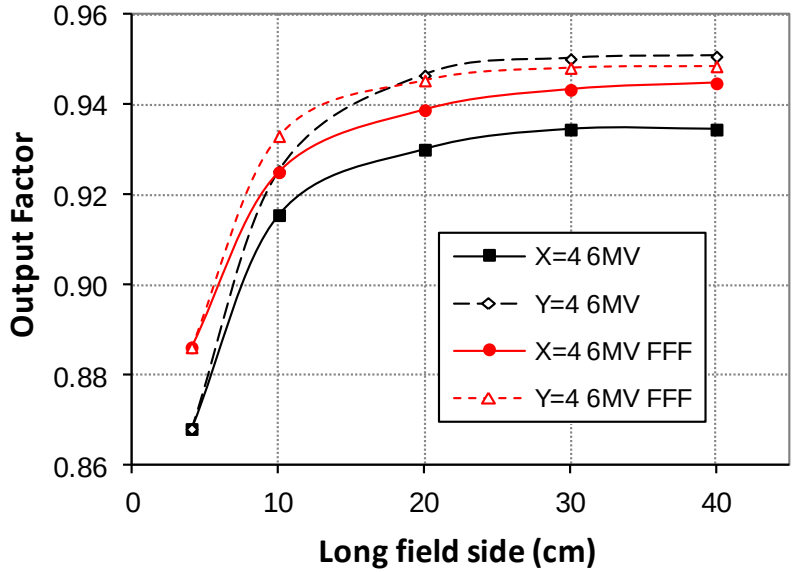

Figure 2.6. Collimator exchange effect. Output factor is plotted as a function of the long field side, keeping either the X or Y collimator fixed at 4cm. Black lines represent the conventional beam and red lines with the filter removed.

2.2.6 Leakage radiation

Reduced head scatter should also lead to a reduction in leakage radiation from the treatment head. Leakage measurements were taken in the patient plane as recommended by the Elekta acceptance documentation (Elekta 2005) *'The absorbed dose due to leakage radiation at any point in a horizontal plane that passes through the isocentre and outside the maximum useful beam area, shall not exceed 0.1% of the dose at the isocentre.'*

A Farmer chamber (with 1.5cm buildup cap) is placed at the cardinal angles at 50 and 100cm from the isocentre (see figure 2.7). With the diaphragms closed the absorbed doses at these points are compared to a 'reference dose' measured using a 10 x 10cm^2 field at the isocentre. Table 2.1 shows the results of patient plane leakage measurements.

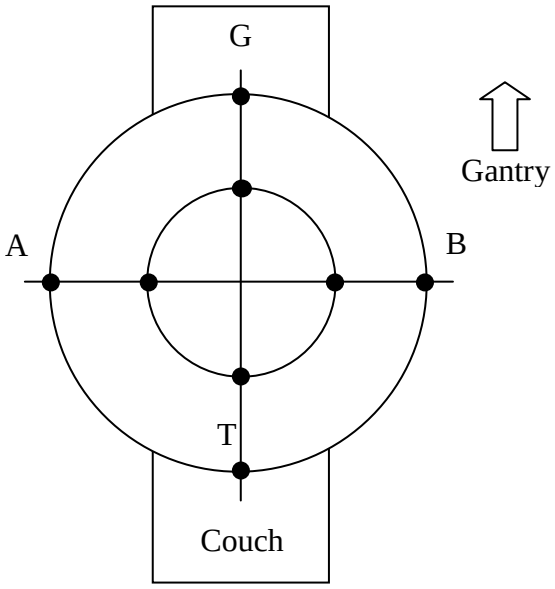

Figure 2.7. Specification of points used to measure patient plane leakage. The circles are of radii 50 cm and 100 cm. Readings at these points are taken with the collimators in the closed position and compared to a central axis reading for a 10×10 cm² field.

Table 2.1. Patient plane leakage measurements. G and T refer to movements towards the Gun and Target. A and B refer to movements left and right of centre when standing facing the gantry.

Leakage radiation (% of reference reading)			
Position	**Filter In**	**Filter Out**	**% Decrease**
50cm G	0.012	0.0068	42.2
50cm T	0.005	0.0029	45.9
50cm A	0.018	0.0079	55.4
50cm B	0.019	0.0072	62.0
100cm G	0.013	0.0054	58.5
100cm T	0.011	0.0032	69.6
100cm A	0.018	0.0079	55.4
100cm B	0.025	0.0061	76.0
	Average decrease		**58.1%**

The leakage dose should not exceed 0.1% of the dose at the isocentre and this is easily achieved during normal use, however, for IMRT delivery the number of monitor units required can be raised significantly (2-4 times) compared to open beam delivery and hence leakage radiation will increase proportionally.

Operating without the flattening filter the dose is seen to be, on average, 58% lower than those recorded for normal use, representing a large decrease in the out-of-field doses that would be received by the patient.

2.2.7 Depth doses

The FFF beam clearly shows significant differences to the conventional beam. To investigate the changes in the beam spectrum sample depth dose (DD) curves were measured to compare with standard data.

The flattening filter significantly hardens the radiation beam on the central axis but due to its physical shape the beam quality decreases with distance from the central axis. Production of contaminant electrons also affects depth doses beyond d_{max} but differences due to this are mainly observed in the surface region.

Table 2.2. Comparison of beam quality parameters.

Nominal Energy (MV)	**Beam Description**	**PDD at 10cm deep, D_{10} (%)**	**Depth of 80% dose, d_{80} (cm)**	**Depth of dose max. d_{max} (mm)**	**QI (TPR $_{20/10}$)**
6	FF in	67.6	6.7	15	0.679
6	FF out	65.2	6.3	13.5	0.653
5	BJR 5MV	65.0	6.2	12.5	0.646

Central axis depth doses were measured at 100cm SSD and normalised at a depth of 15mm for open and wedged square field sizes from 5x5 to 40x40cm² (30x30cm² for wedge). Beam profiles and depth dose measurements were taken using a PTW MP3 Tandem watertank with Semiflex 0.125cc chambers and running Mephysto 7.4 water phantom software.

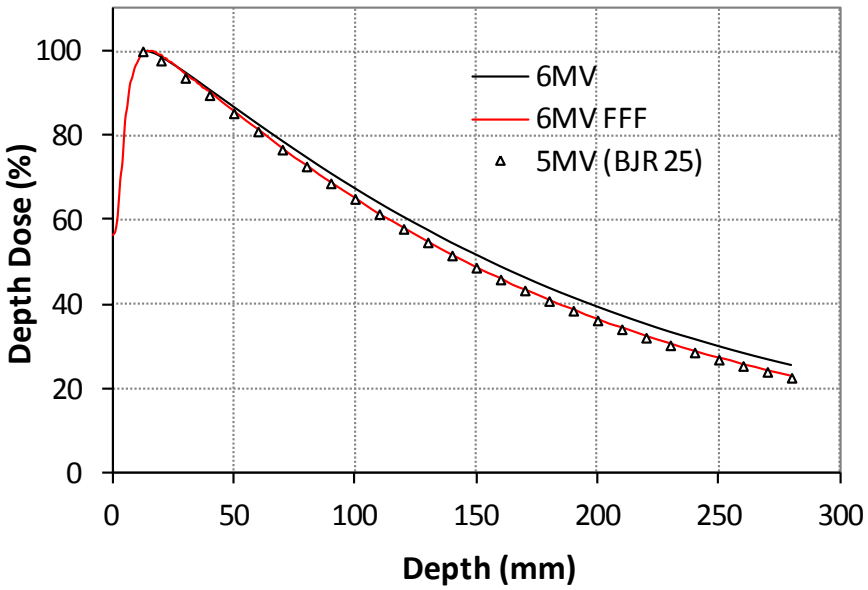

Figure 2.8. Depth doses for a 10x10cm² field at 100cm SSD. Lack of beam hardening is seen as an energy decrease to approx. 5MV.

In a conventional beam the filter attenuates the low energy component of the spectrum increasing the apparent energy of the beam. With FFF beams these soft x-rays pass through and the addition of these to the beam spectrum lowers the observed energy. To quantify this change %DD curves were compared to published data (BJR 25, Jordan *et al* 1996). FF removal at 6MV produces a beam with characteristics similar to a 5MV beam (figure 2.8). Table 2.2 shows comparisons for most of the commonly used beam specification parameters which also demonstrate a good match to 5MV data. The flattening filter obviously hardens the beam appreciably, but this drop in energy could easily be compensated for by adjusting

accelerator parameters to raise the beam energy to match, if so desired. As yet there is very little published depth dose data for unflattened beams and non for Elekta accelerators or wedged beams, so if BJR25 were to be updated at some point it might be a good opportunity to include FFF data.

2.2.8 Surface dose

Changes in beam spectrum and scatter will affect the dose in the build-up region, and in particular, surface doses. Measurements in the build-up region (made with a NACP-02 parallel plate chamber embedded in solid water (Radiation Physics, St Bartholomew's Hospital, London) show that there is a slight increase in surface dose with the flattening filter removed (figure 2.9). The reduced head scatter however produces appreciably less variation in dose near the surface (measured at 3mm depth) with field size (figure 2.10) than is seen for flattened beams.

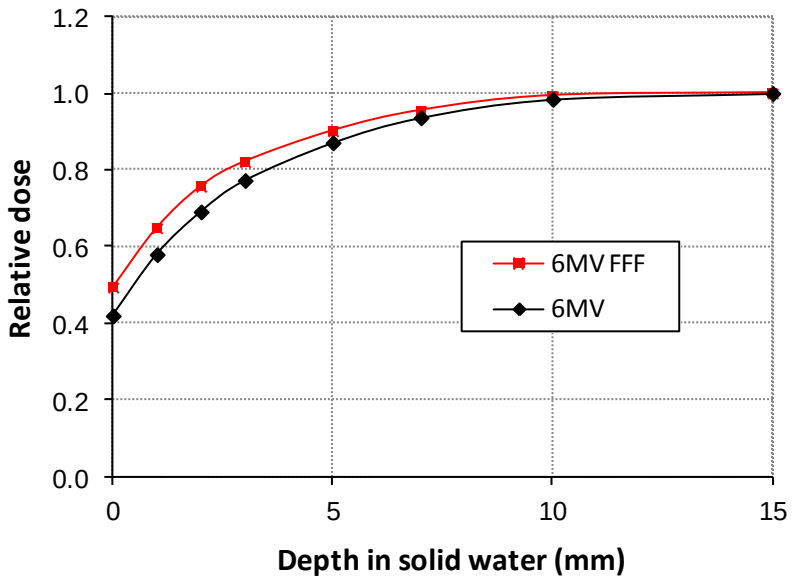

Figure 2.9. Build-up curves for a 10x10cm² field measured in solid water. Filter free beams show slightly increased surface dose compared to filtered beams at 6MV.

It is also useful to look at the variation in surface dose with increasing field size. The reduced head scatter produces appreciably less *variation* in dose near the surface (measured at 3 mm depth) with field size (figure 2.10) than is seen for flattened beams.

The target, primary collimator and flattening filter all act as both producers, and absorbers of electrons. Contamination electrons arising from the primary collimator act to increase surface doses in the patient. The filter removes the majority of these but generates is own electrons. One of the benefits of electrons generated here is that as they deliver a *position-dependant* dose into the ion chamber, which in turn is used to servo the beam. If the filter is simply removed the contamination electrons from the primary collimator reaching the ion chamber directly. These hold no positional information, so cannot be used to control the beam steering. A certain amount of material is therefore necessary to provide the correct signals, however, too much material will increase surface doses. The material used for the plate, and its thickness, need to be optimised.

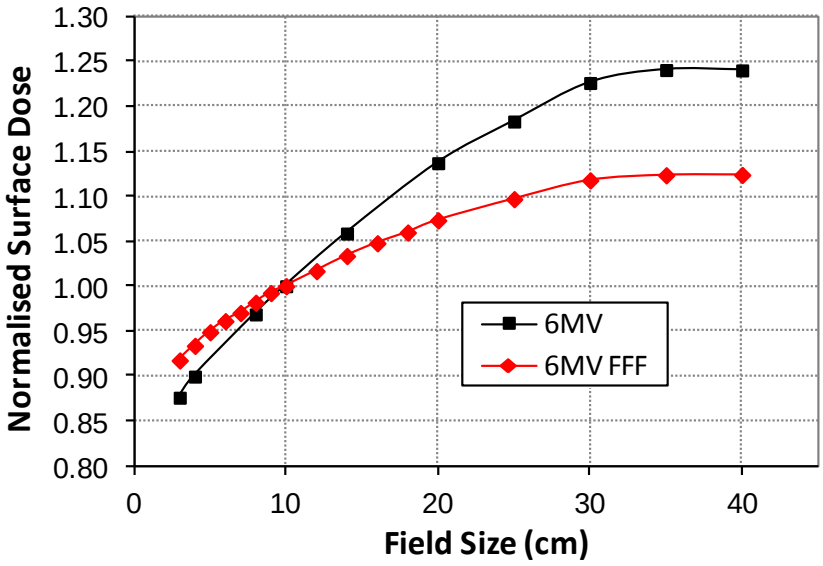

Figure 2.10. Variation of surface dose (at 3mm depth) with equivalent square normalized to a 10x10cm² field. Maximum to minimum ratio is 1.42 with the flattening filter in and 1.23 without, i.e. half the variation.

Monte Carlo studies have demonstrated that the low-energy components of the beam spectrum are significantly enhanced with FF removal (Tsechanski *et al* 2005, Mesbahi 2007) and that these photons would be expected to deposit energy in the buildup region. The fact that surface doses are not universally lower indicates that the electron contamination in the beam must be lowered by a similar amount. This role reversal has a twofold benefit; firstly x-rays are much easier to model than electrons leading to possible improvements in the modelling of the buildup region, and secondly these low kV photons may act to improve the contrast of portal images.

As well as utilising an open port in the carousel the additional unused ports were also used to house various thicknesses of copper and aluminium (figure 2.11) to study the effects of electron contamination on surface dose and machine operation.

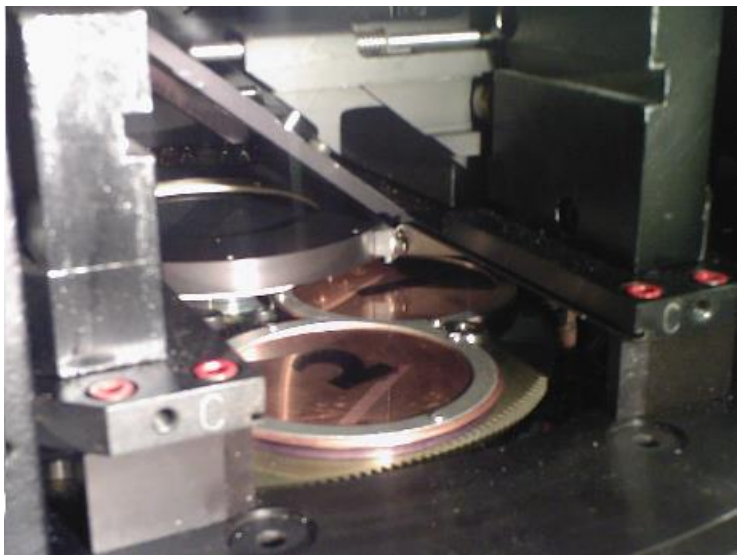

Figure 2.11. Two copper plates (1.1mm and 1.9mm) mounted in the carousel.

A variety of plates have been used in the literature. O'Brien originally used a 13mm Al plug for SRS studies on their Therac-6 linac (O'Brien *et al* 1991). In a Monte Carlo study Titt *et al* (Titt 2006) investigated the use of both 11mm nylon and a 2mm Cu plates. Nylon was found to decrease the photon fluence by 7% and the electron fluence by 54% compared to normal operation. For the copper plate these figures

were 9% and 78% respectively. Stathekis *et al* (2009) used a 1mm steel plate in a Varian 2300 linac, and Kragl *et al* (2009) and Tyner *et al* (2009) have reported data using a 6mm Cu plate in an Elekta Precise accelerator. Georg *et al* have provided an excellent summary of this data (Georg *et al* 2011).

Buildup measurements were performed with thin sheets of copper and aluminium (1.1mm Al, 1.9mm Cu, 1.9mm Al) in place of the flattening filter with the hope of reducing surface dose, but no appreciable reduction was seen (figure 2.12).

Lind *et al* (2009) studied the optimum thickness for the plate and found 1-2mm of Cu to be sufficient, but that a thicker plate may be recommended for additional safety. Measurements presented here indicate that a metal plate with a thickness of 1 to 2mm seems sufficient to allow the monitor chamber to operate correctly, offering a good compromise between efficiency, safety and scatter production. Each manufacturer is likely to choose a different configuration due to variations in operating energy and head design etc.

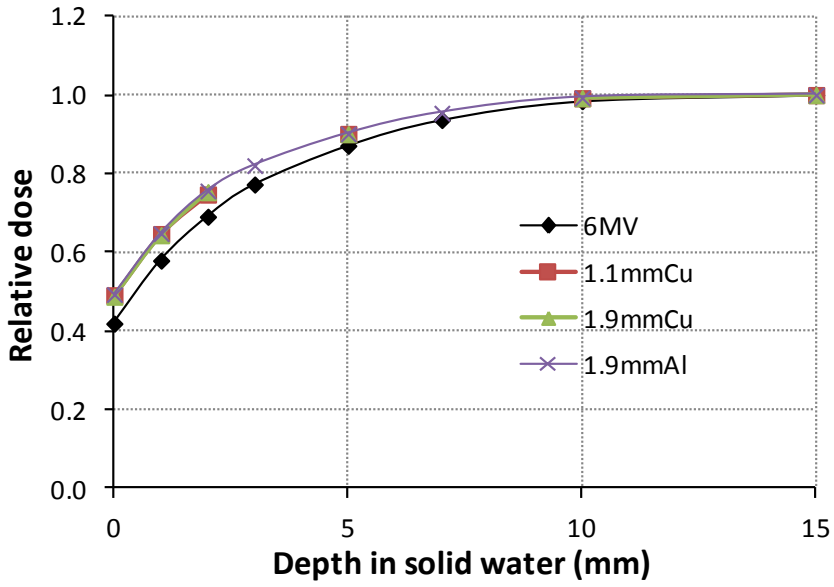

Figure 2.12. Build-up curves for a 10x10cm² FFF field (measured in solid water) through different materials compared to filtered beams at 6MV.

2.2.9 Beam profiles

Beam profile scans in a water tank illustrate the forward-peaked nature of open beam profiles (figure 2.13). Flattening filters are designed to give a flat beam over the maximum field size (usually 40 x 40cm²) and scans at small field sizes (5x5cm² and below) exhibiting little or no change in profile. Larger field sizes show enhanced central axis dose with a rounding of the profiles; similar results have been shown for open beams with a Clinac 21EX (Vassiliev *et al* 2006b). Outside the treatment field the doses are lower for non-flattened beams due to the reduction in out-of-field scatter. This would effectively act to reduce the dose to surrounding normal tissues. At 90cm SSD, 10cm deep for a 10x10cm² field the dose 2cm outside the field edge is reduced from 7.9% to 7.0% (11.3% relative change).

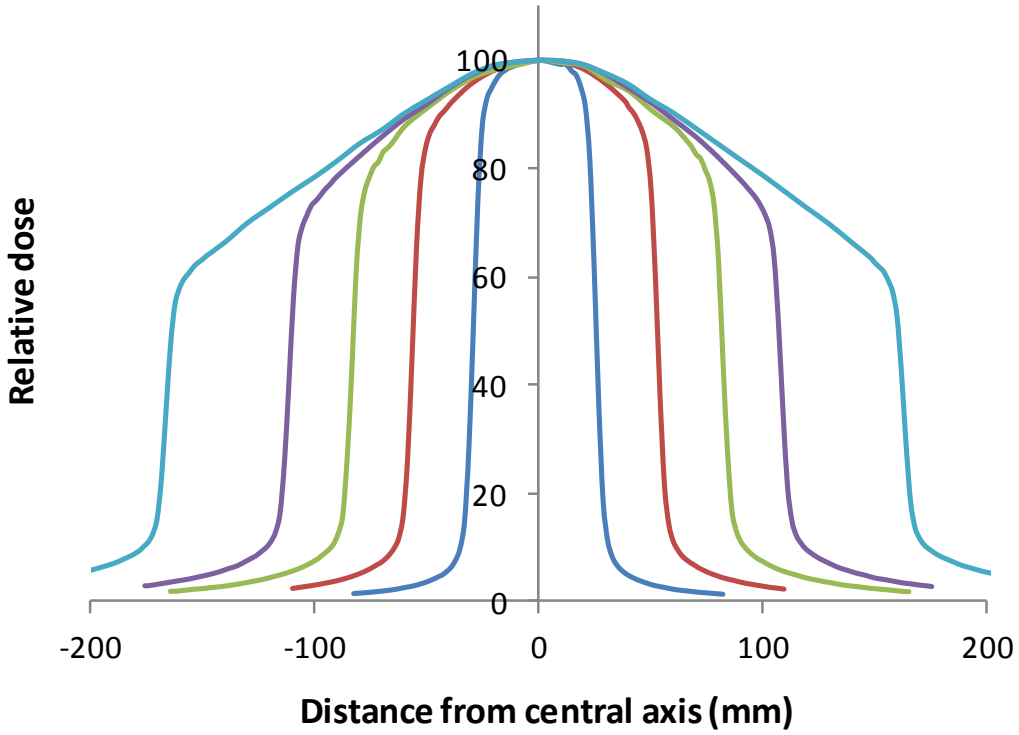

Figure 2.13. Lateral dose profiles of unflattened beams at a depth of 10cm. Field sizes are 5, 10, 15, 20 & 30cm.

2.2.10 Beam steering

Mechanical positioning of the flattening filter and accurate steering of the electron beam are crucial to flat beam production as any misalignment will lead to non-flat, asymmetrical beams. Only if the electron beam axis coincides with the flattening filter axis will the resulting x-ray beam have symmetrical, flat-beam characteristics. In this aspect the flattening filter acts as an amplifier, compounding any effects of inaccurate beam steering. For this reason the beam shape is closely monitored by a series of ionisation chambers and under active servo control to restore flatness and symmetry if the beam is misaligned (section 1.3.1.3).

The *flatness* of an X-ray field is specified as '*the ratio of the maximum absorbed dose (anywhere in the radiation field) to the minimum absorbed dose in the flattened area'*. The ratio should not be greater than 106% for field sizes 10x10cm to 30x30cm, and no greater than 110% for those fields >30x30cm. Field *symmetry* is defined as '*the ratio of the absorbed dose at any two points symmetrically displaced about the beam axis and within the flattened area'*. The ratio should not exceed 103%. Both flatness and symmetry were designed to specify standard flattened X-ray profiles and cannot be used for filter-free beams. These regulations (IEC BS EN 2001) will need to be re-defined for these beams, most probably based on maintaining a match to a base-line non-flat profile measured during commissioning.

Although the ion chamber in the head is designed to maintain flatness and symmetry by servo control of the steering currents, these currents and control amplifiers can drift over time, leading to beam asymmetries.

The beam exhibits two different kinds of instability: angular divergence and lateral displacement, both of which lead to asymmetrical beams (figure 2.14). In practice, beam instability is usually a combination of both effects and can be difficult to decouple.

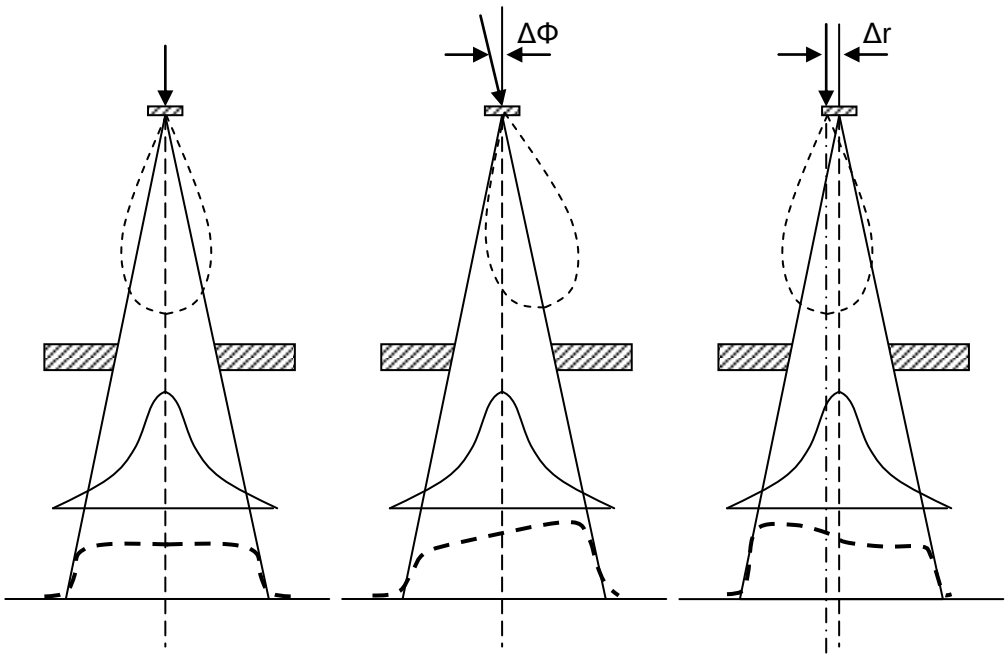

Figure 2.14. Only when the beam is central is a flat, symmetrical beam produced. If lateral or angular displacements are introduced the beam quickly becomes asymmetrical. Beam asymmetry for 2R (angular divergence) and Bf (lateral displacement) instabilities is shown. Adapted from Karzmark, 1993.

To investigate the influences of these two effects bending fine (B_f) and 2R were manually altered (with servos turned off) and the beam shape investigated. Starting from a symmetrical beam the 2R current (controlling symmetry in gun-target axis) was varied by ±50mA and bending fine by ±20mA. Measurements with a Schuster BMS96 linear array (88 diodes with 5mm spacing) demonstrate that for variations in beam steering and bending currents the unflattened beam exhibits almost half the variation in field asymmetry (ratio of absorbed dose at points ±12 cm about the central axis) compared to the flattened beam (see table 2.3).

For flattened beams the dose is seen to 'see-saw' about the central axis with the actual shape and magnitude of the shifts depend on a complex interaction of steering and bending currents. For FFF beams, rather than altering the beam shape these variations simply act to shift the beam off-axis, with the profile remaining the same

relative shape (figure 2.15). The relative stability of the FFF beam is demonstrated by the fact that, as these currents are pushed further, the first interlock to be triggered is that for 'Low Dose Rate', which is due to a loss of beam current as the beam is driven away from the target.

Table 2.3. Beam symmetry measurements recorded at ±12cm off central axis with a Schuster array. Values quoted are the percentage difference of readings ±12cm off axis compared to the central axis value.

		6MV	6MVFFF
2R	**+50mA**	+7.3%	+3.8%
	-50mA	-7.5%	-4.4%
Bf	**+20mA**	+4.1%	+1.5%
	-20mA	-6.5%	-2.4%

In practice, although the flattening filter acts as an amplifier for any beam steering problems, it also acts as a useful indicator of steering inaccuracies as any changes in beam transport produce large errors which are easily noticed. With the filter removed the beam is inherently more stable, but this might make any changes in beam steering more difficult to notice. Further work will be required to investigate the effects of this to determine whether the current configuration (dose cards) remain suitable.

Small changes in energy and beam positioning during start-up are magnified by passing through the flattening filter. This can be a significant problem for IMRT where segments may be delivered with low numbers of monitor units (Sharpe *et al* 2000). If the beam is unable to stabilise itself fully before the dose has been delivered then clearly any delivered dose distributions could be adversely affected by this. Since

the flattening filter acts as an amplifier for any changes in beam steering and energy these problems are reduced with its removal. The Schuster array again was used to study beam start-up characteristics by integrating the dose over a low dose delivery. Whereas repeat measurements for a conventional beam shows a 1.5% tilt in beam symmetry for a 5mu beam (symmetry measured as defined previously), for the unflattened beam this is only 0.3%.

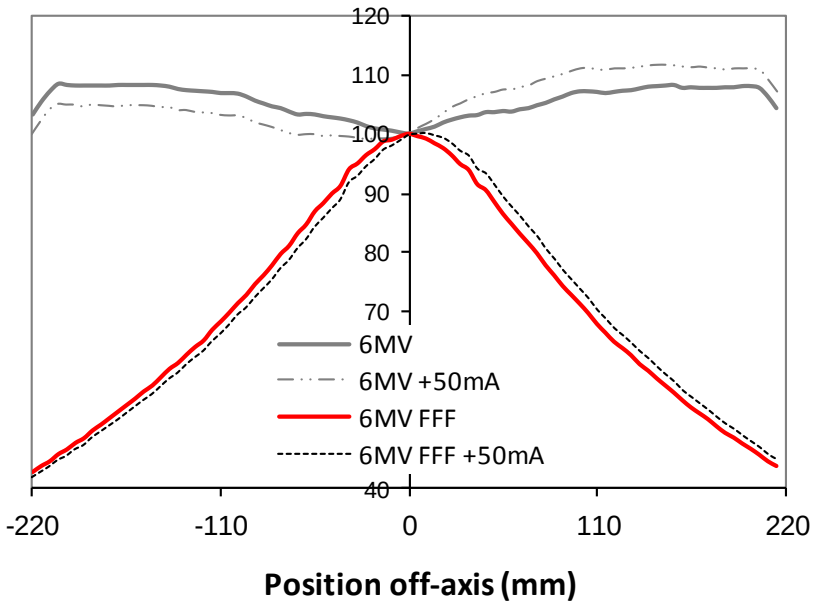

Figure 2.15. Profiles from a Schuster array demonstrating changes in beam symmetry for variations in 2R bending current of ±50mA. For the flattened beam the asymmetry (ratio of absorbed doses ±12cm from the central axis) amounts to 7.4% compared to 4.1% with the filter removed.

The flattening filter is an energy sensitive component producing changes in beam profile as the beam energy varies. Elekta machines take advantage of this to servo the beam energy by monitoring the differences in the inner and outer plate signals (hump error) of the ionisation chamber (figure 1.10). Although the beam runs well under normal conditions the energy sensitivity with the filter out may not operate correctly under these circumstances and needs further study. In other accelerators the energy

is regulated by other means (such as by controlling the voltage on the PFN to achieve maximum ion chamber current, Varian), so this might not be problematic.

2.2.11 Penumbra

The finite dimensions of ion chambers used for water tank measurements means that a blurring effect is added to beam profiles; any subtle changes in beam penumbra can therefore be missed. Penumbra measurements were assessed by exposing films at 100cm SSD under 15mm of solid water using Kodak X-Omat V film. Penumbra itself was defined in the usual way as the distance between the 20 and 80% isodose lines at the field edge. Analysis was performed using a VIDAR scanner and ImageJ software (Rasband). Filter removal produces a small change in beam penumbra probably due to a reduction in the extra-focal radiation, these effects however are of the order of 0.5mm and although this is of course a good thing it will probably be of little practical advantage.

As the field size increases in a FFF beam the 80% point will no longer be positioned at the field edge and another definition of penumbra is needed to make these values meaningful. The most likely definition involves redefining the position of the 100% reference point to be at the inflexion point of the curve rather than at the central axis. These definitions have been discussed by Ponisch *et al* (2006) and Fogliata *et al* (2012) but standardisation is still required.

2.2.12 Wedge data

2.2.12.1 Wedge profiles

Data for wedged beams was also measured as the effect of filter removal on wedge characteristics was completely unknown. As well as shaping the beam profile, the

wedge also acts as an absorber, and can indicate information about the relative contributions of low-energy photons and electron contamination. Central axis depth dose measurements were measured for square fields from 5x5 to 30x30cm² at 100cm SSD and profiles taken at 5 depths.

Beam profiles of the internal motorised wedge (nominal 60°) again show that there is a slightly faster drop-off in dose at the beam edge and lower dose outside of the field (figure 2.16). The wedge profiles are slightly convex rather than concave but importantly the overall effect of the wedge is retained. The wedge angle itself drops slightly from 56° to 53° for a 10x10cm² field but these factors can easily be taken into account within the beam model.

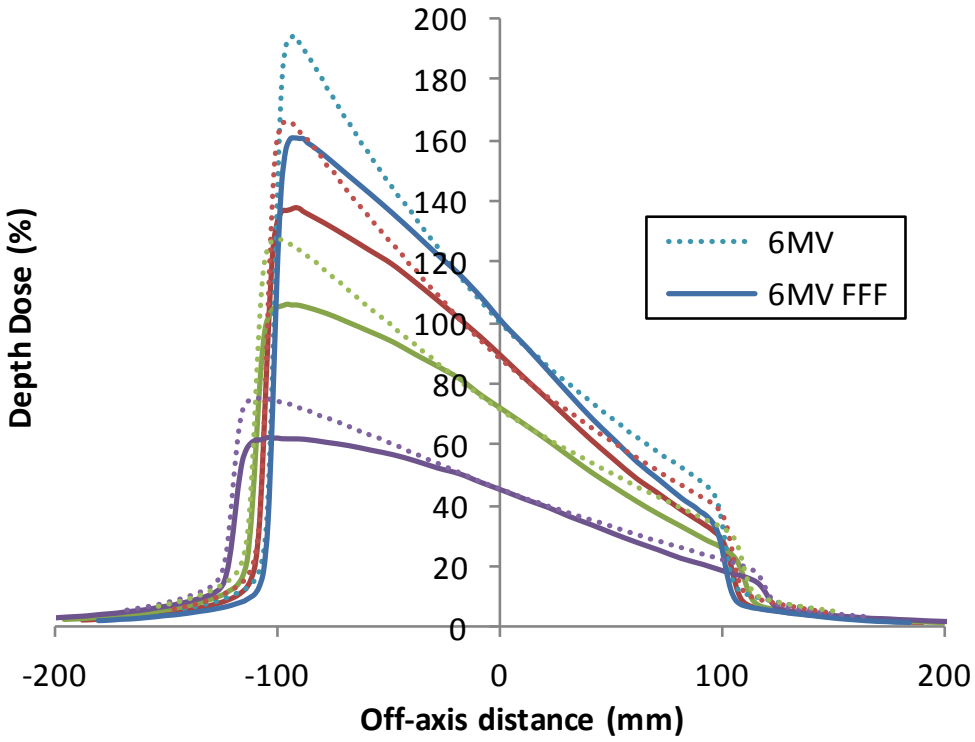

Figure 2.16. Comparison of measured wedge profiles for a 20x20cm² field, normalized at d_{max}. Profiles are at depths of 15, 50, 100 and 200mm.

2.2.12.2 Wedge transmission

Wedge factors were measured using a NE2571 Farmer chamber in solid water (100cm SSD, 5cm deep). The softer spectrum and associated decrease in beam energy to approx. 5MV leads to an increase in x-ray attenuation and hence to reduced transmission. Reduced head scatter also leads to less variation with field size; the ratio of 30x30 to 3x3cm² readings for the flattened beam is 1.098 compared to 1.055 with the flattening filter out, i.e. half the relative range (figure 2.17). Again filter removal is seen to reduce the variation in field size dependant parameters.

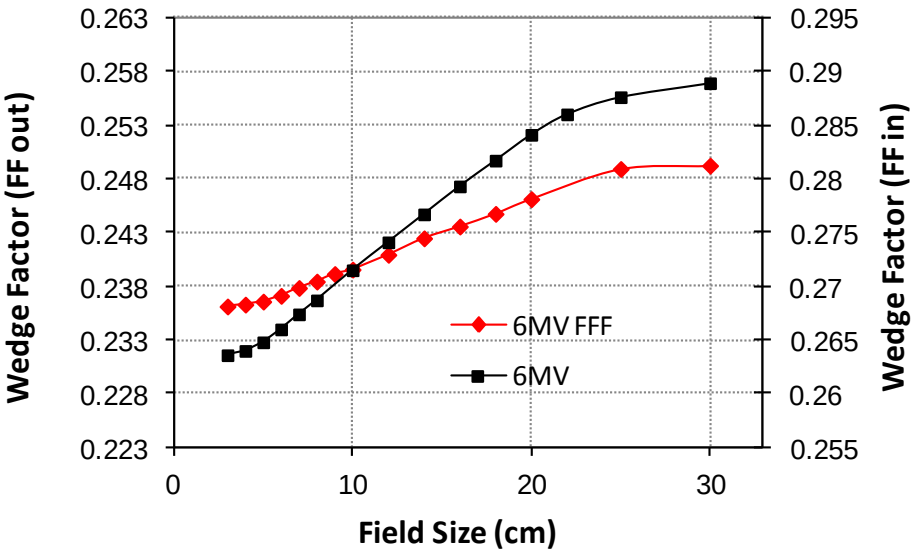

Figure 2.17. Wedge factors plotted on the same scale to compare variation with field size. The ratio of 30x30cm to 4x4cm readings is 1.098 with filter in and 1.055 filter out.

2.3 Discussion

Linear accelerator design has evolved around the need for flat radiation fields and a certain number of problems must be expected when the flattening filter is removed. Measurements reported here show that these problems, however, are fairly minimal

and most likely to be resolved with relatively simple software modifications since the vast majority of all machine running parameters remain unchanged. The only differences are observed at the ionisation chamber where beam parameters such as flatness, symmetry and uniformity need to be reset, but this can be performed relatively easily and, with a thin metal plate in place of the filter, the chamber servos continue to operate well. In fact with the filter removed the beam symmetry is half as sensitive to changes in beam steering, retains a more consistent profile with these changes and is more stable during start-up irradiation.

To operate the machine clinically however it would be necessary to modify current IEC specifications (BS EN 2001) which are based upon having square, flattened radiation fields. The standards are written to ensure the protection of the operator and patient and to define a number of parameters by which users can compare accelerator performance. With unflattened beams terms such as 'flattened area' are meaningless. Uniformity, flatness, symmetry, penumbra and field size definitions may need to be redefined for these beams.

The major benefit of filter removal is in the reduction of head scatter and leakage radiation, both of which cause significant problems in radiotherapy and come as a direct consequence of producing a flattened beam i.e. forcing a large proportion of the beam to interact in the flattening filter. Removal leads to a decrease in head scatter (potentially improving dose calculations) and to lower whole body doses (reducing the risk of secondary cancers). Reduced scatter also leads to a reduction in penumbra, dose outside of the field edge and results in less variation in field size dependent factors. Reduced head scatter and increased dose rate should lead to simpler, faster and more accurate dose delivery with reduced dose to normal tissues; all useful properties.

2.4 Summary

The basic dosimetric properties of filter free beams and linac operation have been investigated. In summary:

- The flattening filter is mounted on a 'carousel' that can be rotated out of the beam line.
- It is necessary to use a thin metal plate in place of the flattening filter to maintain servo control and to reduce surface doses.
- Dose rates are approximately doubled by filter removal.
- The beam positioning and shape are more stable in filter free mode.
- The magnitude of the scatter component of the beam is much reduced.
- The variation of field size dependant factors is substantially lowered.
- Leakage doses are reduced.
- The beam has similar depth dose characteristics to a 5MV beam.
- Surface doses are slightly higher.
- Penumbra is similar or even slightly reduced.
- It is still possible to produce wedged beam profiles.
- Definitions of parameters such as penumbra, flatness and symmetry will need to be reassessed / redefined.

CHAPTER 3

ENERGY MATCHING AND FURTHER CHARACTERISATION

Flattening filter removal produces numerous changes in beam characteristics, many of them large, but also some that are subtle. In particular the changes in leakage dose and in surface doses could be as much due to the change in beam energy as from any inherent property of FFF beams. It is also difficult to assess any changes in treatment planning is the beam energy is different between models. For these reasons a decision was made to alter the beam energy, bringing it back up to '6MV'. In this chapter we will consider the changes made to the beam in order to 'match' the FFF beam energy to that of the conventional 6MV beam, and report in detail some of the dosimetric effects of this.

Sections of this chapter concerning surface doses have been submitted for publication in the journal *Physics in Medicine & Biology* (Appendix D).

3.1 Machine configuration

This work was performed on the linear accelerator at University Hospital Birmingham (UHB) with the linac operated through an independent hard drive to keep all work separate from anything available clinically. At this stage a decision was also made to use a 2mm copper plate rather than 2mm aluminium for the enhancing plate as copper filters had been distributed to other Elekta centres interested in FFF research. These copper filters were of a thickness of 6mm however, and it was felt that this was too thick. A 2mm plate was therefore retained at UHB.

3.2 Energy matching

A FFF beam can never be completely matched to a conventional beam as there are too many changes to the beam spectrum, and in the relative contributions of low-energy photons and electrons to make this possible. There is also the issue of the beam profile – in a conventional beam the flattening filter causes beam hardening on the central axis, which gradually reduces with distance towards the field edge. These changes in off-axis beam spectrum have been well described by Georg *et al* (2009).

A fixed parameter and field size must therefore be chosen to match the beam onto. The most common specifiers of beam energy used are D_{10}, the relative dose at 10cm depth, and the quality index ($TPR_{20/10}$), usually for a 10 x 10cm^2 beam. For the 6MV beam the D_{10} = 67.5% and the quality index = 0.675. Matching was carried out on the central axis for a 10 x 10cm^2 beam by repeat depth dose plots in a PTW watertank as the beam energy was increased. For the beams in question it was possible to simultaneously match both D_{10} *and* ($TPR_{20/10}$), but this is not expected to be the case at all beam energies.

Table 3.1. Changes in bending and gun currents in the FFF beam required to maintain quality index of 0.675.

Parameter	6MV	6MV FFF
Bending Course (B_c)	39.5	49.5
Bending Fine (B_f)	2.07	2.62
Gun current (I_g)	7.89	7.71

At the same time the gun, hump, beam uniformity and 2R and 2T lookup tables etc. were reset to enable efficient operation around these new running parameters. Several other machine parameters were also changed (not detailed here) as recommended by an internal report from Elekta on their investigations into FFF operation. Gross changes to bending and gun currents are detailed in table 3.1.

3.3 Head scatter (Sc)

As the beam energy increases so will the proportion of radiation scattered in the treatment head so increasing the beam energy to match the 6MV depth dose will increase the amount of head scatter from the treatment head. Figure 3.1 shows the new plot of Sc vs. field size for the matched beam (red line) compared to both the conventional 6MV beam (black) and to the filter-free beam pre energy-matching (green). Increasing the beam energy to obtain the central axis depth dose match increases the amount of scattered radiation in the beam, raising the head scatter above that seen for the un-matched beam. However, head scatter variation is still significantly reduced compared to standard operation.

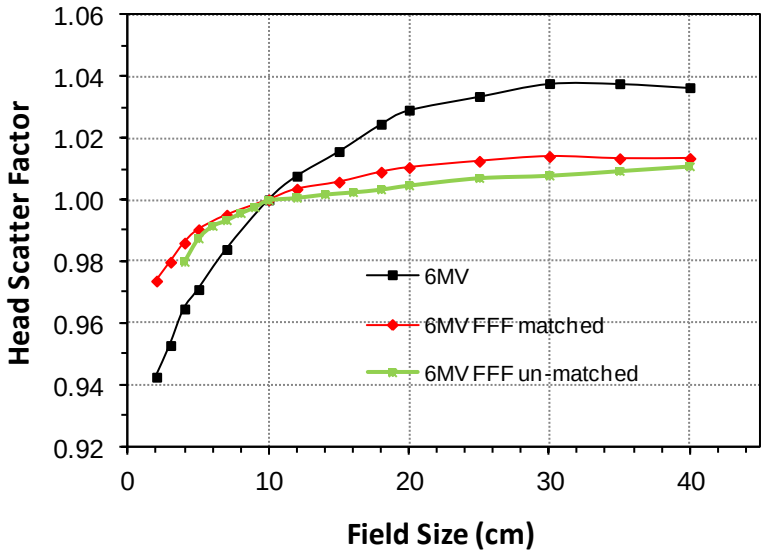

Figure 3.1. The variation of head scatter (as measured with a mini-phantom) with field size for conventional use (filter in) and with filter out. Removal of the flattening filter results in approximately 70% less head scatter.

3.4 Leakage radiation

Measurements were again taken as recommended by the Elekta acceptance documentation (Elekta 2005) using a Farmer chamber (with 1.5cm buildup cap) placed at the points indicated in figure 3.2. With the diaphragms closed the absorbed doses at these points are compared to the reference dose measured for a 10 x 10cm^2 field at the isocentre.

Table 3.2 shows the results of patient plane leakage measurements. The overall reduction in patient plane leakage for FFF operation is seen to be 65.7% at 6MV and 61.4% at 10MV.

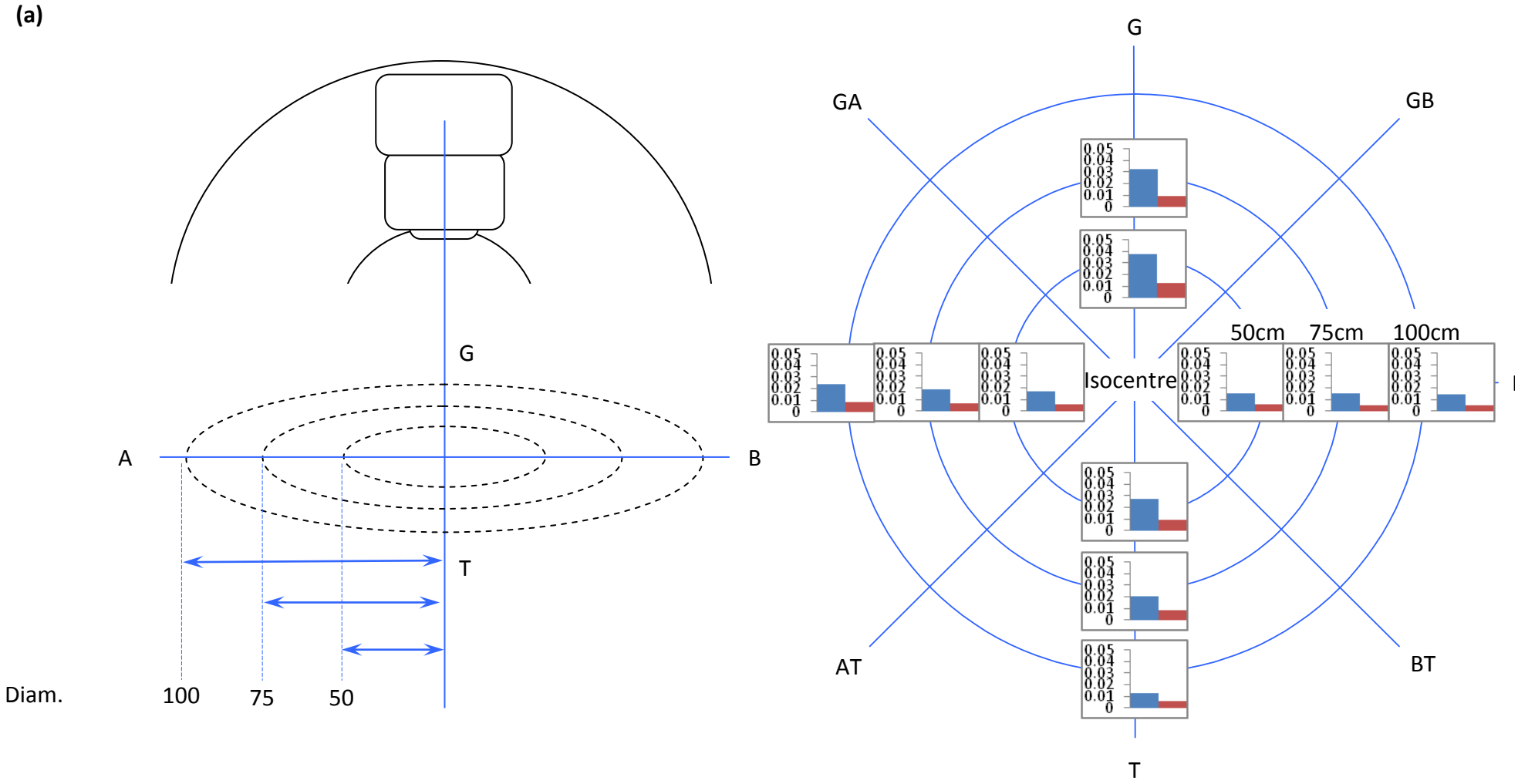

Figure 3.2. (a) Specification of points used to measure patient plane leakage. The circles are of radius 50, 75 and 100cm. (b) Leakage measurements (taken with the collimators in the closed position and compared to a central axis reading for a 10x10cm² field) for conventional (blue) and FFF (red) beams.

Table 3.2 Leakage measurements in the patient plane at points specified in figure 3.2. Figures are presented as a percentage of the dose at isocentre for a 10x10cm² field. The ratio represents the leakage of the FFF beam in comparison to the 6MV beam [100 x (MV FFF / MV)]. (a) 6MV, (b) 10MV.

(a) 6MV

	G			T			A			B		
	6MV	**FFF**	**Ratio**	**6MV**	**FFF**	**Ratio**	**6MV**	**FFF**	**Ratio**	**6MV**	**FFF**	**Ratio**
50	0.038	0.013	0.348	0.027	0.009	0.339	0.017	0.005	0.319	0.016	0.016	0.345
75	0.032	0.010	0.296	0.020	0.008	0.402	0.019	0.006	0.332	0.016	0.016	0.305
100	-	-	-	0.013	0.006	0.428	0.024	0.008	0.342	0.015	0.015	0.315

(b) 10MV

	G			T			A			B		
	6MV	**FFF**	**Ratio**	**6MV**	**FFF**	**Ratio**	**6MV**	**FFF**	**Ratio**	**6MV**	**FFF**	**Ratio**
50	0.039	0.025	0.638	0.034	0.009	0.265	0.014	0.005	0.346	0.014	0.014	0.359
75	0.030	0.018	0.619	0.024	0.008	0.338	0.017	0.006	0.352	0.016	0.016	0.301
100	-	-	-	0.015	0.005	0.362	0.021	0.008	0.362	0.014	0.014	0.306

Leakage radiation is not only responsible for whole body dose levels to the patient, but will also needs to be taken into account when designing bunker shielding.

Measurements were performed to assess both the instantaneous dose rate and cumulative dose for FFF beam delivery. Due to the increased dose rate of the FFF beams compared to those seen under normal operation instantaneous dose rates are expected to be higher. Cumulative doses will depend not only on the relative levels of leakage radiation associated with each beam, but also on the efficiency of delivery of IMRT plans and are presented in chapter 7 and Appendix H.

Table 3.3 shows the instantaneous dose rates measured (with a compensated GM tube) at the gate, within the control area and on the roof of the bunker. These measurements were carried out by trainee physicists within the department working under supervision. A 40x40cm^2 field size was used for all measurements. Readings are normalised to clinical dose rate for each energy.

Table 3.3. Instantaneous dose rates measured at 6 and 10MV at the positions indicated (in μSv/hr).

	Filtered	**FFF**	**Position**
6MV	30.0	19.2	@ Gate
10MV	30.0	18.8	
6MV	4.0	1.9	In control area
10MV	6.5	3.0	
6MV	150	124	On roof *
10MV	300	113	

**With gantry at 180°*

It can be seen that the bunker provides much greater shielding for the FFF beams. Operating at the higher dose rate expected during FFF delivery the readings will scale accordingly, and instantaneous doses will be higher for FFF operation compared to those seen for normal use. Similar effects have been shown by Kry *et al* who investigated the treatment vault shielding for a Varian FFF prototype (Kry *et al* 2009), finding that the thickness of the primary and secondary barriers could be reduced by 10-20% for FFF operation. This reduction matches well with the observed drop in beam energy from 6 to 4 MeV.

3.5 Surface doses

3.5.1 Introduction

It is well known that megavoltage (MV) photon beams provide a skin-sparing effect, but the actual magnitude of this can depend on a number of treatment parameters. Changes in field size, source-to-surface distance (SSD) and beam energy all cause changes in surface dose. In particular the introduction of materials into the beam line such as shadow trays and patient support devices can cause large increases in dose to the skin. At the same time it is also important that doses to targets close to the surface (such as for head & neck and breast treatments) are accurately known so that under-dosage does not occur.

Doses received by the basal skin layer can result in a range of problems from minor (such as erythema/epilation) to serious (desquamation/necrosis) depending on the levels of radiation received. A full knowledge and understanding of this is therefore necessary if clinical decisions are to be made, and these effects have been studied by a number of authors for conventional 'flattened' beams (Carl and Verstergaard 2000, Lamb and Blake 1997, Kim *et al* 1998, Parsai *et al* 2008).

Several authors have reported surface dose variations with field size in FFF beams (Vassiliev *et al* 2006, Cashmore 2008, Kragl *et al* 2009, Wang *et al* 2012), generally reporting higher doses under FFF operation, but data for changes in SSD, tray, wedge, couch etc. are unavailable. With this in mind measurements of surface doses for FFF beams are required to assess any potential changes in dose that may damage the skin.

The purpose of this investigation was to evaluate and compare trends in surface dose for 6 and 10 MV flattened and FFF beams under conditions routinely experienced in radiotherapy treatments. Conditions studied were:-

- variations in field sizes (square fields, sizes 3x3 to 40x40 cm^2);
- variation in source-surface-distance (SSD) (55 to 140cm);
- the presence of
    - motorized wedge (0–60°);
    - shadow tray
    - carbon fibre couch

3.5.2 Background

3.5.2.1 Skin doses

Skin doses arise from a combination of effects and will depend on the magnitude and relative contributions from contamination electrons, low-energy photons and backscattered radiation. Contamination electrons in particular can give rise to significant doses in the skin and will be influenced by several factors including head design, beam energy, SSD, field size or the introduction of materials into the beam close to the patient. Skin dose can therefore vary significantly from one setup to another and can be a limiting factor in some treatments (Carl and Vestergaard 2000).

Since the flattening filter is responsible for the majority of contamination electrons reaching the patient surface (Nilsson and Brahme 1986) its removal is therefore likely to *reduce* this contribution. However, the filter also acts as a beam hardener, removing low-energy photons from the spectrum. With the filter removed the low-energy component is allowed to pass through to the patient and act to *increase* the surface dose.

The use of motorized wedges and Perspex shadow trays (blocking trays) in conjunction with filter removal could also change these characteristics significantly. Since conventional planning with unflattened beams has been shown to be of use (Cashmore 2007, Stevens 2011) data has also been measured for the motorized wedge and shadow tray. Dose measured under different conditions (wedge, SSD, tray etc.) can also be a good indicator of the relative levels of dose from low energy photons and from contamination electrons (although no attempt has been made to separate these two components here).

3.5.2.2 Dose measurement

In the buildup region of high energy photon beams electronic equilibrium does not exist, therefore percentage depth ionization (PDI) and percentage depth dose (PDD) are not equal. Under these conditions electronic fluence perturbations in the air-sensitive volume of the cavity cause ionization chambers to exhibit an 'over-response', and determining PDD from PDI measurements is difficult. This will occur for measurements carried out in the dose build-up region (and in the transition zones between different media), with a magnitude depending on the geometrical characteristics of the chamber. The over-response will be greatest at the surface and decrease as dose maximum (d_{max}) is approached, and electronic equilibrium restored.

In these circumstances it is generally accepted that extrapolation chambers provide the most accurate means of measurement. These chambers, however, are

unavailable in most departments and are also very time consuming to use, therefore parallel plate chambers are routinely used to measure surface and buildup doses, and corrections must be applied to convert ionisation to dose.

The over-response of chambers has been shown to be mainly due to electron in-scattering from the side walls, which is determined by the width of the guard ring (Nilsson and Montelius 1986, Gerbi and Kahn 1990). Perturbation factors will therefore depend on the dimensions of the chamber and several methods have been introduced to correct for the effects seen when using parallel plate chambers in the build-up region of high-energy photon beams. These are based either on correction-based methods from extrapolation chamber measurements, or by direct derivation of individual perturbation factors.

In the first method the chamber reading is corrected by a subtractive factor that depends on the beam energy, chamber geometry and depth of measurement (Nilsson and Montelius 1986, Gerbi and Kahn 1990, Velkley *et al* 1975, Rawlinson *et al* 1992). These factors are essentially independent of field size but increase with decreasing energy.

Velkley *et al* used extrapolation chamber data to develop a correction term for parallel plate chambers to account for the in-scattering of electrons in the buildup region, introducing an over-response correction factor based on the plate separation of the chamber:

$$P'(d) = P(d) - \xi(E, d/d_{\max}) \times l \qquad (3.1)$$

where d is the depth to the front surface of the chamber, E is the nominal maximum energy of the beam, P is the percentage maximum ionisation obtained using a chamber with plate separation of l mm, and P' is the corrected percentage maximum

ionisation. $\xi(E, d/d_{max})$ is the correction factor in units of percent per mm of plate separation.

These correction factors were intended to be applied to all types of parallel plate chambers, but further work by Nilsson showed that the factors are specific to the chamber design and depend on guard size, plate separation and volume.

Gerbi and Kahn extended this to take into account wall perturbation effects by introducing the distance to the side wall (thickness of guard ring) into the equation:

$$P'(d,E) = P(d,E) - \xi(0,E) \times l \times e^{-\alpha \times (d/d_{max})} \quad (3.2)$$

where d is the measuring depth, d_{max} is depth of dose maximum of the X-ray beam with energy quality E. The ξ function is the correction to the surface %DD per mm of plate separation independent of the ion chamber used. l is the plate separation of the chamber, and α is an exponent that decreases the correction with depth.

In some chamber designs the guard ring is very small leading to large correction factors. Gerbi and Khan (1990) show that Markus-type chambers require greater correction than most chambers due to small guard ring (0.1mm), with corrections exceeding those recommended by Velkley. Mellenberg (1995) reported a complete set of over-response correction factors for the Markus-type chamber at several photon energies.

Rawlinson *et al* (1992) then developed an empirical method which accounted for side wall effects in the chamber. This was an improvement on the original method developed by Velkley and later adapted by Gerbi and Khan. Here, the collector edge to wall distance is assumed to be the appropriate parameter. This method works well for chambers with small collector diameters but over-estimates the correction for larger chambers.

Perturbation factors can also be derived explicitly. For parallel-plate chambers the PDD at depth *d* can be expressed as

$$PDD(d) = PDI(d)\frac{\left[\left(\frac{\bar{L}}{\rho}\right)_{air}^{med} P_{fl}P_{wall}P_{cel}\right]_{d}}{\left[\left(\frac{\bar{L}}{\rho}\right)_{air}^{med} P_{fl}P_{wall}P_{cel}\right]_{d_{\max}}} \qquad (3.3)$$

Where $\left(\overline{L_\Delta}/\rho\right)_{air}^{med}$ is the mean restricted collision stopping power from medium to air and P_{fl}, P_{wall} and P_{cel} are perturbation factors for the fluence, wall and central electrode respectively. When $d>d_{max}$ these factors do not change and can be considered as invariant and the dose ratio is then equal to the ionization ratio (PDD = PDI) (Abdel-Rahman *et al* 2005). In the buildup region however, perturbations in the electron fluence cause these chambers to over-respond so that PDI>PDD. Since perturbation factors are known to have a strong dependence on chamber design, depth of measurement and beam energy, P_{fl}, P_{wall}, P_{cel} and $\left(\overline{L_\Delta}/\rho\right)_{air}^{med}$ must be independently evaluated.

Recent studies have shown that the product $P_{fl}P_{wall}P_{cel}$ changes by less than 1% from the surface to d_{max} (Gerig *et al* 2009, McEwen *et al* 2008) and that $\left(\overline{L_\Delta}/\rho\right)_{air}^{med}$ changes by less than 4% for beams up to 18MV. The maximum deviation occurs at the phantom surface and will be less than 5%, reducing to 0% at d_{max}.

For certain ion chambers and beam energies some of these factors have been evaluated (e.g. Mellenberg 1995). The presence of beam modifiers such as the wedge can change the photon beam spectrum appreciably, so removal of the flattening filter and associated changes in the beam spectrum are therefore likely to cause significant

changes to this. For FFF beams in general these are unknown and an independent set of over-response factors would be required for more accurate prediction.

In more recent years work has been concentrated on Monte Carlo modelling and the discrepancies observed between measurements using extrapolation chambers and those from Monte Carlo simulations. McEwen *et al* (2008) has shown that with advances in the physics and description of beam geometry MC results match well provided the correct effective point of measurement (EPOM) for the chamber is used. The EPOM method has therefore been employed to calculate dose in the buildup region, accepting limitations.

3.5.3 Materials and methods

The Elekta Synergy FFF prototype linear accelerator (Elekta AB, Stockholm, Sweden) with a standard 80 leaf MLCi head has been used for measurements. The linac is fitted with a motorized wedge (nominal 60° wedge angle) and an iBEAM evo carbon fibre couchtop, both of which were assessed.

The flattening filter is replaced with a 2mm stainless steel plate that is used to shield out contamination electrons from the primary collimator, and to provide build-up into the ionisation chamber. This is now the standard configuration expected for clinical use.

Removing the flattening filter changes the energy spectrum of the beam since lower energy photons are no longer removed from the beam. This results in unflattened beam having 'softer' beam spectra than their filtered counterparts. The 6MV beam can be energy matched to the conventional beam by adjusting the beam running parameters. In this way the depth doses at 10cm depth, $TPR_{20/10}$ QI/$TPR_{20/10}$ [0.675] for a 10x10cm^2 field are the same. FF removal also affects the variation in the energy spectrum across the beam (making it much more uniform) but energy

matching across the beam is not possible. In contrast, and for consistency with other work (Kragl *et al* 2009, Georg *et al* 2010) the 10MV beam has *not* been adjusted. The $TPR_{20/10}$ for the 10MV and 10MV FFF beams are 0.737 and 0.716, respectively.

3.5.3.1 Experimental setup

Measurements were taken in a phantom composed of 30x30cm² WT1 Solid Water slabs (Radiation Physics, St Bartholomew's Hospital, London) of varying thickness, with 15 cm of backscatter material to ensure full phantom scatter conditions. Further sheets of Solid water were added to take readings in the buildup region (maintaining SSD) (Figure 3.3a). Doses were measured with an NACP-02 (Scanditronix, IBA Dosimetry) parallel plate ionization chamber. The NACP chamber has a 'coin-shaped' sensitive volume with a diameter of 10mm, a height of 2mm and a guard ring of 3mm in width (NACP 1981). In the literature a guard ring of at least 5mm is recommended for measuring skin doses (Gerbi and Kahn 1990), but both Carl (Carl and Vestergaard 2000) and McEwen (McEwen *et al* 2008) have investigated its use and found it to be suitable.

The chamber is embedded in the phantom such that the entrance window of the chamber was flush with the surface with the central axis perpendicular to this. Doses at depth were measured by adding layers of phantom material while maintaining the SSD at 100cm to the top of the phantom (Figure 3.3a). The effective point of measurement itself was taken as the inside of the entrance window which, for the NACP-02 chamber (with a composite window of 0.1 mm Mylar and 0.5 mm graphite) is equivalent to 1 mm of water. Surface dose measurements therefore represent a measurement depth of 1mm, and all results are plotted relative to the dose measured at d_{max} (15mm 6MV, 22mm 10MV) for the same field size.

Surface dose readings are reported as relative surface dose (RSD) where:

$$RSD = d_{surface} / d_{\max}$$

Buildup curves through the carbon fibre couch we measured according to the setup shown in figure 3.3 (b, c), with the gantry rotated to 180° to deliver radiation through the couch. Couch transmission factors were measured using a Farmer type chamber (NE2577 Nuclear Enterprises Ltd. (now supplied by QADOS, UK)) set at isocentre within 10cm of WT1 (Figure 3.3c). Couch factors are expressed as the ratio of the posterior to anterior electrometer readings.

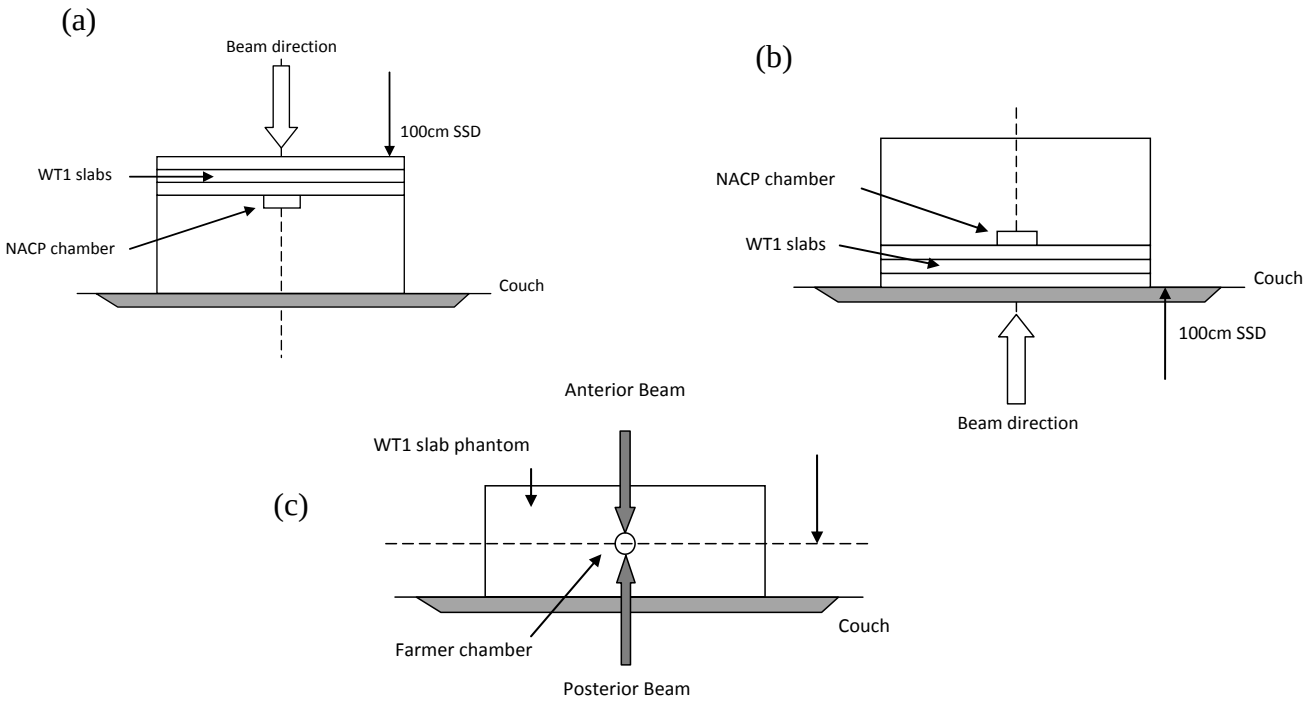

Figure 3.3. Experimental setup for (a) surface dose and buildup, (b) surface dose and buildup through the couch, (c) couch transmission factors.

Polarity corrections in x-ray beams are generally small, but can become significant for parallel plate chambers, especially in the buildup region (Gerbi and

Kahn 1987). It is expected that the largest differences will occur at the surface, and that this will reduce as d_{max} is approached. To estimate polarity effects buildup curves were measured at ±200V over the buildup region, representing the full range of contamination conditions at 6 and 10 MV.

3.5.4 Bias effects

Surface doses were measured at positive and negative polarity (±200V) under representative high and low conditions (surface and d_{max}). Figure 3.4 shows these buildup curves for both 6 and 10MV FFF beams (for a 10x10cm² field), and the ratio of these readings (+ve/-ve) vs. depth.

As expected, the correction becomes larger as the measurement point moves closer to the surface and was found to differ by <1.3% (1.3% at 6MV, 1.1% at 10MV) and fall to unity at d_{max}. This was considered to be of small enough magnitude to disregard as the main purpose is to compare surface doses and evaluate trends. Readings were therefore taken at -200V only for the remainder of the study.

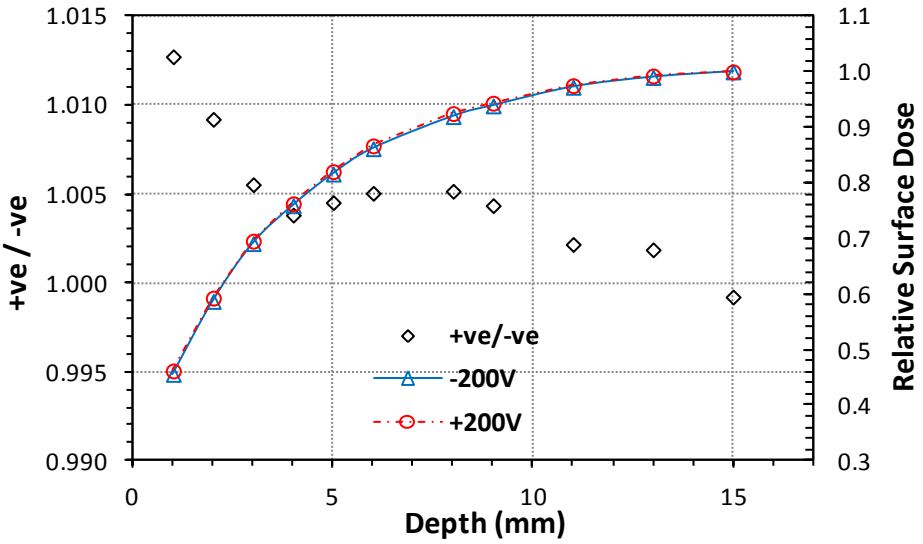

(a)

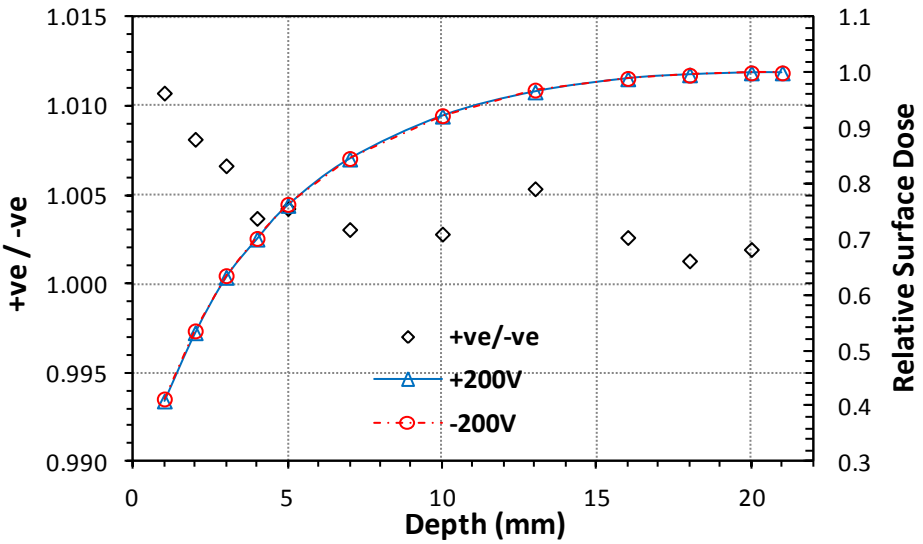

(b)

Figure 3.4. Fractional surface dose as a function of depth for +ve and –ve polarization voltages for (a) 6MV and (b) 10MV photons. The +ve/-ve ratio shows the increasing disequilibrium towards the surface.

3.5.5 Field size variation

Surface doses are seen to increase fairly linearly with increasing field size, albeit at a shallower incline for FFF beams than for the conventional (figure 3.5). At 6MV the unflattened beam shows a slight increase in RSD at smaller field sizes (+3.4% at 3x3cm²) but a decrease at larger (-7.1% at 40x40cm²) with equivalency at 15x15cm².

At 10MV there is again far less variation in the RSD with field size for the FFF beams, but the conventional beam generally exhibits lower surface doses. At small field sizes the unmatched 10MV FFF shows an increase of 10% in absolute terms over the conventional 10MV beam; in contrast, the largest field size the FFF beam shows a 5% decrease. The surface doses are equivalent for a field size of 25x25cm².

For the 6MV beam there is a variation in RSD of 26.7% (absolute) in changing from a 3x3 to 40x40cm² field (0.353 to 0.620) compared to only 16.2% (0.387 to 0.549) for the FFF equivalent. At 10MV these values are 31.0% for 10MV (0.242 to 0.552) and 16.0% for FFF (0.344 to 0.504).

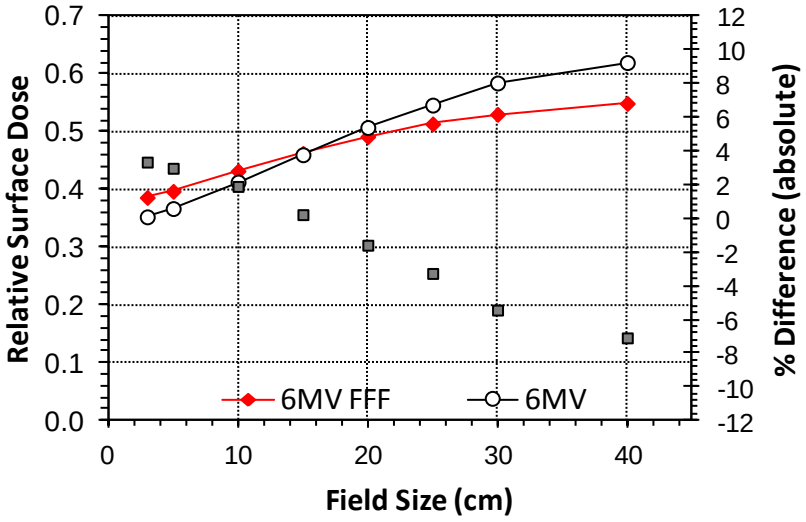

(a)

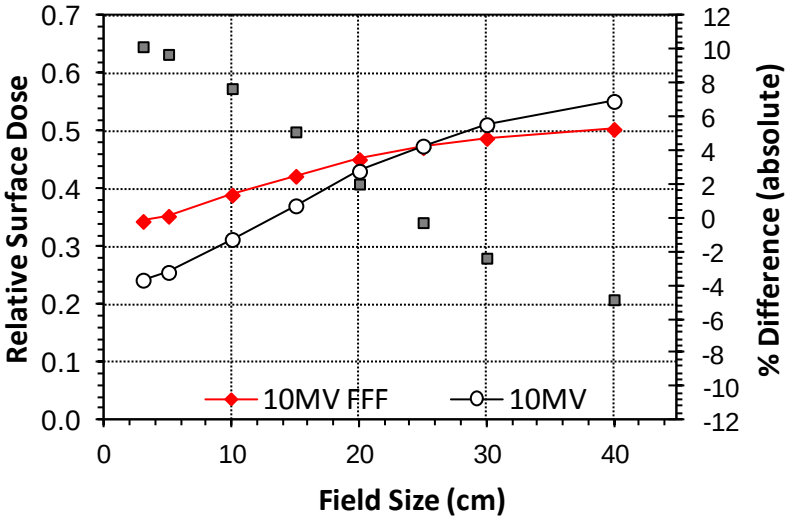

(b)

Figure 3.5 Variation of surface dose with field size for Flattened and FFF beams for jaw settings of 3x3 to 40x40cm². (a) 6MV and (b) 10MV.

The variation of surface dose with field size is very similar for the 6 and 10MV FFF beams showing only minor differences with field size (0.44%cm^{-1} FFF at 6MV and 0.43%cm^{-1}) at 10MV. For conventional operation these gradients are 0.72%cm^{-1} at 6MV and 0.84%cm^{-1} at 10MV.

3.5.6 Wedge

The skin dose for wedged field increases as field size is increased in a similar manner to the skin dose for open fields. With the wedge in place surface doses at both 6 and 10MV are seen to be generally lower for FFF beams. This is true for all field sizes at 6MV (figure 3.6a) and those beyond 12x12cm² for 10MV (figure 3.6b). The slope of the curves is also much shallower for the unflattened beams. This is demonstrated clearly in figure 3.6c where wedge only data is plotted for each beam.

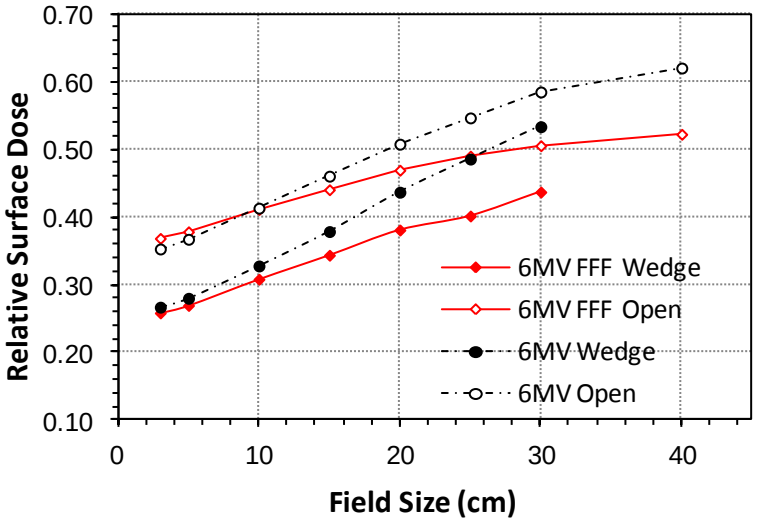

(a)

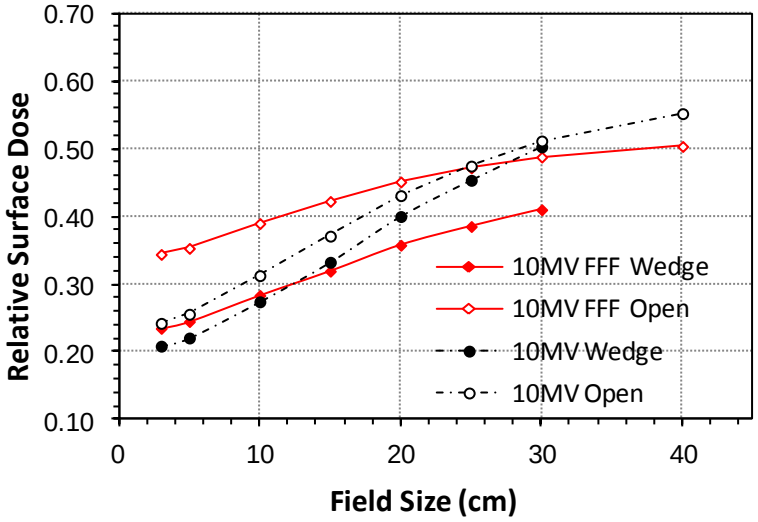

(b)

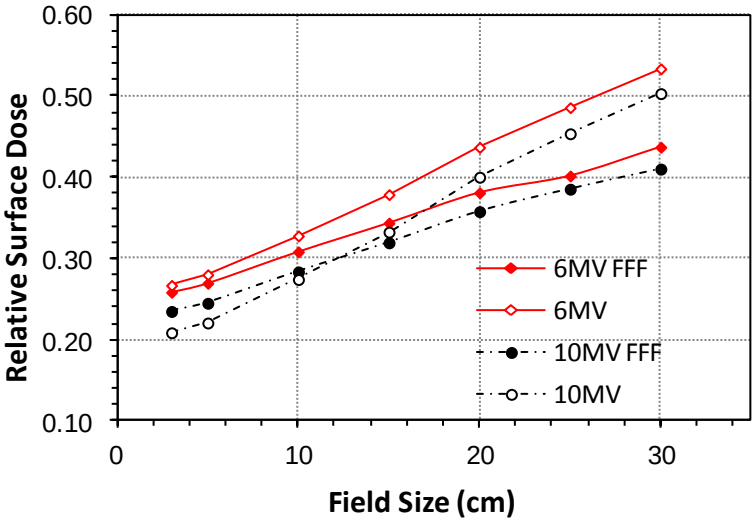

(c)

Figure 3.6. Variation of RSD with field size for wedged beams. (a) 6MV FFF and conventional open and wedged beams, (b) variation at 10MV, (c) wedge only data for 6 and 10MV.

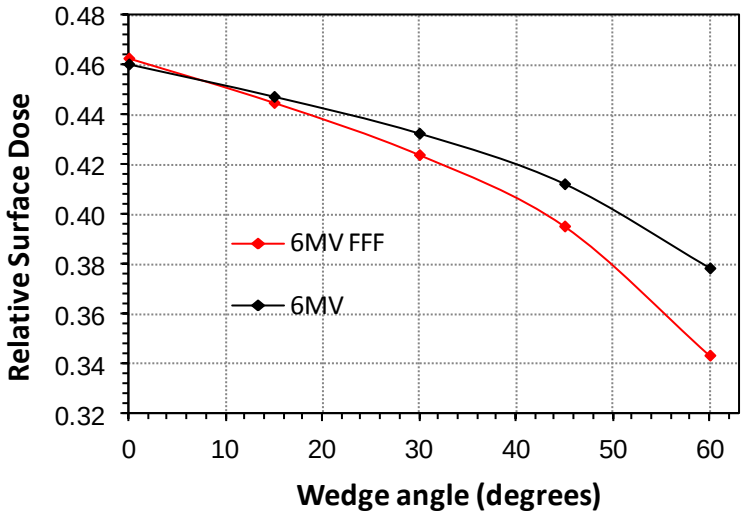

Figure 3.7. RSD variation with wedge angle for motorized wedge, 6MV. Field size is 15x15cm².

The gradient of these lines is 0.66%cm^{-1} vs. 0.99%cm^{-1} (6MV FFF vs. 6MV) at 6MV and 0.65%cm^{-1} and 1.09%cm^{-1} at 10MV, again demonstrating much less variation with field size for filter free operation.

Skin doses for wedge angles of 15°, 30°, 45°, and 60° were also measured for the motorized wedge at 6MV only (figure 3.7). Since the wedge is shown to reduce RSD the greatest difference is observed when the field is fully wedged.

3.5.7 SSD variation

At 6MV there is little difference between the FFF and conventional beams, except near the treatment head where the FFF beams show a reduction in surface dose of up to 5%. Increasing the beam energy to 10MV shows the typical reduction in surface dose. The FFF beam again shows reduced doses at the shortest SSD's, but this quickly reverses with the conventional 10MV beams exhibiting a marked reduction in dose beyond 60cm SSD (figure 3.8).

RSD is very stable between 90 and 140cm SSD then shows a sharp rise for measurements closer to the treatment head. Again, there is a reduction seen in the variation in FFF beams than for conventional beams.

SSD variations were also investigated with the wedge in place. At both 6 and 10MV a larger dose difference is seen between FFF wedge and open data than is seen for the conventional beams. The highest RSD is seen for 10MV FFF beams, and lowest for the 10MV wedge. A 10% reduction in RSD is seen for 10MV FFF compared to only 4% for 10MV. At 6MV these figure are 11% vs. 7%.

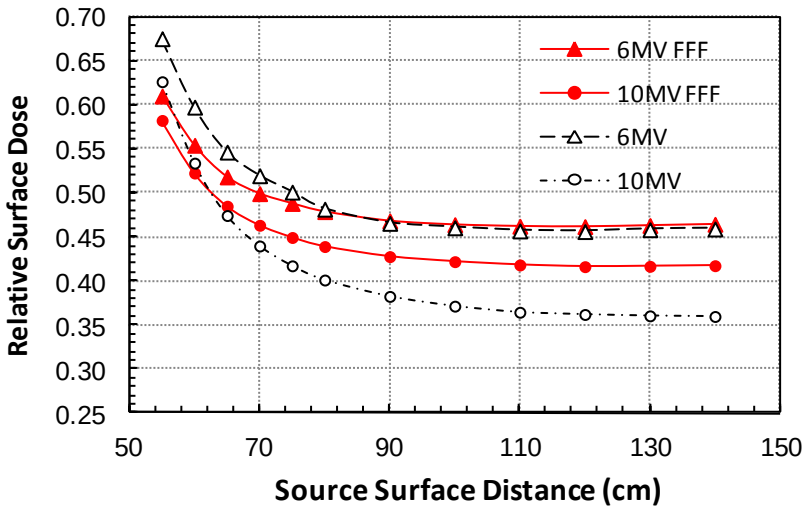

(a)

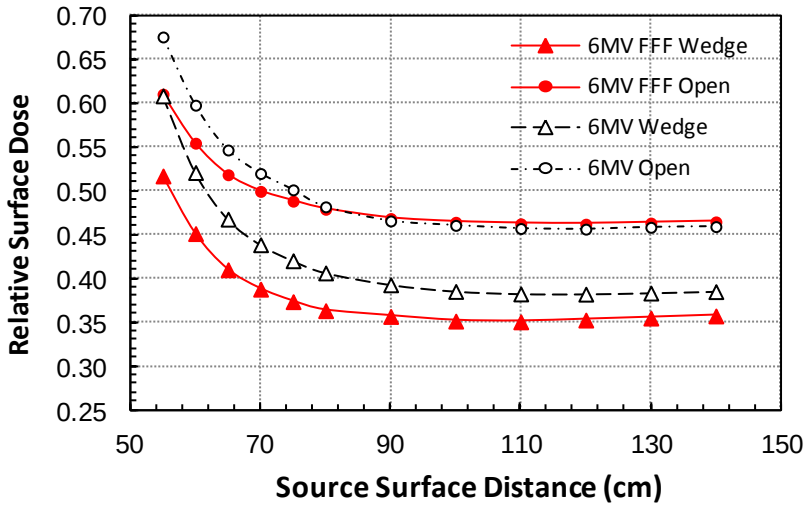

(b)

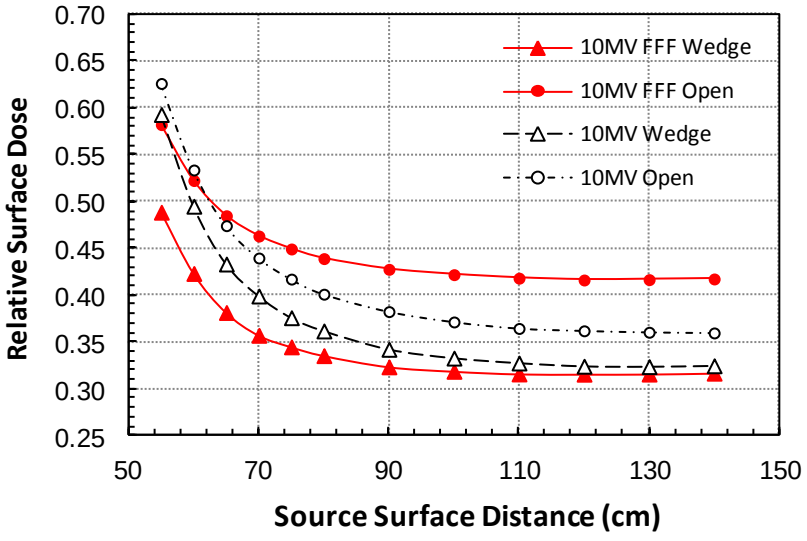

(c)

Figure 3.8. Effect of changes in source to surface distance on surface dose for 6MV and 10MV beams for open and wedged beams (15x15cm²).

3.5.8 Shadow tray

Inevitably the insertion of an acrylic shadow tray (10mm thick acrylic [polymethyl methacrylate]) into the beam causes an increase in the observed surface dose. At 6MV the smallest field sizes exhibit very similar readings, but these rapidly diverge as field size increases with the FFF beam having a much shallower slope (figure 3.9a).

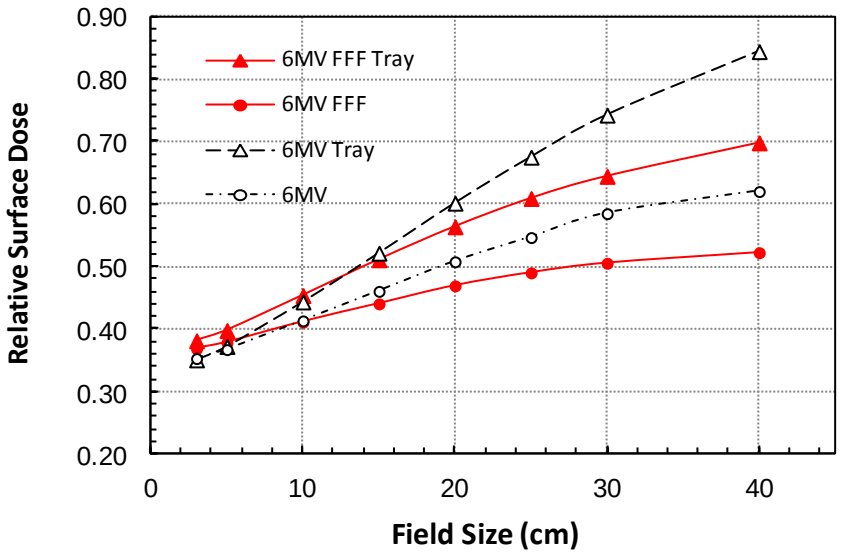

(a)

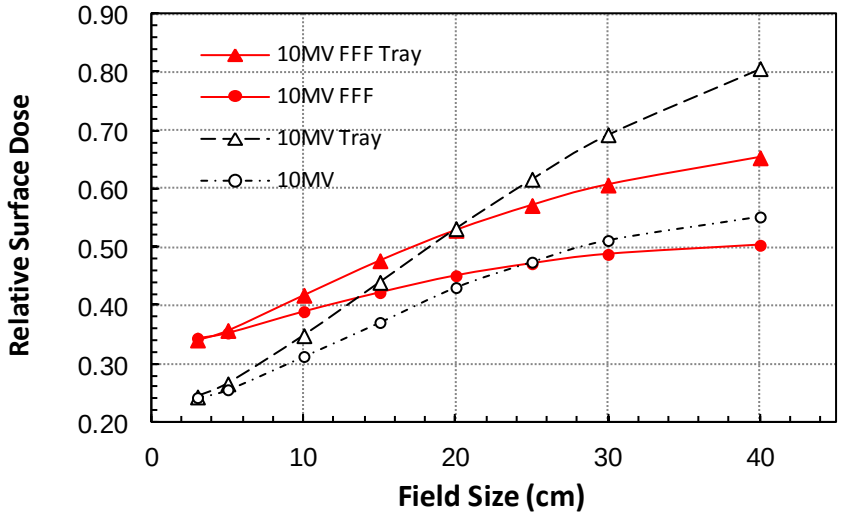

(b)

Figure 3.9. Variation of RSD when passing through Perspex shadow tray for (a) 6MV and (b) 10MV.

For a 40x40cm² field the reduction rises to 12% for the FFF beam. For the 10MV beams the slope is once again much shallower for the FFF energy (figure 3.9b). There is a switch over from higher to lower surface doses at around 20x20cm² with doses being approximately 10% higher for 3x3cm² and 15% lower for 40x40cm².

3.5.9 Carbon fibre couch

Figure 3.10 (a, b) show the buildup characteristics when passing through the iBEAM evo treatment couch. The curves for both 6 and 10MV show very little difference between FFF and conventional beams. At 6MV there is a slight decease for FFF (~3%) at the surface, but nothing large enough to be of clinical significance.

As the field size is varied from 5x5 to 40x40cm² the difference is slightly exaggerated (up to 6%) (Figure 3.10 c, d).

Couch transmission factors follow a similar pattern between FFF and conventional energies with the FFF beams showing a greater factor at both energies, 0.976 vs. 0.982 for 6MV and 0.982 vs. 0.988 for 10MV.

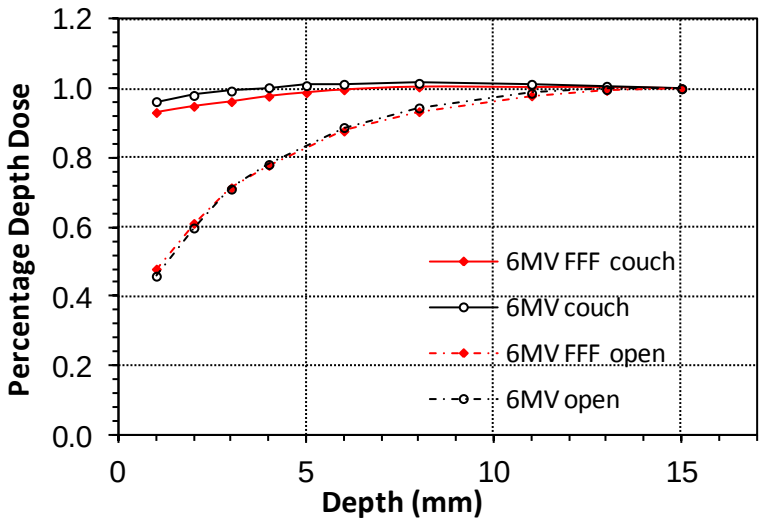

(a)

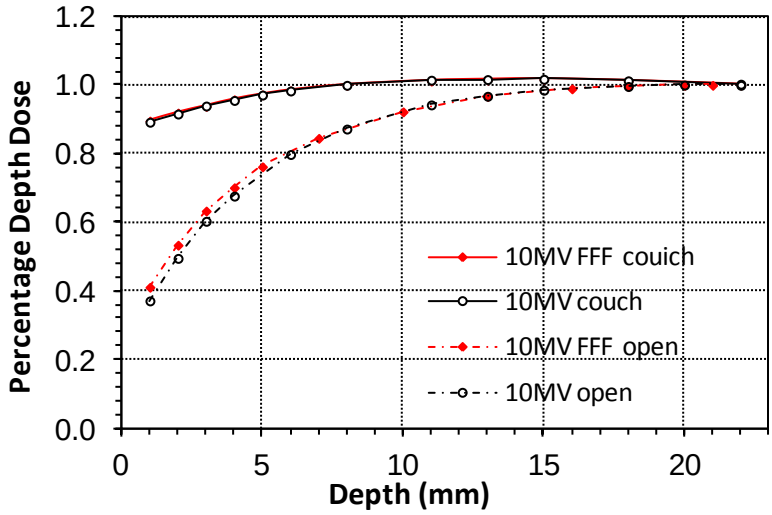

(b)

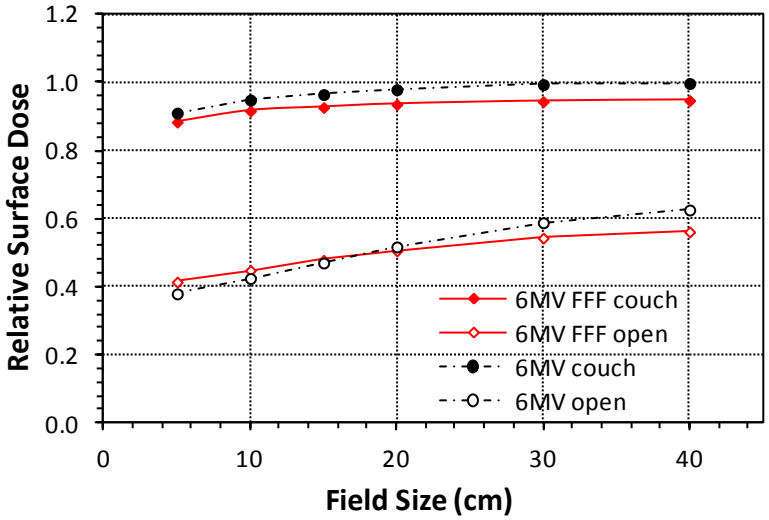

(c)

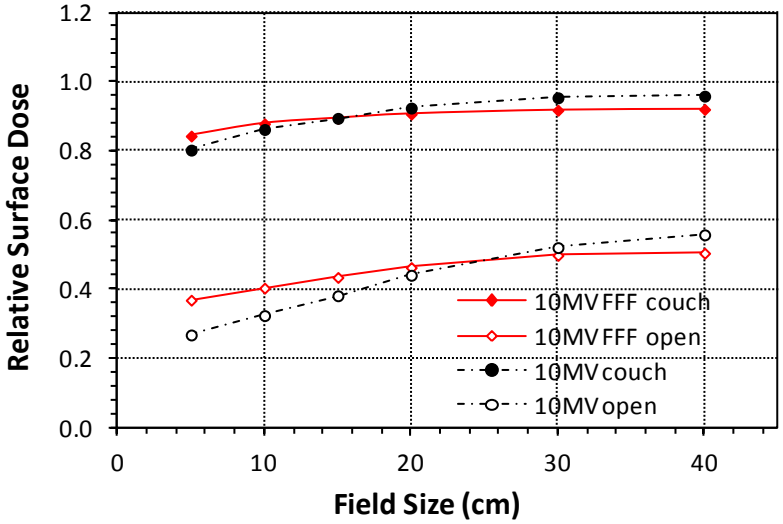

(d)

Figure 3.10. Buildup curves for (a) 6MV and (b) 10MVwith and without the treatment couch intersecting the beam. Relative surface dose vs. field size for (c) 6MV and (d) 10MV.

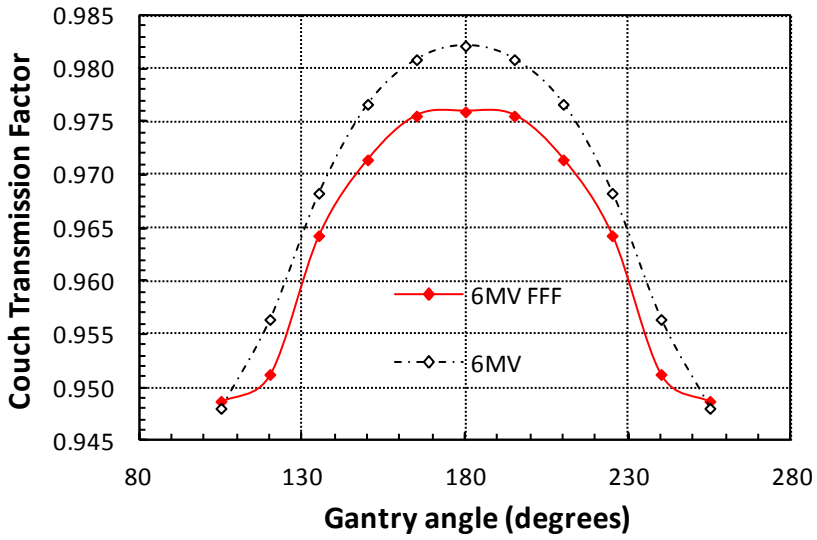

(a)

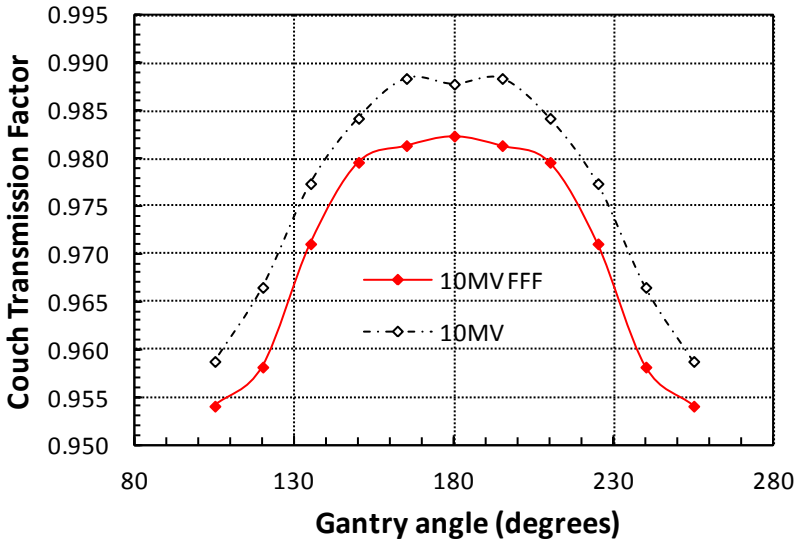

(b)

Figure 3.11. Couch transmission factors vs. gantry angle at 6MV (a) and 10MV (b).

The variation of couch transmission factor with changing gantry angle and with field size show a similar trend to conventional beams at both energies, albeit with greater attenuation, and are shown in figures 3.11 (a) and (b).

3.6 Discussion & Conclusions

By passing through the flattening filter conventional beams exhibit a hardened beam spectrum so they tend to contain less low-energy x-rays, leading to lower surface doses, but high amounts of contamination electrons which act to raise surface doses. FFF beams on the other hand contain larger amounts of low-energy photons, since these are no longer filtered out by the flattening filter, but less contamination electrons, reversing the situation seen in the conventional filtered beam. In practice it seems that these effects almost cancel each other out so that the overall magnitude of surface doses from FFF beams are not too dissimilar to those seen in the original beams.

The increase in surface dose with increasing field size is a well known effect and it is electron contamination that gives rise to most of this variation (Lopez Medina et al 2005), so the overriding effect of filter removal is a reduction in the *variation* of surface doses with field size. Here, the reduction in electron contamination means that the FFF beams exhibit much less variation with changes in field size compared to filtered beams. In general surface doses for FFF are higher for small field sizes and lower for larger field sizes with a cross-over point at approx. 15x15cm^2 for 6MV, and at 25x25cm^2 for 10MV.

Kragl *et al* (2009) observed a similar variation in surface dose with field size for a 6MV energy-matched Elekta linac (42.3% at 5x5cm^2, 56.5% at 30x30cm^2 compared to 39.7% and 53.1% seen here). Their readings are 2-3% higher than those seen in this study but can be explained by the use of a 6mm Cu plate in earlier versions of the filter plate, instead of the 2mm stainless steel plate used in this work. Kragl also reported data for a non energy-matched Elekta linac at 6MV reporting surface doses of 47.1% at 5x5cm^2 and 61.6% at 30x30cm^2, and increase of approx. 5% over those values seen for operation in the energy-matched linac. For an un-matched machine

the average energy is reduced to around 5MV by filter removal so this increase in surface doses (by approx. 5%) can be explained by the change in beam quality.

A similar situation is seen for the Varian TrueBeam accelerator where the beam energy is not adjusted and FFF doses are seen to be higher at all field sizes for both 6 and 10MV compared to operation with the filter in place (Vassiliev *et al* 2006, Wang *et al* 2012). Surface doses are strongly dependent on beam energy, so by altering the beam energy to match, maintaining $TPR_{20/10}$ on the central axis, surface doses can be reduced.

Materials in the path of the beam can both generate electrons and absorb them from further upstream. Since it is relatively thin, and of low-Z material, the shadow tray generates more electrons than it stops, and these pass through to reach the patient, raising skin doses. As the field size increases more electrons are emitted from the shadow tray, therefore higher doses are expected for larger field sizes compared to open fields.

Fontenla *et al* (1994) showed an increase in skin dose of approximately 16% when a tray was added into a 25x25cm^2 field at 6 MV. Our data shows an increase of 13% for the conventional beams and 9.5% for the 6MV FFF. At 10MV these figures are 14.2 and 10% respectively.

Electrons generated by the shadow tray are likely to be similar in both beams indicating that the initial contamination from upstream must be higher in the conventional beam.

The wedge is of sufficient thickness to absorb all of the contamination electrons arising from the head of the linac (Rao *et al* 1988), but surface doses will be influenced by electrons generated within the wedge. These are produced in a thin layer close to the exit surface equivalent in thickness to the range of the secondary electrons.

Regardless of beam energy the presence of the wedge is seen to reduce surface doses, by up to 10% for larger field sizes. Compared to conventional fields the FFF beams again show a reduction in RSD across all field sizes with the slope of the curve being much shallower for FFF operation, and filter removal is seen to have a much larger effect on the 10MV FFF beam than the 10MV (10% at 10MV FFF compared to 4% for 10MV). Considering the blocking tray, wedged fields and open fields together the overall reduction in the slope of the curves with field size is seen to be reduced by 36.1% at 6MV and 44.4% at 10MV.

Considering the variation of RSD with SSD at 6MV it seems that this remains very stable at SSD's beyond 90cm. At shorter SSD's there is a significant rise in surface dose for both beams, but to a greater extent for the conventional 6MV. This again indicates the presence of greater number of contamination electrons in the filtered beam, which are gradually absorbed by the air column as SSD increases. At 10MV the surface dose is generally higher for the FFF beams at all but the shortest SSD's, but the variation is much reduced for FFF operation. Again an approximate 10% reduction in RSD is seen on filter removal at both beam energies with the wedge in place, and this is consistent across all SSD's.

Increasing the beam energy is known to reduce surface doses,, so even though 10MV FFF doses are seen to be slightly higher than for standard 10MV operation, they are still *lower* than those seen at 6MV. At 10MV differences in surface dose may be due to the lower effective energy of the beam compared to the standard, since the 10MV FFF beam has not been energy matched. However, the small variation seen between 6MV FFF and 10MV FFF over a range of conditions indicates that a change in beam energy to a matched 10MV beam is likely to have little overall effect.

Several authors have studied the effects of carbon fibre couchtops on surface dose (e.g. Smith *et al* 2010, McCormack *et al* 2005, Meydanci and Kernikler 2008). The proximity of the patient to the couch means that the skin sparing effect is almost

completely lost and surface doses increase to 85-95% of that seen at d_{max}, and for FFF beams a similar pattern is observed. At 6MV a very slight reduction in %DD is seen for FFF operation, and at 10MV the buildup curves are almost identical. The variation of RSD with field size is again seen to be reduced for FFF use being universally lower for 6MV over all field sizes, and lower at 10MV beyond 15x15cm^2.

Since the unflattened beams contain more low-energy photons than conventional beams the transmission factor of the couch is greater for both FFF energies (by approx. 0.5%), showing a similar variation with gantry angle to that observed for normal use.

3.7 Summary

Removal of the flattening filter has been shown to have many benefits over conventionally filtered beams for the delivery of treatments techniques such as (but not limited to) SRT, SBRT and IMRT. The present study indicates that the surface doses from these beams are very similar to those experienced for conventional flattened beams, and are therefore unlikely to cause concern in a clinical setting. However, as variations in electron contamination with SSD, or from the introduction of wedges, trays and couches are not taken into account in most treatment planning systems (Lopez Medina *et al* 2005), it is possible that the use of FFF beams may help to reduce the uncertainty of dose calculations in the buildup region by reducing the potential range of these values.

By increasing the beam energy to maintain the quality index of the beam it is hoped that any reported differences in dosimetric characteristics or treatment planning can be more readily related back to filter removal rather than changes in beam energy. This energy matching procedure is in contrast to research reported for other accelerators.

CHAPTER 4

BEAM MODELLING

The dosimetric characterisation of FFF beams has shown that they are of potential benefit in radiotherapy, but this can only be translated into use if patient treatments can still be planned and delivered on the accelerator. Three treatment planning systems have been commissioned for FFF use: XiO, Monaco and Brainlab – and these are described below.

This chapter therefore discuses the beam data requirements of each treatment planning system and the modelling of the FFF within the software, concentrating on the implementation and commissioning of the Monaco TPS, as this is where most effort was required. The implementation of FFF for Monaco has been published in the journal *Medical Physics* (Cashmore *et al* 2012), and was performed in conjunction with staff at Elekta based in large part on work performed by Marcin Sikora and Markus Alber (Sikora *et al* 2007, Sikora *et al* 2009, Sikora 2011).

4.1 XiO

Commissioning data has been measured and used to create a beam model within the XiO treatment planning system (Elekta AB, Stockholm, Sweden, version 4.34.02). XiO is a treatment planning system for both 3D conformal radiotherapy and IMRT, and is the main software package for radiotherapy planning at UHB. Within the software is a separate program for beam modelling called 'Source File Maintenance'. Here it is possible to create, edit and copy existing machine data files.

To create the FFF beam model the existing 6MV model for this linac was used as a starting point. The beam remains unaffected up until the FF so the basic machine parameters for the model (machine limits etc.) obviously remain the same but a new beam spectrum, depth doses and profiles along with total scatter ($S_{c,p}$) and phantom scatter (S_p) factors are required. In practice total scatter and head scatter (S_c) have been measured (and S_p calculated) since published S_p data are inaccurate for unflattened beams (Satherberg *et al* 1996, Kragl *et al* 2009).

Beam profiles and depth dose measurements were taken using a PTW MP3 Tandem watertank with Semiflex 0.125cc chambers and running Mephysto 7.4 water phantom software. For scatter and wedge factor measurements an NE2571 Farmer chamber was used. Build-up measurements were made with a NACP-02 parallel plate chamber in WT1 solid water.

A full set of commissioning data as recommended by Elekta (CMS XiO 2003) were measured along with surface and out-of-field doses to compare with concurrently measured 6MV data (table 4.1).

Central axis depth dose measurements were measured for square fields from 5x5 to 30x30cm^2 at 100cm SSD and profiles taken at 5 depths. Wedged beam data was also measured as the effect of filter removal on wedge characteristics has not been

studied previously. A 40x40cm open field diagonal profile was also taken for beam modelling purposes.

Table 4.1. Measurements made for XiO commissioning. Depth doses and profiles were measured with a Semiflex 0.125cc chamber, scatter factors with a Farmer NE2571 chamber and build-up and surface doses with a NACP chamber in solid water.

Depth Doses	Open / Wedge	5, 10, 15, 20, 30 cm^2
Profiles	Open / Wedge	15, 50, 100, 150, 200mm depths For 5, 10, 15, 20, 30 cm^2
	Open Diagonal	40x40 cm^2
Total Scatter Factors		3, 4, 5, 6, 7, 8, 9, 10, 12, 14, 16, 18, 20, 25, 30, 40 cm^2
Head Scatter Factors		3, 4, 5, 6, 7, 8, 9, 10, 12, 14, 16, 18, 20, 25, 30, 40 cm^2
Wedge Factors		3, 4, 5, 6, 7, 8, 9, 10, 12, 14, 16, 18, 20, 25, 30 cm^2
Build-up	Open	5, 10, 15, 20 cm^2 0-17mm depths
Surface dose	Open	3, 4, 5, 6, 7, 8, 9, 10, 12, 14, 16, 18, 20, 25, 30, 40 cm^2 at 3mm depth
Leakage		50cm and 100cm from isocentre, patient plane
Dose rate	Open / Wedge	10x10, d_{max} (15mm)

4.1.1 Modelling variations in energy spectrum

The flattening filter significantly hardens the radiation beam on the central axis but, due to its physical shape, the average beam energy decreases with distance from the central axis (due to differential absorption of soft x-rays).

The conical shape of the flattening filter therefore produces a variation in beam spectrum across the field. This can be modelled to some extent in the XiO TPS by the use of central axis and off-axis spectra. Modelling of the beam spectra is a matter of informed trial and error through an iterative process. Low-energy components are added to increase dose near the surface, and higher energy for doses at depth, all the while trying to maintain a smooth spectrum.

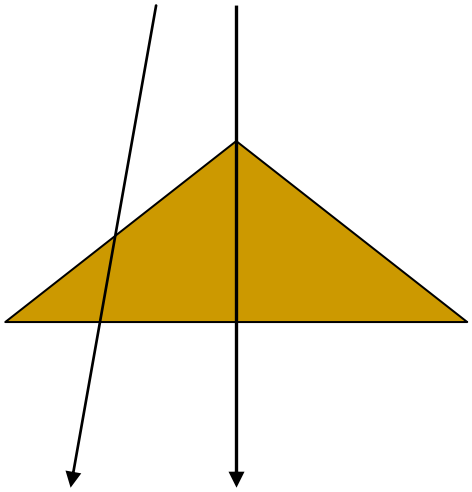

Figure 4.1. A simple diagram to illustrate the need for different beam spectra on and off axis.

Figure 4.1 illustrates the need for an off-axis spectrum for treatment planning. The XiO system uses two spectra for beam modelling to account for changes in beam quality across the flattening filter, one on the central axis and the other 7° off-axis. Figure 4.2 (a) shows the spectra used to model a conventional 6MV unit in XiO; in black is the central-axis (CAX) spectrum and in brown is the off-axis spectrum. For dose calculation at fan-lines between these two angles the spectrum is interpolated.

As yet there are no published spectra for unflattened beams, but conventional central axis spectra are simple to derive from standard published spectra (Mohan *et al* 1985). Some off-axis spectra have also been published (Sheikh-Bagheri and Rogers, 2002) and are used to modify attenuation towards the field edge, giving a better fit to measured data in the shoulder region of beam profiles.

(a)

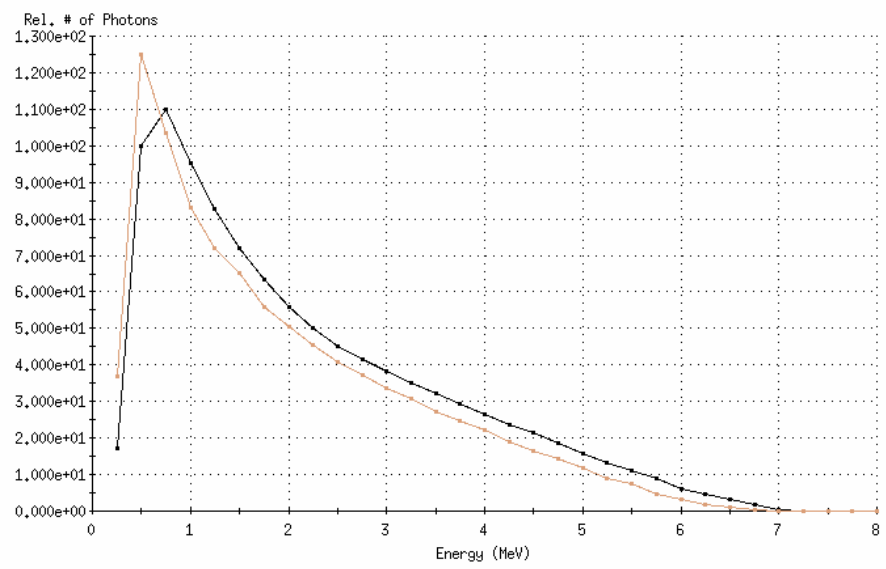

(b)

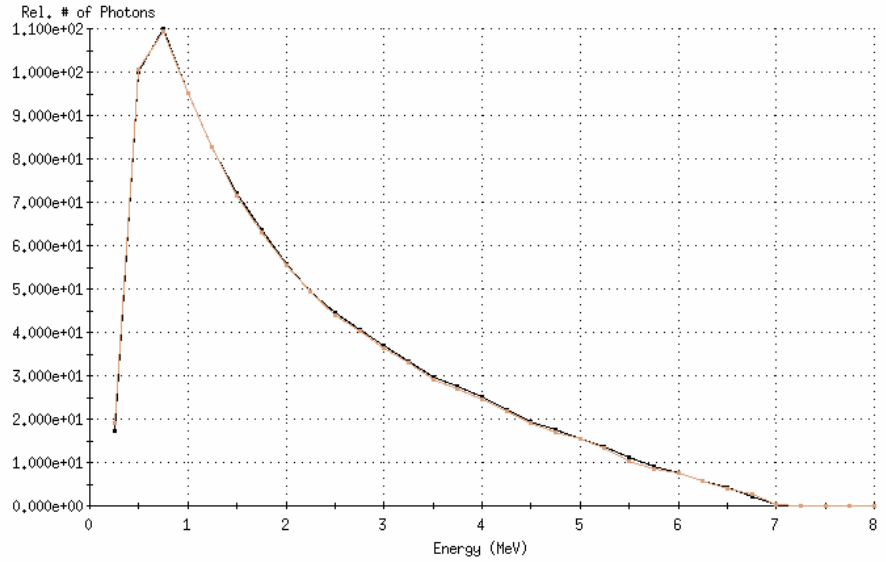

Figure 4.2. Central and off-axis spectra used for beam modelling. (a) 6MV. (b) 6MV FFF beam, notice the coincidence of the off-axis spectrum for the FFF beam.

Although there is still a change in beam spectrum across the field with the flattening filter removed it is much reduced and a separate spectrum is not required in XiO to model the off-axis component and fit to measured profiles (figure 4.2b).

A selection of beam profiles and depth dose measurements are presented in figures 4.3 and 4,4 respectively. At smaller field sizes the filter has no observable effect on the beam shape, but as the size increases the forward-peaked nature of the beam becomes more apparent.

Figure 4.5 shows a selection of beam profiles for a 30x30cm² field normalised to remove beam divergence and output. In the shoulder region the beam profiles for the conventional beam show considerable variation, which is the reason why flattening filter can only be designed to give a 'flat' field at one particular depth. The FFF plot shows the reduction in this variation due to the similarity of the energy spectrum across the portal.

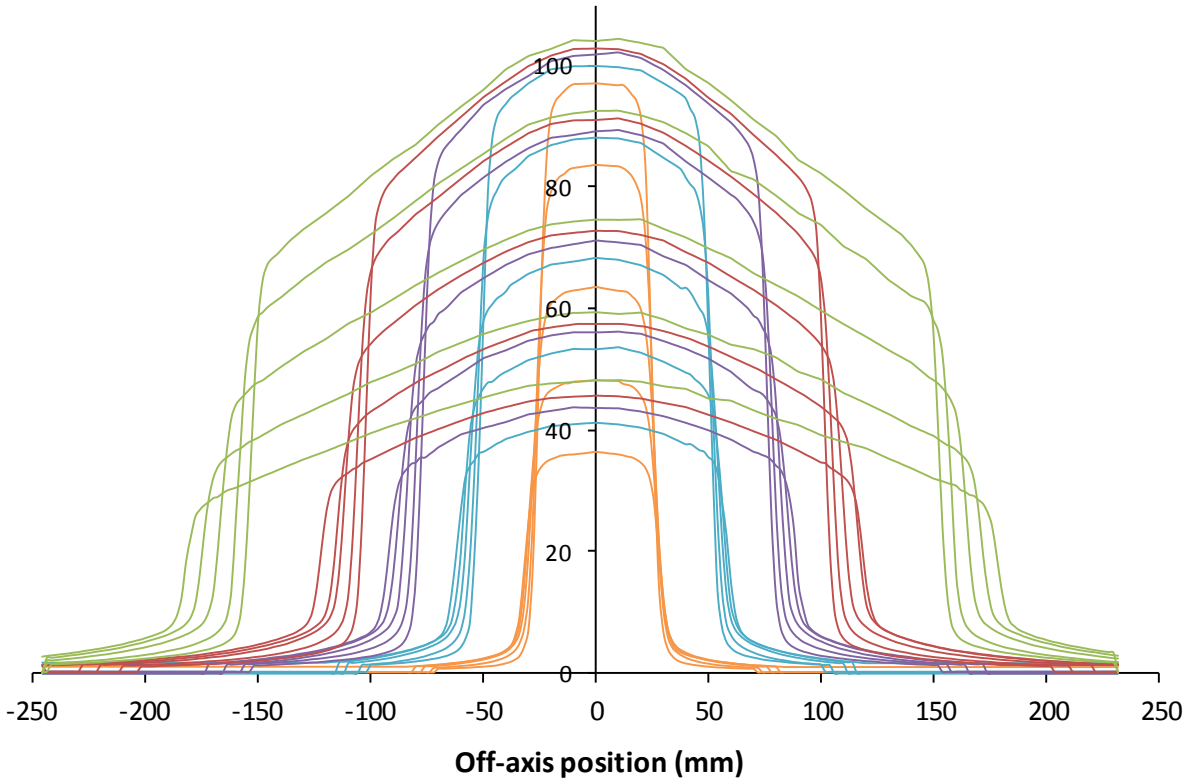

Figure 4.3. FFF beam profiles for field sizes of 5, 10, 15, 20, 30cm² at depths of 1.5, 5, 10, 15, 20cm.

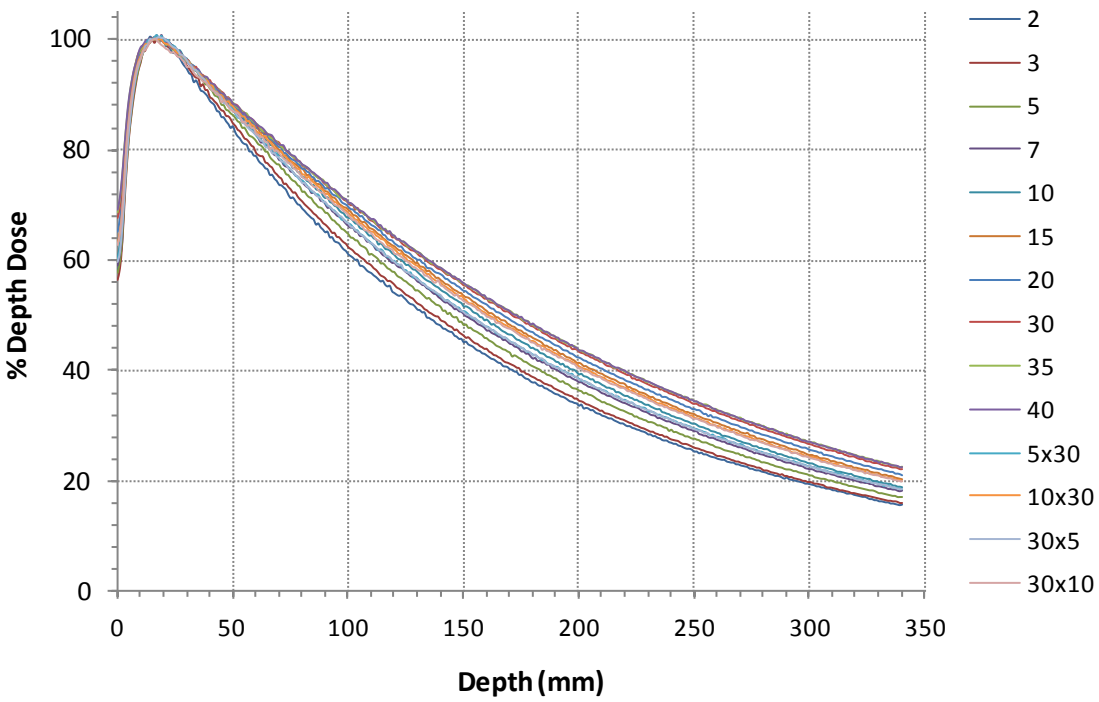

Figure 4.4. Percentage depth dose plots for FFF beam (100cm SSD) for the field sizes indicated.

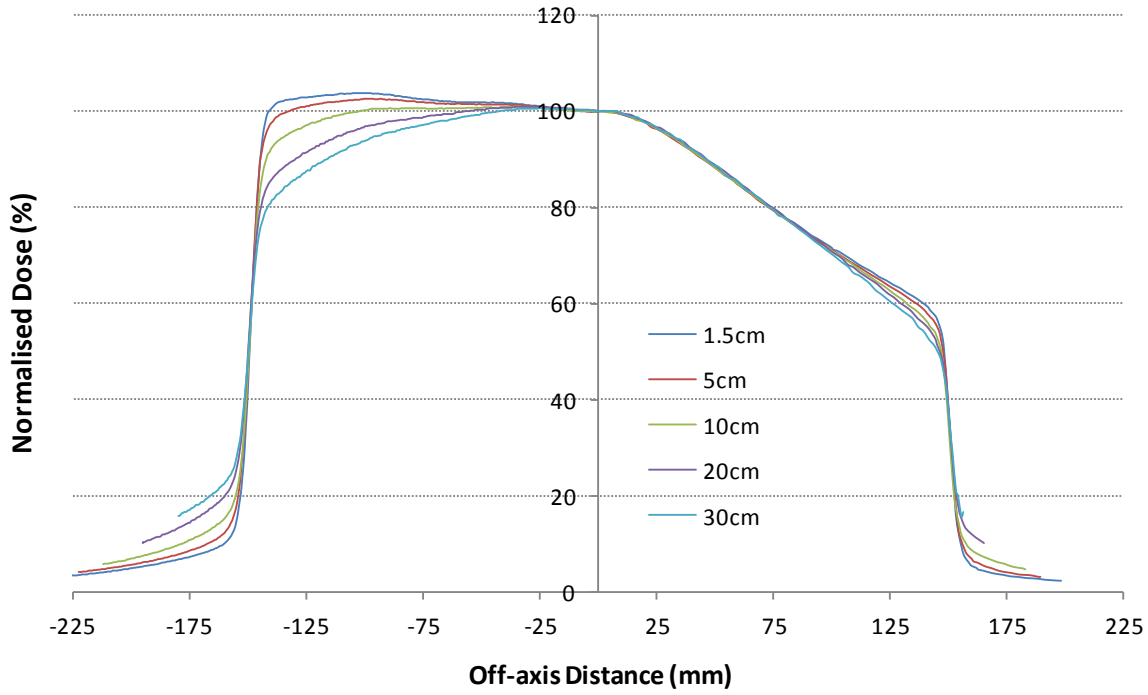

Figure 4.5. A half-beam profile plot comparing standard 6MV flattened beam (left of plot) against the energy matched FFF equivalent (right) for a 30x30cm² beam. Profiles are normalised to 100% on the central axis and scaled to remove divergence, this illustrates the changes in beam profile with depth. Note the relative reduction in beam shape change with depth for the FFF beam.

Figure 4.6 (a to e) shows example beam profiles and percentage depth doses from beam model calculations in XiO (vs. measured data) to illustrate the quality of the beam model. A good match to measured data is achieved at all field sizes.

(a)

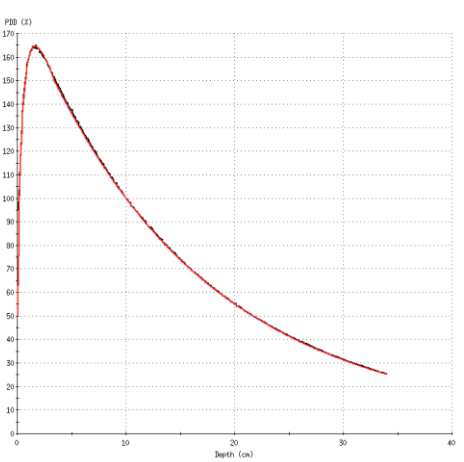

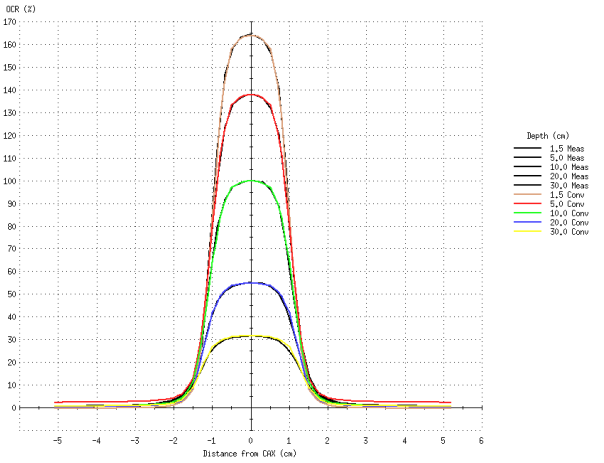

(b)

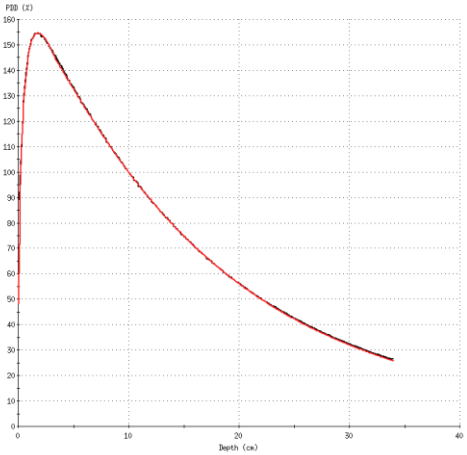

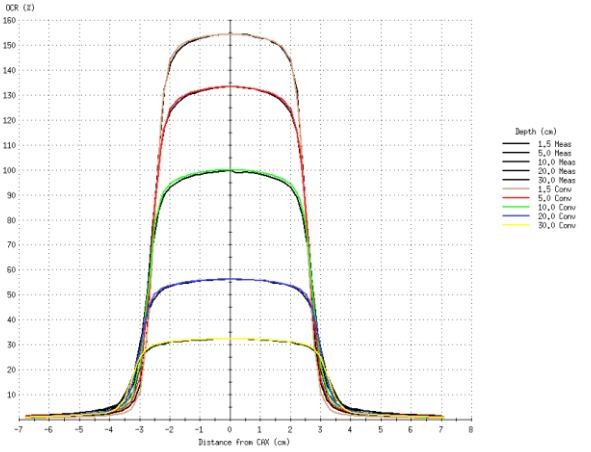

(c)

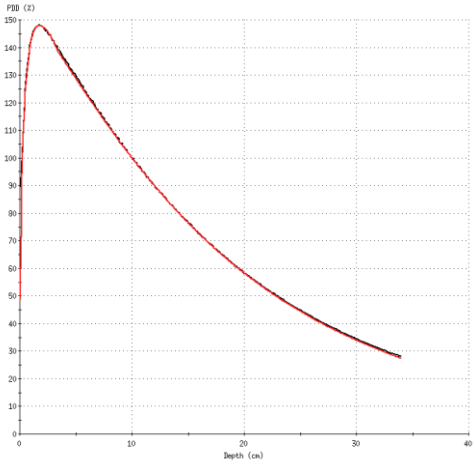

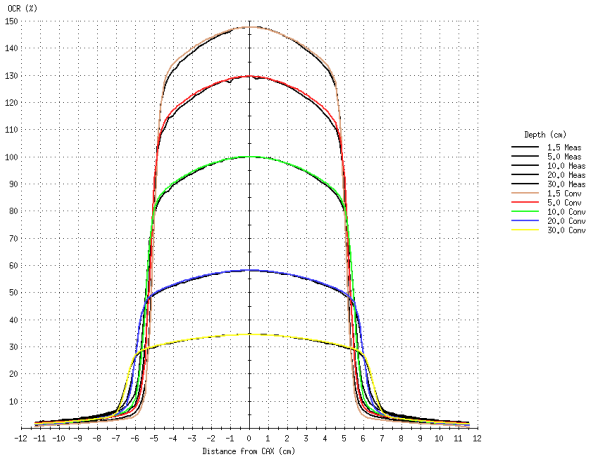

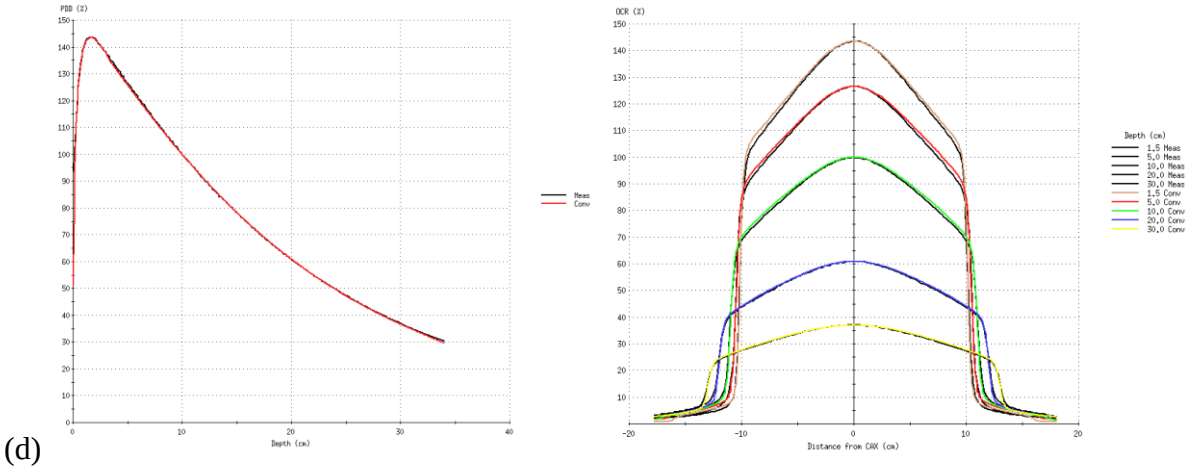

(d)

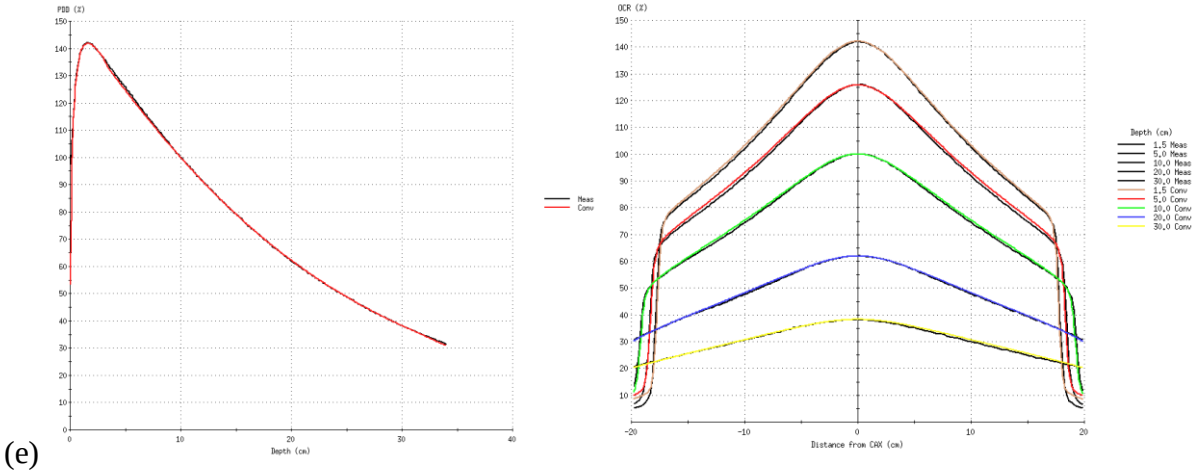

(e)

Figure 4.6. Depth dose and beam profile comparisons (measurements vs. TPS predictions) for field sizes of (a) 2x2, (b) 10x10, (c) 15x15, (d) 20x20 and (e) 35x35cm² fields to illustrate beam modelling of FFF.

4.2 Monaco

Monaco™ (Elekta AB, Stockholm, Sweden) is a treatment planning system that uses biological cost functions and constrained optimisation for IMRT treatment planning. Plan optimisation is carried out using a pencil beam algorithm for speed, but final dose calculations are computed using a Monte Carlo dose engine.

In the standard clinical release (version 2.03) the TPS was not capable of modelling the triangular profiles of the FFF beams, and modifications were needed by to support FFF modelling and dose calculation. Alterations to the Monaco

software were implemented by Elekta staff based on dosimetric, beam modelling and verification data acquired for FFF beams at UHB.

To maintain consistency, all IMRT specific beam data for both the 6MV and 6MV FFF modes were measured concurrently using the same equipment and techniques. Both models were generated at the same time and to the same standard.

The following sections describe the beam modelling within Monaco and the modifications to the model needed to support FFF beams.

4.2.1 VSM - Source densities and particle fluence distribution

For MC simulations a beam can be described by the phase space parameters (position, direction of motion and energy) of the constituent photons and electrons. It is possible to generate these parameters analytically in a phase space plane in front of the patient and use MC transport for particles passing through the patient. A 'virtual source model' (VSM) allows for efficient generation of particle parameters and can be commissioned for conventional linear accelerators with semi-automatic modelling tools. The VSM-based MC computes dose in the following way:

1) Source type, energy, position and direction of particles are sampled from the VSM. The required number of particles is generated on the fly in an arbitrary plane above the collimators to achieve a predefined level of statistical noise in the patient.
2) The particles are transported through collimators or transmission probability filters (Sikora 2011), e.g. in the multileaf collimator (MLC) plane.
3) The dose deposited in the patient is calculated using the XVMC code (Fippel 1999, Kawrakow and Fippel 2000)

The VSM treats particles coming from different parts of the accelerator as if they were coming from three different virtual sources. These sources are the primary photon source, the secondary photon source and the electron contamination source, with relative contributions P_{pri}, $P_{\sec}$, and P_{econ} respectively. The primary source is defined in the plane of the electron beam target. The secondary source then models all of the photons that result from interactions occurring in places other than the target. The positions of the secondary source and the electron contamination source are free parameters which are set according to the machine geometry. The secondary source is located at the base of the primary collimator and the electron contamination source at the base of the FF (or the build-up plate).

It is assumed that each of the sources has a Gaussian shape with standard deviations $\sigma_{pri}, \sigma_{sec}(E), \sigma_{econ}(E)$ for primary photon distribution, energy-dependent secondary photon distribution and energy-dependent electron contribution respectively, according to the following expressions:

$$\sigma_{\sec}(E) = \Sigma_{\sec}\left(\frac{E}{E_0}\right)^{-0.34} \qquad \text{if E} \geq 0.511 \text{ MeV} \qquad (4.1)$$

$$\sigma_{\sec}(E) = \Sigma_{\sec}\left(\frac{0.511}{E_0}\right)^{-0.34} \qquad \text{if E} < 0.511 \text{ MeV} \qquad (4.2)$$

where:

E = particle energy

$E_0 = 1$ MeV

$\Sigma_{\sec}$ = free parameter, the base data standard deviation of the secondary source.

$$\sigma_{econ}(E) = \Sigma_{econ}(E / E_0)^{-0.18} \qquad (4.3)$$

Σ_{econ} = free parameter, the base data standard deviation of the electron source.

Upon generation of a photon in the source location, the particle fluence in a phase space plane that is located above the collimators is initially flat. The particle weight is altered depending on the angle between its direction and the central axis (CAX) according to a tabulated profile.

4.2.2 VSM – Energy spectra

The primary photon spectrum (S_{pri}) on the central axis before the flattening filter is described by

$$S_{pri}(E) = \omega_0 \qquad \text{if } E_{bin} \le E < E_{\min} \qquad (4.4)$$

$$S_{pri}(E) = \left(\frac{E}{E_{\max}}\right)^{-b_{pri}} - 1 \qquad \text{if } E \ge E_{\min} \ . \qquad (4.5)$$

where:

E = photon energy (MeV)

$E_{\min}, E_{\max}$ = are minimum and maximum photon energies.

For $E_{\min}$ a fixed value of 0.5 MeV is used.

ω_0 ,= low energy bin parameter

b_{pri} = free parameter.

In the implementation of this VSM for flattened beams this primary spectrum is attenuated with an appropriate, radially-dependent filter function (Sikora and Alber 2009).

The secondary photon spectrum $S_{sec}(E)$ describes the secondary photons on the CAX after the flattening filter.

$$S_{\sec}(E) = \omega_S \qquad \text{if } E_{bin} \le E < E_{\min} \qquad (4.6)$$

$$S_{\sec}(E) = e^{-b_{\sec}E} - e^{-b_{\sec}E_{\max}} \qquad \text{if } E \ge E_{\min}, \qquad (4.7)$$

where:

E_{bin}, ω_S = low energy bin parameters

$b_{\sec}$ = free parameter.

The off-axis energy softening is approximated by two parameters (δb_{pri} and $\delta b_{\sec}$) which define the relative change of the primary and secondary spectrum with respect to the tangent of angle to the CAX ($\tan(\nu)$) at the scoring plane.

$$b_{pri}(\nu) = b_{pri} + \delta b_{pri} \tan(\nu) \qquad (4.8)$$

$$b_{\sec}(\nu) = b_{\sec} + \delta b_{\sec} \tan(\nu) \qquad (4.9)$$

The energy spectrum of the contaminating electrons is approximated by an exponential function

$$S_{con}(E) = N_e \exp(-\frac{E}{\langle E_e \rangle}), \qquad (4.10)$$

where:

N_e = Normalization factor

$\langle E_e \rangle$ = mean electron energy

The VSM is defined by fixed and open parameters. Fixed parameters are derived from a BEAMnrc (Rogers *et al* 1995) simulation of the treatment head which is performed only for a given accelerator type. Open parameters are fitted in the poly-

energetic kernel superposition commissioning routine for each individual linac (Fippel 1999). The free parameters of the VSM are derived from basic beam data measurements performed in water, and by minimizing the differences between calculated and measured data.

For the purpose of verifying the dose calculation accuracy of this model the Monaco treatment planning system (TPS) (Elekta CMS software, St. Louis, Mo) was used (version 3.1), which incorporates a commercial implementation of this VSM model (VSM v.1.6).

Beam modelling (parameter fitting) was carried out by Elekta staff.

4.2.3 Beam data requirements

Measurements for beam modelling included depth dose curves and profiles for various field sizes measured in a water phantom (Blue Phantom2, IBA Dosimetry, Germany). Measurements were performed at SSD = 100cm with suitable detectors (CC01, CC13 IBA Dosimetry, NE2577 Nuclear Enterprises Ltd, (now QADOS, UK)).
At the time of implementation, the model required both in air and in water scans to be performed (see table 4.2).

Table 4.2. Beam data requirements for Monaco. Depth doses and profiles were measured with a Semiflex 0.125cc chamber, scatter factors with a Farmer NE2571 chamber.

In Water		
Depth Doses	Square	2, 3, 4, 5, 7, 10, 15, 20, 30x30 cm^2
	Rectangular	5x30, 10x30, 30x5, 30x10 cm^2
Profiles	Square Rectangular	2, 3, 4, 5, 10x, 20, 30x30 cm^2 5x30, 10x30, 30x5, 30 10 cm^2 At d_{max}, 5, 10, 20, 30 cm depths
Output	Square	1, 2, 3, 4, 5, 7, 10, 15, 20, 30, 40cm^2
In Air		
Profiles	Square	2, 3, 4, 5, 7, 10, 15, 20, 30, 40x40 cm^2
	Rectangular	5x30, 10x30, 30x5, 30 10 cm^2 at 85, 100 and 115cm SCD
CAX scan	Square	2, 3, 4, 5, 7, 10, 15, 20, 30, 40x40 cm^2
	Rectangular	5x30, 10x30, 30x5, 30 10 cm^2 From 85 to 115cm SCD
Relative output factors		2, 3, 4, 5, 7, 10, 15, 20, 30, 40x40 cm^2 5x30, 10x30, 30x5, 30 10 cm^2 Normalized to 40x40cm^2
Films	Square	1x1, 2x2, 3x3, 4x4, 5x5cm^2 10x10cm^2 shaped by 4x4 MLC

The dataset consisted of water, air and film measurements of depth dose curves, in-plane and cross-plane profiles for field sizes, diagonal profiles for the largest field size: 40x40cm^2 and output factors. These measurements are detailed in table 4.2.

Monaco is used clinically at UHB with conventional flattened beams and the data set and equipment used for FFF measurements matched those originally used to commission this beam energy. In this way the FFF and FF data can be said to be of the same standard and can be directly compared against one another.

4.2.4 Model commissioning

The unique feature of the VSM is that it represents the primary photon spectrum before it reaches the flattening filter. Therefore, turning off the flattening filter correction corresponds to physically removing the flattening filter from the accelerator head. The procedure for modelling the FFF machine is very similar to modelling a standard machine and as a starting point a previously created model of the FF linear accelerator from the same vendor was used. The model parameters were modified as follows:

1) The radially dependent, differential attenuation of the FF in the conventional model was turned off. Further variations in off-axis spectrum were kept constant (eq. 4.8).
2) The relative contribution from primary photons P_{pri} was increased.
3) $E_{\max}$ was increased along with b_{pri} to provide a better agreement of the depth dose, especially in the D_{max} region. This accounts for the re-tuning of the machine to produce a typical 6 MV quality index.
4) The secondary source Gaussian sigma was made wider by a factor of approx. two, due to the fact that in the absence of the flattening filter, the primary collimator contributes most of the scatter.

5) To correct the fluence profile for FFF beams the tabulated parameters for radial energy fluence variation were adjusted to the diagonal cross-profiles at D_{max}.

The results of the VSM phase space reconstruction are independent of the calculation engine used; therefore it can be coupled with other MC dose engines. MC simulation and treatment planning were performed in the Monaco TPS using a water phantom of size 50x50x35 cm^3. The voxel size was set at 2mm for the smallest 2x2 cm^2 field and 3mm for the rest of the fields with statistical uncertainties set to 0.5%.

4.2.5 Results of water phantom data verification

Figure 4.7 shows a plot of output factor variation with field size for FFF and conventional beams (a) and also the difference in calculated relative output factor curve against measurement (b). These are absolute values as predicted by the planning system and not scaled to measured data. The absolute outputs can be predicted within 1.5% of measurements over the entire range of field sizes.

To illustrate the match achieved figure 4.8(a) shows a sample depth dose curve for a 2x2 cm^2 field size, and figure 4.8(b) profiles for a 30x30cm^2 field at depths of d_{max}, 5cm, 10 cm, and 20 cm for a 30x30 cm^2 field. Good agreement is seen in each case.

A more detailed analysis is presented in figure 4.9 where, for various depths and fields sizes, the percentage difference between measured and calculated depth dose curves is presented. The spread in values is approximately 1.5% (+0.5 to -1.0) in both cases indicating that the beam model is of similar quality for both FFF and conventional beams, and is within the measurement uncertainty for these fields.

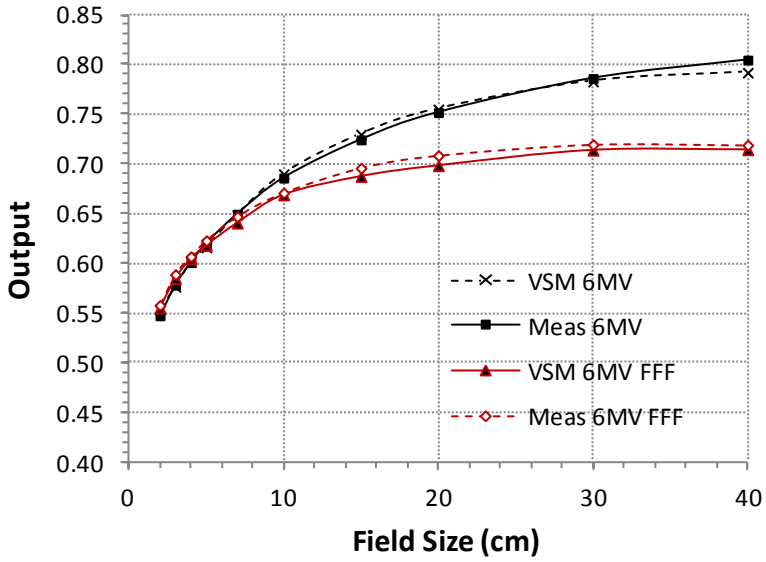

(a)

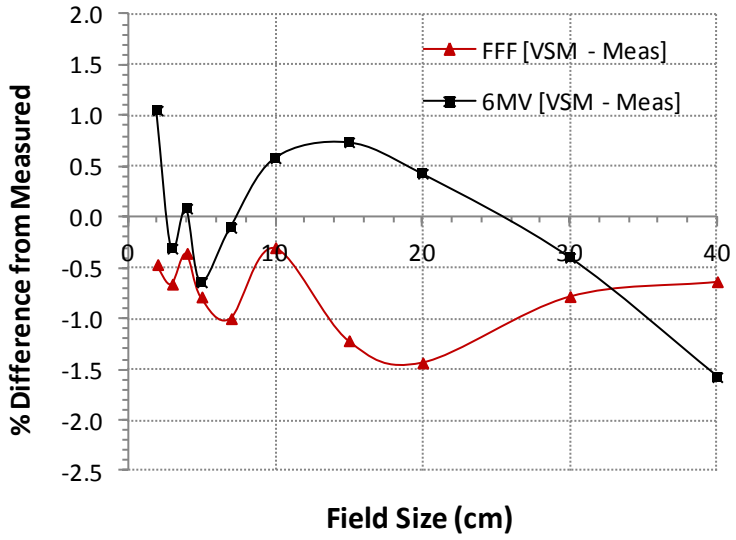

(b)

Figure 4.7 (a) Absolute output factors as a function of field size for FFF and conventional 6MV beams as predicted by the TPS compared to measurement. b) Difference in output factors, calculated minus measured.

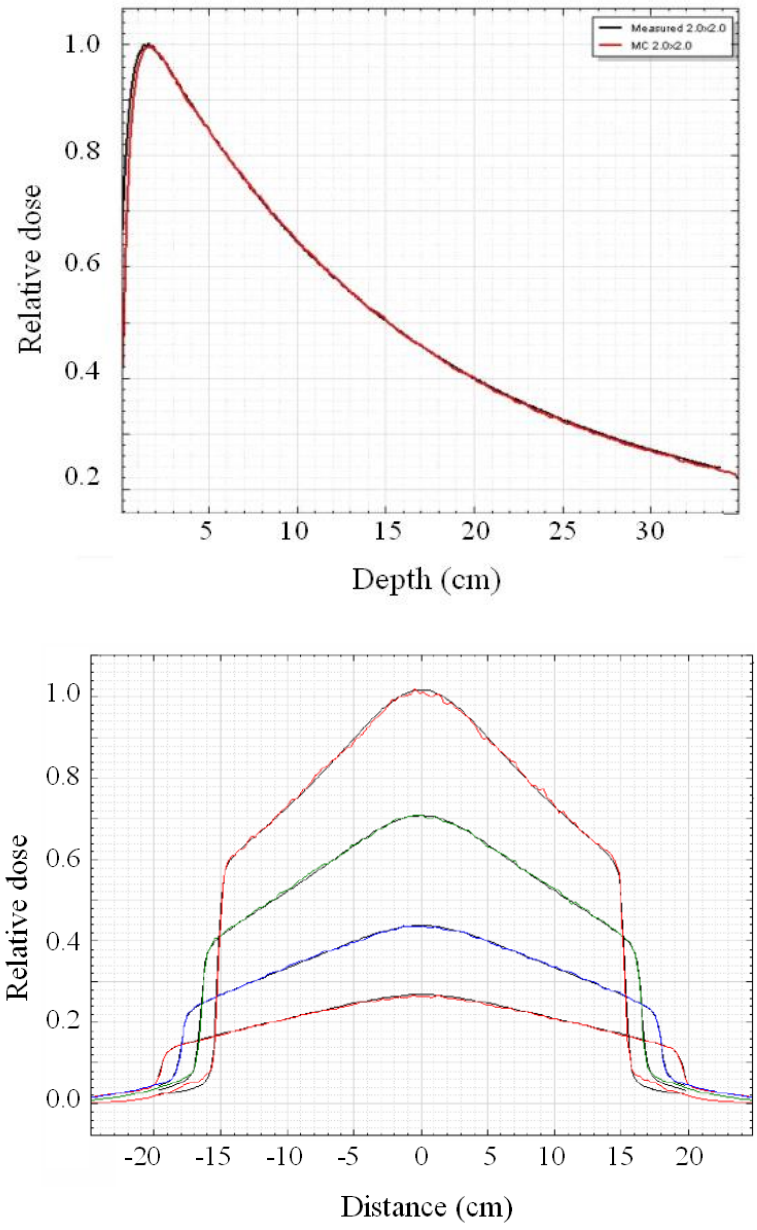

Figure 4.8. Sample beam data (a) PDD curve for 2x2 field, (b) cross-profiles for a 30x30cm² field for the FFF model.

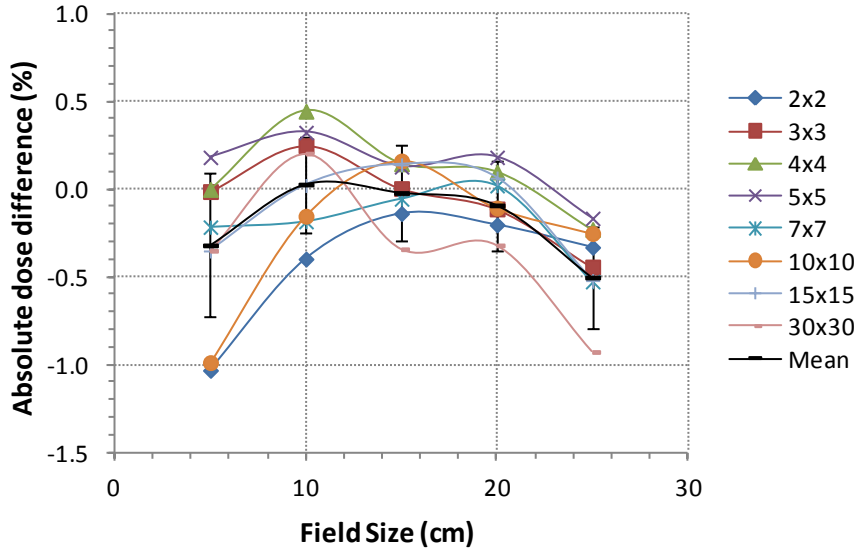

(a)

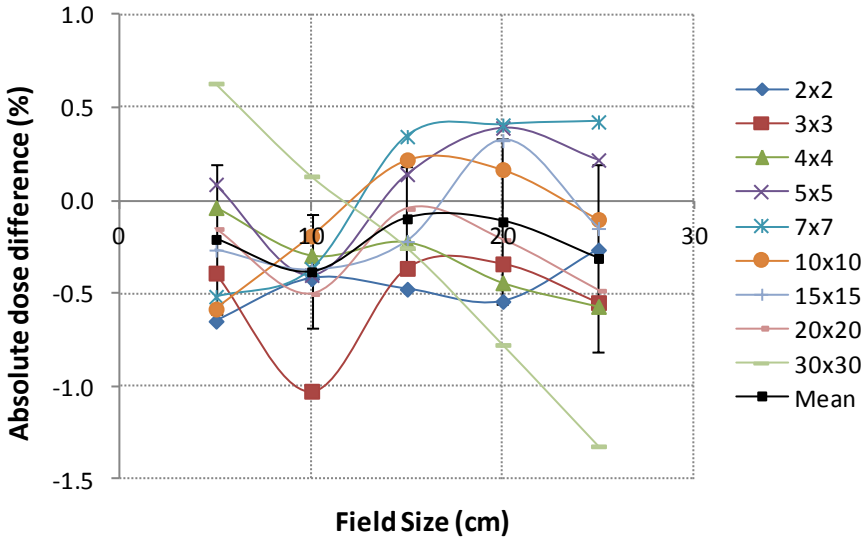

(b)

Figure 4.9. Absolute dose difference between measured and calculated depth doses curves (100cm source-surface distance) for the field sizes indicated for (a) the 6MV FFF beam, and (b) 6MV. Monte Carlo variance is set at 0.5%.

Beam profiles are analysed in figure 4.10 which shows comparisons of FFF beam profile measurements against TPS predictions for field sizes from 2x2 to 30x30cm². A 1D γ-analysis (written by Mark Ramtohul at UHB) was performed for each profile with criteria of 2% / 2mm. It can be seen that all points had γ <0.8. For set criteria of 1% / 1mm 93% of all points had γ<1 (figure 4.10).

a)

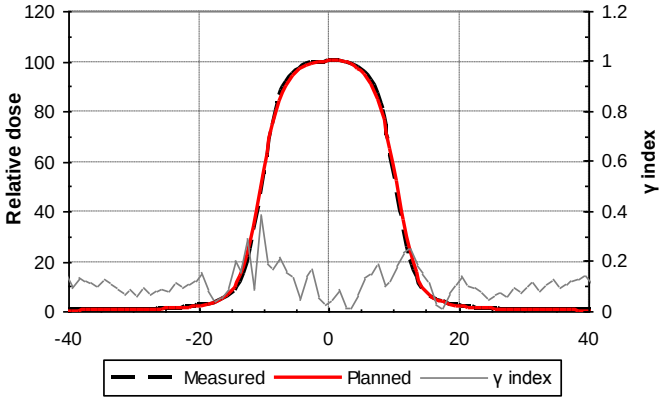

b)

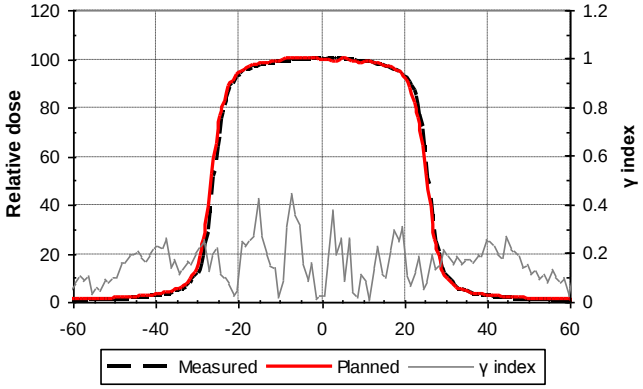

c)

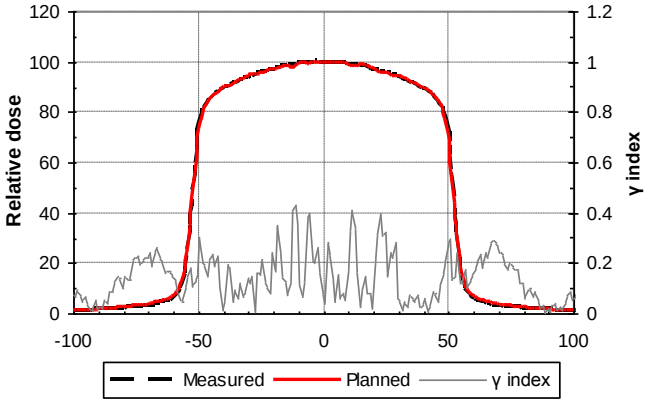

d)

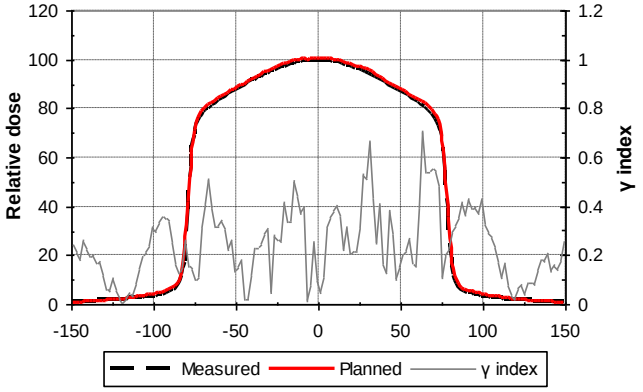

e)

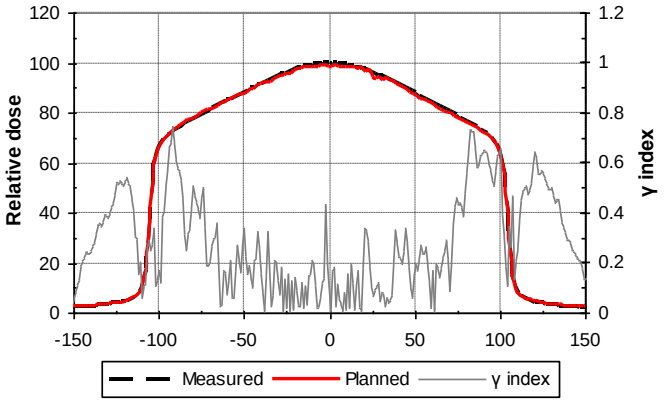

f)

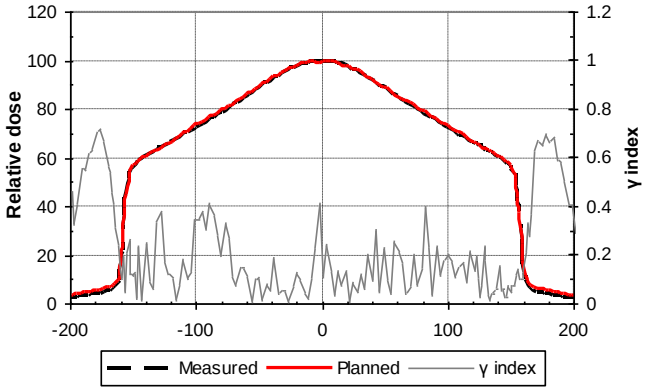

Figure 4.10. Comparison of calculated vs. measured beam profiles for sample field sizes of a) 2x2, b) 5x5, c) 10x10, d) 15x15, e) 20x20 and f) 30x30cm² at 100cm SSD and a depth of 5cm. Criteria for gamma analysis are 2%/2mm.

Beam modelling of the 6MV FFF beam within Monaco is seen to be as accurate as that used clinically. Depth dose predictions are generally within 0.5% for the FFF beam, with only a few outliers up to 1% which is more consistent than for the conventional beam model. 1D gamma analysis of beam profiles for selected criteria (2%/2mm) also show excellent agreement. This matches well with commissioning results reported by Hrbacek *et al* (2011), and Kragl *et al* (2011b) for FFF beams from Varian and Elekta linacs respectively. Any differences between prediction and measurement where γ exceeded 1 occurred mainly within the out-of-field regions of the beam profiles and only for the larger (>15x15cm^2) field sizes.

4.3 BrainLab

Commissioning data has also been measured for six BrainLab stereotactic collimators (10, 12.5, 15, 17.5, 20 and 22.5mm diameter). These have been commissioned in both conventional and FFF modes (at 6MV) to compare beam data and treatment plans. Profiles and depth doses were measured with a CC01 chamber in a BluePhantom2 watertank (iBA dosimetry) at 92.5cm SSD.

The beam profile is preserved on filter removal, with only small deviations from those seen under normal operation. Figure 4.11 shows half-beam profile plots of the standard 6MV and FFF beams normalised to reflect the changes in output observed.

Small differences are seen in the beam penumbra (20-80%) measured for each beam, as well as the output factor. These are detailed in table 4.3 below.

There are additional changes in the beam profile outside of the treatment area, where the doses are approx. half of those seen for conventional operation. This is discussed in more detail in section 7.7 and appendix H.

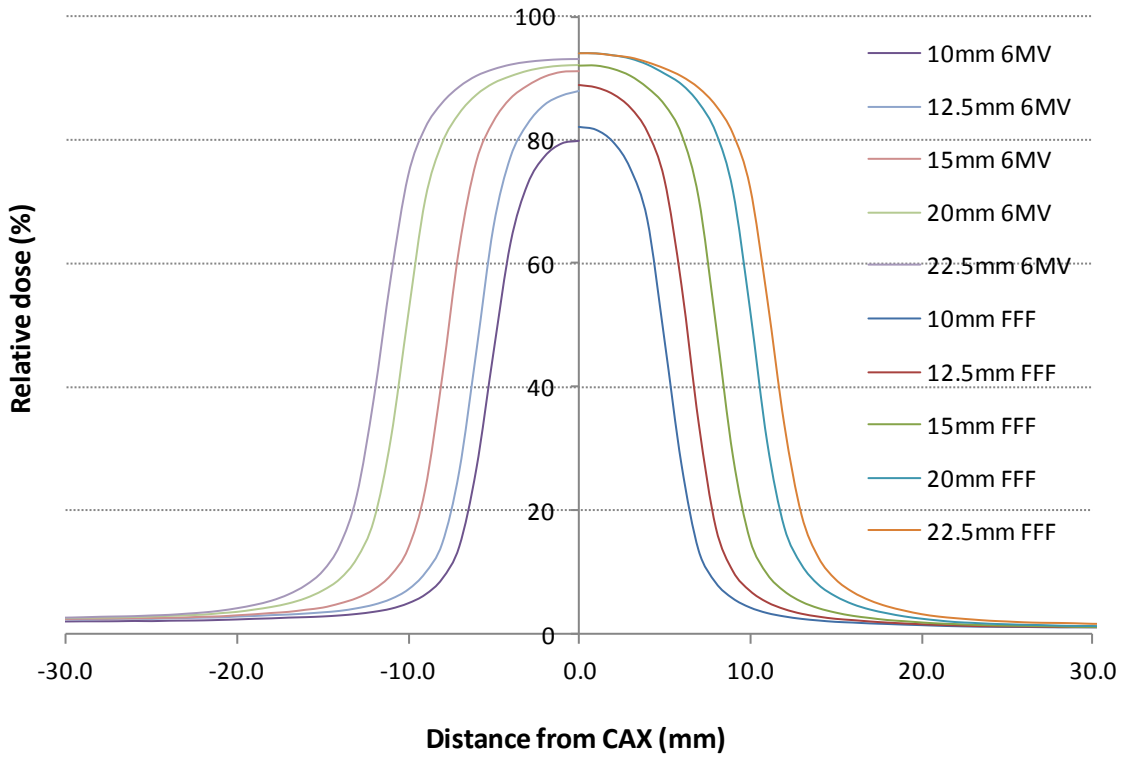

Figure 4.11. Half-beam profiles normalised to the output factor for each cone (relative to a 5x5cm² field). 6MV data is on the left of the plot, 6MV FFF data on the right.

Table 4.3. Field with and penumbra (80-20%) measurements for stereotactic cones (10 to 22.5mm) for 6MV and 6MV FFF operation.

	Field width (mm)		Penumbra (mm)		Output Factor *	
Collimator	**6MV**	**FFF**	**6MV**	**FFF**	**6MV**	**FFF**
10	10.5	10.4	5.3	4.8	0.806	0.825
12.5	12.9	12.8	5.5	5.2	0.883	0.896
15	15.5	15.5	6.0	5.6	0.918	0.927
17.5	18.0	18.0	6.4	5.9	0.923	0.936
20	20.5	20.4	6.6	6.3	0.928	0.942
22.5	23.0	22.9	6.9	6.6	0.932	0.948

- *Output factor is relative to a 10x10cm² field.*

The TPS used for SRS is the BrainLab (BrainLAB, AG, Germany) BrainSCAN (version 5.31), which utilises a simple ray-tracing algorithm for dose predictions. These are based on the input of %DD and beam profile data along with output factors, so beam modelling is not required.

4.4 Summary

Removal of the flattening filter invalidates the assumption of energy fluence and phantom scatter homogeneity in the incident beam a TPS must be able to model an arbitrary shape of the energy fluence. It is therefore important to be able to handle the incident particle fluence either by means of a sufficiently general calculation algorithm or through modelling of changes in the beam spectrum with off-axis position.

Within the XiO TPS it is seen that the use of two energy spectra, on and off-axis is sufficient to model standard filtered beams, and that removal of the flattening filter only acts to reduce the variation in the beam spectrum. Although some variation still exists, it is possible to model the FFF beam with a single energy spectrum and match %DD and beam profile variations with depth and off-axis position.

In Monaco the virtual source model for flattened beams was successfully adapted to a flattening-filter free beam production by modifying the energy spectrum to account for the lack of angular differential absorption and general beam hardening. Since the VSM model was initially derived from studies of phase spaces created by BEAMnrc (Rogers *et al* 1995) it captures the salient features of the various sources of radiation in a linear accelerator without overly-limiting assumptions, and thereby provides enough latitude to model flattening filter removal.

Beam modelling within BrainSCAN is not an issue as dose calculation is via a simple ray-tracing algorithm utilising tabulated data.

CHAPTER 5

TREATMENT PLANNING

Unflattened photon beams have been shown to have many beneficial properties such as reduced leakage and increased dose rate. Although these beams can be modelled within modern treatment planning systems there is still the potential issue of whether the triangular intensity profile can be of use when planning treatments. In principle this beam shape may be useful in many conventional planning circumstances and should be suitable for IMRT provided an algorithm is used that takes the beam profile into account.

This chapter discuses the basic beam properties of FFF beams and their use in planning conformal and IMRT treatments.

5.1 Introduction

The use of a flattening filter to produce large, flat fields has been considered to be a prerequisite for single beam and parallel pair techniques used to treat large slabs or boxes of tissue, but modern radiotherapy techniques often require the *active production* of non-flat fields; the most obvious example of this being IMRT. Non-flat

distributions are also produced by field-in-field techniques (to treat boost volumes) and more mundanely by the simple use of wedges.

The characteristics of flattening filter free linacs show many potential benefits for radiotherapy treatments. The only problem with these beams, of course, has always been the forward-peaked intensity profile of the beam.

So far the possibility of utilising FFF beams for conventional treatment planning has not been explored or quantified but the forward-peaked profile in essence provides a central axis boost to the distribution which could potentially be useful in many planning situations.

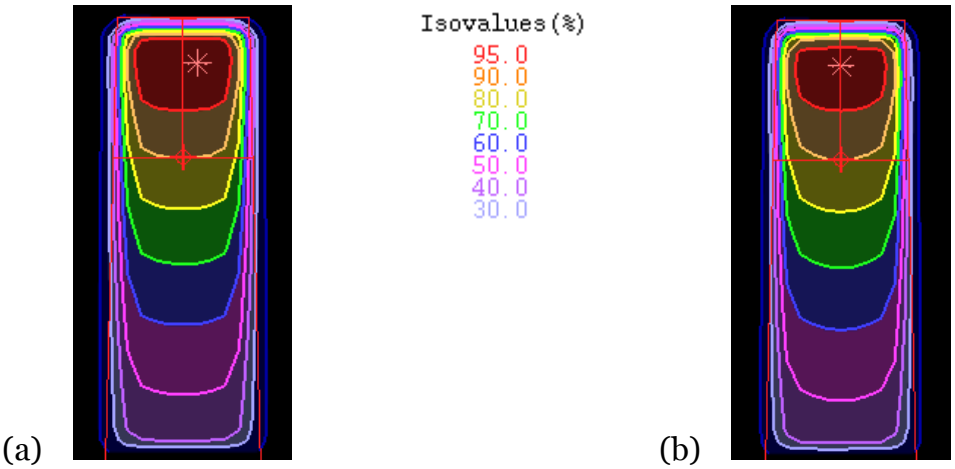

Figure 5.1. Comparison of isodose distributions for a 5x5cm² square field a) 6MV flattened beam, b) 6MV unflattened beam, illustrating the minor changes seen for small field sizes.

Figure 5.1 shows a single 5x5 beam both with and without the flattening filter in. As beam flatteners are designed to give a uniform field over large areas (typically 40x40cm²) at these small field sizes the filter has no real effect on the beam profile. This means that small field work could be performed as usual with no real effect on the plans produced. Although treatment machines are capable of delivering treatment fields up to 40x40cm² these size fields are rarely ever used (exceptions being whole or

half body techniques TBI, CNS). Over 50% of planned treatments at UHB are seen to have an equivalent square of 10cm² or less, with very few greater than 15cm². Modern treatments therefore require small fields.

5.2 Basic beam properties

The use of single applied beams is now a relatively unusual occurrence and the properties of a single beam, flat or otherwise, are not of huge relevance. It is the properties of beam *combinations* that are important and these are best studied by examining the basic situations encountered in treatment planning. An interesting effect is illustrated by considering the 4-field brick technique using 10x10cm² fields (figure 5.2). Although the distribution for the FFF beams in figure 5.2(b) is different to that seen in 5.2(a), there are several potentially beneficial features in that (1) the 95% isodose has rounded, not square corners and (2) the normal tissues near the surface receive a lower dose than normal. A 3D rendering of the 95% isodose contour (figure 5.2 c, d) shows that the high dose region for the conventional beams is cuboid in shape (hence the name 4 field 'brick'), whilst the same combination of FFF beams produces a spherical distribution. This is more likely to be of use in treatment planning terms as tumours tend to be more spherical in nature.

(a) 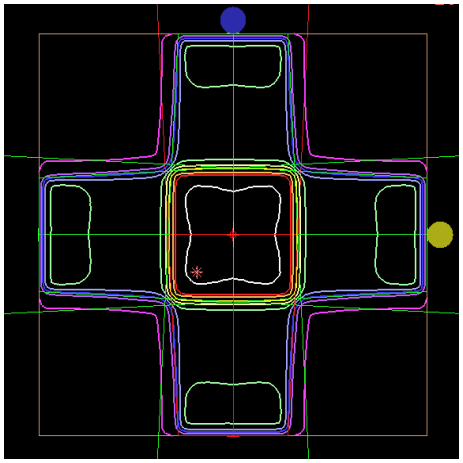 (b) 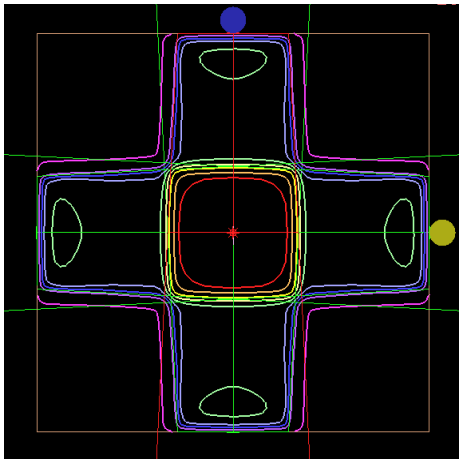

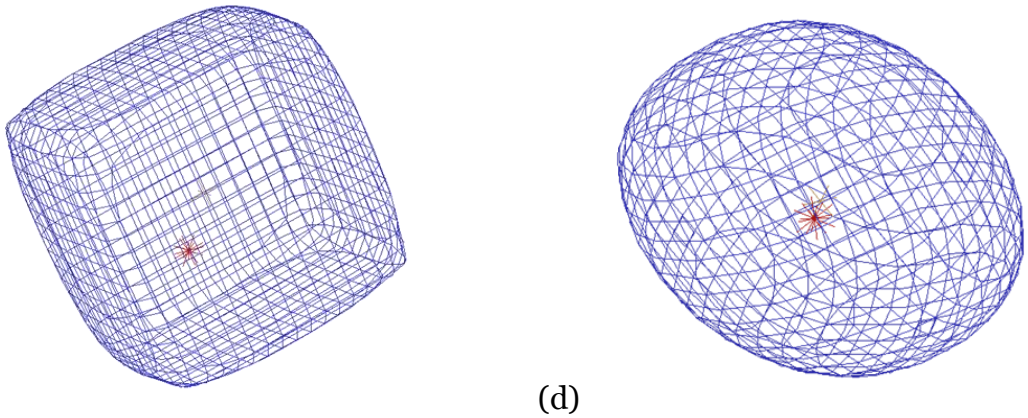

(c) (d)

Figure 5.2. For a 4-field 'brick' plan the unflattened distribution (b) shows a smaller 50% isodose (green) in the normal tissues near the phantom surface compared to the conventional plan (a). The central target region in (b) also has a rounded 95% region (d) that tends to match the general shape of tumours rather than the square distributions seen in normal planning situations (c).

On moving to larger fields the forward peaked nature of the beam becomes more apparent. Figure 5.3 shows an isodose distribution for a 20x20cm² beam and a beams eye view of this field to illustrate the conical nature of the beam intensity. The utilisation of these beams requires some consideration.

(a) (b)

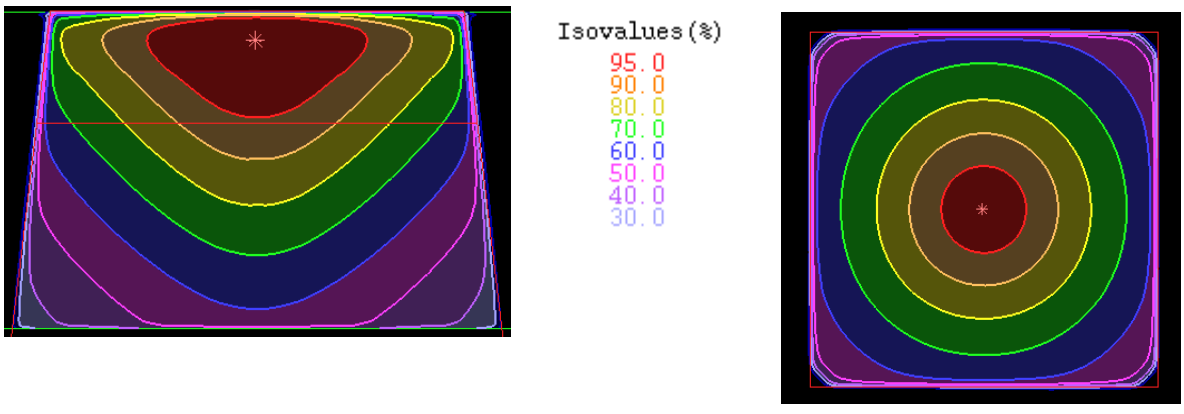

Figure 5.3. (a) Axial and (b) coronal isodose distributions for a 20x20cm² FFF beam (6MV FFF).

Historically, flat, uniform fields have been used almost exclusively for treatment planning, but modern radiotherapy often relies more on modulated radiation profiles. In particular, the uptake of forward-planned IMRT (field-in-field) techniques are rapidly increasing as they can be used to provide uniform doses over a region or to enhance (boost) the dose to a particular volume.

The forward peaked shape could therefore be a useful property if utilised correctly. The addition of a conventional flat beam with the FFF beam in different weightings can produce a beam anywhere between the fully 'flat' and fully 'unflat' simply by changing the relative weights of the two beams (much the same as for a motorised wedge) (figure 5.4).

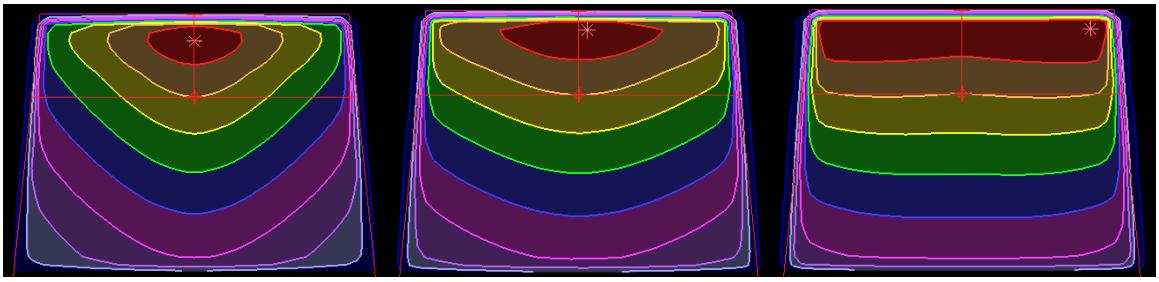

Figure 5.4. A dose distribution anywhere between 'unflat' and 'flat' can be produced by mixing the beams together in differing weights.

In this way the peak can be customised to the planning situation raising the central dose by the required amount to produce a uniform distribution. This is illustrated in figure 5.5 where a whole brain radiotherapy treatment is to be planned. The target area (the skull) is convex in both dimensions, causing problems for regular flattened beams (figure 5.5a), with hotspots occurring towards the edge of the beam. The use of the FFF beam in figure 5.5b overcompensates for the curvature of the skull, producing a central hotspot, but the combination of these two beams can produce an even dose distribution (figure 5.5c). When an opposing beam is applied

the overall distribution removes the original hotspots of either technique. The degree of boosting required can therefore be tailored to the situation.

(a) (b)

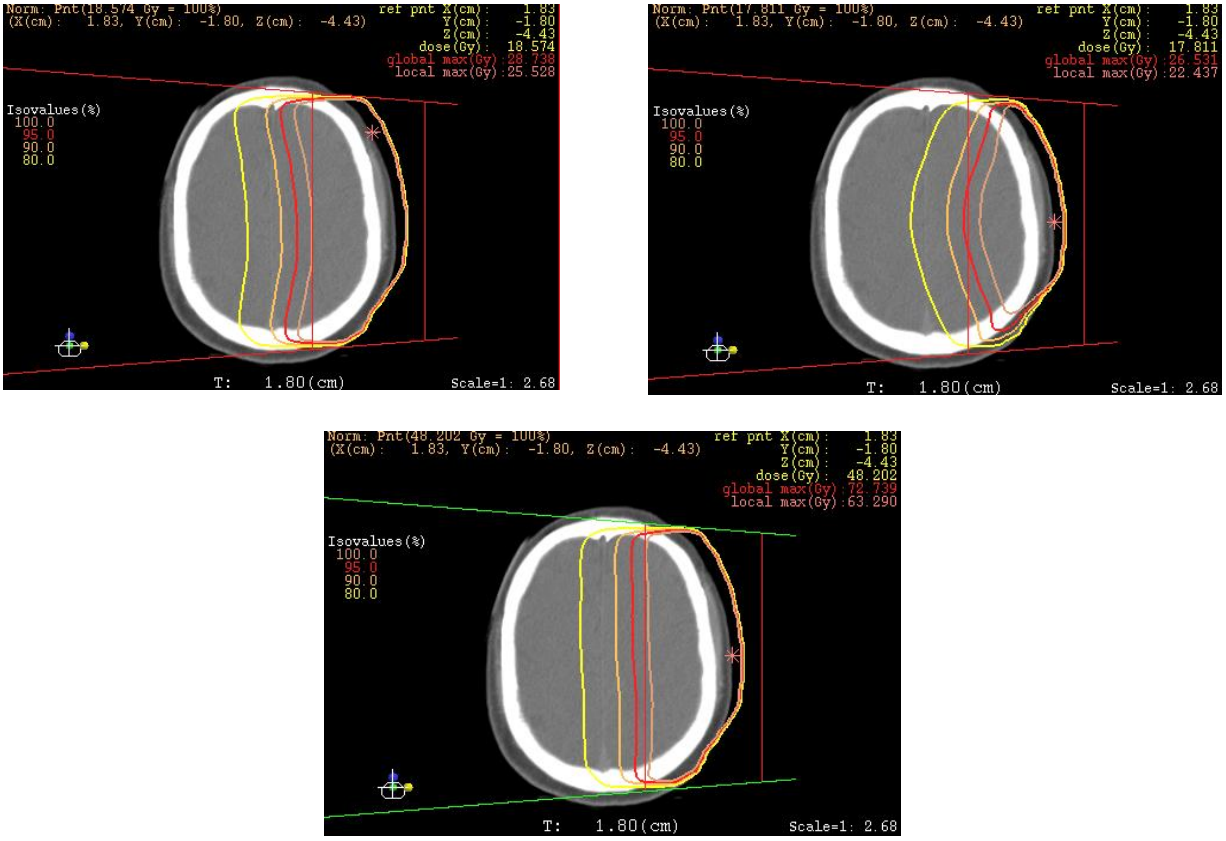

(c)

Figure 5.5. (a) Whole brain radiotherapy with conventional beams tends to produce hotspots. The addition of the FFF beam in (b) gives an overall distribution that is much more even in dose (c).

One of the most commonly used conventional planning techniques is the use of angled wedged pairs as seen in figure 5.6. Although the wedges act to even out the dose distribution to produce a box shape, it also generally produces two hotspots under the thin parts of the wedges. For the 10x10cm^2 beams shown these hotspots are at 105% and this value is seen to increase as the field size increases. Whilst these values are acceptable within the +7/-5% ICRU recommendations they are obviously not ideal, especially since they occur away from the centre of the tumour. If hotspots

are to exist then it is preferable for them to be within the tumour itself, away from surrounding normal (dose limiting) tissues.

By simply substituting these for FFF beams the hotspot drops to only 101% and target coverage is maintained. This effect could obviously be achieved by other means (e.g. by IMRT, or the addition of a lateral beam) but this achieves the same result with no further complications in technique.

(a) 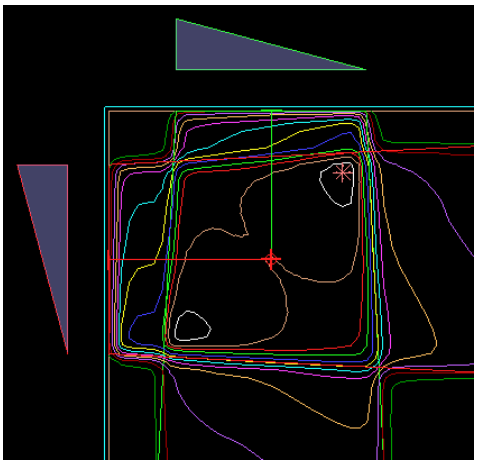 (b) 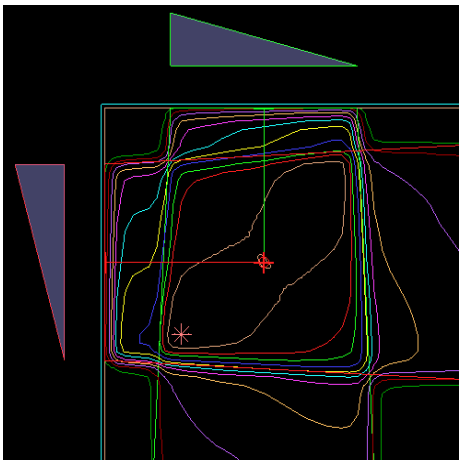

Figure 5.6. Comparison of plans for an angled wedged pair arrangement with 10x10cm² beams. The conventional plan (a) exhibits hotspots of 5% compared to the plan with unflattened beams (b) in which the forward peak of the radiation beam 'fills-in' the dose to the beam centre.

Unflattened wedges retain the characteristic shape of wedged fields, albeit with a more rounded profile. This is useful as many wedge applications occur in situations where the body is curved (such as the head & neck or breast) and/or at shallow depth (<10cm). Under these conditions the beam is *over-flattened* by the flattening filter producing horns (figure 5.7), leading to hotspots at the beam edge. The use of an unflattened wedge reduces the dose at the periphery, evening out the dose distribution.

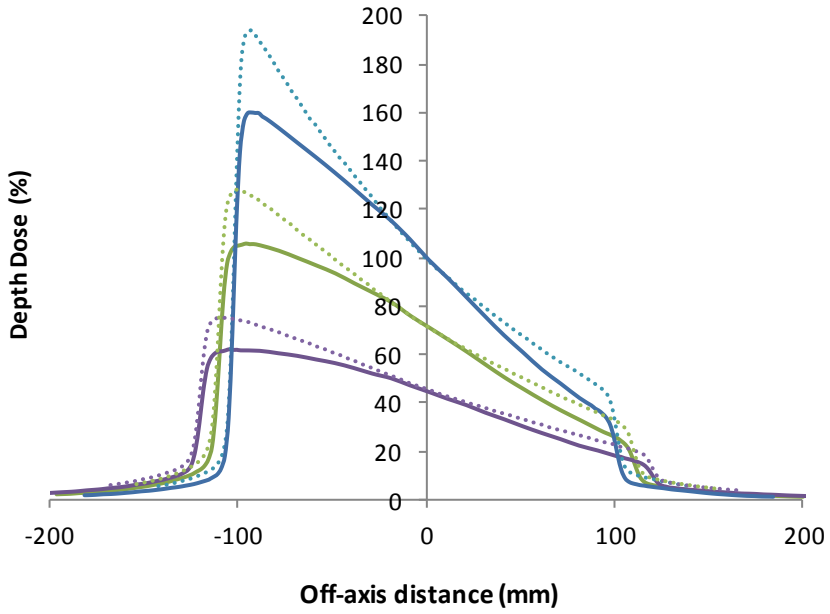

Figure 5.7. Comparison of measured wedge profiles for a 20x20cm² field, normalised at d_{max}. Profile depths are at 15, 50 and 100mm.

Figure 5.8 shows the results of increasing field size on an angled wedged pair applied to a phantom. As the field size increase so does the size of the hotspot. The FFF beams act to counteract this by filling in the dose to the centre of the target.

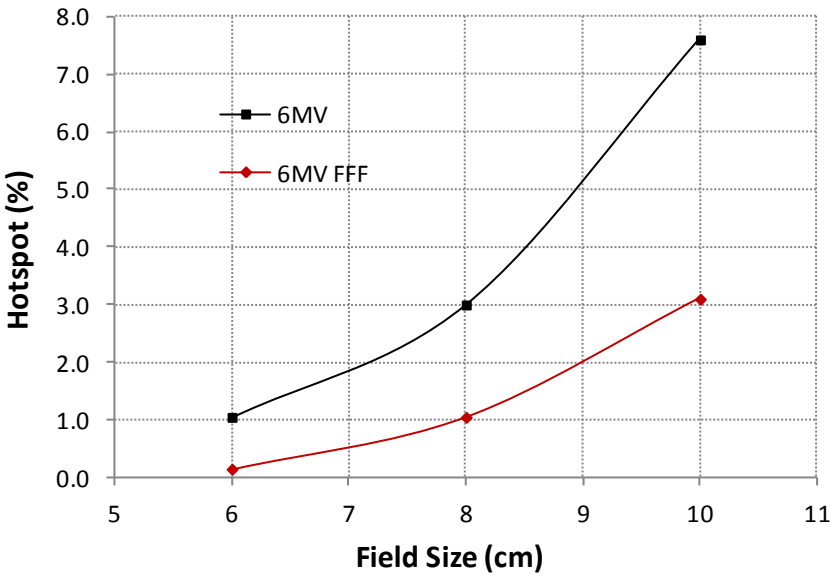

Figure 5.8. Graph depicting the increasing value of the planning hotspot with increasing field size for a wedged-pair distribution.

Another interesting situation is the half-beam block which, for a FFF beam, is seen to produce a wedge-shaped distribution. Again this wedge angle can be modified by altering the relative weighting of flattened to unflattened beams. The shape of the wedge is like a half cone, falling off in all directions from the central value (figure 5.9).

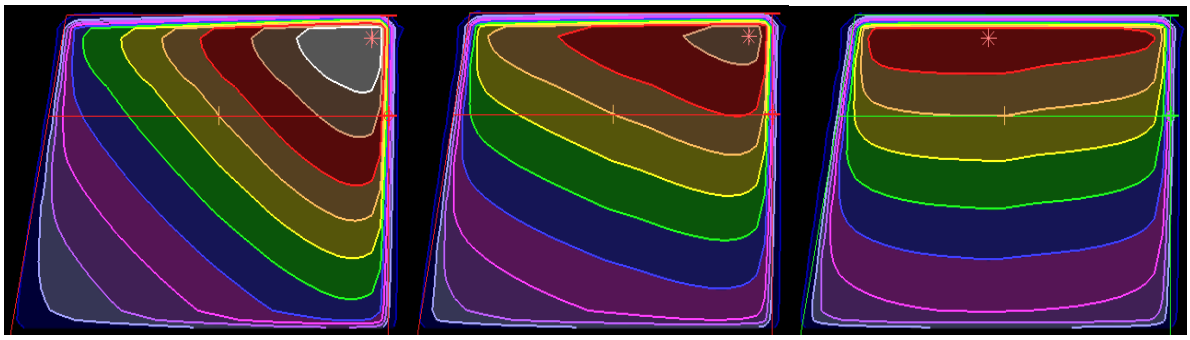

Figure 5.9. A half-beam blocked FFF beam produces a dose distribution similar to that of a conventional wedged beam. By changing the relative weights of the FFF and 6MV beams it is possible to create a 'wedge' angle between these two extremes.

The addition of a conventional flattened beam can again be used to modify this 'wedge' angle anywhere between the maximum (fully FFF) and minimum (fully flattened) by changing the relative weights of each beam. A three-quarter beam block produces a field that slopes from one diagonal to the other i.e. that is wedged in two directions at the same time.

5.3 Breast planning

Breast planning has been traditionally performed in a relatively simple manor using tangential wedged fields but has undergone a revolution in recent years with the advent of forward-, inverse- and hybrid planning techniques. Hotspots of 10-15% in

the dose distributions are not untypical and are located at the superior and inferior portions of the breast where the entrance-exit distance of the tangential beams is significantly shorter than on the central plane (figure 5.10). This is a direct consequence of using flat radiation fields on such a curved target region.

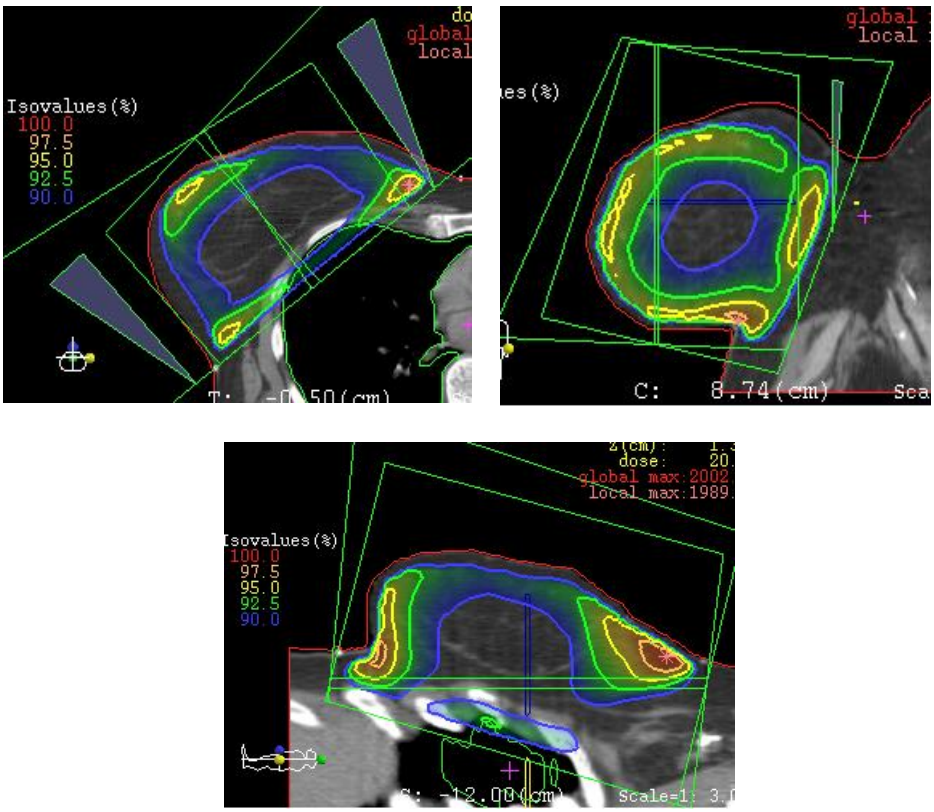

Figure 5.10. A typical breast plan highlighting the hotspots seen in a conventional plan.

To cover the entire volume uniformly a plan really needs to incorporate forward/inverse planning techniques or the use of custom made tissue compensators. The unflattened beam can be used to boost the dose to this central region, evening out the dose across the target volume with no further complication in technique (figure 5.11). The degree of boosting can be tailored by the relative weighting of flat and unflattened beams.

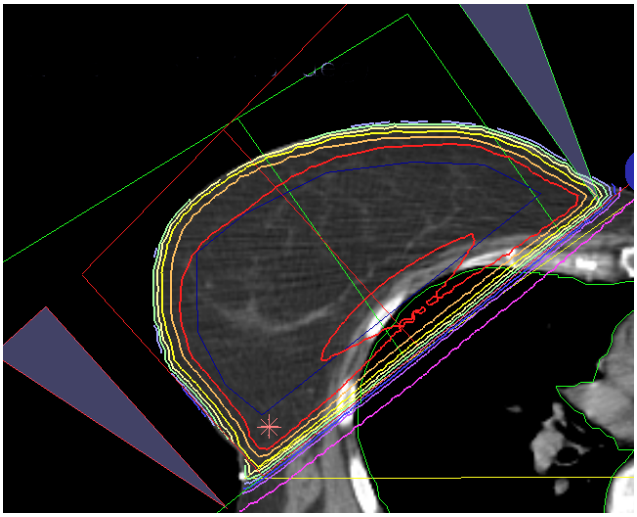

Figure 5.11. By combining the conventional plan with a FFF beam the central region can be boosted (without further field shaping) to produce an even dose distribution.

5.4 Lung planning

In general small beams are used when planning treatments for lung tumours, with the main objective being to treat the tumour without compromising lung function. Figure 5.12 shows a comparison of plans for a typical lung case. No real differences are seen in the dose distribution except for small variations above 90-95% of the prescription dose. No real gains are seen in planning with un-flattened beams, but a significant benefit may come from the increased dose rate and associated benefits to gated breathing; a doubling in dose rate obviously allows the treatment to be performed in half the time.

(a) 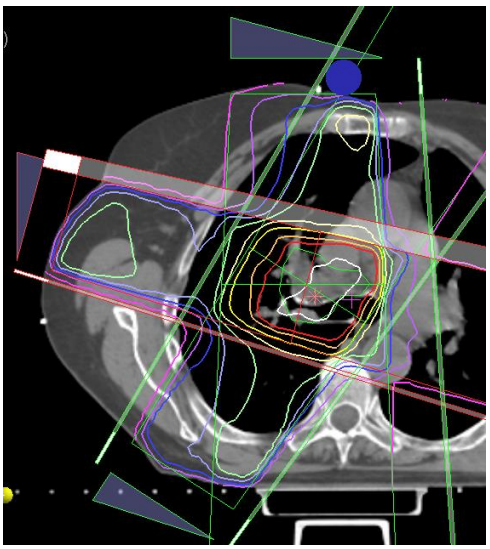 (b) 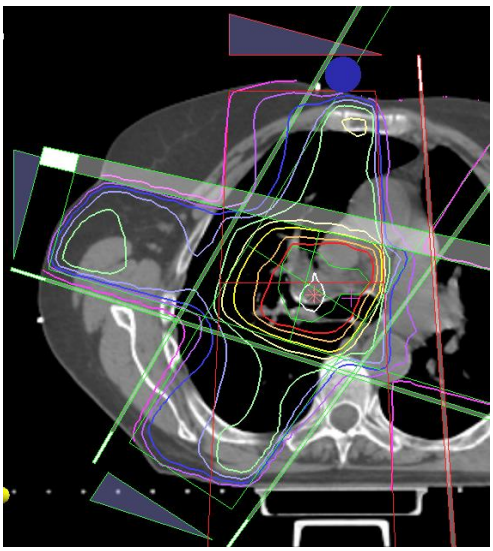

Figure 5.12. No major differences are seen in the plans produced (a) with and (b) without the flattening filter in place except in the central target region.

5.5 Stereotactic radiosurgery

It has already been shown (chapter 4) that the flattening filter has very little effect on beam profiles for small fields (i.e. <5cm²). For these beams the flattening filter is essentially an unnecessary component.

To test the FFF beam model a series of clinically accepted patient plans were re-calculated with the FFF model. Three plans were selected: an acoustic neuroma, a two lesion brain metastisis and an ateriovenous malformation (AVM). BrainLab's BrainSCAN version 5.31 (BrainLAB, AG, Germany) was used to generate a treatment plan using a Clarkson dose algorithm.

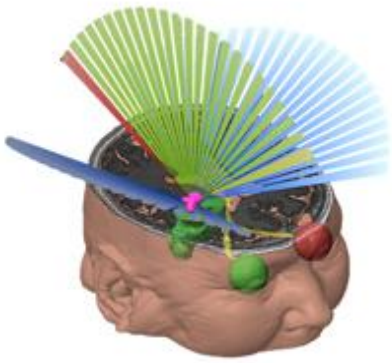

Figure 5.13. Typical beam arrangement for SRS plans designed with non-opposing beams so that the entrance and exit doses do not overlap.

The acoustic neuroma plan required 2 isocentres to cover the 2.42cc PTV. One isocentre used a 20mm collimator of 4 arcs (100^{o}, 100^{o}, 85^{o}, and 100^{o}) and the second used a 10mm collimator with three 100^{o} arcs (figure 5.13). The dose to the lesion (2.42cc), brainstem (14.31cc) and normal brain (3005.58cc) were assessed. The number of arcs and monitor units required for each plan are presented in table 5.1.

Table 5.1. Monitor units required to deliver each of the SRS plans for the cases indicated.

Plan	Arcs	6MV	6MV FFF
Acoustic Neuroma	7	3703	3715 (+0.3%)
2 Metastasis	9	6105	6091 (-0.2%)
AVM	12	9971	10026 (+0.6%)

No significant changes in the number of monitor units needed to deliver the plans are seen. The treatment plans show very little effect when switching to the FFF beam model, as would be expected as the flattening filter has no real effect at small field sizes (figure 5.14). The dose coverage and dose volume histograms for the targets remain unchanged in each case; however additional tissue sparing is seen for brainstem and normal brain for FFF. The most significant differences were observed for the low isodoses. These effects are studied further in chapter 7.

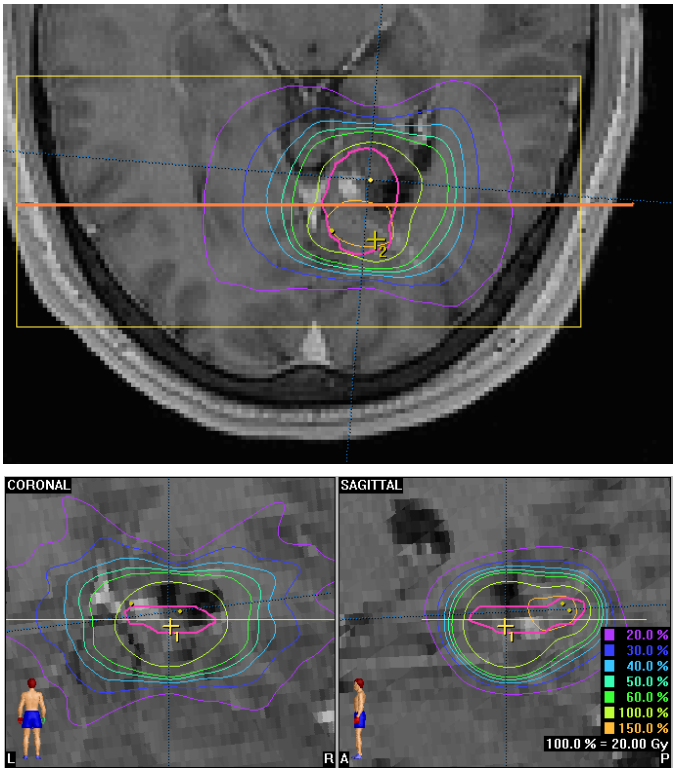

Figure 5.14. Axial, sagital and coronal sections through an ateriovenous malformation (AVM) (6MV FFF plan).

5.6 IMRT planning

Studies have shown that IMRT plans can be successfully generated with FFF beam models to produce usable plans but with an increase in the number of segments and monitor units needed. These studies, however, used the beam energy as it exits the machine (4MV Varian (Vassiliev *et al* 2006), 5MV Elekta (Fu *et al* 2004) so any differences observed could simply be due to this change in energy rather than any inherent property of unflattened beams. Critically in this work the beam energy has been raised back to the nominal energy by matching D_{10} (67.5%) and $QI/TPR_{20/10}$ (0.675). By raising the beam energy back to nominal values any differences in treatment plans can be correctly evaluated without reference to changing beam energy.

5.6.1 XiO IMRT

A series of 11 paediatric head and neck patients were outlined by a consultant paediatric oncologist for IMRT planning. For each case a plan has been produced using the conventional IMRT beam model in the XiO TPS. When a set of dose constraints had been found to produce an optimised plan they were used in turn to produce conventional and unflattened treatment plans (thus removing any inter-planner or inter-plan bias from the system). Plans have been evaluated for target coverage using the criteria in table 5.2.

Table 5.2. Summary of dosimetric parameters used for IMRT plan evaluation.

V_{90}	Volume of target (%) receiving 90% of prescribed dose
V_{95}	Volume of target (%) receiving 95% of prescribed dose
V_{100}	Volume of target (%) receiving 100% of prescribed dose
V_{107}	Volume of target (%) receiving 107% of prescribed dose
D_2	Dose to 2% of volume
D_{98}	Dose to 98% of target volume
HI	Homogeneity index (D_2-D_{98}/Dose prescribed)*100
V_{PTV}	Volume of PTV
CI	Conformity Index V_{95}/TV

Dose priorities changed for each case but in general the PTV was given priority and doses to critical structure lowered until the PTV dose started to become compromised. The number of beams and their gantry angles remained the same in each case (generally 5 equally spaced fields) unless significant differences were observed between plans or planning objectives not met. There should, of course, be no reason why IMRT without the flattening filter could be not be used as long as the beam is accurately modelled within the TPS and the segmentation process takes this into account.

Table 5.3. Target coverage for each of the indicated IMRT plans.

	Plan1		**Plan2**		**Plan3**		**Plan4**		**Plan5**	
	6MV	**6MV FFF**	**6MV**	**6MV FFF**	**6MV**	**6MV FFF**	**6MV**	**6MV FFF**	**6MV**	**6MV FFF**
V_{90}	99.1	99.1	98.1	98.3	99.8	99.6	99.4	99.5	98.6	98.9
V_{95}	96.4	95.7	91.3	91.9	97.9	96.6	93.3	94.2	90.5	90.9
V_{100}	50	50	50	50	50	50	50	50	50	50
V_{107}	0.05	0	1.2	0.7	0	0.5	0.1	0.1	0	0
D_2	56.2	56.1	57.3	57.1	56.0	56.8	56.1	56.2	56.1	56.4
D_{98}	50.5	50.3	48.6	48.9	51.2	50.7	50.1	50.2	49.2	49.3
HI	11.3	11.5	17.3	16.3	9.5	12.1	11.9	11.9	13.7	14.1
V_{PTV}	310	310	362.9	362.9	60.2	60.2	431.6	431.6	471.9	471.9
CI	0.964	0.957	0.913	0.919	0.979	0.966	0.933	0.942	0.905	0.909

Table 5.4. Organ at risk sparing for each of the indicated IMRT plans.

	Plan1		**Plan2**		**Plan3**		**Plan4**		**Plan5**	
	6MV	**6MV FFF**	**6MV**	**6MV FFF**	**6MV**	**6MV FFF**	**6MV**	**6MV FFF**	**6MV**	**6MV FFF**
Lt Eye	27.9	28.6	-	-	7.9	6.3	44.0	43.5	12.5	12.4
Rt Eye	30.7	30.2	41.8	42.1	7.7	6.6	51.6	52.1	14.0	13.4
Optic Chiasm	-	-	-	-	23.5	21.1	-	-	-	-
Brainstem	-	-	53.9	53.9	-	-	55.7	55.5	-	-
Spinal cord	-	-	40.8	41.3	-	-	-	-	-	-
Lt cochlea	-	-	38.3	39.9	-	-	-	-	41.9	41.7
Rt cochlea	-	-	-	-	-	-	-	-	41.1	41.2
Pituitary	54.3	53.2	-	-	-	-	-	-	-	-

Table 5.5. Segments and monitor units required to deliver identical plans by different each method.

Case	No. fields	6MV		6MV FFF		Ratio of segments	Ratio of MUs
		Segments	MUs	Segments	MUs		
Plan1	5	123	22856	111	26327	0.90	1.15
Plan2	7	168	24808	162	24502	0.96	0.99
Plan3	5	103	18239	103	20363	1.00	1.12
Plan4	7	164	22258	161	22528	0.98	1.01
Plan5	5	90	18681	90	20291	1.00	1.09
Plan6	5	121	25516	118	25820	0.98	1.01
Plan7	5	70	15300	71	14798	1.01	0.97
Plan8	5	61	13928	56	13883	0.92	1.00
Plan9	5	94	16884	95	18762	1.01	1.11
Plan10	5	86	14883	87	15992	1.01	1.07
Plan11	5	100	26452	108	27477	1.08	1.04
Plan12	5	54	12557	58	13453	1.07	1.07
Plan13	5	86	17624	85	17924	0.99	1.02
					Average	**0.99**	**1.05**

Conventional 5-field IMRT 6MV FFF 5-field IMRT

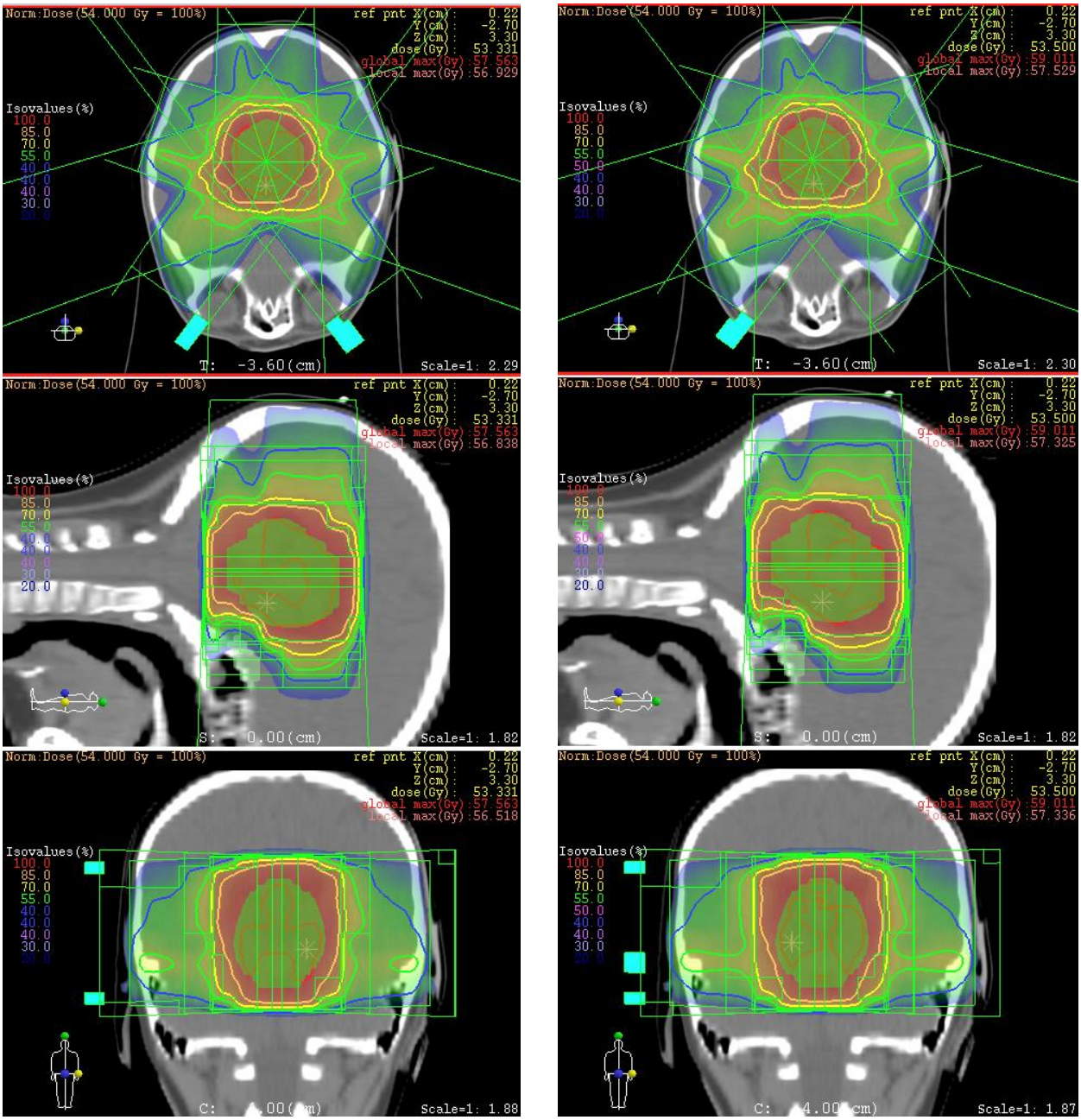

Figure 5.15. Transverse, sagital and coronal slices through the target region showing comparison between techniques conventional IMRT a) and IMRT with flattening filter removed, b) for a midbrain astrocytoma.

For all planned cases the target coverage, homogeneity and OAR doses both with and without the flattening filter were the same (within statistical bounds). Figures 5.14 shows slices through the target centre for one of the cases to illustrate the

similarity of the plans. Tables 5.3 and 5.4 list the target coverage, homogeneity and OAR doses for 5 planned cases with and without the flattening filter. Table 5.5 compares the number of segments and MUs required to deliver the same dose distribution with the two techniques.

The average ratio for the number of segments required for the 5 plans was 0.99 and the MU ratio is 1.05 over 11 patients (13 plans). Where large differences are seen between conventional and unflattened delivery in terms of segments or MU it can be seen that moving to a 7-field plan brings these back in line with each other.

There is therefore no significant effect on target coverage, OAR sparing, segments or monitor units required to deliver IMRT with unflattened beams compared to conventional use for these plans. The question remains as to whether the beams are more deliverable and simpler to calculate etc.

5.6.2 Monaco IMRT

In order to expose the FFF model to a range of conditions and test the beam model and the accuracy of the dose calculation, a series of treatments with increasing complexity and treatment volume were planned. These sites consisted of skull base, oesophagus, prostate, and head and neck cases. To test the model under the extreme influence of the unflattened beams, the isocentre for the prostate and head and neck plans were placed asymmetrically so that large parts of the fields were exposed to the off-axis region of the beam.

For each plan, a set of constraints were found to give an optimal distribution. The plans were then re-optimised using the FFF beam model and adapted as necessary to fulfil the dose constraints.

Table 5.6. Number of segments and monitor units needed for each treatment plan, and the relative increase in each necessary to deliver the FFF plans.

	PTV Volume (cm^3)	**Segments**			**Monitor Units**		
		6MV	**FFF**	**% Diff**	**6MV**	**FFF**	**% Diff**
Skull Base	23.2	20	21	+5.0	416	446	+7.2
Esophagus	555.4	64	67	+4.7	785	931	+18.6
Prostate	804.5	66	68	+3.0	828	951	+14.9
Head & Neck	918.7	168	183	+8.9	1343	1682	+25.2

As the volume of the tumour (treatment length) and complexity of the plan increase there is a tendency to see an under-dosage in regions far from the central axis, which is seen as a sloping shoulder on the DVH curve. It is possible to compensate for this by further penalizing cold spots within the tumour, and in the Monaco TPS this can be achieved by increasing the cell sensitivity (α) of the tumour or adding a quadratic underdose penalty. This acts to maintain plan quality but brings about an increase in both the number of segments and monitor units needed to deliver the plan. It can be seen from Table 5.6 that as the treatment volume and plan complexity increase there is a corresponding increase in the number of segments and MU needed to deliver the FFF plans. Figure 5.16a shows a colour-wash dose distribution on sagital and coronal CT slices through the tumour for a head and neck

FFF IMRT plan. The dose volume histogram (figure 5.16b) indicates that the plans are equivalent in terms of both PTV coverage and organ at risk sparing.

a)

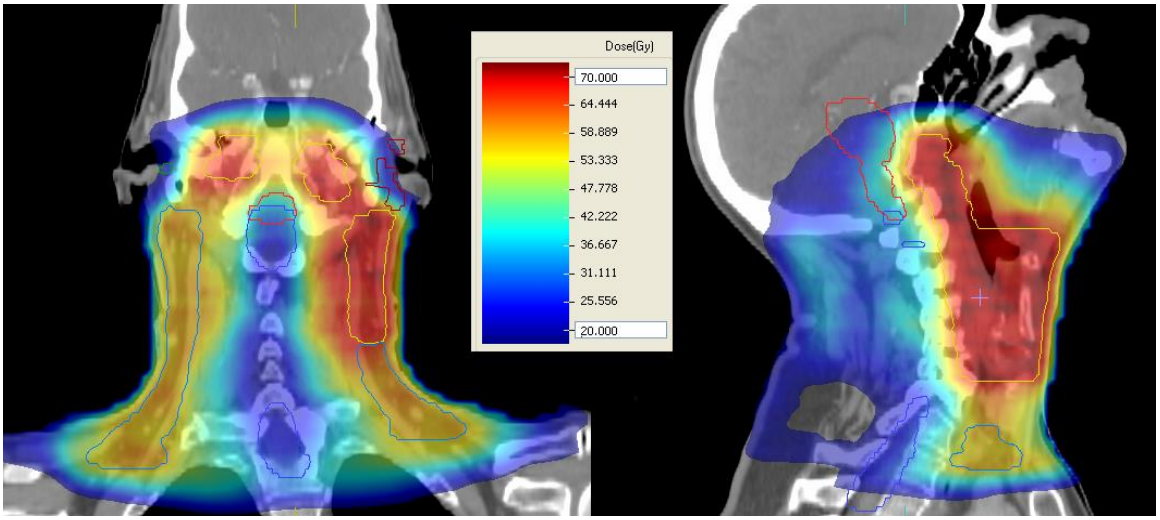

b)

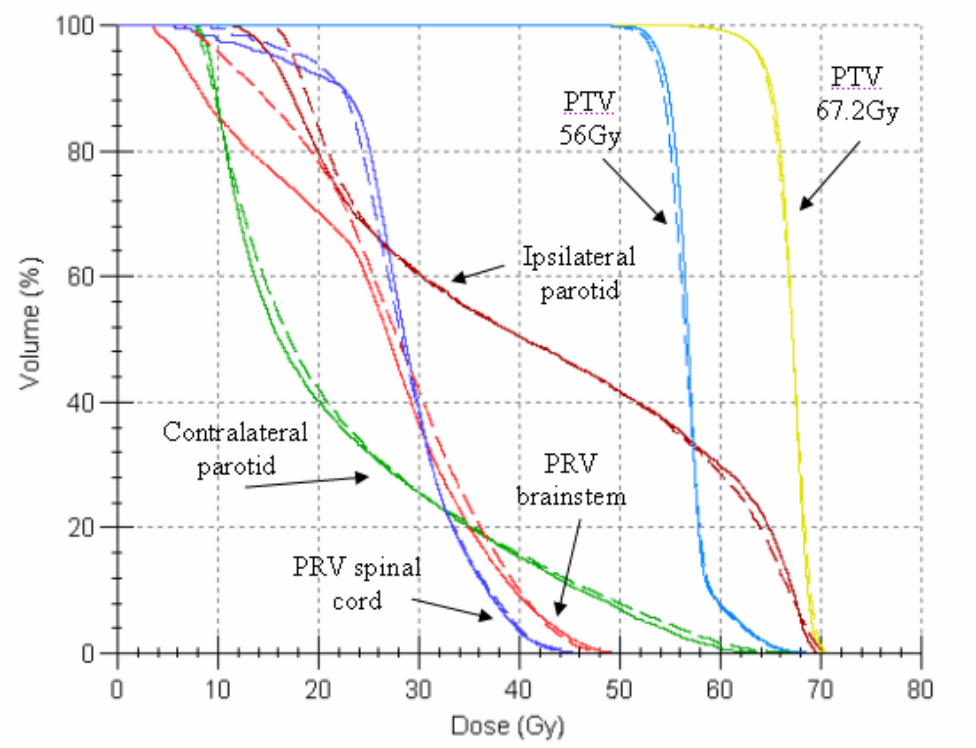

Figure 5.16. Beam setup for IMRT planning of a head and neck case showing sagital and coronal colorwash maps (a) and dose volume histogram (b). The FFF beam is displayed as the dotted line, 6MV solid.

It has been observed that as the field sizes needed for planning increase then so do the number of MU required to deliver these plans; this is a natural consequence of the FFF beam profile since it will require longer beam on times to deliver doses off-axis. The complexity of the plan is also seen to increase the number of segments required to treat the FFF plans compared to the conventional IMRT plans if plan quality is to be maintained. This may be more specifically related to the fact that segmentation algorithms are optimized for flattened rather than unflattened beam profiles. Commercial planning systems do not currently consider the non-flat beam profile during optimization. This is discussed in further detail in chapters 6 and 8.

5.7 VMAT

5.7.1 Prostate

Retrospective studies (e.g. Zelefsky *et al* 2001 & 2002) show that IMRT can provide lower treatment toxicity than 3DCRT for localised prostate cancer without compromising tumour control. VMAT is now used routinely in many centres around the world as a technique to provide fast IMRT delivery using either single or multiple arcs (see Appendix A), resulting in significantly reduced delivery times.

A study was carried out to retrospectively compare standard 3DCRT with IMRT and VMAT techniques using conventional 6MV and 6MV FFF beams. Five patients were randomly selected and re-planned and assessed according to departmental protocol. The PTV coverage for each plan is summarised in table 5.7, and the doses to organs at risk presented in table 5.8.

Significant differences (determined by a 2-tailed, paired T test) were seen for a number of dose parameters, as noted in each table. On moving to modulated techniques extra sparing of the bladder was possible and a reduction in the mean and

maximum doses received by the hips. No significant differences were observed between 6MV and 6MV FFF plans. Comparing VMAT plans the only parameter that reached significance was the (near-) maximum dose (D2) delivered to PTV2, but in reality, although significant, this only amounts to a dose difference of 0.1Gy. IMRT and VMAT are therefore of very similar quality for 6MV flattened or unflattened beams.

As expected, significantly more MU are required to deliver IMRT compared to 3DCRT (table 5.9). For the 6MV beam the average increase was 38.0%, and for the FFF beams this increased to 66% representing a 20.2% overall increase in MU in moving from conventional to FFF delivery. This is expected because of the shape of beam and the necessity to deliver dose off-axis. There is also a much larger *variation* in the number of MU required for FFF delivery compared to standard IMRT, but no increase in the number of segments required or the delivery time.

For VMAT delivery further MU are needed, with an extra 15.2% for 6MV and 3.4% for FFF compared to IMRT. There is also a reduction in delivery time transferring from IMRT to VMAT of approx. 54% using either technique. The FFF beam model does not include the dose rate enhancements that will be available on the clinical machine, both models delivering dose at a maximum of 600 MU/min, so a shorter delivery time will be expected for FFF in reality.

Figure 5.17 shows a screenshot from the Monaco TPS to illustrate the beam arrangements used for the treatment planning techniques. The VMAT plans are optimised over a reduced gantry rotation to avoid entering through the treatment couch as this is not currently modelled to sufficient accuracy within the TPS.

Table 5.7. Summary of PTV coverage and OAR doses for prostate plans optimised by 3DCRT, IMRT and VMAT for standard and FFF delivery. Numbers in brackets are ±1SD.

			IMRT		VMAT		Significance
Organ	**Parameter**	**3DCRT**	**6MV**	**6MV FFF**	**6MV**	**6MV FFF**	
PTV3	**D_{99}**	71.1 (0.5)	71.2 (0.2)	71.0 (0.2)	71.1 (0.3)	71.1 (0.2)	
140.2cc (±133.8cc)	**D_{95}**	72.0 (0.6)	72.0 (0.2)	71.9 (0.2)	72.1 (0.1)	72.0 (0.1)	
	D_{50}	74.1 (0.3)	74.0 (0.0)	74.0 (0.0)	74.0 (0.0)	74.0 (0.0)	
	D_{2}	75.9 (0.5)	76.5 (0.2)	76.5 (0.2)	76.5 (0.1)	76.6 (0.1)	b, e,
PTV2	**D_{99}**	68.3 (0.4)	68.6 (0.1)	68.5 (0.5)	69.0 (0.3)	68.3 (0.3)	b, d, f
211.4 (±172.5)	**D_{50}**	73.6 (0.2)	73.3 (0.2)	73.4 (0.1)	73.4 (0.2)	73.3 (0.2)	
PTV1	**D_{99}**	58.9 (3.1)	59.9 (1.3)	59.3 (1.8)	60.0 (2.1)	59.6 (2.1)	
292.0 (±173.4)	**D_{50}**	71.5 (2.2)	71.6 (2.0)	71.6 (2.0)	71.6 (2.1)	71.5 (2.2)	

a = 3DCRT vs. IMRT, b = 3DCRT vs. 6MV VMAT, c = 6MV IMRT vs. 6MV FFF IMRT, d = 6MV IMRT vs. 6MV VMAT, e = 6MV FFF IMRT vs. 6MV FFF VMAT, f = 6MV VMAT vs. 6MV FFF VMAT.

Table 5.8. Summary OAR doses for prostate plans optimised by 3DCRT, IMRT and VMAT for standard and FFF delivery. Numbers in brackets are ±1SD.

			IMRT		VMAT		Significance
Organ	**Parameter**	**3DCRT**	**6MV**	**6MV FFF**	**6MV**	**6MV FFF**	
Rectum	**V_{50}**	50.5 (9.0)	48.1 (6.6)	47.9 (5.8)	46.6 (8.0)	47.5 (8.0)	
67.2 (±12.8)	**V_{60}**	32.2 (6.4)	30.9 (6.8)	30.4 (6.7)	31.3 (8.0)	31.5 (6.9)	
	V_{65}	17.2 (2.0)	16.7 (2.7)	16.8 (2.2)	21.4 (9.2)	21.2 (8.3)	
	V_{70}	5.6 (2.0)	7.7 (2.4)	7.2 (2.1)	13.4 (11.1)	12.6 (11.0)	
	V_{74}	0.2 (0.4)	2.5 (4.3)	0.5 (0.4)	6.4 (12.6)	6.3 (12.4)	b,
Bladder	**V_{50}**	37.4 (11.6)	32.4 (9.7)	32.4 (9.8)	34.4 (8.2)	34.7 (8.6)	a, b, d, e
229.1 (±109.9)	**V_{60}**	26.5 (10.8)	23.4 (9.0)	23.6 (9.1)	25.0 (81.)	25.0 (8.4)	a, b,
	V_{74}	2.4 (1.0)	3.0 (2.3)	3.5 (2.8)	6.2 (5.5)	6.1 (5.6)	
Lt Hip	**Max**	46.9 (3.9)	42.2 (10.3)	42.9 (9.3)	40.1 (4.1)	40.8 (4.0)	b,
59.0 (±4.6)	**Mean**	35.4 (13.3)	27.3 (12.4)	27.2 (12.3)	23.2 (6.8)	23.3 (7.0)	a, b,
Rt Hip	**Max**	47.6 (1.9)	46.8 (6.1)	47.2 (4.5)	39.0 (7.7)	37.6 (7.1)	e
62.2 (±8.2)	**Mean**	36.2 (10.5)	31.9 (5.4)	31.6 (4.7)	21.8 (5.3)	21.9 (6.4)	b, d

a = 3DCRT vs. IMRT, b = 3DCRT vs. 6MV VMAT, c = 6MV IMRT vs. 6MV FFF IMRT, d = 6MV IMRT vs. 6MV VMAT, e = 6MV FFF IMRT vs. 6MV FFF VMAT, f = 6MV VMAT vs. 6MV FFF VMAT.

Figure 5.17. Sample screenshot from Monaco showing prostate plans for three treatment techniques. Top left: 5 field IMRT, bottom left: VMAT, bottom right: field-in-field 3DCRT (XiO). In the top right is DVH comparing the PTV coverage and OAR sparing of each technique. 74Gy in 37# prescribed.

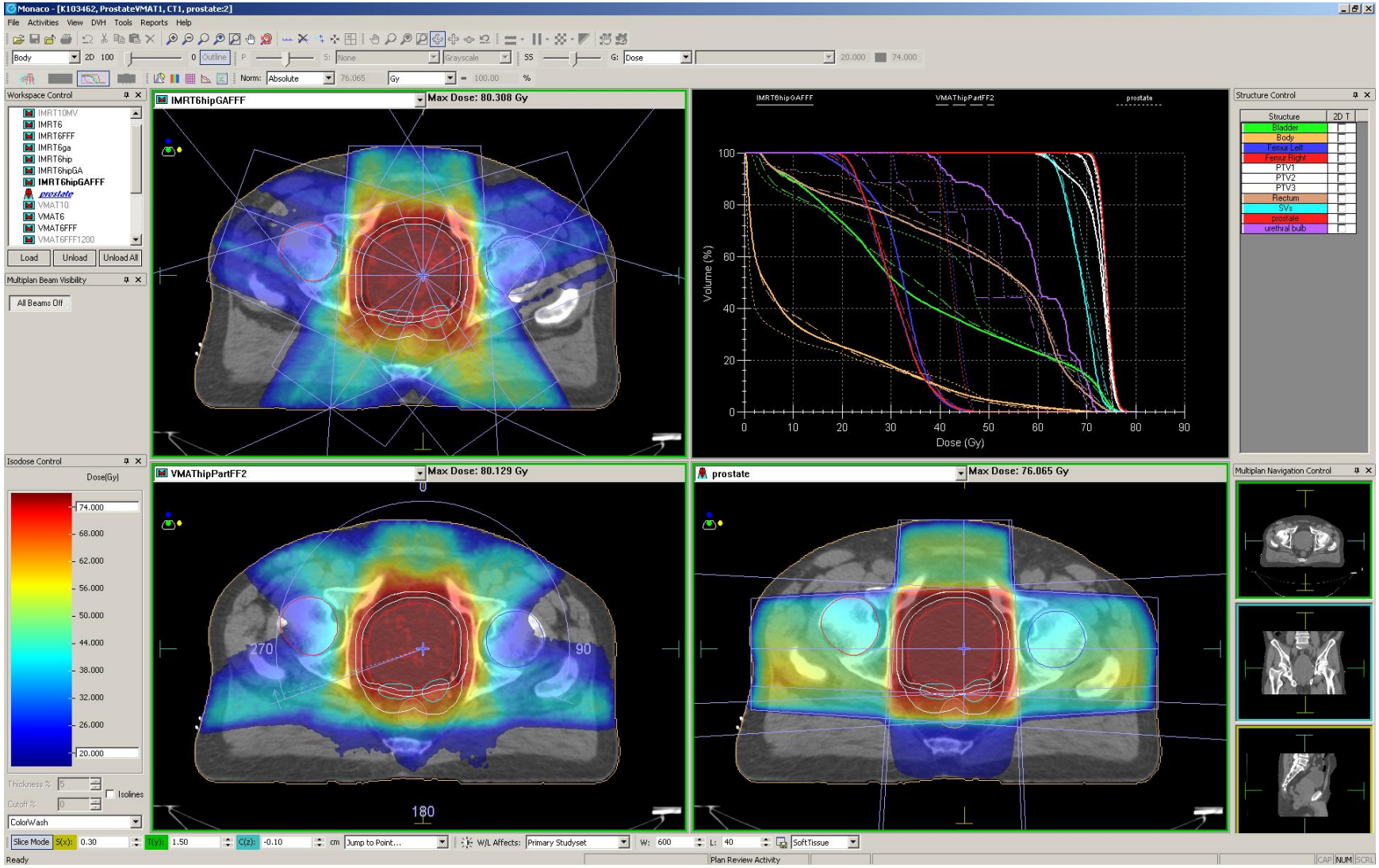

Table 5.9. Number of MU, segments and estimated time to deliver prostate radiotherapy by 3DCRT, IMRT and VMAT (averaged over 5 patients). Numbers in brackets are ±1SD.

	MU	Number of Segments	Time (s)
3DCRT	526 (35.0) a, b	6	-
IMRT	726 (80.3) a, c, d	56.8 (8.9) d	300 (32.1) d
IMRTFFF	873 (180.2) c	55.8 (13.8) e	315 (47,.2) e
VMAT	836 (55.8) b, f	101.6 (14.8) d, e	139 (7.7) d
VMATFFF	903 (63.1) f	95.8 (2.2)	142 (7.0) e

a = 3DCRT vs. IMRT, b = 3DCRT vs. 6MV VMAT, c = 6MV IMRT vs. 6MV FFF IMRT, d = 6MV IMRT vs. 6MV VMAT, e = 6MV FFF IMRT vs. 6MV FFF VMAT, f = 6MV VMAT vs. 6MV FFF VMAT.

5.7.2 SBRT / SABR

Stereotactic body radiotherapy is intimately tied to image-guidance, without which it would not be possible to deliver the high doses of radiation with the necessary precision. SBRT was first developed at the Karolinska Institute in the 1990s along the same lines as intra-cranial radiosurgery. Multiple beams are directed towards the target to deliver a high radiation dose, sparing the surrounding critical organs, typically heart, spinal cord, oesophagus, and the lungs themselves. Recently SBRT has been renamed to SABR (stereotactic ablative radiotherapy) to standardise the naming used across countries. SABR techniques are used most often in the treatment of lung cancers where local control rates of >95% are seen for peripheral stage 1 non small cell lung cancer (NSCLC) (Timmerman *et al* 2003).

A range of planning techniques can be used for SABR treatments including 3DCRT, IMRT and VMAT. Because of the small field size and relatively low modulation involved in these plans it is desirable to use VMAT as this should be able to deliver the radiation in the shortest time period. In fact, because of the high dose per fractions used the use of FFF should significantly reduce treatment times when operating in high dose-rate mode.

A short planning study was undertaken to ensure the plan quality of FFF VMAT plans against the standard technique used in our centre (3DCRT) and against conventional VMAT at 6MV. Three patients treated under SABR protocol were planned by each method and the target and OAR doses recording according to standard protocol. The data for these comparisons are reported in tables 5.10 and 5.11 below. Figures 5.18 and 5.19 show plan comparisons for Plan1 and Plan2 respectively.

There is a significant increase in the number of MU required to deliver FFF plans via VMAT compared to the standard beam (20.2%) which is much greater than for other series reported in the literature e.g. Zhang *et al* saw an increase of 8.7% for FFF VMAT delivery on the Varian TrueBeam accelerator. This difference is explained by the fact that the plans produced in this study have the beam isocentre not at the centre of the PTV, but at the centre of the body. This allows the patient to be set up in the middle of the couch allowing unrestricted rotation of the cone-beam CT unit for image-guidance (see figure 5.18). The tumour is then a considerable distance off-axis, requiring more MU for the FFF delivery.

Table 5.10. PTV coverage and OAR doses for 3 SABR lung cases. Each case has been planned with 3DCRT, 6MV VMAT and 6MV FFF VMAT as indicated.

	Volume (cc)	XiO	6MV	6MV FFF	Volume (cc)	XiO	6MV	6MV FFF	Volume (cc)	XiO	6MV	6MV FFF
Prescription		**Plan 1: 55Gy / 5#**				**Plan2: 60Gy / 8#**				**Plan 3: 55Gy / 5#**		
PTV	129.4				97.6				29.5			
D_{95}		55.2	55.0	55.0		60.1	60.0	60.0		55.31	55.0	55.0
D_{99}		52.9	52.3	52.3		56.5	57.5	57.5		52.9	54.1	54.2
1cc max		69.1	72.2	69.9		71.7	72.6	71.7		75.3	62.5	62.1
$V_{100}\%/V_{PTV}$		1.03	1.09	1.06		1.10	1.04	1.06		1.17	1.28	1.21
$V_{50}\%/V_{PTV}$		3.23	3.33	3.36		4.02	4.00	4.15		5.54	6.91	7.02
Max > 2cm		35.86	36.31	34.31		39.27	39.86	37.88		76.6	64.7	64
OAR												
$D_{0.01}$ Cord	62.7	20.95	20.3	19.5	79.3	11.1	7.8	5.4	74.3	6.7	9	9.7
$D_{0.1}$ Oesophagus	22.5	14.05	14.05	12.6	48.7	12.2	11.1	9	31.2	10.4	7	4.2
Heart 0.1	465.9	23.95	24.3	23.5	956.0	49.2	44.2	45	625.9	10.8	6.8	3.6
$D_{0.1}$ Trachea/Bronchus	31.7	26.2	28.6	26.2	37.4	6.75	14.6	14.6	61.6	12.5	9.4	11
V_{20} Lungs - GTV $_{exhale}$	4179.7	11.55	10.93	10.81	5957.9	6.35	6.31	6.9	5976.7	4.45	7.16	6.59

Table 5.11. MU, segments and delivery time for each of the plans in table 5.10.

	Plan 1			Plan 2			Plan 3			Average (±SD)		
	3DCRT	**6MV**	**FFF**	**3DCRT**	**6MV**	**FFF**	**3DCRT**	**6MV**	**FFF**	**XiO**	**6MV**	**FFF**
MU	1680.1	2743	3760	1086.5	2449	2916.4	2316.4	3602.7	4465.6	1694.3 (615.1)	2931.6 (599.5)	3714.0 (775.6)
Segments	7	72	85	8	91	91	7	85	98	7.3 (0.6)	82.7 (9.7)	91.3 (6.5)
Time (s)		288.1	376.3		251.2	296.4		428.8	499.6		322.7 (93.7)	390.8 (102.4)

Figure 5.18. Lung SABR plan (Plan1 of Table 5.10) showing the 7-field 3DCRT beam arrangement (top left), and single arc VMAT plans for 6MV (bottom left) and 6MV FFF (bottom right).

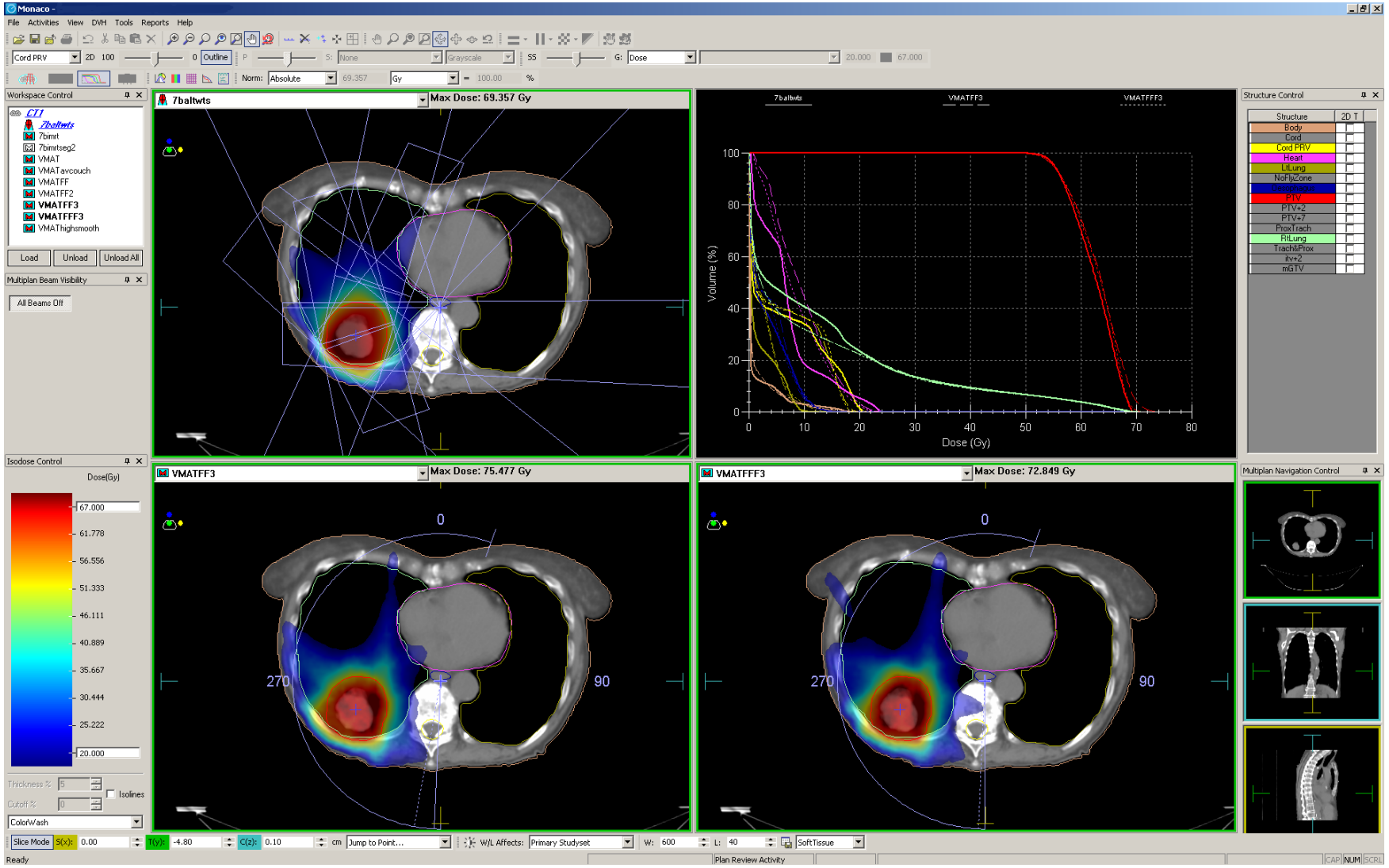

Figure 5.19. 6MV and 6MV FFF VMAT plans for Plan 3 showing a 3-arc beam arrangement to avoid the right arm.

5.8 Discussion and conclusions

Treatment without the flattening filter offers many potential benefits both in terms of treatment planning and machine operation. The main application for unflattened beams is seen to be for small-field applications where the beam profile is unaffected by FF removal, and for modulated techniques since the intensity profile can easily be modulated by the MLCs to alter the profile as necessary. Now that treatment machines are clinically available for unflattened delivery these FFF techniques should quickly gain popularity as a way of providing faster, more accurate dose delivery with whole body doses half that of current levels. The possibility of using non-flat beams in general planning only strengthens the case.

The literature covering the uses of FFF beams for 3DCRT is currently very limited with only one author dedicating any time to their properties (Kretschmer *et al* 2013).

Far from being unusable the forward peak could be very useful as this central axis boost is exactly what is needed under many treatment circumstances. An unflattened beam is, of course, not appropriate in all planning situations in much the same way as a wedge is not always appropriate. As with all treatment planning the choice of energy/wedge angle etc. is chosen according to the individual needs of the case at hand; the same reasoning should be applied here.

FFF VMAT techniques have now been studied for a variety of treatment sites (Nicolini *et al* 2012, Zwahlen *et al* 2012, Scorsetti *et al* 2011, Zhang *et al* 2011, Zhuang *et al* 2012, Alongi *et al* 2013) and found to produce plans of equivalent quality to those seen for standard flattened beams.

The greatest gain in moving towards FFF delivery comes from the increased dose rate and associated reductions in treatment time. Intra-fraction movement of the tumour and surrounding tissues is still an issue, even with daily image-guidance, so

reducing the time for delivery is still of great benefit. Reduced treatment times also aid throughput on the accelerator allowing more patients to be treated, and for the patient to be more comfortable. The potential of FFF to reduce scatter and leakage doses is also of importance and is discussed in chapter 7.

It is interesting to note that even though treatment planning systems are not yet fully optimised for FFF beams (see chapter 8) plan quality is still maintained between techniques. The variation in the number of MU required for VMAT delivery for FFF techniques (seen in table 5.9) might be indicative of this fact. Hopefully once these modifications take place further increases in plan quality, calculation accuracy and speed may be possible.

CHAPTER 6

IMRT VERIFICATION

In the previous chapters it was demonstrated that unflattened beams can be successfully modelled and used to create treatment plans for both conventional and intensity modulated treatments. It is a logical step to then assess the accuracy of the dose prediction against machine measurements. A key benefit of filter removal is the reduction in head scatter which could possibly lead to greater accuracy in dose calculation.

In this chapter we will discuss the verification of IMRT delivery on the linac for plans generated in the XiO and Monaco treatment planning systems.

Parts of this chapter have been published by the author (Cashmore *et al* 2011, Cashmore *et al* 2012).

6.1 Introduction

The key to any improvements in the accuracy of dose calculations for FFF beams originate in the reductions in head scatter, as discussed in previous chapters. The flattening filter adds further degrees of complexity to dose modelling by creating a significant source of extra-focal radiation and the need to model the changing energy

spectrum with off-axis position. This makes the small, complex, off-axis and often elongated fields used for IMRT delivery particularly problematic, leading to uncertainties in the dose calculation. The consequences of this are the need to perform patient specific quality assurance tests on IMRT plans before delivery to the patient (appendix A).

With a key source of extra-focal radiation removed both the magnitude and variation of head scatter with field size is reduced as discussed in chapters 2 and 3.

6.2 Head scatter predictions

To test the validity of these arguments a simple test was devised: a step-and-shoot IMRT plan for a head & neck treatment was delivered segment-by-segment in order to measure the head scatter component of each field and compare these against XiO predictions. The plans for each delivery mode were optimised independently to achieve the dose objectives using the XiO TPS. These were then transferred to the linac and measurements of head scatter made using a Farmer chamber (NE 2571) fitted with a 2mm brass cap. For each segment of a beam the chamber was moved to a suitable point to take a measurement of the Sc for that field. Head scatter measurements are presented relative to a 10x10cm^2 field and compared to the predictions from XiO.

Referring to figure 6.1 it is clear that for each of the FFF segments delivered the variation in head scatter is reduced compared to that seen for the standard 6MV beam. In each case the TPS predictions for Sc are also closer to the measurements for the FFF beam.

In figure 6.2 these results are plotted showing the difference between prediction and measurement for each segment. The mean error, represented by the horizontal lines, is reduced from 0.9% to 0.5% for FFF operation.

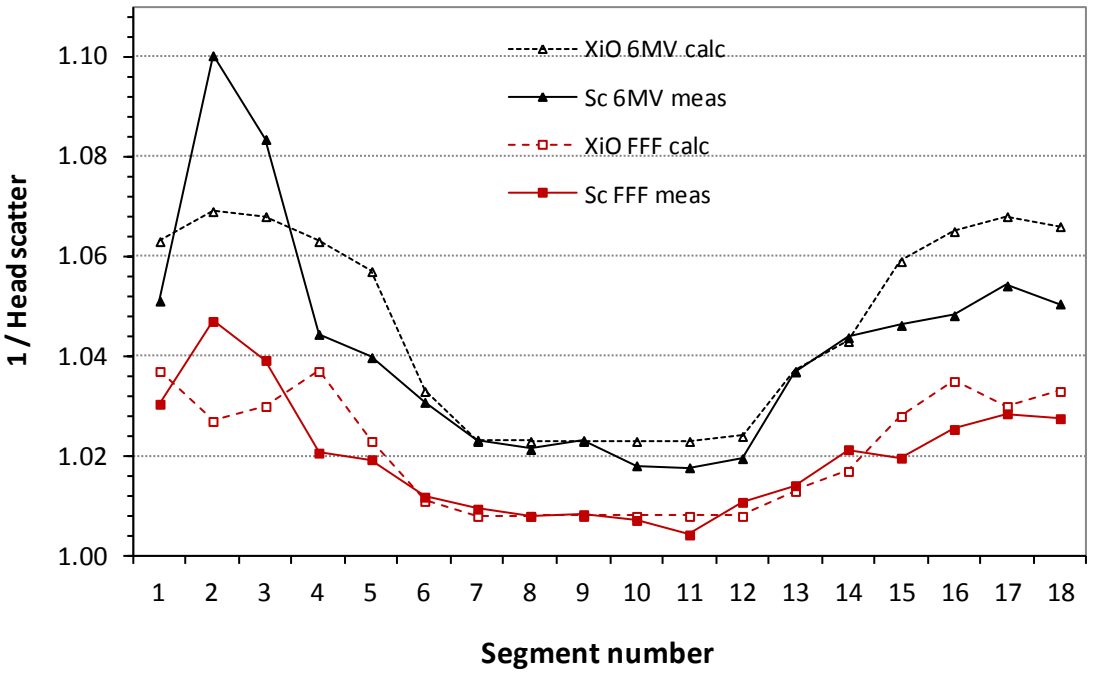

Figure 6.1. Head scatter measured using a brass build-up cap vs. segment number. Measurements were made at the centre of the segment and are relative to a 10x10cm² reading at the same position. 100 x (Measured - XiO) / Measured.

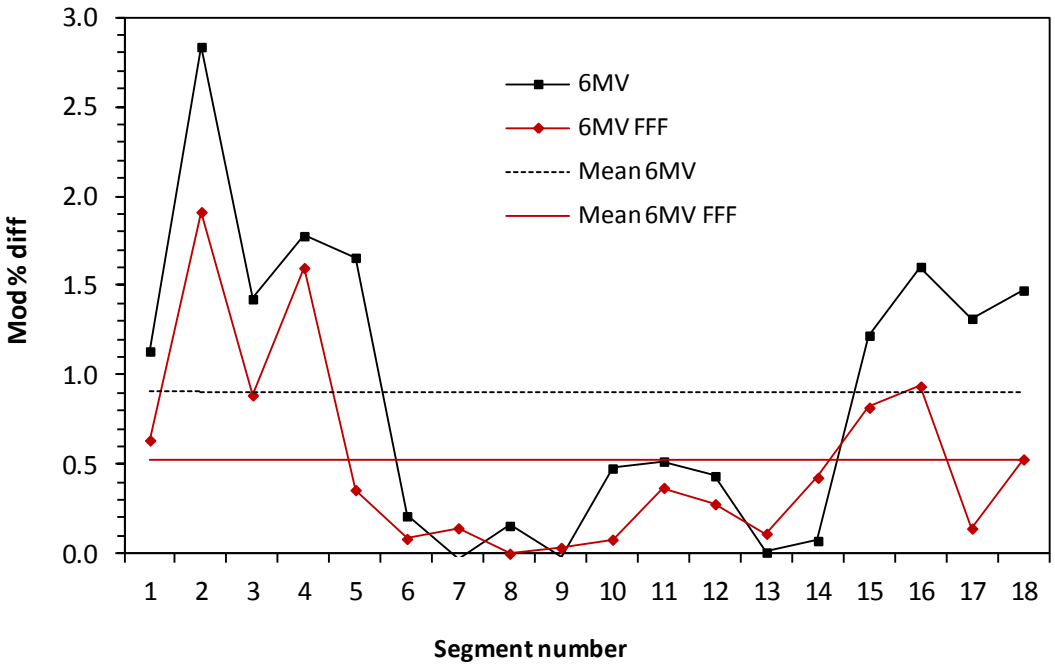

Figure 6.2. Percentage difference from TPS predicted value for each segment. The horizontal lines indicate the mean error for each of the two beams.

It is also interesting to note the variation in the magnitude of the error with segment number. Segments at the beginning and end of the beam delivery have a much larger deviation from predictions than those in the middle (segments 7 to 13). This can be explained with reference to figure 6.3. XiO uses a sliding window segmentation algorithm, attempting to optimise fluence delivery by minimising leaf travel between segments over the course of the delivery. Segments therefore sweep from one side to the other.

The mid-range segments are usually fairly large and centrally placed compared to those at the beginning and end of the beam that are often small, elongated and off-axis. These are the situations where dose modelling is most problematic and the dose predictions are therefore less accurate for these segments.

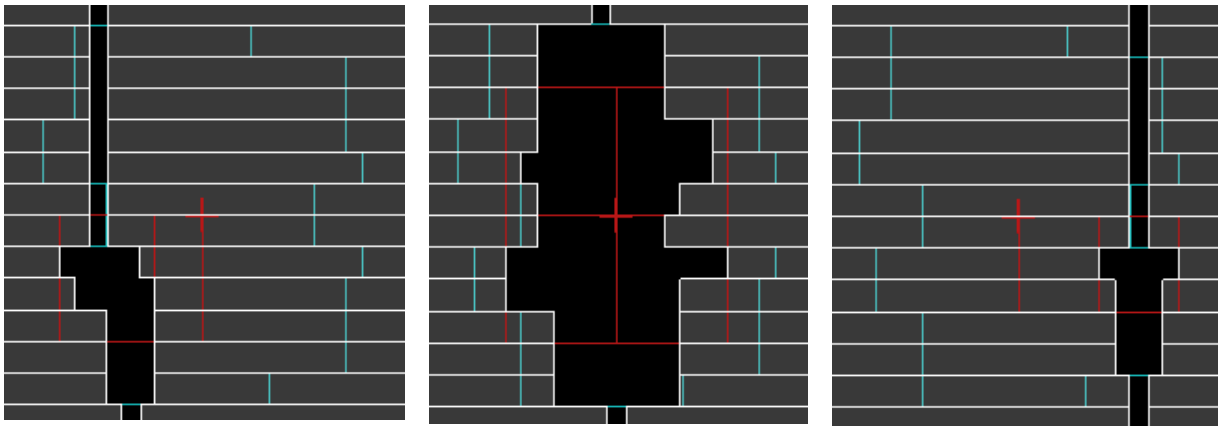

Segment 1 Segment 10 Segment 18

Figure 6.3. Sample segments from the measured field to illustrate the variation in beam size/shape and position with increasing segment number. Segments at the beginning and end tend to be smaller and off-axis, whilst midpoint segments are larger and nearer the central axis.

This helps to validate the assumption that by reducing the range of possible values for head scatter (less variation with field size) it is possible to more accurately predict its value.

6.3 XiO IMRT

Treatment plans were generated for 3 cases; breast (40Gy in 15 #, with a 5 Gy boost to the tumour bed), a parotid carcinoma (2 dose levels, 65Gy to PTV1, 54Gy to nodes in 30#) and an oropharynx case (65Gy to PTV1, 60Gy PTV2, 54Gy PTV3 in 30#). Each was planned according to standard departmental or clinical trials guidelines. For each case a set of dose constraints was found to give an optimal plan for both the flattened and unflattened beam models.

These plans were then transferred to a solid water (WT1) phantom setting a nominal gantry angle of 0° (95cm SSD), and re-calculated. Fluence maps were generated at a depth of 5cm within the phantom and transferred to a 2D array (MatriXX, IBA, Germany) for verification.

The MatriXX is a two dimensional array consisting of 1024 parallel plate cylindrical ionisation chambers in a 32x32 matrix arranged over a 24x24cm area. Each detector has a diameter of 4mm and a height of 5.5 mm giving a sensitive volume of 70 mm^3. The centre to centre distance between each ionisation chamber is 7.5mm. The array is calibrated both for uniformity (to account for variations in detector response across the array), and for absolute dose by reference to a 10x10cm^2 field. The FFF beam exhibits not only a variation in fluence across the field compared to standard operation, but a significant change in beam spectrum too. An independent set of calibration factors were therefore determined for the FFF beam before measurements were taken. Each reading is background corrected.

Figure 6.4 shows the array response to an exposure from a 24x24cm^2 FFF beam to demonstrate the detector spacing and response to the forward peaked beam.

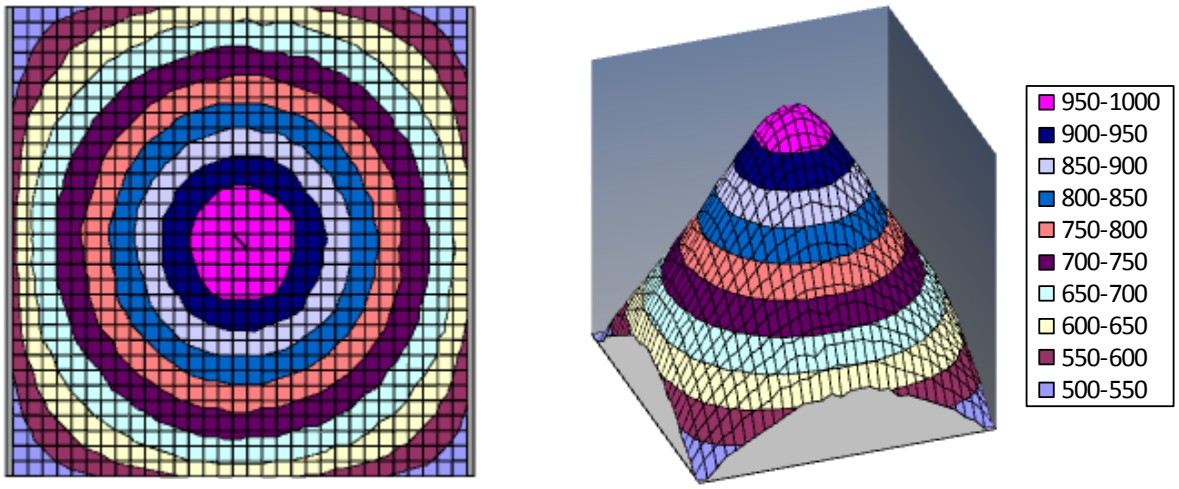

Figure 6.4. 24x24cm² open field delivered to the MatriXX array demonstrating chamber separation and forward-peaked nature of the FFF beam.

The fluence maps are also corrected for difference in output by delivering a 100 MU 10cmx10cm² field, measuring the dose at the centre of the field and then rescaling the fluence maps to correct for the difference in output on the day of measurement.

A region of interest encompassing the whole segment was used when calculating the gamma value and a tolerance of 3% dose and 3mm distance was used. Gamma index evaluation was performed using OmniPro I'mRT (v1.6, IBA dosimetry). Figure 6.5 shows a sample fluence map and gamma analysis from one of the plans. In figure 6.6 (a) to (c) individual pass rates for each of the fields for plans 1 to 3 are presented.

The number of points with $\gamma < 1$ should be greater than 95% in order for that beam to pass and it can be seen from these figures that all of the beams from all plans pass this comfortably. With the filter removed there is a trend towards greater consistency and a higher percentage of points passing the gamma evaluation than for conventional delivery - this trend was observed for relative and absolute doses in all of the plans delivered.

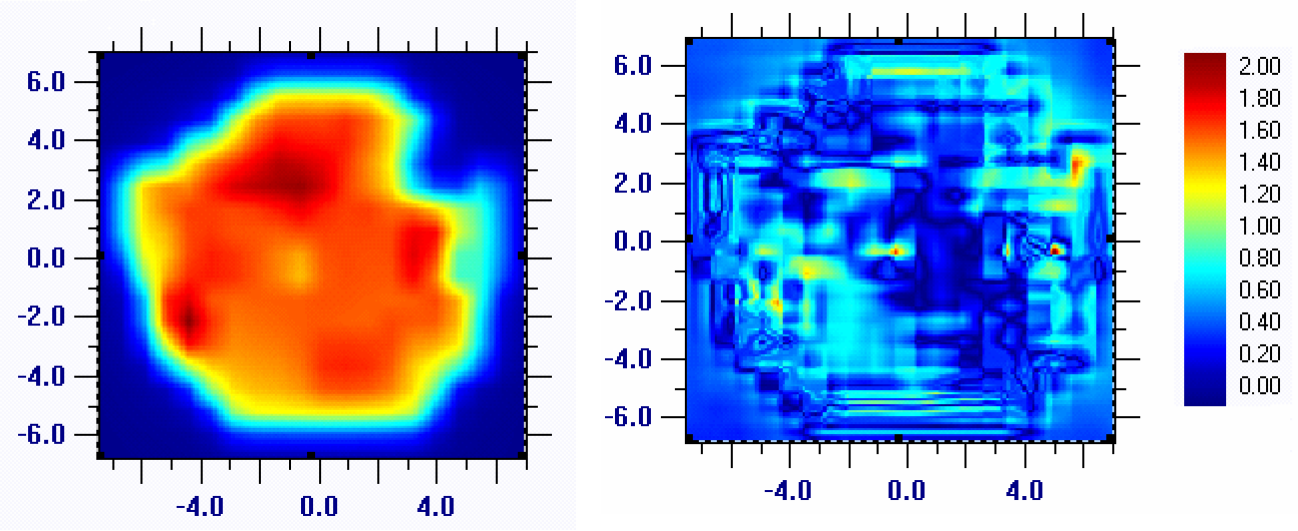

Figure 6.5. Results from the intensity-modulated radiotherapy quality assurance analysis of Case 3. (a) typical fluence map (beam 1), (b) gamma analysis (3%/3 mm) two-dimensional array vs. treatment planning system.

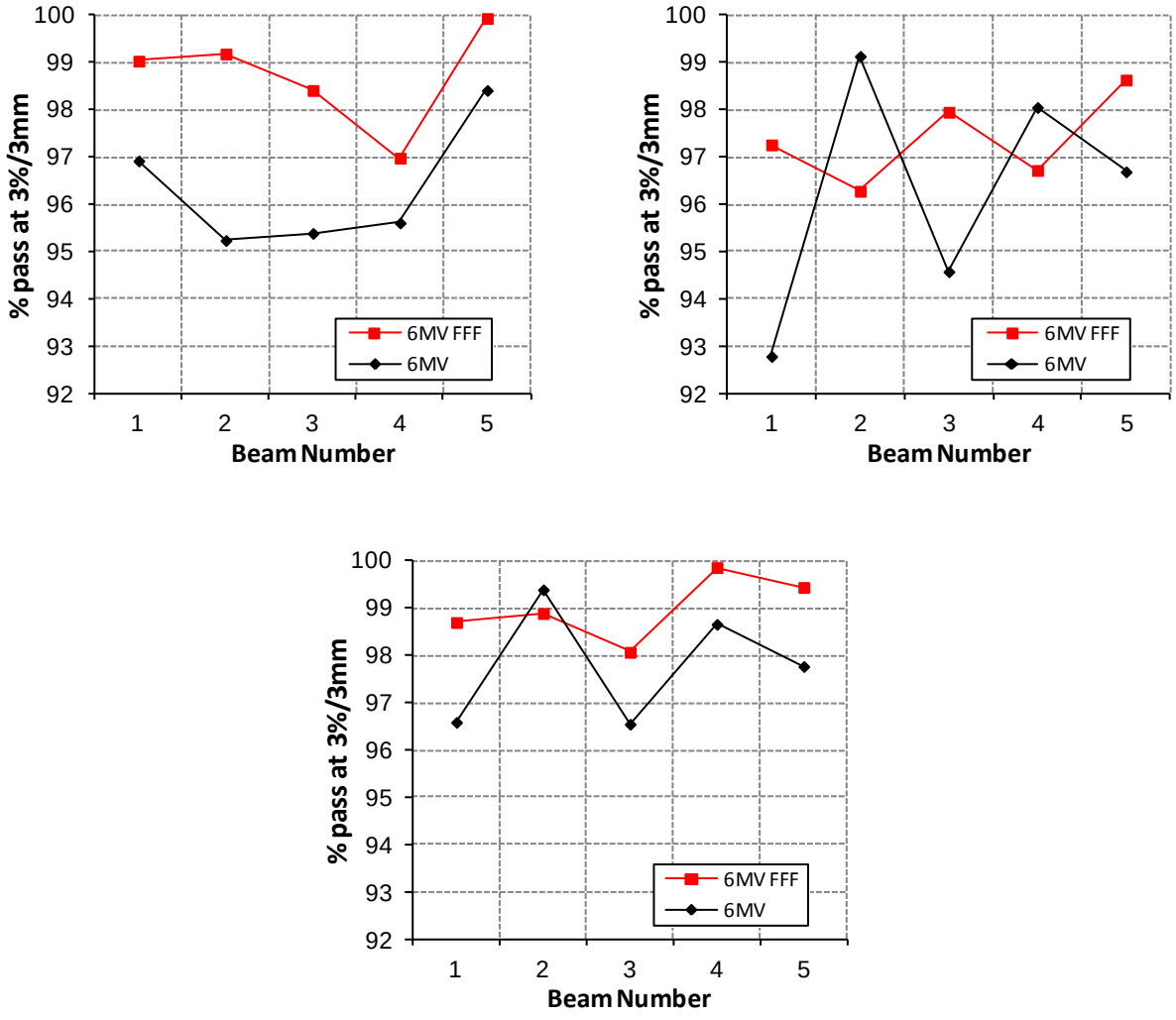

Figure 6.6. Gamma pass rates for each of the 3 IMRT plans. Plot of percentage of points passing evaluation for each beam.

6.4 Monaco IMRT

A similar experiment was carried out with the Monaco TPS as part of the validation of the virtual source model (VSM 1.6) for FFF beams. In order to expose the FFF model to a range of conditions a series of plans in the head and neck, skull base, oesophagus and prostate were generated. To test the model under the extreme influence of the unflattened beams, the isocentre for the head and neck plan was placed asymmetrically, so that large parts of the fields were exposed to the off-axis region of the beam. Plans were calculated on a 2mm grid spacing and a MC variance of 2%. Figure 6.7 shows a colourwash representation of the dose in the sagital plane of the head and neck case, and the associated fluence map.

a) b)

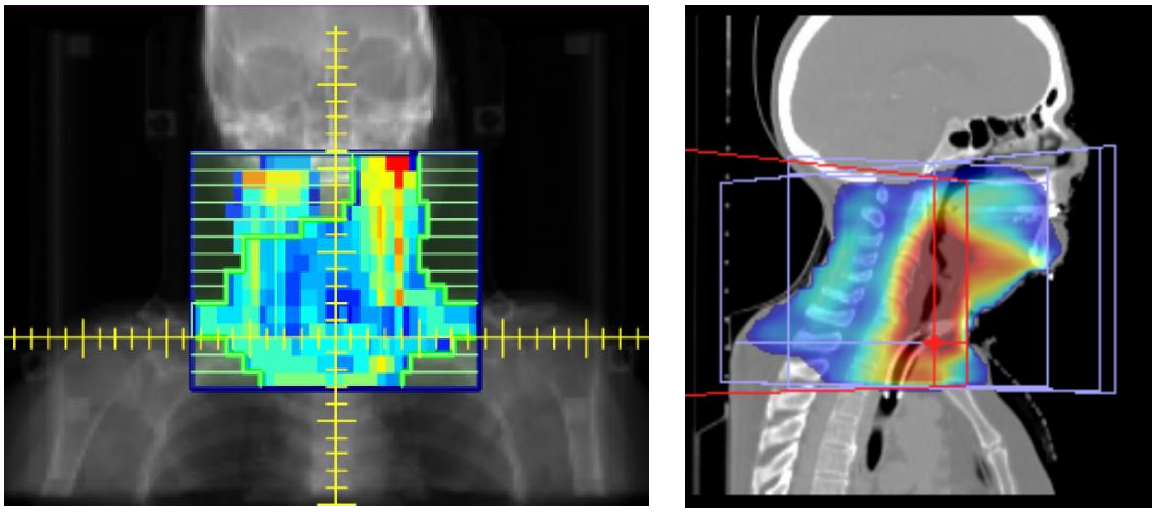

Figure 6.7. Beam setup for IMRT planning of a head and neck case showing relative fluence map (a) and colourwash dose display (b).

The beams for each plan were transferred to a cylindrical phantom representing the Delta^4 QA device and re-calculated. The Delta^4 (ScandiDos, Uppsala, Sweden) is a cylindrical phantom for pre-treatment patient QA. Absolute dose is measured using

1069 p-Si diode detectors arranged in two orthogonal detector arrays. The spacing between each detector is 5mm over the central region (8x8cm^2) and 10mm outside this (20x20cm^2). The diameter of each detector is 1mm. Properties of the phantom have been described in detail by Bedford et al (2009).

Figure 6.8 shows a sample beam from an the head and neck plan demonstrating a) the fluence map generated by Monaco, b) the fluence recorded for that field and c) the difference map between calculated and measured data.

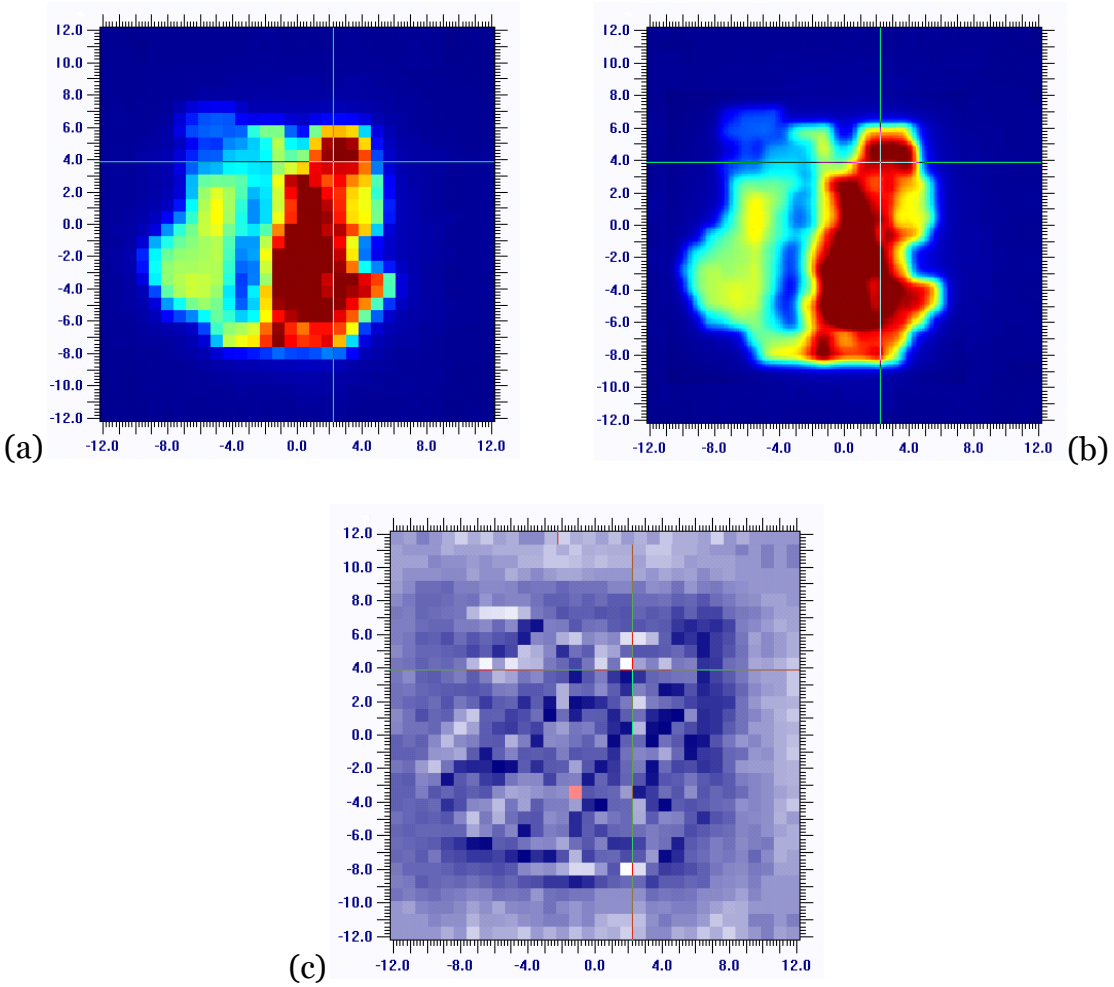

Figure 6.8. Sample beam from an asymmetric Head and Neck plan a) Fluence map generated by Monaco, b) fluence recorded by 2D array, c) difference map.

Table 6.1. Gamma analysis and absolute dose difference of individual beams for the IMRT plans. Percentage of points passing gamma analysis (γ < 1) at 3%/3mm and 2%/2mm for the individual beams of each plan.

Treatment site	Beam	Gamma analysis 3%/3mm		Gamma analysis 2%/2mm		Absolute dose difference (%)	
		6MV	FFF	6MV	FFF	6MV	FFF
Skull base	1	100.0	100.0	99.5	100.	-0.8	0.2
	2	99.8	100.0	93.5	92.4	-0.2	0.5
	3	100.0	99.8	90.6	89.4	-0.9	-0.1
	4	99.8	99.3	92.9	92.3	-0.1	0.0
	5	99.8	100.0	92.4	91.2	-0.6	0.1
Oesophagus	1	100.0	99.0	98.3	89.9	0.6	1.2
	2	100.0	99.8	99.1	95.9	0.0	1.0
	3	100.0	100.0	100.0	99.8	-0.1	0.3
	4	100.0	100.0	100.0	99.1	-0.7	0.5
	5	100.0	99.8	98.8	97.2	0.2	1.0
Prostate + nodes	1	99.4	97.2	93.5	86.2	0.8	1.4
	2	99.8	100.0	97.6	98.4	0.2	0.7
	3	100.0	99.8	97.7	92.8	0.1	0.9
	4	100.0	100.0	98.8	98.8	0.0	0.7
	5	100.0	99.9	98.0	94.9	0.0	0.6
Head & neck	1	97.7	98.3	87.8	84.8	0.9	1.4
	2	100.0	98.8	97.6	94.6	0.4	1.1
	3	99.7	99.5	97.5	94.3	0.3	1.1
	4	99.5	100.0	95.7	96.9	0.3	0.9
	5	99.4	99.2	92.0	84.0	0.4	1.2
	6	99.1	98.3	94.4	87.6	0.6	1.3
	7	99.7	99.8	97.5	95.8	0.3	0.9
				Average		**0.1±0.4**	**0.8±0.4**

Table 6.1 shows the absolute dose differences and statistics for the gamma analysis of the sample plans analyzed at both 3%/3mm and 2%/2mm acceptance criteria. It can be seen that as the volume of tumour and the complexity of the plan increase the pass rate begins to fall (as expected), but all plans pass the standard IMRT acceptance criteria of 95% of points <1 using a 3%/3mm tolerance. The data indicates that the pass rates are slightly higher for the conventional IMRT plans. This is not statistically significant at 3%/3mm but does becomes significant at 2%/2mm ($p<0.001$).

There is also a systematic offset in the absolute doses measured for FFF (0.8%) that is not present in the conventional plans. This figure ties in well with the data presented in figure 4.7(b), where an offset is observed in the output factors curve for FFF beams. This could be minimised by applying a global calibration factor to the beam model.

6.5 Discussion and conclusions

All beams in the planning exercises passed the defined acceptance criteria used for standard IMRT patient specific quality assurance tests. Once the test criteria are tightened to 2%/2mm slight differences can be seen between the flattened and FFF deliveries, with the conventional beams generally receiving slightly higher pass rates. There may be several reasons for this including the increased number of segments delivered and also the fact that the linac is still a prototype (non clinical) release. Once the Elekta FFF linac is released for clinical use with fully optimized hardware and dosimetry these tests should be repeated to assess any possible improvements in dose calculation and delivery.

Several other authors have now demonstrated the accuracy of IMRT QA for FFF delivery. Stathekis *et al* (2009) studied flattening filter delivery on the Varian 23EX

linac using the Pinnacle TPS, finding equivalence in treatment plan quality and delivery. Lang *et al* (2012b) have shown equivalence in 224 pre-treatment plan deliveries for FFF delivery for a combination of Eclipse TPS and TrueBeam accelerator. Kragl *et al* (2011b) tested the dosimetric accuracy of the Monaco TPS using an older version of the VSM (VSM 1.5 within Monaco version 2.03), finding improvements in dose calculation accuracy for off-axis profiles. This did not directly translate into better verification results for IMRT QA delivery, as seen in this study (reported in Cashmore *et al* 2012).

Treatment planning systems, like linear accelerators, have evolved around the use of the flattening filter. In a TPS with simplistic beam modelling, like XiO, the reduction in the magnitude and range of head scatter is likely to have a direct impact on the accuracy of dose predictions, as this will be a dominating factor in calculation uncertainty. In more sophisticated planning systems like Monaco, with much more accurately modelled treatment head and scatter, it is more likely that additional factors will come into play. In particular these IMRT systems do not contain leaf sequencers optimised for FFF segmentation and delivery. The optimisation of non-uniform beam profiles has been discussed by Kim *et al* (2010) who found that number of segment required for FFF beams can be significantly reduced once this is taken into account in the optimization process. Such an addition is likely to reduce the number of segments required to deliver modulated FFF plans. This is discussed further in chapter 8.

CHAPTER 7

PERIPHERAL DOSES

This chapter focuses on the measurement of those doses received by the patient outside of the treated area. These out-of-field, or peripheral doses are increased for IMRT delivery, and planning studies (chapter 5) have shown that more MU are required to deliver modulated beams without the flattening filter This increase in MU can only be justified if the overall scatter received by the patient is reduced during delivery. Data is also presented for stereotactic treatments where the change in MU is not significant but the advantages of increased dose rate (and hence faster delivery) make FFF attractive.

Parts of this chapter forms the basis of an article published by the author in *Int. J. Radiat. Oncol. Biol. Phys.* (Cashmore *et al* 2011).

7.1 Background

Intensity modulated radiotherapy (IMRT) is now a well established technique used to concentrate dose into a target region/s whilst sparing normal tissues, and is recognised as superior to 3D conformal radiotherapy (3D-CRT) in these respects (see Chapter 5). However, the increased number of beam directions used in IMRT

compared with 3D-CRT means that a low level 'dose-bath' is given to a larger volume of normal tissues. Leakage radiation from the treatment head is also raised since IMRT delivery is wasteful of monitor units (MU), which can increase by a factor of 2-10 (typically 2-3) depending on the techniques and equipment used. Since leakage radiation is proportional to the number of monitor units delivered, IMRT is known to increase whole-body doses to the patient.

Several authors have compared the delivery of 3D conformal plans against IMRT and reported that IMRT delivery may double the incidence of solid cancers in long-term survivors (Hall & Wuu 2003, Hall 2006, Kry *et al* 2005, Ruben *et al* 2008, Verellen & Vanhavere 1999). The range of reported values varies considerably (1.2 to 8) since the MU demand for IMRT is largely dependent on both the software and hardware used for planning and delivery and also on the radiobiological models used.

Radiation induced secondary cancers are not a serious concern until at least 5 years after treatment (NCRP report 115, 1993) with patients surviving longer than 10 years being most at risk. Following successful treatment of the original disease secondary cancers are diagnosed on average 15 years after treatment (Bassal *et al* 2006). A recent study (Diallo *et al* 2009) showed that of 115 paediatric patients diagnosed with secondary cancers after radiotherapy 22% of these were >5cm from the PTV, and some were detected up to 1m away. The peak frequency was seen to be in tissues receiving 2.5Gy or less.

With treatments becoming more successful and survival rates rising, the importance and incidence of second cancers will also increase and is likely to be of particular concern in children.

Peripherals doses are influenced by many factors and have been reported for a range of accelerators and beam energies (Followill *et al* 1997, Klein *et al* 2006, Mansur *et al* 2007, Van der Giessen 1994, Xu *et al* 2008). The dose to tissues close to

the target site (within several cm) is dominated by internal scatter and head scatter (Lillicrap *et al* 2000) and is dependent on field size and energy.

At distances beyond the range of internal scatter, peripheral doses are dominated by head leakage and therefore proportional to MU, so are unavoidably higher for IMRT. Since paediatric patients are also physically smaller, geometric factors play an important role in these patients. The distance from the field edge to any organ at risk in a child (and also the depth from surface) will be reduced, raising organ doses relative to comparable exposure in an adult.

One of the major sources of head scatter and leakage radiation from the treatment head is the flattening filter, and operation of an Elekta Precise linear accelerator without the flattener has been shown to reduce patient-plane leakage at 1m by 58% at 6MV (Cashmore 2007, Kragl *et al* 2011). Several groups have investigated the treatment planning aspects of unflattened IMRT (Cashmore 2007, Stathekis *et al* 2009, Vassiliev *et al* 2007) and one author has investigated peripheral doses through Monte Carlo modelling (Kry *et al* 2007), but no direct measurements has been made between out-of-field doses for clinical delivery of comparative plans. If IMRT can be planned and delivered utilising a system with no flattening filter then peripheral doses could be significantly reduced, potentially lowering the incidence of secondary cancers.

This study aims to investigate the potential of IMRT with unflattened photon beams by directly comparing the treatment planning and delivery of unflattened beam IMRT against the conventional IMRT standard. Since peripheral doses are so dependent on the software, hardware and energy used these have been kept constant i.e. the same planning system, plan quality, beam energy and accelerator are used throughout.

Since the dose rate is roughly doubled by filter removal for unflattened beam delivery the pulse repetition frequency has been lowered to maintain the same dose

rate between delivery techniques. Baring any small changes in monitor units (MU) and segmentation the plans therefore took the same time to deliver in each case. Although the dose per pulse is approximately doubled by filter removal the machine had been recalibrated so that 1MU = 1cGy under standard conditions (10x10cm^2, 90cm SSD, D_{max}), as for any other clinical beam.

7.2 Measurements in a slab phantom

To establish a reference and provide base-line measurements, peripheral doses were measured for standard field sizes in a slab phantom consisting of tissue equivalent material (figure 7.1). Peripheral doses are relatively independent of measurement depth and a depth of 5cm was chosen as being representative for the cases studied.

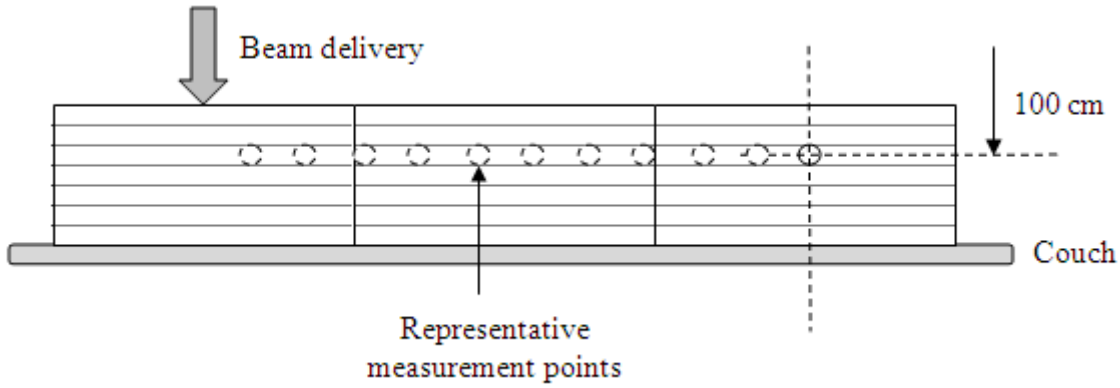

Figure 7.1 Experimental setup for measuring peripheral doses using a slab phantom construction. Three piles of slabs are used, each of dimension 30x30x20cm, giving an overall length of 90cm.

Measurements were taken at regular intervals, from the central axis out to 70cm away from the CAX, and recorded for a variety of field sizes and at collimator rotations of 0 and 90°, both with and without the filter. Readings were performed using a cylindrical ionization chamber (NE2571) and repeated with TLD-100 (Harshaw Chemical Company, Solon, OH) LiF thermoluminescent dosimeters

(TLDs). For each position ten TLDs were used and readings normalised to the dose recorded for delivery under standard conditions (10x10, 90cm SSD, D_{max}). These were then compared to the dose measured under the same conditions with the ionisation chamber to characterise any differences in the energy response of the TLDs due to the altered spectrum of scattered/leakage radiation.

As expected, peripheral doses are seen to decrease with distance from the field edge approximately exponentially, and to increase with increasing field size. In each case the readings generally start to converge beyond 40cm from the central axis, however doses measured with the filter removed drop more quickly and to a lower level (figure 7.2 a-e).

For a 10x10cm^2 field at 40cm from CAX the dose is only 50% of that seen for the standard field, and at 70cm from CAX this falls to 38.5%. For a 3x3cm^2 field the values are even lower at 34.7% and 27.8% respectively. There is a significant drop in dose with the collimator rotation set at 0° due to extra shielding (from the MLC carriage) within the treatment head which is seen in both treatment modes with readings diverging at approximately 10cm from the CAX and then re-converging at approximately 40cm. At 20cm this accounts for a 45% decrease in dose and whenever possible IMRT plans are produced at collimator 0° to reduce this leakage dose.

TLD-100 chips are known to show variations in dose response at low energy, but have been used previously to measure out-of-field doses (Vassiliev *et al* 2006). The differences in beam spectrum between scattered and leakage radiation mean that the TLDs may respond differently. To account for these differences the ratio between ionisation chamber and TLD readings under the same conditions was taken, and these factors used to correct measurements taken in the anthropomorphic phantoms.

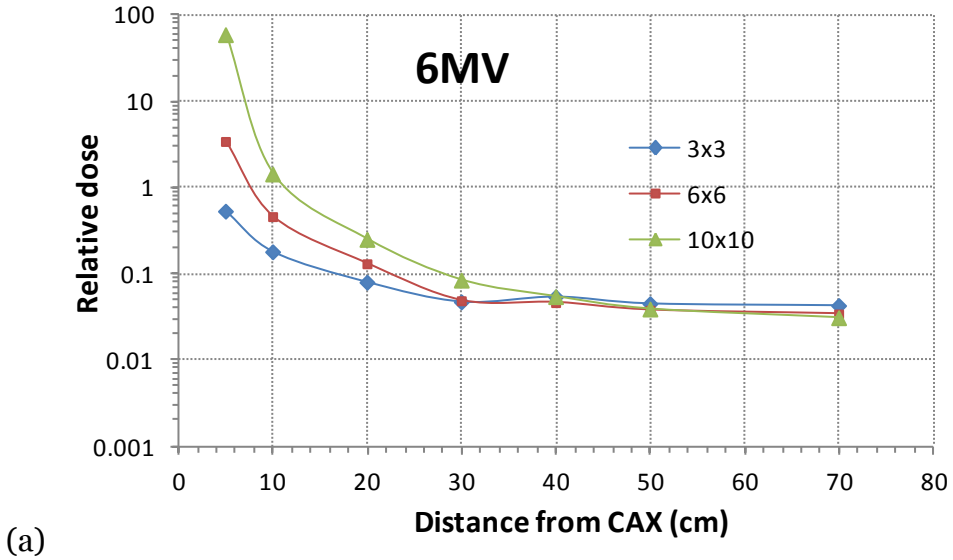

(a)

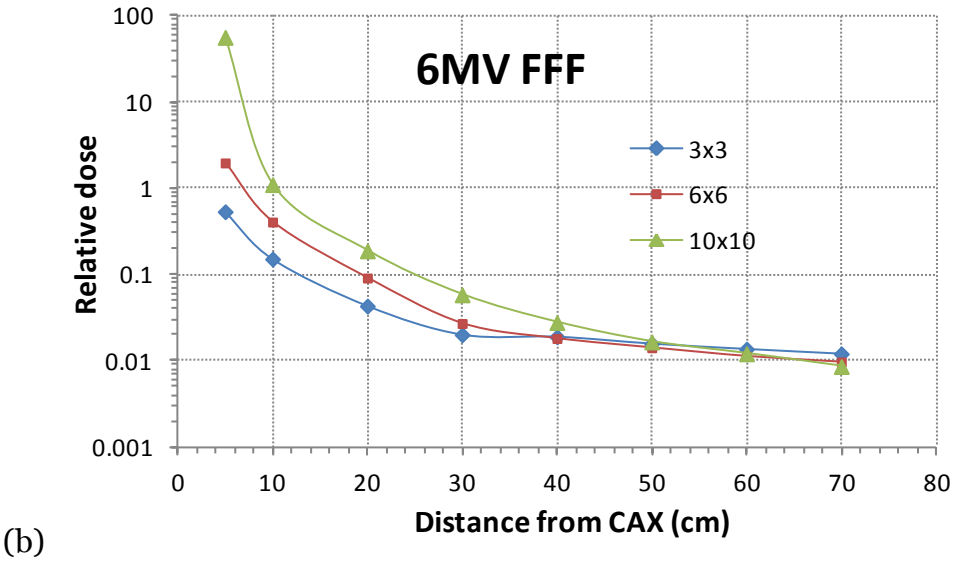

(b)

Figure 7.2. Peripheral dose measurements as a function of distance from the central axis with NE2571 chamber. Measurements are in water equivalent material at a depth of 5cm. a) flattening filter in, b) flattening filter out for field sizes of 3x3, 6x6 and 10x10 cm². c) Shows a comparison between filter in and filter out for 3x3 and 6x6 cm² fields (10x10 cm² removed for clarity). Variation in dose for collimator rotations of 0° and 90° d) filter in, e) with the filter out.

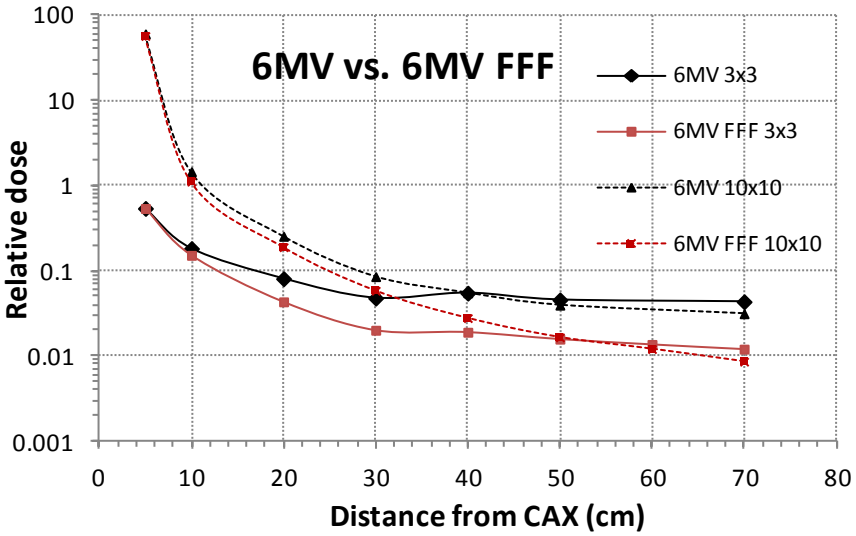
6MV vs. 6MV FFF
6MV 3x3
6MV FFF 3x3
6MV 10x10
6MV FFF 10x10
Relative dose
100
10
1
0.1
0.01
0.001
0
10
20
30
40
50
60
70
80
Distance from CAX (cm)

(c)

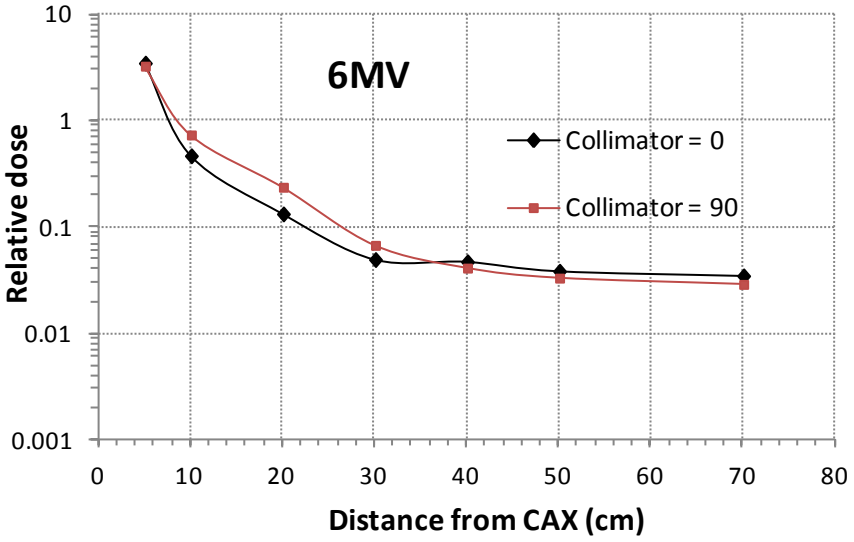
6MV
Collimator = 0
Collimator = 90
Relative dose
10
1
0.1
0.01
0.001
0
10
20
30
40
50
60
70
80
Distance from CAX (cm)

(d)

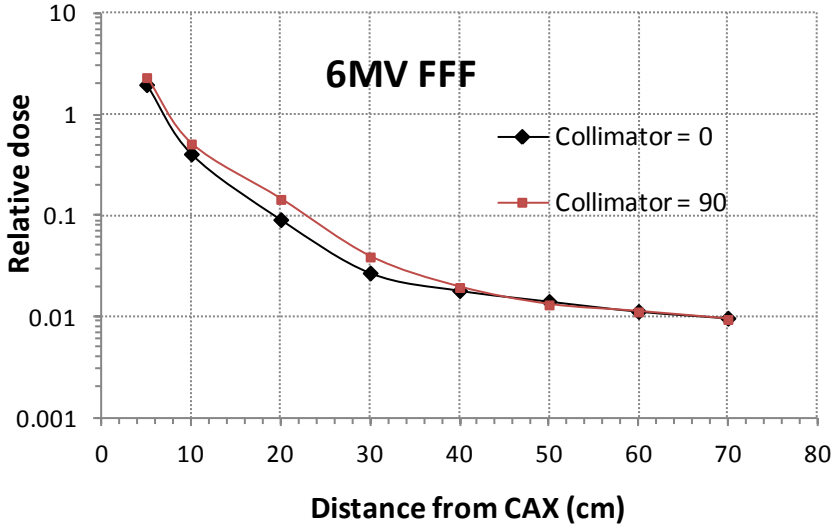
6MV FFF
Collimator = 0
Collimator = 90
Relative dose
10
1
0.1
0.01
0.001
0
10
20
30
40
50
60
70
80
Distance from CAX (cm)

(e)

Under the same delivery conditions the TLDs showed significant differences compared to the ionization chamber readings, with the conventional beams *under*-responding on average by 7.5%, whilst the unflattened beams *over*-responded by almost 17%. These differences are most likely due to the changes in energy spectrum between conventional and FFF delivery but requires further investigation.

For each position ten TLDs were used and readings normalised to the dose recorded for delivery under standard conditions (10x10, 90cm SSD, D_{max}). These were then compared to the dose measured under the same conditions with the ionization chamber to characterise any differences in the energy response of the TLDs due to the altered spectrum of scattered/leakage radiation.

7.3 IMRT Treatment Planning

7.3.1 Patient selection

For this study we retrospectively selected 5 paediatric patients recently treated for intracranial tumours with conventional 3D-CRT at our institution. Additional outlining was then performed by a consultant paediatric oncologist to enable IMRT planning for these patients. Intracranial tumours have been chosen because they offer a challenge for the beam models involved and the opportunity to measure out-of-field doses over a large distance through the rest of the body.

Treatment plans were produced both with and without the flattening filter (10 plans in all). The number of beams and their gantry angles remained the same in each case (generally 5 equally spaced fields). Dose optimisation priorities changed for each case but the planning target volume (PTV) was given priority unless a critical structure was compromised. In many cases organs at risk were contained within the PTV in which case care was taken to avoid dose hotspots occurring in these regions.

All plans received 50.4 Gy in 28 fractions prescribed to the mean of the PTV dose i.e. D_{50} = 50.4Gy. In each case calculations were performed using the superposition algorithm, a step increment of 5mm on the MLCs and a 2mm grid spacing.

For each IMRT case a plan was produced using the conventional IMRT beam model first then, having found a set of dose constraints to drive the optimiser to meet target and OAR limits, these same objectives were used to produce an optimised unflattened treatment plan. This process removes any inter-planner or inter-plan bias from the evaluation. Plans were then evaluated according to standard dose indices to assess PTV coverage, homogeneity and OAR sparing.

7.3.2 IMRT plan evaluation

All 10 plans have been assessed using standard evaluation criteria as shown in table 7.1. Values are reported in table 7.2 for each of the 10 plans created.

Table 7.1. Summary of dosimetric parameters used for plan evaluation

PTV coverage	
V_{90}	Volume of target (%) receiving 90% of prescribed dose
V_{95}	Volume of target (%) receiving 95% of prescribed dose
V_{100}	Volume of target (%) receiving 100% of prescribed dose
V_{107}	Volume of target (%) receiving 107% of prescribed dose
D_2	Dose to 2% of target volume
D_{98}	Dose to 98% of target volume
HI	Homogeneity index (D_2-D_{98}/Prescribed dose)*100
V_{PTV}	Volume of the PTV
CI	Conformity Index volume of tissue $V_{NT\ 95}$/ V_{PTV}
Normal tissue sparing	
$V_{NT\ 5}$	Volume of tissue receiving 5% of prescribed dose
$V_{NT\ 95}$	Volume of tissue receiving 95% of prescribed dose

Figure 7.3 shows slices through the isocentre for Case5 (a midbrain astrocytoma) to illustrate the *similarity* of the plans. For all planned cases the target coverage, homogeneity and OAR doses both with and without the flattening filter were similar with no one technique producing better plans than the other. This can be seen diagrammatically in figure 7.3a which shows the dose volume histogram (DVH) for the 2 plans in figure 7.3a. The correlation between plans for each case was tested and differences were found to be statistically insignificant.

Table 7.2. Summary of doses (in Gy) recorded for PTV coverage in each plan for flattening filter in (In) and filter out (Out) according to evaluation parameters of table 1. Volumes are expressed as a percentage except the PTV volume which is in cc.

	Case1		Case2		Case3		Case4		Case5	
	In*	**Out***	**In**	**Out**	**In**	**Out**	**In**	**Out**	**In**	**Out**
V_{90}	99.4	99.3	99.9	99.9	99.9	99.9	99.1	99	100	100
V_{95}	95.3	94.9	98.1	98.3	99.0	98.9	94.2	95.4	96.2	96.3
V_{100}	50.0	50.0	50.0	50.0	50.0	50.0	50	50	50	50
V_{107}	0.2	0.1	0.1	0.2	0.9	0.3	0.4	0.9	0	0
D_2	52.6	52.4	52.4	52.9	53.2	52.5	52.6	53.1	51.6	51.5
D_{98}	46.8	46.6	47.9	47.9	48.2	48.2	46.6	46.7	47.3	47.4
HI	11.5	11.5	8.9	9.9	9.9	8.5	11.9	12.7	8.5	8.1
V_{PTV}	420.5	420.5	497.8	497.8	309.9	309.9	441.6	441.6	60.3	60.3
CI	1.13	1.10	1.09	1.10	1.22	1.16	1.05	1.07	1.26	1.23
$V_{NT\,5}$	1445.3	1433.9	939.1	934.3	1345.2	1313.2	1053.8	1038.1	1331.7	1321.8
V_{NT}	475.2	462.0	542.3	547.0	378.9	360.6	463.6	471.9	76.1	74

** 'In' refers to the flattening filter in position (i.e. conventional IMRT) and 'Out' refers to unflattened IMRT (flattening filter out).*

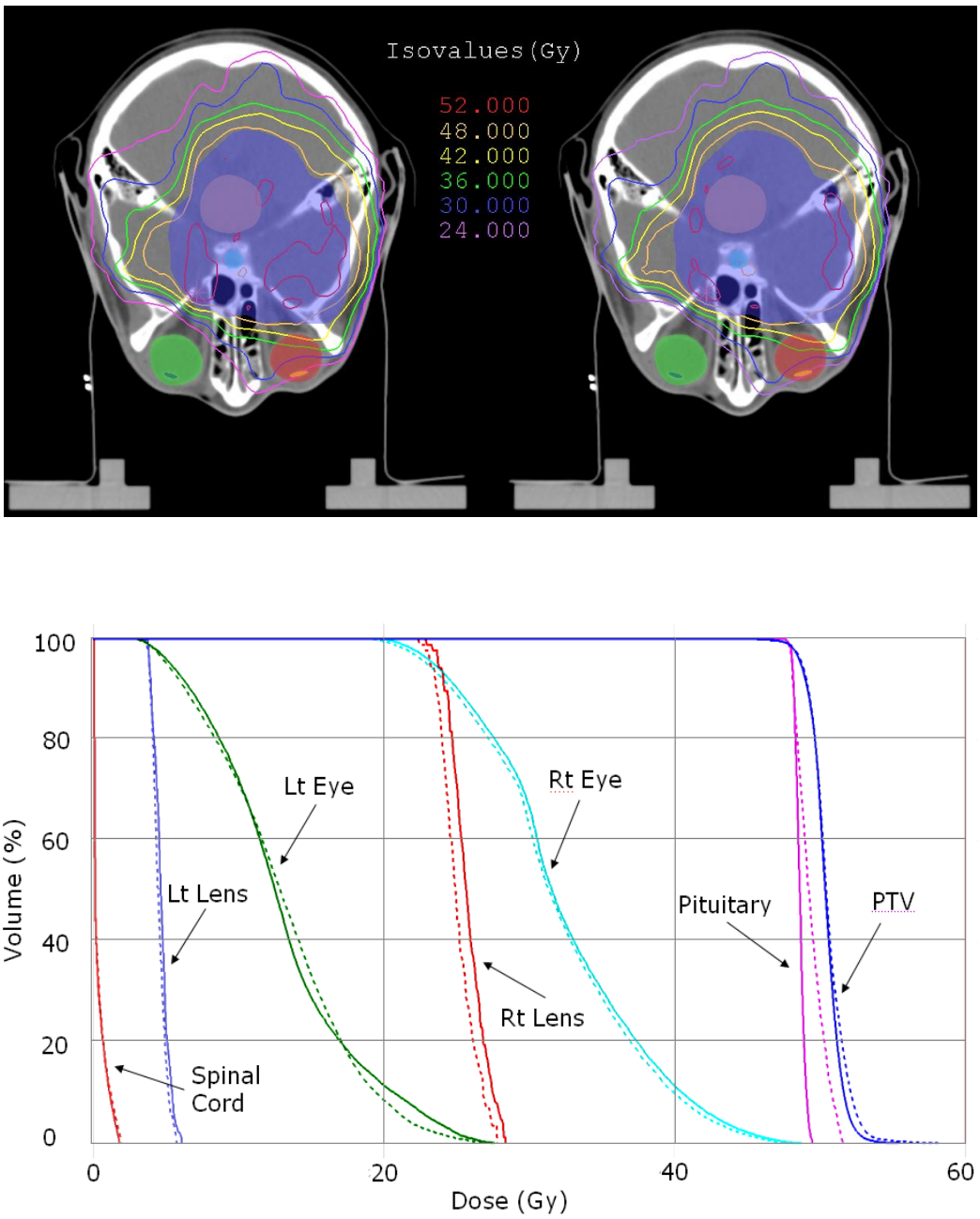

Figure 7.3. Transverse slice through the centre of the target region for Case5 (a midbrain astrocytoma) showing dose distribution comparisons between each technique. On the left (a) is the conventional IMRT plan and on the right (b) that with the flattening filter removed. The PTV is marked in green and the pituitary in red. Figure 7.3b. DVH comparison between conventional (solid lines) and unflattened (dotted lines) plans for Case5.

Table 7.3. Organ at risk doses (in Gy) for the 10 treatment plans (5 cases). All doses are the maximum point dose to that organ unless marked with a † in which case the mean dose is listed.

	Case1		**Case2**		**Case3**		**Case4**		**Case5**	
OAR	***In**	***Out**	**In**	**Out**	**In**	**Out**	**In**	**Out**	**In**	**Out**
Lt Eye †	34.3	33.6	13.3	13.1	32.0	32.4	36.9	36.6	3.7	3.4
Rt Eye †	33.7	33.8	11.5	11.3	12.9	13.0	36.7	35.9	2.6	2.4
Lt lens	38.3	39.5	9.3	9.3	27.8	28.4	40.4	37.1	4.4	4.2
Rt lens	29.6	29.0	5.4	5.2	5.8	6.1	35.8	36.2	3.3	3.1
Optic Chiasm	52.8	52.9	32.7	35.3	50.5	50.4	48.9	49.4	11.8	11.8
Brainstem	50.3	50.6	53.1	52.6	53.2	52.1	49.6	50.6	50.5	50.8
Spinal cord	2.9	2.7	49.8	49.7	2.0	1.8	49.6	48.6	0.6	0.5
Lt cochlea †	42.2	42.8	45.9	45.3	50.4	50.2	38.9	39.0	9.0	8.5
Rt cochlea †	44.6	43.5	45.8	47.7	31.5	33.6	48.8	48.5	8.1	7.6
Pituitary	51.8	51.6	53.6	52.6	51.6	49.5	50.0	51.3	14.9	15.3

** 'In' refers to the flattening filter in position (i.e. conventional IMRT) and 'Out' refers to unflattened IMRT (flattening filter out).*

Table 7.4. Segments and monitor units required to deliver identical plans by the two different delivery methods.

Case	No. fields	Conventional IMRT		Unflattened IMRT		Ratio of segments*	Ratio of MUs*
		Segments	**MUs**	**Segments**	**MUs**		
Case 1	5	89	18146	89	19186	1.000	1.057
Case 2	5	94	18105	98	20695	1.043	1.143
Case 3	5	85	17928	76	17767	0.894	0.991
Case 4	5	100	22462	104	24667	1.040	1.098
Case 5	5	57	10924	59	11310	1.035	1.035
				Average		**1.003 ± 0.063**	**1.067 ± 0.058**

** ratio is taken as Unflattened / Conventional IMRT*

Table 7.3 lists the maximum point doses to the OARs for each case with and without the flattening filter. In many of the cases OARs were within the PTV and so received unavoidably high doses.

Table 7.4 compares the number of segments and MUs required to deliver the same dose distribution with the two techniques. Taking the ratio of (Unflattened IMRT/Conventional IMRT) for each of the 5 cases the average for the number of segments required is 1.003 and the MU ratio is 1.067.

7.4 Anthropomorphic phantom construction

Out-of-field doses are difficult to calculate with any degree of accuracy and peripheral doses to organs at risk cannot be reliably or accurately predicted from large-field phantom studies (Followill *et al* 1997). With an unflattened beam there may be significant changes in the number and shape of the beam segments required and the number of MUs needed to deliver the prescribed dose. Scatter and leakage will also depend on the direction and energy of the scattered radiation so may be affected by the changes in beam spectrum. It is therefore important to measure these changes under representative conditions.

Phantom measurements yield dose values at the correct distance from the isocentre, at the correct depth and for clinically usable plans. Therefore, to measure and compare peripheral doses for IMRT delivery an anthropomorphic paediatric phantom of a 3-year-old child was constructed with dimensions based on published statistical data (Hall 1995, Stovall *et al* 2004) (figure 7.4). The design of the phantom is necessarily simple as the manufacture of a detailed paediatric phantom is beyond the scope of this thesis; no attempt was made to manufacture the phantom from water equivalent materials or include inhomogeneities. The aim of the study is not to provide definitive data for risk of cancer induction but to compare treatment

techniques under the same conditions; therefore it is relative doses that are of interest.

With the beam isocentre in the centre of the head doses were measured at clinically relevant points i.e. thyroid, breast, ovaries and testes. In particular, thyroid cancer is the only tissue with clear evidence for risk even at doses of <0.1 Gy (Shore 1992) and is also the second most frequent secondary cancer reported.

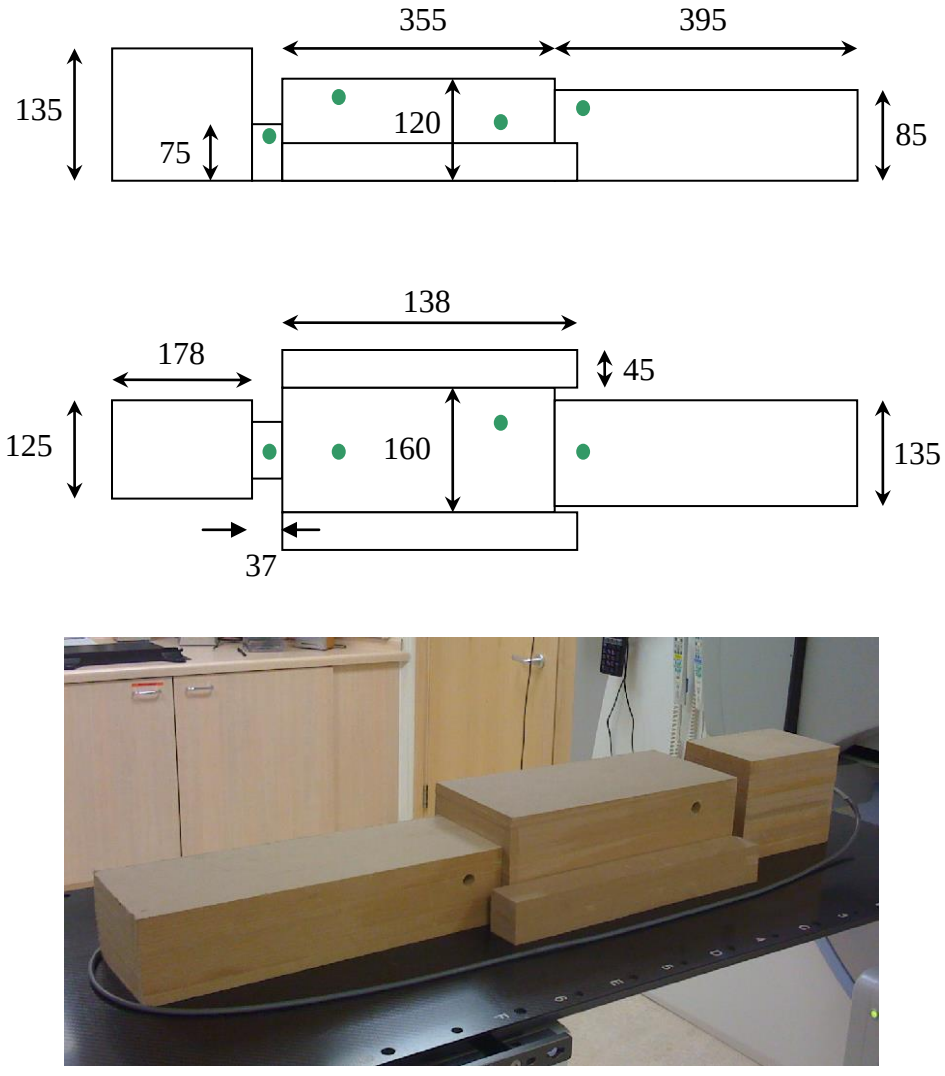

Figure 7.4. Details of the paediatric anthropomorphic phantom used for measurements, distances as marked (mm). Measurements were performed with an NE2571 chamber.

Table 7.5. Summary of doses at specified points of interest in the wood phantom for the five cases treated both with the flattening filter in (In) and out (Out). All doses are relative to the beam isocentre (head) which is equal to 1.8Gy (50.4Gy/28#).

		Case 3			**Case 4**			**Case 5**			
	Distance										**Average**
	(mm)	**In**	**Out**	**Ratio**	**In**	**Out**	**Ratio**	**In**	**Out**	**Ratio**	**Ratio**
Head	0	100	100	**1.00**	100	100	**1.00**	100	100	**1.00**	**1.00**
Thyroid	195	1.085	0.837	**0.77**	1.073	0.789	**0.74**	0.512	0.422	**0.82**	**0.78**
Breast	265	0.260	0.191	**0.74**	0.320	0.206	**0.64**	0.148	0.103	**0.70**	**0.69**
Ovaries	510	0.082	0.034	**0.42**	0.131	0.045	**0.34**	0.062	0.025	**0.40**	**0.38**
Testes	600	0.062	0.021	**0.34**	0.096	0.030	**0.31**	0.049	0.017	**0.34**	**0.33**

Table 7.5 shows the doses received at each of these points for three of the IMRT plan deliveries. In each case the peripheral doses from the flattening filter plans are significantly lower than for conventional IMRT. Figure 7.5 plots the peripheral dose vs. off-axis distance for the average of the datasets.

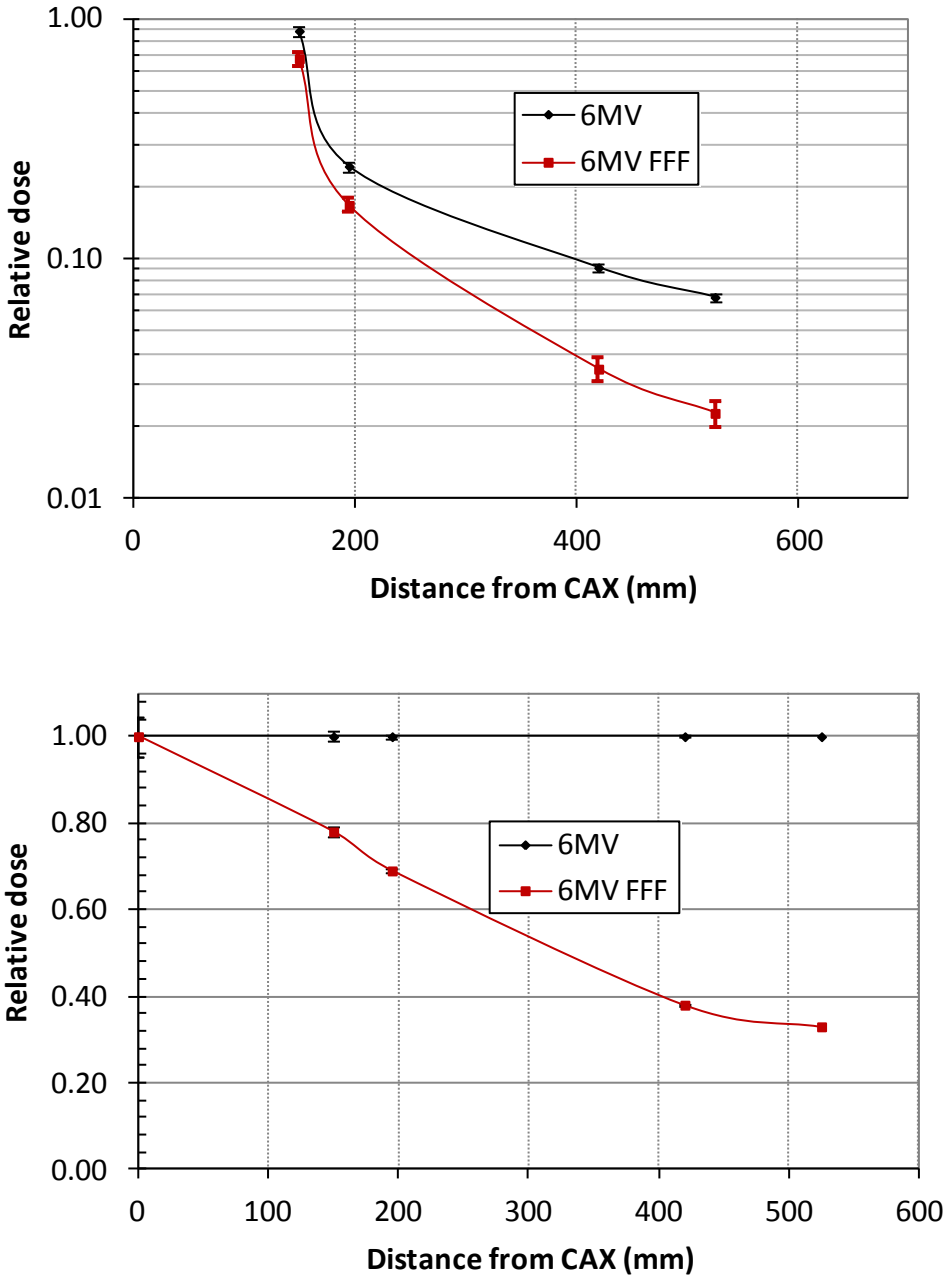

Figure 7.5. Sample data from Case5 illustrating the drop in peripheral dose for the unflattened beam delivery in the clinical IMRT plans (wood phantom). Figure b) shows a plot of relative dose on a linear scale with the point doses for the conventional plans normalised to 1 to illustrate the drop seen in relative dose with the unflattened IMRT plans.

7.5 ATOM phantom

Scatter and leakage will depend on the direction and energy of the scattered radiation so readings may be affected by the phantom material. It is therefore important to measure these changes under representative conditions. For these reasons a commercially available anthropomorphic paediatric phantom (ATOM dosimetry model 706) (CIRS Inc., Norfolk, VA, USA) of a 10-year-old child was used to measure and compare peripheral doses for IMRT delivery (kindly loaned from The Christie NHS Foundation Trust).

The phantom consists of 25mm thick contiguous sections pre-drilled to hold TLDs. For each plan delivery 5 LiF TLDs were placed at each of 6 points within the phantom corresponding to clinically relevant anatomical locations outside of the treated volume representing the thyroid, breast, lung, intestines, ovaries and testes. Plans were delivered with the beam isocentre in the centre of the head and each plan was delivered three times to ensure adequate dose levels were recorded by the TLDs.

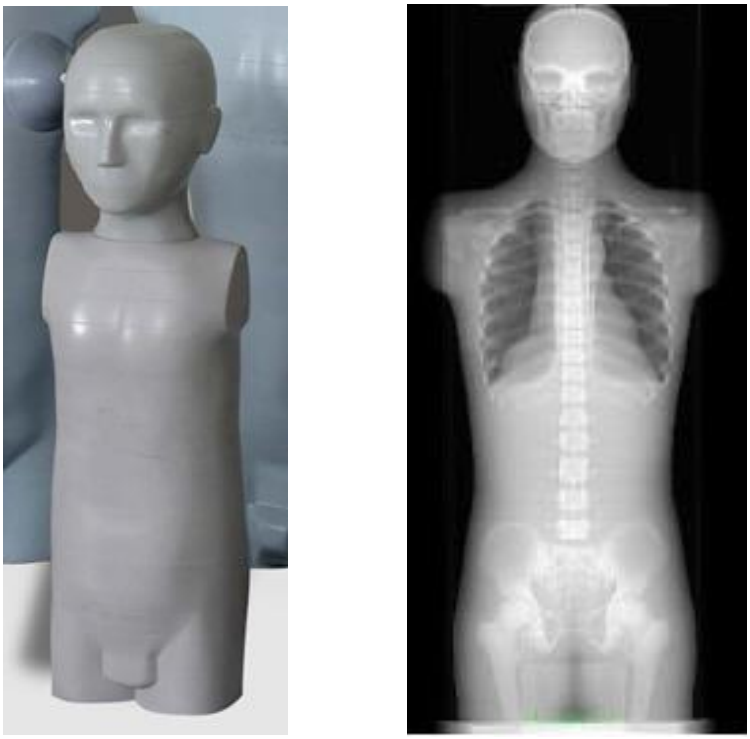

Figure 7.6 CIRS ATOM paediatric phantom used for peripheral dose measurements.

7.5.1 Doses to distant organs

These measurements are summarised in table 7.5 for each of the regions of interest and shown graphically in figure 7.7. Even for doses close to the target volume the doses are seen to be consistently lower for unflattened delivery. On average the thyroid was only 5cm from the field edge but still shows a 24% reduction in dose compared to the standard IMRT delivery.

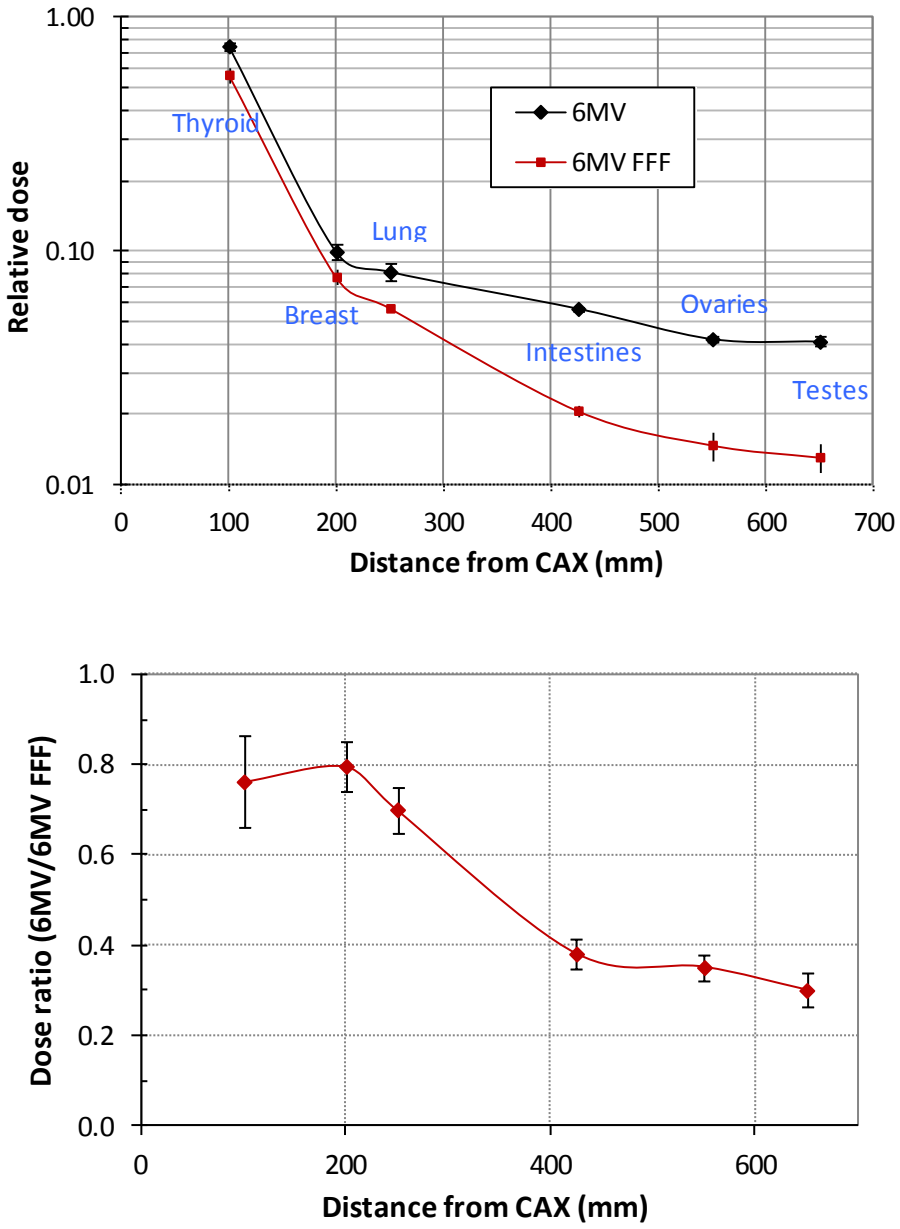

Figure 7.7. Sample data from Case5 illustrating the drop in peripheral dose for the unflattened beam delivery in the clinical IMRT plans (a). Figure b) shows a plot of the average dose ratio (unflattened/flattened) for all of the plans delivered.

Table 7.6. Summary of doses at specified points of interest for three of the five cases treated both with the flattening filter in (In) and out (Out)

		Case 1			Case 2			Case 5			
	Distance (mm)	**In***	**Out***	**Ratio**	**In**	**Out**	**Ratio**	**In**	**Out**	**Ratio**	**Average Ratio**
Head	0	100	100	**1.00**	100	100	**1.00**	100	100	**1.00**	**1.00**
Thyroid	100	1.730	1.288	**0.745**	2.256	1.778	**0.778**	0.755	0.570	**0.755**	**0.763**
Breast	200	0.202	0.167	**0.825**	0.248	0.195	**0.784**	0.010	0.078	**0.781**	**0.797**
Lung	250	0.159	0.112	**0.701**	0.189	0.132	**0.701**	0.082	0.057	**0.700**	**0.701**
Intestines	425	0.082	0.031	**0.374**	0.090	0.036	**0.402**	0.057	0.021	**0.367**	**0.381**
Ovaries	550	0.059	0.019	**0.328**	0.064	0.024	**0.373**	0.042	0.015	**0.353**	**0.351**
Testes	650	0.057	0.015	**0.268**	0.064	0.020	**0.312**	0.041	0.013	**0.321**	**0.300**

** 'In' refers to the flattening filter in position (i.e. conventional IMRT) and 'Out' refers to unflattened IMRT (flattening filter out). Distances are from the central axis (isocentre).*

7.6 Room survey

The reduction in scatter, and hence leakage radiation effectively lowers the whole body dose received by the patient, even taking into account the increased number of monitor units required for IMRT delivery with FFF techniques.

A head and neck IMRT plan was delivered to assess the cumulative doses received at various points around the treatment room. Radiation was delivered to a 20cm thick solid water phantom to simulate patient scatter and doses measured using calibrated Harshaw lithium fluoride TLD-100s (Harshaw Chemical Company, Solon, OH).

Table 7.7 shows the doses received at each position. Despite the FFF plan requiring 33% more MU than the conventional IMRT plan, the cumulative doses are significantly lower for unflattened delivery with a dose reduction of 31.6% averaged over all positions. Dose measurements and analysis for this survey were carried out not by the author, but by trainee physicists within the department working under supervision. Further results are presented in Appendix H.

Table 7.7. Cumulative doses measured during IMRT plan delivery for 6MV and 6MV FFF plans. Doses are in mSv.

TLD Position	6MV	6MV FFF
A side wall	17.0	13.3
B side wall	40.2	23.2
G side wall	-	-
T side wall	11.0	7.8
Maze entrance	8.2	6.4
Machine head	201	115

7.7 Stereotactic radiosurgery (SRS)

The stereotactic cones commissioned for the FFF linac were used to assess the out-of-field doses received during radiation delivery. Figure 7.8 shows the beam profile of two SRS cones on a log scale to illustrate the reduction in dose immediately outside of the field edge for the FFF beams. Doses measured at 25mm from the central axis were lower for all FFF beams compared to the flattened beams for all the collimators due to the reduction in the linac head leakage observed when the flattening filter is removed.

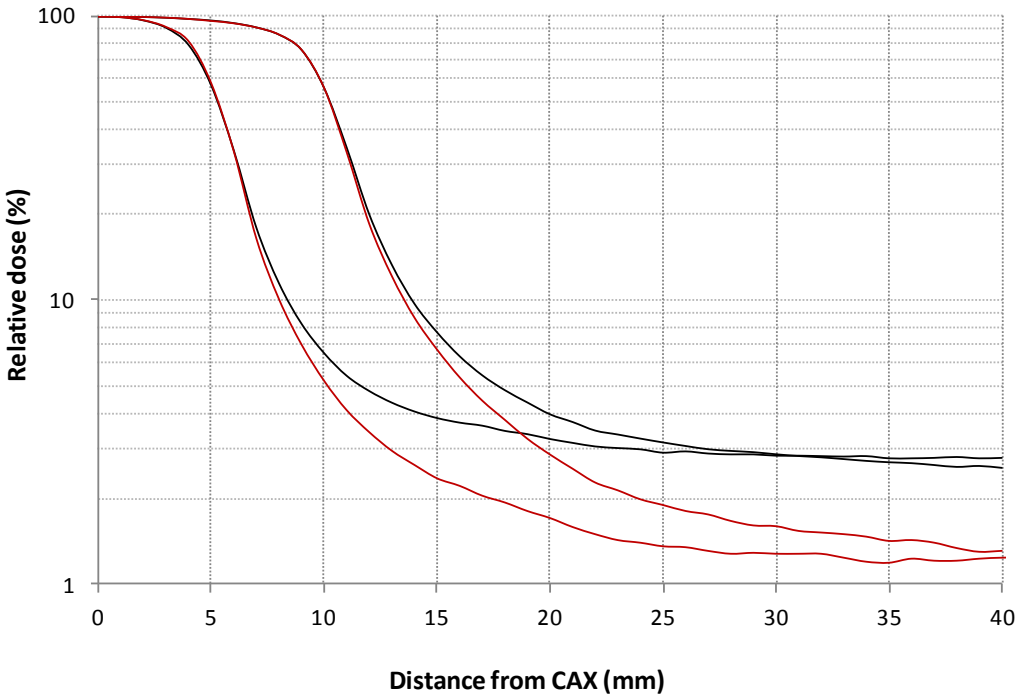

Figure 7.8. Comparison of 6MV (black) and 6MV FFF (red) profiles for 2 conical stereotactic collimators (10 & 22.5mm diameters). On the log plot it is possible to see the reduction in out-of-field dose for the FFF beam compared to standard data.

The peripheral dose measurements of section 7.2 were repeated using a 20mm SRS cone using the slab phantom as illustrated in figure 7.1.

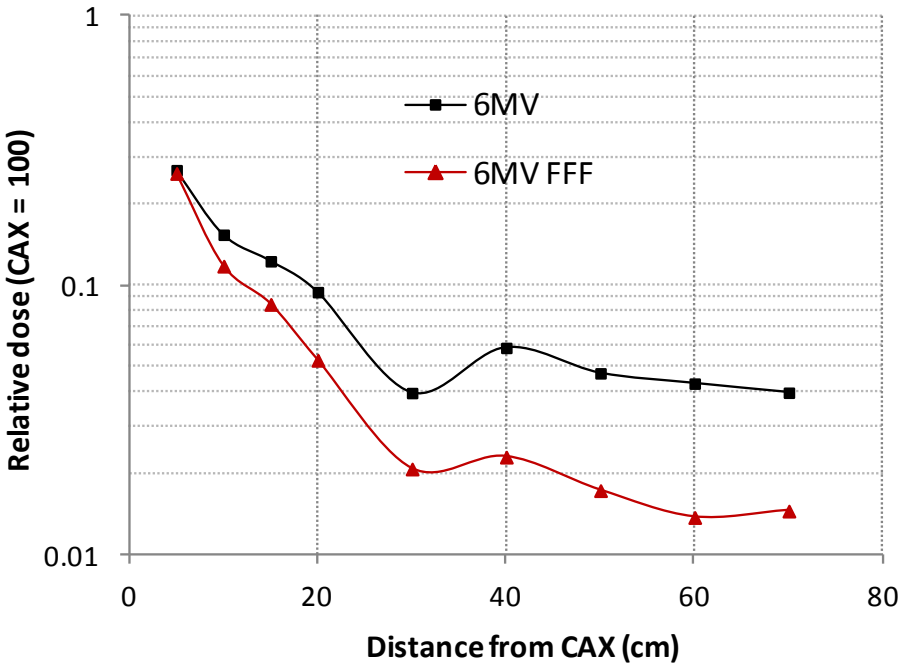

Figure 7.9. Peripheral doses measured for a 20mm SRS cone.

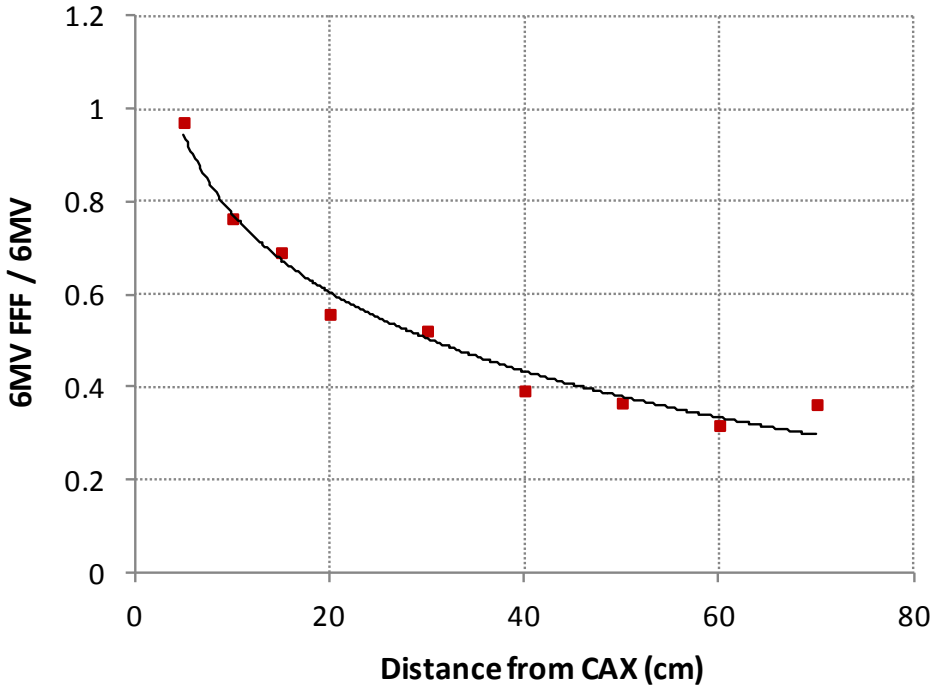

Figure 7.10. Ratio of peripheral doses (6MV FFF / 6MV) measured for a 20mm SRS cone illustrating the increasing reduction in out-of-field dose for the FFF with distance from the field centre.

There is a significant reduction in dose for FFF operation (figure 7.9), and this difference increases with distance from the central axis (figure 7.10). This reduction in the dose outside of the treatment field for FFF beams provides normal tissue sparing within the patient, and this is magnified for stereotactic radiosurgery over conventional radiotherapy due to the fact that the stereotactic plan involves multiple small field arced (typically 100°) beams, each with a high number of monitor units.

The FFF beam shape means that the photon fluence naturally falls off with distance from the central axis (falling to 50% at the beam edge). The magnitude of the leakage radiation through the collimators will scale directly with that of the photon fluence, so the dose outside the field edge (to normal tissues) will also be lower. This is a simple consequence of there being less primary radiation present at off-axis positions.

The plan below (produced by Geoff Heyes [appendix H]) for an acoustic neuroma (figure 7.11) required 2 isocentres to cover the PTV, one using 4 arcs and a 20mm collimator, the second 3 arcs with a 10mm collimator, each arc covering 100°.

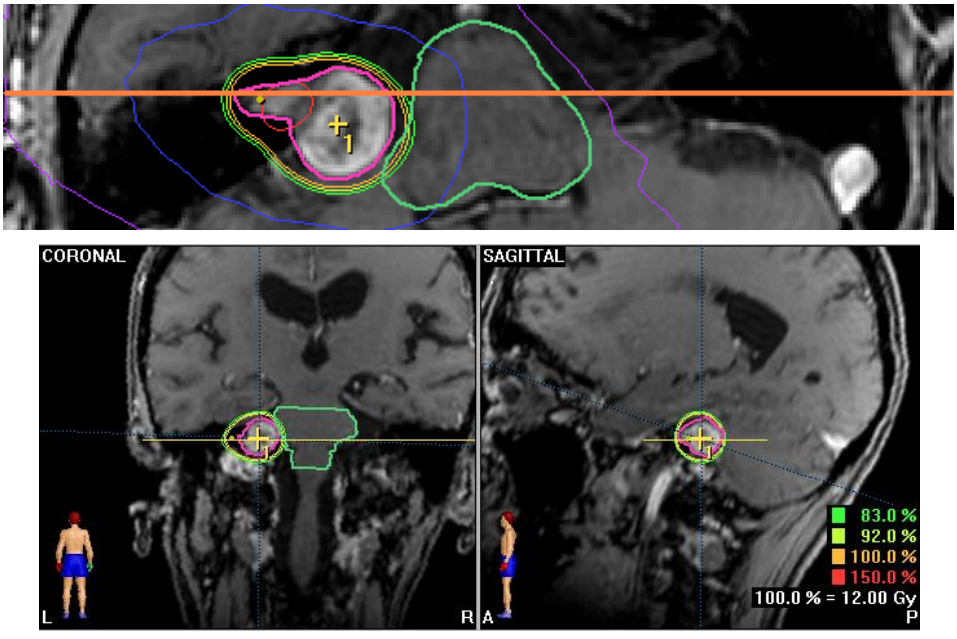

Figure 7.11. Comparison of dose between 6MV and 6MV FFF beams through an axial slice of an acoustic neuroma.

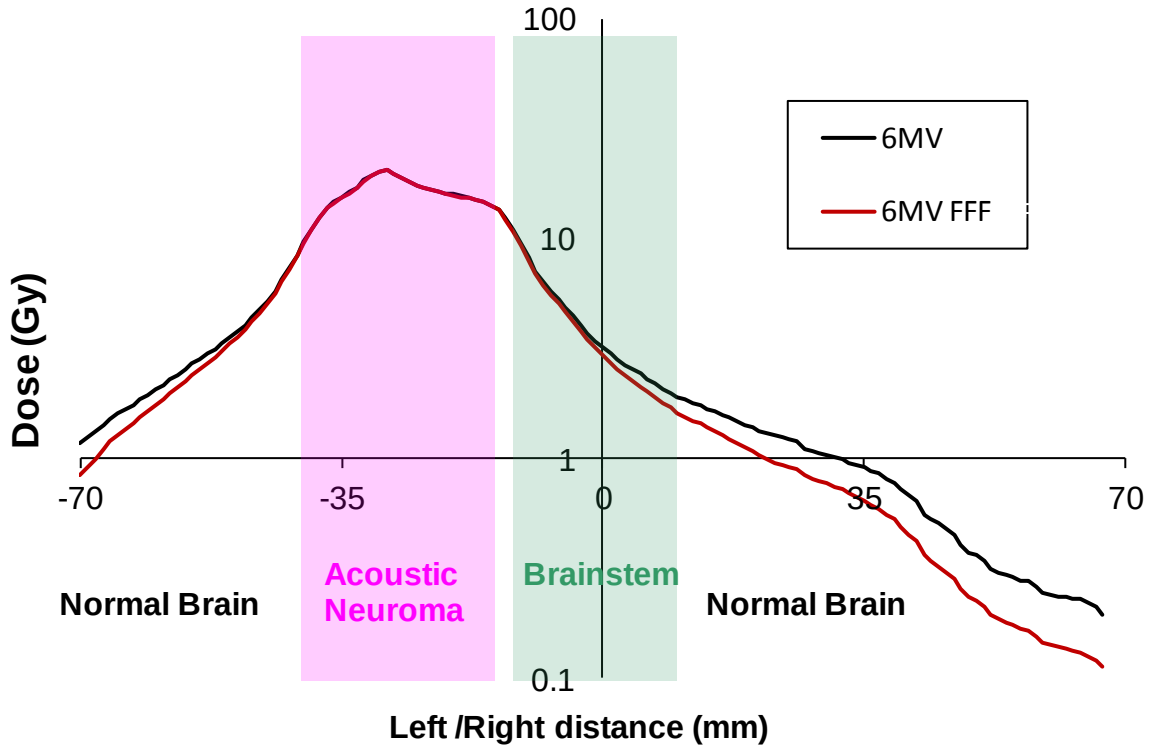

Figure 7.12. A plot of the dose profile through a lesion indicating the reduction in dose for FFF delivery within the close critical structures and more distant normal tissues. Cross-section plane is indicated in figure 7.11.

These treatment plans show very little effect when switching to the FFF beam model, as would be expected as the flattening filter has no real effect for small beams. The dose coverage and dose volume histograms for the targets remain unchanged in each case; however additional tissue sparing is seen for brainstem and normal brain for FFF. The dose to the lesion, brainstem and normal brain were assessed and are shown in table 7.8 below.

The most significant differences were observed for the low isodoses. For a prescribed dose of 12Gy, the V10 for normal brain and brainstem were reduced by nearly 60% and 10% respectively by using the FFF beam model (figure 7.12 & table 7.7).

Table 7.8. Assessment of doses to the Normal Tissue, Brainstem and the Lesion for the acoustic neuroma plan shown in figure 7.11 (from Heyes G and Cashmore J, Appendix H).

		V10 (cc)	V20 (cc)	V50 (cc)	V100 (cc)
Normal Tissue (3005.6cc)	6MV FFF	249.3	61.9	11.7	2.9
	6MV	396.6	80.5	12.6	3.0
	% Reduction using FFF	**-59.1**	**-30.1**	**-7.7**	**-3.8**
Lesion (2.42cc)	6MV FFF	2.4	2.4	2.4	2.4
	6MV	2.4	2.4	2.4	2.4
	% Reduction using FFF	**0.0**	**0.0**	**0.0**	**0.0**
Brainstem (14.31cc)	6MV FFF	12.5	7.5	1.7	0.2
	6MV	13.6	8.7	1.8	0.2
	% Reduction using FFF	**-8.7**	**-15.7**	**-8.5**	**0.0**

7.8 Discussion

There is a slight increase in the number of MU needed to deliver the same dose (6.7% for the cases studied) but this is an expected consequence of unflattened delivery because of the shape of the beam profile; delivering any dose *off-axis* will require the beam to be on for a longer period of time. Even taking this increase into account the rise in MU required for unflattened delivery is modest compared to the reduction in leakage dose seen.

The risk of second cancer induction can be related back to these values and will scale with the ratio of absorbed doses. Taking a nominal distance of 50cm to represent whole-body dose (Xu *et al* 2008), doses here are reduced on average by 64% for unflattened IMRT delivery, and this obviously represents a significant reduction in risk from leakage radiation.

Under both standard and clinical conditions out-of-field doses are seen to be lower at all positions relative to conventional delivery. In a recent Monte Carlo study

by Kry *et al* (2010) however, unflattened beams were seen to increase the dose in the region from 3-15cm from the field edge for IMRT delivery on a Varian accelerator. These differences may be due to variations in head design between Elekta and Varian machines, or due the Varian accelerator having a slightly lower effective energy (4MV). As the field size increases beyond the range used in this study it is possible that there may be similar issues for larger PTVs and in adults, and further study is required to quantify this.

Machines operating without a flattening filter are now commercially available such as the Tomotherapy HI-ART (TomoTherapy, Inc., Madison, WI) and CyberKnife (Accuray, Inc., Sunnyvale, CA), indicating that in a 'bottom-up' design the flattening filter is seen to be unnecessary. Helical delivery systems, however, are inefficient in MU delivery as dose is delivered in a slice-by-slice fashion so to deliver the same dose in clinical treatment plans requires 5-15 times as many MU (Ramsey *et al* 2006). The Tomotherapy system has been designed with this in mind with 23cm of attenuation (tungsten jaws and MLC leaves) meaning that for *static field delivery* leakage doses are reduced by 3-11 times compared to a conventional accelerator. When these factors are combined together, this results in similar, if not lower leakage than for a conventional linac delivering IMRT (Ramsey *et al* 2006).

Leakage may be reduced by increasing the shielding around the head, but this is both costly and cumbersome. Removal of the flattening filter is a relatively simple way of achieving the same effect on a conventional linac, and since the flattening filter doesn't actually seem to be required for IMRT one can argue that it should be removed for IMRT treatments. A filter free conventional linac could combine the best aspects of both delivery methods - a machine that combines the inherent dose delivery efficiency of a linac combined with the reduction of scatter from flattening filter removal.

7.9 Summary

Removal of the flattening filter for IMRT removes an unwanted and *unnecessary* source of scatter from the treatment head significantly reducing whole-body radiation doses.

The flattening filter has no effect on beam profiles for the small field sizes employed in stereotactic treatments. In these cases there is no reason why the filter should be in place and its removal for these treatments is recommended. FFF offers the opportunity for faster treatment times with reduced out-of-field doses to the patient.

If IMRT is to be used then this risk must be balanced by an increase in local control and reduced toxicity. Any increase in whole-body dose must be justified for paediatric patients who have the potential for such long-term survival and as much as possible should be done to reduce these doses and lower the risk of cancer induction.

CHAPTER 8

SUMMARY & FURTHER WORK

This final chapter provides a summary of the research presented in this thesis and discusses the scope for continuing research into FFF beams.

8.1 Overview

Removal of the flattening filter from the beam line produces profound changes in the operation and dosimetric characteristics of the treatment beam. Without the filter the electron contamination from the primary collimator is not only allowed to reach the ionisation chamber, but also has a negative effect on servo control as the direction of these electrons is somewhat random. By mounting a 2mm stainless steel plate in its place the electron contamination is reduced, and electrons generated in the plate have a strong directional component, which allows the beam steering servos to operate correctly.

The beam hardening offered by the flattening filter is obviously lost with its removal, but so also is the strong variation of the energy spectrum with distance from the central axis. The beam energy can be raised to maintain the same beam quality

and depth dose profile for the FFF beam, but matching off-axis is not possible, or in fact desirable.

By removing the differential absorption effect of the flattening filter the beam becomes far simpler to model, and commercial treatment planning systems seem capable of modelling these beams with the same accuracy as that observed for conventional beams.

The key benefit to filter removal comes from the reduction in scattered radiation from the treatment head. Not only do parameters like head scatter, output factors and surface doses show much less variation with field size, the leakage radiation reaching the patient is significantly reduced, as is the dose received by staff outside of the treatment bunker. The introduction of IMRT into routine use has raised questions regarding the additional out-of-field radiation received by patients. These techniques, which are inherently inefficient in MU delivery, can raise peripheral doses by a factor of 2 and raise concerns for secondary cancer induction later in life, particularly for paediatric patients. By introducing FFF the reduction in scatter, and hence leakage radiation, means that these doses are reduced by a similar factor, returning these doses to the levels seen for 3DCRT delivery.

The rapid expansion of IMRT delivery as the technique of choice for many treatment sites also removes the reason for having flattening filters in the first place. Previously, a flat radiation field was a prerequisite for treatment planning as radiotherapy was based on the delivery of radiation to 'box-like' structures within the body. With improvements in, and the widespread use of, imaging techniques such as CT, MRI the accurate identification and delineation of tissues is possible, and the delivery of radiation is sculpted to match the shape of the tumour, avoiding surrounding normal tissues as much as possible. This active production of 'non-flat' beams contradicts the use of a flattening filter – why flatten the beam only to go onto modulate the fluence to actively change this?

Although modern treatment planning systems were not specifically designed to cope with FFF beams the inherent flexibility of these systems to model treatment beams from various linac manufactures and energies means they also seem capable of modelling FFF beams accurately. Fluence optimisation of these beams for IMRT delivery remains the same, provided the beam profile is taken into account, and commercial planning systems have been shown to demonstrate equivalency in plans generated for conventional and FFF beams for a variety of treatment sites. Likewise the verification of these plans has shown no particular concerns for FFF delivery.

8.2 FFF linacs

Several medical accelerators are now available operating in FFF mode. The CyberKnife and TomoTherapy systems (Accuray) have shown that in a bottom-up design the flattening filter is not deemed a necessary component for either SRS (CyberKnife) or IMRT (TomoTherapy) delivery. Varian have also released the TrueBeam accelerator, and now Elekta have recently (March 1st 2013) released their version of the FFF linac (figure 8.1), the VersaHD (http://www.versahd.com/) incorporating the research and development and publications of data from this work and others.

Figure 8.1 The Elekta FFF linac, VersaHD, released March 1st 2013 (http://www.versahd.com/).

8.3 Scope for future work

Although the FFF linac has now been commercially released for medical use there is still a considerable amount of scope for continued research.

8.3.1 Beam specification and QA

Although FFF accelerators have been released there is still some ambiguity surrounding the specification of beam parameters and the quality control tests necessary. Parameters such a beam flatness and penumbra take on a different meaning for these beams and several attempts have been made to standardise these specifications (Ponisch *et al* 2006, Fogliata *et al* 2012). Many of these tests rely on reference to a flat beam, but this obviously relies on having filtered and FFF beams of the same energy on the linac. IMRT continues to increase in popularity and since the flattening filter is not necessary for modulated treatments it is likely that the use of flattened beams will decrease. It can therefore be envisioned that the FFF linac may

become the standard, so beams specification and QA tests must be designed so as not to be reliant on a flattened equivalent. The use of the Elekta AutoCAL software for MLC leaf calibration has been investigated by Mark Ramtohul (Appendix H) and found to be suitable for FFF beams (providing strict procedures are followed), but further testing will be required.

There is also the issue of long term performance under FFF operation. In theory the FFF beam is more stable, so this should result in increased reliability of the beam steering. Any improvements in this will need to come from long-term monitoring of QC tests. By operating in FFF mode there is also a reduced wear on the HT components of the linac as the beam needs to be on for only half the time (at 6MV) compared to normal operation. Again, in theory, this should translate into greater reliability and increased component lifetime. This remains to be seen.

8.3.2 Dose calculation (TPS)

FFF beams naturally lend themselves to SRS and IMRT treatments as, for small fields the flattening filter essentially has no effect on the beam profile, and for IMRT the fluence optimisation takes the non-flat profile into account. The subject of 3DCRT with FFF beams has not really been addressed and there is certainly scope for these to be used in conventional planning. The wedge profile is maintained without the filter in place, and the central axis boost inherent to these beams could be useful in many situations and warrants further investigation beyond that reported here.

Regarding the treatment planning systems themselves, there is still much work that could be done to optimise the calculation algorithms for FFF use. In particular the scatter kernels used for dose calculation are based on Monte Carlo studies using energy spectra from conventional beams, incorporating beam hardening from the

flattening filter. Ideally these kernels should be re-calculated and incorporated into the TPS.

IMRT plans generated with FFF beams also tend to contain more segments that those seen for flattened beams, so there is scope to improve the fluence optimisation and segmentation for FFF beams by taking the beam profile more fully into account. Hopefully this will improve the efficiency of the delivery, making full use of the increase in dose rate.

It is expected that the reduced scatter in FFF beams will increase the dosimetric accuracy of patient dose distributions, but so far this has not been demonstrated. This may be due to the reasons discussed above, and once treatment planning systems are optimised for FFF delivery it should be possible to determine if this is true.

8.3.3 Beam steering and isocentre accuracy

As discussed in section 2.2.10, when operating with a flattening filter in place (i.e. under standard operating conditions) the beam positioning is critical, as any misalignment will lead to asymmetrical beams. This is therefore closely monitored and under constant feedback control. The FFF beam is inherently more stable as the amplifying effect of the flattening filter is no longer present; the beam steering coils therefore perform a slightly different function in FFF beams. Instead of acting to maintain a symmetrical beam, the 2R and 2T currents simply move the beam from side to side, maintaining the initial beam shape (figure 2.15). Removing this restriction means that the bending and steering coils could be used for another purpose.

The intercept of the beam central axis with the gantry, collimator and couch rotation axes is known as the isocentre (figure 1.11). Ideally this is a single point in space, but due to the weight of the gantry arm and the torque exerted by the

treatment head the isocentre is realistically confined to a sphere with a diameter of approx. 1mm (figure 8.2). For stereotactic treatments this is on the limit of what would be acceptable, and improvements on this would be desirable. By changing the 2R, 2T and bending fine (Bf) currents the beam can be shifted in space, therefore it should be possible to actively *reposition* the beam as the gantry rotates so that the variation in radiation isocentre is minimised. This concept is not possible on a non-FFF linac due to the reasons discussed earlier, but as the need for these servo systems is reduced and their original function is changed it might be a possibility to utilise this effect. The 2R and 2T lookup tables would therefore be used, not to maintain a flat beam, but to reposition the central axis of the beam according to a set pattern as the gantry rotates, counteracting the effects of gantry sag (figure 8.3).

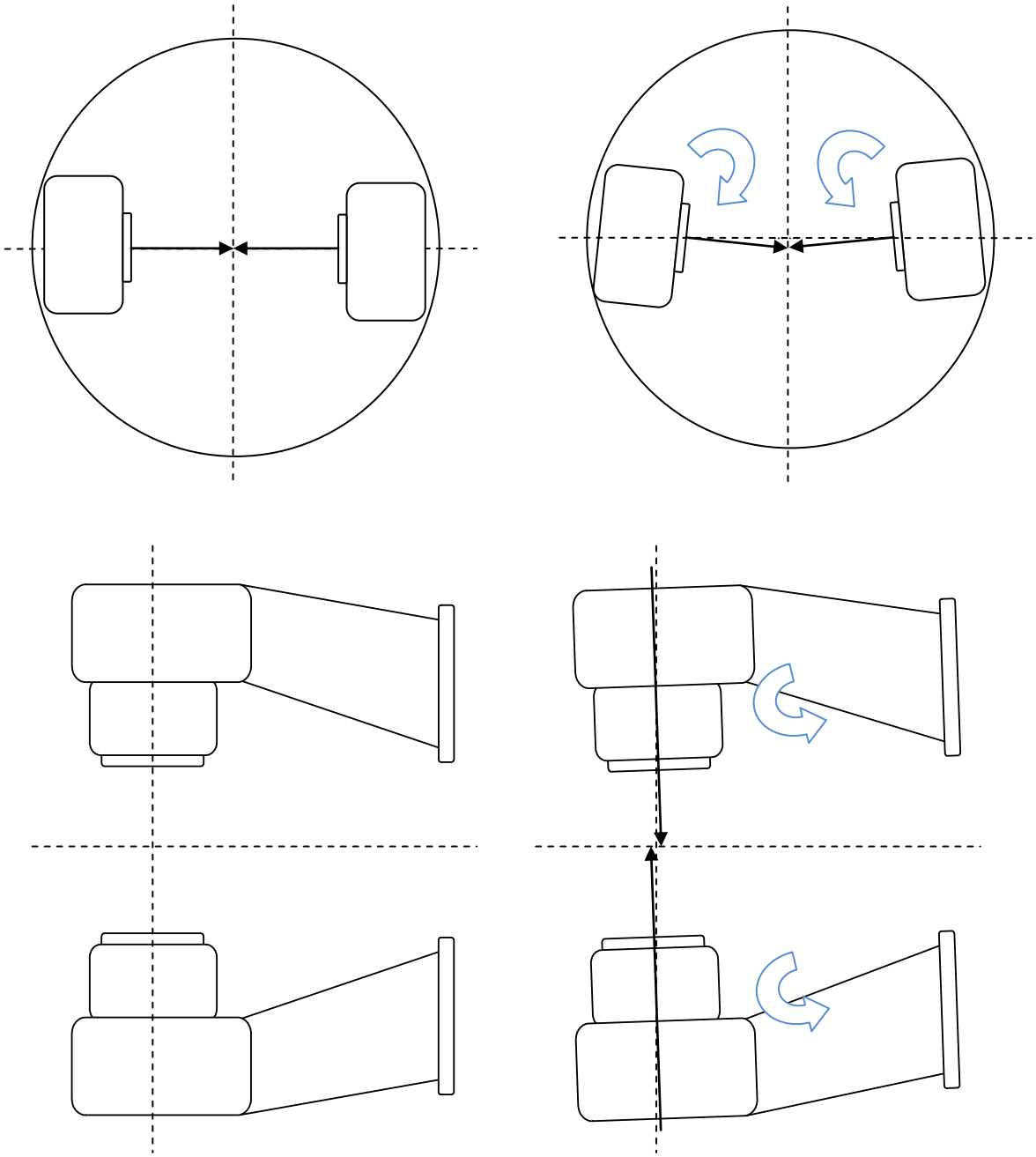

Figure 8.2. Ideally, the mechanical and radiation isocentre should form a single point in space (a) and (b). As the gantry rotates the sag and twist of the treatment head causes the isocentre form an ellipse of approx. 1mm diameter (c) and (d).

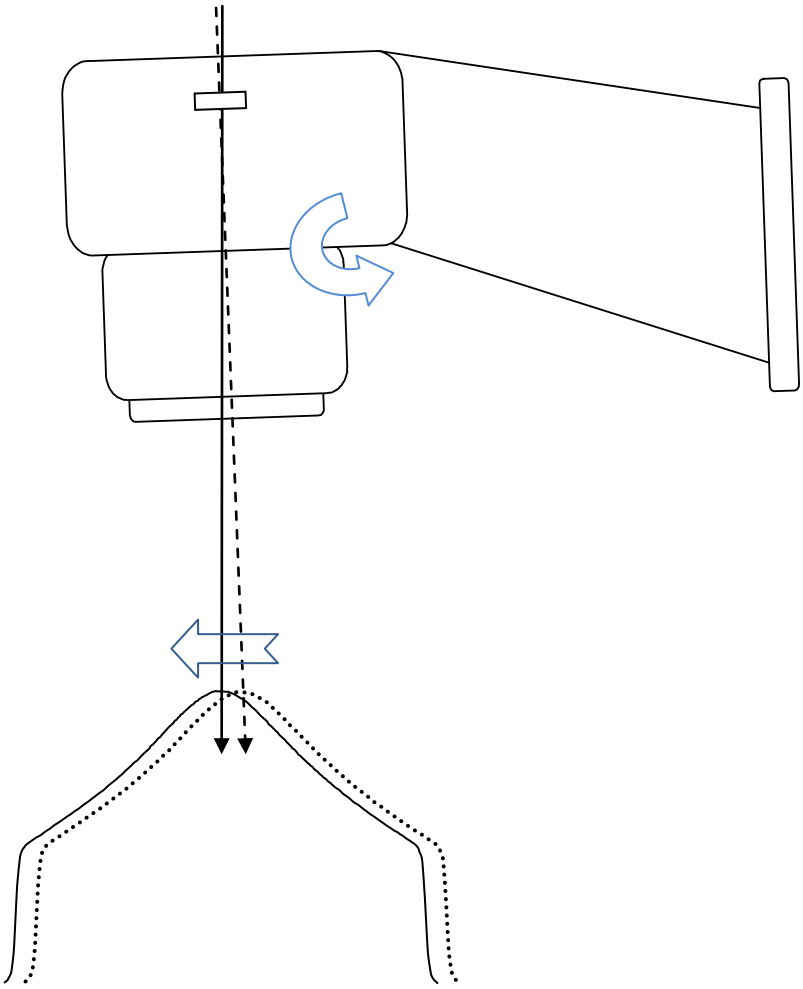

Figure 8.3. By changing the currents in the bending magnets and steering coils it could be possible to redirect the beam along a path to counteract the sag of the treatment head with gantry rotation. This would reduce the size of the isocentre enabling more accurate stereotactic treatments.

LIST OF REFERENCES

Abdel-Rahman W, Seutjens JP, Verhaegen F *et al*, "Validation of Monte Carlo calculated surface doses for megavoltage photon beams," *Med. Phys.* **32**(1): 286-298, (2005).

Almberg S, Frengen J, Lindmo T "Monte Carlo study of in-field and out-of-field dose distributions from a linear accelerator operating with and without a flattening-filter" *Med. Phys.* **39**(8): 5194-5203, (2012).

Alongi F, Fogliata A, Clerici B *et al*, "Volumetric modulated arc therapy with flattening filter free beams for isolated abdominal/pelvic lymph nodes: report of dosimetric and early clinical results in oligometastatic patients," *Radiat. Oncol.* **7**(1), 204 (2012).

Anand P, Kunnumakara AB, Sundaram C *et al.* "Cancer is a preventable disease that requires major lifestyle changes". *Pharm. Res.* **25** (9): 2097–2116, (2008).

Barton MB, Gebski V, Manderson C, Langlands AO. "Radiation Therapy: are we getting value for money?" Clin Oncol **7**: 287-292, (1995).

Bassal M, Mertens AC, Taylor L *et al,* "Risk of selected subsequent carcinomas in survivors of childhood cancer: a report from the Childhood Cancer Survivor Study" *J Clin Oncol* **24:** 476–483, (2006).

Bedford J, Lee YK, Wai P, "Evaluation of the Delta4 phantom for IMRT and VMAT verification," *Phys. Med. Biol.* **54**(9): N167-176, (2009).

Bortfeld T, "Optimized planning using physical objectives and constraints" *Semin. Radiat. Oncol.* **9**: 20-34, (1999).

Bortfeld T, Schlegel W "Optimization of beam orientations in radiation therapy: some theoretical considerations" *Phys. Med. Biol.* **38**: 291-304, (1993).

Bortfeld T, Schmidt-Ulrich R, De Neve W, Wazer DE, "Image-Guided IMRT," Springer-Verlag, Germany, (2006).

Bostwick DG, Eble JN *Urological Surgical Pathology*. St. Louis: Mosby. p. 468. ISBN 0-323-01970-6, (2007).

Brahme A, Kraepelien T, Svensson H, "Electron and photon beams from a 50 MEV racetrack microtron," *Acta. Radiol. Oncol.* **19**(4): 305-319, (1980).

Brahme A, Roos JE, Lax I "Solution of an integral equation in rotation therapy" *Phys Med Biol* **27**: 1221-1229, (1982).

Bruggmoser G, Saum R, Schmachtenberg A, Schmid F, Schüle E. "Determination of the recombination correction factor kS for some specific plane-parallel and cylindrical ionization chambers in pulsed photon and electron beams" *Phys. Med. Biol.*. **52**(2):N35-50, (2007).

BS EN 60976:2001, Medical electrical equipment – Medical electron accelerators – Functional performance characteristics, (2001).

Carl J, Vestergaard A. "Skin damage probabilities using fixation materials in high-energy photon beams" *Radiother. Oncol.* **55**: 191-198, (2000).

Cashmore J, "Flattening filter free radiotherapy", 9th Biennial Meeting on Physics and Radiation Technology for Clinical Radiotherapy *Radiother. Oncol.* ***84****, S100, (2007).*

Cashmore J, "The characterisation of unflattened photon beams from a 6MV linear accelerator", *Phys Med Biol.* **53**: 1933-1946, (2008).

Cashmore J, Ramtohul M, Ford D, "Lowering whole-body radiation doses in pediatric intensity-modulated radiotherapy through the use of unflattened photon beams" *Int. J. Radiat. Oncol. Biol. Phys.* **80**(4): 1220-1227, (2011).

Cashmore J, Golubev S, Dumont JL *et al,* "Validation of a virtual source model for Monte Carlo dose calculations of a flattening filter free linac" *Med.Phys.* **39** (6): 3262-3269, (2012).

CMS Monaco Beam Data Requirements Doc: 9415-953-01B, (2003).

CMS XiO Beam Data Collection List Doc: 9000-959-24H, (2003).

Das S, Cullip T, Tracton G *et al,* "Beam orientation selection for intensity-modulated radiation therapy based on target equivalent uniform dose maximization" *Int. J. Radiat. Oncol. Biol. Phys.* **55**: 215-224, (2003).

Derikum K, Roos M, "Measurement of saturation correction factors of thimble-type ionization chambers in pulsed photon beams" *Phys. Med. Biol.* **38**(6): 755–763, (1993).

Diallo ID, Haddy N, Adiadi E *et al*, "Frequency distribution of second solid cancer locations in relation to the irradiated volume among 115 patients treated for childhood cancer" *Int. J. Radiat. Oncol. Biol. Phys.* **74**: 876-83, (2009).

Dzierma Y, Licht N, Nuesken F *et al* "Beam properties and stability of a flattening-filter free 7 MV beam-An overview" *Med. Phys.* **39**(5): 2595-2602**,** (2012).

Elekta customer acceptance tests, Doc 4513 370 2065 04, (2005).

Ezzel G, Galvin J, Low D *et al* "Guidance document on delivery, treatment planning, and clinical implementation of IMRT: Report of the subcommittee of the AAPM radiation therapy committee" *Med. Phys.* **30**(8): 2089-2115, (2003).

Ezzel G, Eisbrauch A, Yu C *et al*, "Implementing IMRT in clinical practice: a joint document of the American Society for Therapeutic Radiology and Oncology and the American Association of Physicists in Medicine," *Int. J. Radiat. Oncol. Biol. Phys.* **58**(8): 1616-1634, (2004).

Fippel M "Fast Monte Carlo dose calculation for photon beams based on the VMC electron algorithm" *Med. Phys.* **26**: 867-878, (1999).

Fogliata A, Garcia R, Knoos T *et al* "Definition of parameters for quality assurance of flattening filter free (FFF) photon beams in radiation therapy" *Med. Phys.* ***39*** *(10)***:** 6455-6464, (2012).

Followill D, Geis P and Boyer A, "Estimates of whole-body dose equivalent produced by beam intensity modulated conformal therapy" *Int J Radiat Oncol Biol Phys* **38**: 667–672, (1997).

Fontenla DP, Napoli JJ, Hunt M *et al*, "Effects of beam modifiers and immobilization devices on the dose in the build-up region," *Int. J. Radiat. Oncol. Biol. Phys.* **30**(1): 211-219, (1994).

Fraumeni JF; Schottenfeld D, Marshall JM. *Cancer epidemiology and prevention*. Oxford [Oxfordshire]: Oxford University Press. pp. 977. ISBN 0-19-514961-0. (2006).

Fu W, Dai J, Hu Y, Han D, Song Y, “Delivery time comparison for intensity-modulated radiation therapy with/without flattening filter: a planning study” *Phys. Med. Biol.* **49**(8): 1535-47, (2004).

Georg D, Kragl G, Wetterstedt S *et al*, “Photon beam quality variations of a flattening filter free linear accelerator” *Med Phys* **37**(1): 49-53, (2009).

Georg D, Knoos T, McClean B, “Current status and future perspective of flattening filter free photon beams,” Med. Phys. **38**(3): 1280-1293, (2011).

Gerbi BJ, Khan FM. “The polarity effect for commercially available plane-parallel ionization chambers,” *Med. Phys.* **14**(2): 210-215, (1987).

Gerbi BJ, Khan FM. “Measurement of dose in the build-up region using fixed-separation plane-parallel ionization chambers” *Med. Phys.* **17**(1): 17-26, (1990).

Gerig LH, Niedbala M, Nyiri BJ, “Dose perturbations by two carbon fiber treatment couches and the ability of a commercial treatment planning system to predict these effects,” *Med. Phys.* **37**(1): 322-328, (2009).

Hall EJ, Wuu C, “Radiation-induced second cancers: The impact of 3D-CRT and IMRT” *Int. J. Radiat. Oncol. Biol. Phys.* **56**: 83-88, (2003).

Hall EJ. “Intensity-modulated radiation therapy, protons, and the risk of second cancers” *Int. J. Radiat. Oncol. Biol. Phys.* **65**: 1-7, (2006).

Hall J, Froster-Iskenius UG, Allanson JE. Handbook of normal physical measurements. Oxford University Press; (1995).

Hounsell AR, Wilkinson JM. “Head scatter modelling for irregular field shaping and beam intensity modulation” *Phys. Med. Biol.* **42**(9): 1737-49, (1997).

Hounsell AR, Wilkinson JM. “Electron contamination and build-up doses in conformal radiotherapy fields” *Phys. Med. Biol.* **44**(1): 43-55, (1999).

Hrbacek J, Lang S, Klöck S “Commissioning of photon beams from a filter-free linear accelerator and the accuracy of beam modelling using an anisotropic analytical algorithm”, *Int. J. Radiat. Oncol. Biol. Phys.* **80**(4): 1228-1237, (2011).

IAEA TECDOC 734, “Radiation dose in radiotherapy from prescription to delivery (1994)

IAEA TECDOC 1540 “Specification and acceptance testing of radiotherapy treatment planning systems”. International Atomic Energy Agency, Vienna, Austria, (2007).

IAEA Technical Report Series No. 430. Commissioning and quality assurance of computerized planning systems for radiation treatment of cancer. International Atomic Energy Agency, Vienna, Austria, (2004).

Institute of Physics and Engineering in Medicine. Guidelines for the clinical implementation of IMRT. Report 96. York, IPEM, (2008).

International Commission on Radiation Units and Measurements: *ICRU report 50: prescribing, recording, and reporting photon beam therapy*. Bethesda, MD, (1993).

International Commission on Radiation Units and Measurements: *ICRU report 62: prescribing, recording, and reporting photon beam therapy (supplement to ICRU report 50)*. Bethesda, MD (1999).

International Commission on Radiation Units and Measurements: *ICRU report 83: prescribing, recording, and reporting photon beam intensity-modulated therapy (IMRT). Journal of the ICRU* **10**:1, (2010).

International Commission on Radiological Protection.Recommendations. Annals of the ICRP Publication 60. Oxford, England: Pergamon Press, (1990).

Jiang SB, Boyer Al, Ma C. "Modelling the extra focal radiation and monitor chamber backscatter for photon beam dose calculation" *Med. Phys.* **18**: 55-66, (2001).

Jordan TJ. "Central axis depth dose data for use in radiotherapy" *Br. J. Radiol.* (Suppl. 25): 72, (1996).

Karan T, Moiseenko V, Gill B *et al* "Radiobiological effects of altering dose rate in filter-free photon beams" *Phys. Med. Biol.* **58**: 1075-1082, (2013).

Karlsson M, Nystrom H, Svensson H, "Photon beam characteristics on the MM50 racetrack microtron and a new approach for beam quality determination," *Med. Phys.* **20**(1): 143-149, (1993).

Karwakow J and Fippel M "Investigation of variance reduction techniques for Monte Carlo calculation using XVMC" *Phys. Med. Biol.* **45**: 2163-2183, (2000).

Karzmark CJ, Nunan CS, Tanabe E, *Medical Electron Accelerators* (McGraw-Hill Health Professions Division) p127. (1993).

Kim S, Liu CR, Zhu TC and Palta JR, "Photon beam skin analyses for different clinical setups," *Med. Phys.* **25**(6): 860-866, (1998).

Kim T, Zhu L, Suh TS *et al*, "Inverse planning for IMRT with nonuniform beam profiles using total-variation regularization (TVR)," *Med. Phys.* **38**(1): 57–66 (2010).

Klein EE, Esthappan J, Li Z. “Surface and buildup dose characteristics for 6, 10, and 18 MV photons from an Elekta Precise linear accelerator” *J. Appl. Clin. Med. Phys.* **4**(1), (2003).

Klein EE, Maserang B, Wood R, Mansur D. “Peripheral doses from pediatric IMRT” *Med. Phys.* **33**(7): 2525-31, (2006).

Knöös T, McClean B, “Dose calculations for external photon and electron beam therapy”, 9th Biennial ESTRO meeting. Barcelona, Spain, (2007).

Kragl G, Albrich D, Georg D, “Radiation therapy with unflattened photon beams: Dosimetric accuracy of advanced dose calculation algorithms” *Radiother. Oncol.* **100** 417-423, (2011a).

Kragl G, Baier F, Lutz S *et al*, “Flattening filter free beams in SBRT and IMRT: Dosimetric assessment of peripheral doses,” *Z. Med. Phys.* **21**(2): 91-101, (2011b).

Kragl G, Wetterstedt S, Knäusl B, *et al*, “Dosimetric characteristics of 6 and 10MVunflattened photon beams” *Radiother. Oncol.* **93**: 141–146, (2009).

Kretschmer M, Sabatino M, Blechschmidt A *et al*, “The impact of flattening-filter-free beam technology on 3D conformal RT,” *Radiother. Oncol.* **8**(1), 133 (2013)

Kry SF, Salehpour M, Followill D *et al*, “The calculated risk of fatal secondary malignancies from intensity-modulated radiation therapy” *Int. J. Radiat. Oncol. Biol. Phys.* **62**: 1195-1203, (2005).

Kry SF, Price M, Followill D *et al,* “The use of LiF (TLD-100) as an out-of-field dosimeter” *J Appl Clin Med. Phys.* **8**(4): 169-175, (2007).

Kry SF, Howell RM, Polf J *et al*, “Treatment vault shielding for a flattening filter-free medical linear accelerator” *Phys. Med. Biol.* **54**: 1265-1273, (2009).

Kry SF, Vassiliev ON, Mohan R, “Out-of-field photon dose following removal of the flattening filter from a medical accelerator” *Phys. Med. Biol.* **55**: 2155-66, (2010).

Lam KL, Muthuswamy MS, Tan Haken RK. “Flattening filter based empirical methods to parameterise the head scatter factor” *Med. Phys.* **23**: 343-52, (1996).

Lamb A, Blake S “Investigation and modelling of the surface dose from linear accelerator produced 6 and 10MV photon beams”, *Phys. Med. Biol.* **43**: 1133-1146, (1997).

Lang SL, Hrbacek J, Leong A, Klock S, “Ion-recombination correction for different ionization chambers in high dose rate flattening-filter-free photon beams” *Phys. Med. Biol.* **57**: 2819-2827, (2012).

Lang SL, Reggiori G, Vaque JP *et al*, "Pretreatment quality assurance of flattening filter free beams on 224 patients for intensity modulated plans: A multicentre study" *Med. Phys.* **39**(3): 1351-1356, (2012).

Lillicrap SC, Morgan HM, Shakeshaft JT, "X-ray leakage during radiotherapy" *Br. J. Radiol.* **73**: 793–794, (2000).

Lind M, Knöös T, Ceberg C, Wieslander E, McClean B, and Georg D, "Photon beam characteristics at the Monitor chamber level in a flattening filter free linac: A Monte Carlo study," *Radiother. Oncol.* **92**: S57, (2009).

Liu HH *et al* "A dual source photon beam model used in convolution/superposition dose calculations for clinical megavoltage x-ray beams" *Med. Phys.* **24**(12): 1960-1974, (1997).

Lopez Medina A, Teijeiro A, Garcia J *et al,* "Characterization of electron contamination in megavoltage photon beams," *Med. Phys.* **32**(5): 1281-1292, (2005).

Mansur DB, Klein EE, Maserang BP. "Measured peripheral dose in pediatric radiation therapy: A comparison of intensity-modulated and conformal techniques" *Radiother. Oncol.* **82**: 179-184, (2007).

Mayles P, Nahum A, Rosenwald JC, "Handbook of radiotherapy physics: theory and practice," Taylor & Francis, (2010).

McCormack S, Diffey J, Morgen A, "The effect of gantry angle on megavoltage photon beam attenuation by a carbon fiber couch insert," *Med. Phys.* **32**(2): 483-487, (2005).

McEwen MR, Kawrakow I, Ross CK, "The effective point of measurement of ionization chambers and the build-up anomaly in MV x-ray beams," *Med. Phys.* **35**(3): 950-958, (2008).

Mellenberg DE. "Dose behind various immobilization and beam modifying devices" *Int. J. Radiat. Oncol. Biol. Phys.* **32**(4): 1193-1197, (1995).

Mesbahi, A. "Dosimetric characteristics of unflattened 6MV photon beams of a clinical linear accelerator: A Monte Carlo study" *App. Radn and Iso.* **65**: 1029-1036, (2007).

Meydanci TP, Kemikler G," Effect of a carbon fiber tabletop on the surface dose and attenuation for high-energy photon beams," *Radiat. Med.* **26**(9): 539-544, (2008).

Mijnheer B, Bridier A, Garibaldi C *et al*, "Monitor unit calculation for high energy photon beams – practical examples," ESTRO Booklet 6, Brussels (2001).

Mohan R, Chui C, Lidofsky L. “Energy and angular distributions of photons from medical linear accelerators” *Med. Phys.* **12**(5): 592-597, (1985).

Morgan G, Ward R, Barton M, “The contribution of cytotoxic chemotherapy to 5-year survival in adult malignancies,” *Clin. Onc.* **16**(8): 549-560, (2004).

Mundt AJ and Roeske JC, “Intensity modulated radiation therapy: a clinical perspective,” BC-Decker, Ontario, (2005).

NCRP Report No. 115, Risk Estimates for Radiation Protection. National Council on Radiation Protection and Measurements (NCRP, Bethesda, Maryland) 1993.

Nicolini G, Ghosh-Laskar S, Shrivastava SK et al, “Volumetric Modulation Arc Radiotherapy With Flattening Filter-Free Beams Compared With Static Gantry IMRT and 3D Conformal Radiotherapy for Advanced Esophageal Cancer: A Feasibility Study,” *Int. J. Radiat. Oncol. Biol. Phys.* **84**(2): 553-560, (2012).

Nilsson B and Brahme A, “Electron contamination from photon beam collimators,” *Radiother. Oncol.* **5**(3): 235-244, (1986).

Nilsson B, Montelius A. “Fluence perturbation in photon beams under nonequilibrium conditions”, *Med. Phys.* **13**(2): 191-5, (1986).

Nordic Association of Medical Physics. Electron beams with mean energies at the phantom surface below 15 MeV. Supplement to the recommendations by the Nordic Association of Clinical Physics (NACP) 1980. *Acta Radiol. Oncol.* **20**(6): 401-415, (1981).

O’Brien PF, Gillies BA, Schwartz M, Young C, and Davey P, "Radiosurgery with unflattened 6-MV photon beams." *Med. Phys.* **18**: 519-521, (1991).

Palta J, Liu C, Li J “Quality assurance of intensity-modulated radiation therapy” *Int. J. Radiat. Oncol. Biol. Phys.* **71**, S108-S112, (2008).

Parsai EI, Shvydka D, Pearson D *et al*, “Surface and build-up region dose analysis for clinical radiotherapy photon beams,” *Appl. Radiat. Isot.* **66**: 1438-1442 (2008).

Petti PL, Goodman MS, Gabriel TA and Mohan R, “Investigation of buildup dose from electron contamination of clinical photon beams” *Med. Phys.* **10:** 18–24, (1983).

Podgorsak EB, Radiation Oncology Physics: A handbook for teachers and students. IAEA (2005).

Ponisch F, Titt U, Vassiliev ON, Kry SF, Mohan R. “Properties of unflattened photon beams shaped by a multileaf collimator” *Med. Phys.* **33**(6): 1738-46, (2006).

Pugachev A, Li JG, Boyer AL *et al* "Role of beam orientation optimization in intensity-modulated radiation therapy", *Int. J. Radiat. Oncol. Biol. Phys.* **50**: 551-560, (2001).

Purdy *et al*, IMRT Collaborative Working Group, "Intensity-modulated radiotherapy: current status and issues of interest," *Int. J. Radiat. Oncol. Biol. Phys.* **51**(4): 880-914, (2001).

Quinn M J, Babb P, Brock A, Kirby L and Jones J, *Cancer trends in England and Wales 1950–1999*. Studies in Medical and Population Subjects Series No.66, TSO: London, (2001).

Ramsey CR, Seibert R, Mahan SL *et al, "*Out-of-field dosimetry measurements for a helical tomotherapy system", *J. Appl. Clin. Med. Phys.* **7**(3): 1–11, (2006)

Rao BM, Prasad SG, Parthasaradhi K *et al,* "Investigations on the near surface dose for three 10-MV x-ray beam accelerators with emphasis on the reduction of electron contamination," *Med. Phys.* **15**(2): 246-249, (1988).

Rasband W, ImageJ 1.36b, National Institutes of Health, USA, http:/rsb.info.nih.gov/ij.

Rawlinson JA, Arlen D, Newcombe D. "Design of parallel plate ion chambers for build-up measurements in megavoltage photon beams". *Med. Phys.* **19**(3): 641-8 (1992).

Rogers DWO *et al,* "BEAM: a Monte Carlo code to simulate radiotherapy treatment units" *Med. Phys.* **22**: 503-24, (1995).

Ruben JD, Davis S, Evans C *et al*, The Effect Of Intensity-Modulated Radiotherapy On Radiation-Induced Second Malignancies *Int. J. Radiat. Oncol. Biol. Phys.* **70**(5): 1530-1536, (2008).

Satherberg A, Karlsson M, Karlsson M. "Theoretical and experimental determination of phantom scatter factors for photon fields with different radial energy variation". *Phys. Med. Biol.* **41**(12): 2687-94, (1996).

Scharf WH and Siebers JV, "Biomedical particle accelerators," New York, American Institute of Physics, (1994).

Scorsetti M, Alongi F, Castiglioni S *et al,* "Feasibility and early clinical assessment of flattening filter free (FFF) based stereotactic body radiotherapy (SBRT) treatments," *Radiat Oncol.* **6**: 113, (2011).

Sharpe MB, Miller MB, Yan D, and Wong JW. "Monitor unit settings for intensity modulated beams delivered using a step-and-shoot approach," *Med. Phys.* **27**: 2719–2725, (2000).

Sheikh-Bagheri and D.W.O. Rogers, "Monte Carlo calculation of nine megavoltage photon beam spectra using the BEAM code", *Med. Phys.* **29**(3): 391-402, (2002).

Shore RE, "Issues and epidemiological evidence regarding radiation-induced thyroid cancer," *Radiat. Res.* **131**: 98–111, (1992).

Sikora M and Alber M "A virtual source model of electron contamination of a therapeutic photon beam" *Phys. Med. Biol.* **54**(24): 7329-7344, (2009).

Sikora M, Dohm O and Alber M "A virtual source model of an Elekta linear accelerator with integrated mini MLC for Monte Carlo based IMRT dose calculation" *Phys. Med. Biol.* **52**: 4459-4463, (2007).

Sikora M, "Virtual source modelling of photon beams for Monte Carlo based radiation therapy treatment planning," Ph.D. dissertation, University of Bergen, Norway, (2011).

Smith DW, Christophides D, Dean C *et al*, "Dosimetric characterisation of the iBEAM evo carbon fiber couch for radiotherapy," *Med. Phys.* **37**(7): 3595-3606, (2010).

Stathekis S, Esquivel C, Gutierrez A *et al*, "Treatment planning and delivery of IMRT using 6 and 18MV photon beams without a flattening filter", *Appl. Radiat. Isot.* **67**(9): 1629-37, (2009).

Stein J, Mohan R, Wang XH, "Number and orientation of beams in intensity-modulated radiation treatments," *Med. Phys.* **24**(2): 149-160, (1997).

Stevens S, Rosser KE, Bedford JI, "A 4 MV flattening filter-free beam: commissioning and application to conformal therapy and volumetric modulated arc therapy" *Phys. Med. Biol.* **56**: 3809-3824, (2011).

Stovall M, Donaldson SS, Weathers BS *et al,* "Genetic effects of radiotherapy for childhood cancer: gonadal dose reconstruction," *Int. J. Radiat. Oncol. Biol. Phys.* **60**(2): 542-552, (2004).

Svensson H, 1st international symposium on quality assurance in radiation therapy**,** *Int. J. Radiat. Oncol. Biol. Phys.* **10**: 59-65, Suppl 1, (1984).

The British Institute of Radiology. Geometric uncertainties in radiotherapy: Defining the planning target volume. London. BIR, (2003).

The Royal College of Radiologists, Society and College of Radiographers, Institute of Physics and Engineering in Medicine. On Target: ensuring geometric accuracy in radiotherapy. London. RCR, (2008).

Timmerman R, Papiez L, McGarry R *et al*, "Extracranial stereotactic radioablation: Results of a phase I study in medically inoperable stage I non small cell lung cancer," *Chest* **124**: 1946-1955, (2003).

Titt U, Vassiliev O, Ponisch F,*et al* "A flattening filter free photon treatment concept evaluation with Monte Carlo" *Med. Phys.* **33**(6): 1595-1602 (2006).

Titt U, Vassiliev ON, Ponisch F, Kry SF, Mohan R. "Monte Carlo study of backscatter in a flattening filter free clinical accelerator" *Med. Phys.* **33**(9): 3270-3, (2006).

Tsechanski A, Krutman Y, Faermann S. "On the existence of low-energy photons (<150 keV) in the unflattened x-ray beam from an ordinary radiotherapeutic target in a medical linear accelerator" *Phys. Med. Biol.* **50**(23): 5629-39, (2005).

Tyner E, McClean B, McCavana P, af Wetterstedt S, "Experimental investigation of the response of an a-Si EPID to an unflattened photon beam from an Elekta Precise linear accelerator", *Med. Phys.* **36**(4): 1318-1329, (2009).

van der Giessen PH. "Calculation and measurement of the dose at points outside the primary beam for photon energies of 6, 10 and 23 MV" *Int. J. Radiat. Oncol. Biol. Phys.* **30**: 1239-46 (1994).

Van Esch A, Bohsung J, Sorvari p *et al*, "Acceptance tests and quality control (QC) procedures for the clinical implementation of intensity modulated radiotherapy (IMRT) using inverse planning and the sliding window technique: experience from five radiotherapy departments," *Radiother. Oncol.* **65**(1): 53-70, (2002).

Vassiliev ON, Titt U, Kry SF, Ponisch F "Monte Carlo study of photon fields from flattening filter-free clinical accelerator" *Med. Phys.* **33**(4): 820-7 (2006a)

Vassiliev ON, Titt U, Ponisch F *et al* "Dosimetric properties of photon beams from a flattening filter free clinical accelerator" *Phys. Med. Biol.* **51:** 1907-17 (2006).

Vassiliev ON, Kry SF, Kuban DA *et al* "Treatment planning study of prostate cancer intensity modulated radiotherapy with a Varian Clinac operated without a flattening filter". *Int. J. Radiat. Oncol. Biol. Phys.* **68**(5): 1567-1571, (2007).

Velkley DE, Manson DJ, Purdy JA, Oliver GD. "Build-up region of megavoltage photon radiation sources". *Med. Phys.* **2**: 14-24 (1975).

Verellen D, Vanhavere F, "Risk assessment of radiation-induced malignancies based on whole-body dose equivalent estimates for IMRT in the head and neck region" *Radiother. Oncol.* **53**: 83-88, (1999).

Wang Y, Khan MK, Ting JY *et al*, "Surface Dose Investigation of the Flattening Filter-Free Photon Beams" *Int. J. Radiat. Oncol. Biol. Phys.* **83**(2): E281-E285 (2012).

Webb S. "The physical basis of IMRT and inverse planning," *Br. J. Radiol.* **76**: 678-689, (2003).

Weiss E, Hess CF, "The impact of gross tumour volume (GTV) and clinical target volume (CTV) definition on the total accuracy in radiotherapy," *Strahl. Onkol.* **179**(1): 21-30, (2003).

Xu George X, Bednarz B, Paganetti H, "A review of dosimetry studies on external-beam radiation treatment with respect to second cancer induction" *Phys. Med. Biol.* **53**: R193-R241, (2008).

Yu CX, "Intensity-modulated arc therapy with dynamic multileaf collimation: an alternative to tomotherapy," *Phys. Med. Biol.* **40**(9): 1435-1449, (1995).

Zefkili S, Kappas C, Rosenwald JC. "On-axis and off-axis primary dose component in high energy photon beams" *Med. Phys.* **21**(6): 799-808, (1994).

Zelefsky MJ, Fuks Z, Hunt M, *et al,* "High dose radiation delivered by intensity modulated conformal radiotherapy improves the outcome of localized prostate cancer," *J. Urol.* **166**: 876–881, (2001).

Zelefsky MJ, Fuks Z, Hunt M, *et al,* "High-dose intensity modulated radiation therapy for prostate cancer: Early toxicity and biochemical outcome in 772 patients," *Int. J. Radiat. Oncol. Biol. Phys.* **53**: 1111–1116, (2002).

Zhang GG, Ku L, Dilling TJ *et al,* "Volumetric modulated arc planning for lung stereotactic body radiotherapy using conventional and unflattened photon beams: a dosimetric comparison with 3D technique," *Radiat. Oncol.* **6** (1): 152 (2011).

Zhu TC, Bjärngard BE, "The fraction of photons undergoing head scatter in X-ray beams", *Phys. Med. Biol.* **40:** 1127-34, (1995).

Zhu TC, Bjärngard BE. "Head scatter off-axis for megavoltage x rays" *Med. Phys.* **30**(4): 533-43, (2003).

Zhu XR, Kang Y, Gillin MT," Measurements of in-air output ratios for a linear accelerator with and without the flattening filter" *Med. Phys.* **33**(10): 3723-33, (2006).

Zhuang M, Zhang T, Chen Z *et al*, "Advanced nasopharyngeal carcinoma radiotherapy with volumetric modulated arcs and the potential role of flattening filter-free beams," *Radiat. Oncol.* **8**(1): 120 (2013).

Zwahlen DR, Lang S, Hrbacek J *et al*, "The use of photon beams of a flattening filter-free linear accelerator for hypofractionated volumetric modulated arc therapy in localised prostate cancer," *Int. J. Radiat. Oncol. Biol. Phys.* **83**(5): 1655-60 (2012).

APPENDIX A

INTENSITY MODULATED RADIOTHERAPY (IMRT)

Starting in the 1980s and through the 1990s the mainstay of treatment planning was 3D conformal radiotherapy (3DCRT). However, depending on the size, shape and position of a tumour it is often found that the use of uniform intensity beams is often not sufficient to adequately treat the tumour whilst sparing surrounding tissues, especially if the target has concave surfaces. The ability to adjust the intensity of individual rays within a beam can be utilised to achieve better target homogeneity, conformity and/or better sparing of normal tissues. This need for beams with non-uniform intensity was first described by Brahme *et al* in 1982 and is the basis of intensity modulated radiotherapy (IMRT), and refined since by many authors (e.g. Bortfeld 1993 and 1999, Webb 2003).

IMRT is therefore a radiation delivery technique where multiple beams are incident on a target site from *different directions* in which at least some of the beams are intensity-modulated so that each beam *intentionally* delivers a non-uniform dose to the target (figure A.1).

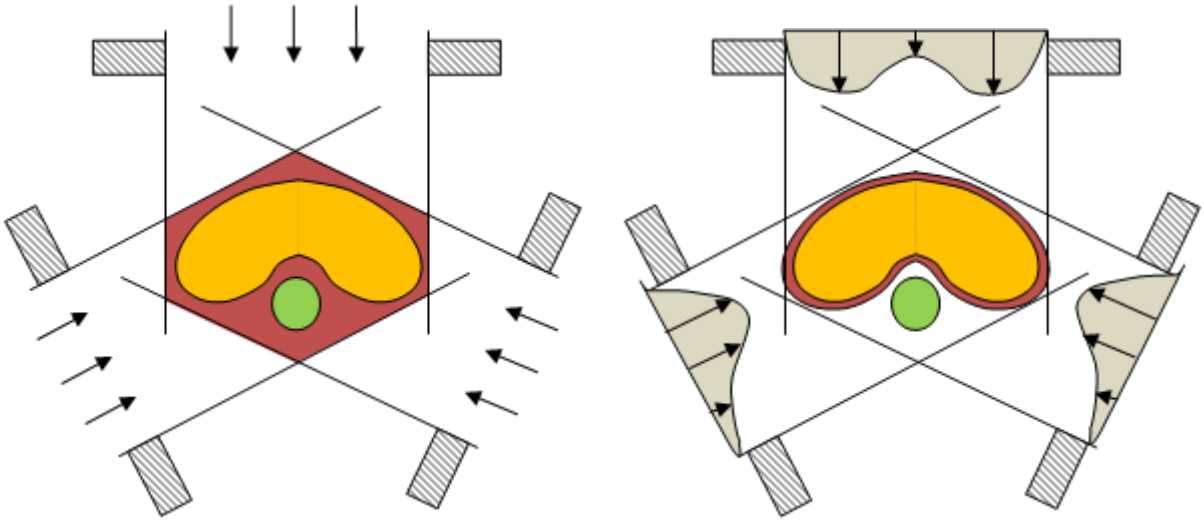

Figure A.1. In (a) the tumour (orange) is treated with 3D conformal therapy using three beams of radiation, all of uniform intensity. The red region shows the area treated by this combination of beams which includes the organ at risk (green). By using non-uniform beam intensities (b) the treatment area can be created to match the tumour shape, sparing the OAR from the high dose region.

The traditional approach in treatment planning is for the planner to create a plan based on a manual trial-and-error process using a suitable arrangement of beams. The treatment goal is to maximise the dose to the target while minimising the dose to the surrounding anatomy and critical structures. This is achieved by manually manipulating the beam parameters such as beam angle, shape, weighting etc. to achieve a suitable dose distribution.

'Inverse' planning reverses this process by defining the clinical goals upfront, and using an optimisation algorithm to find the best beam parameters to meet the solution. 'Intensity modulation' means that the intensity of radiation in a given treatment field varies across the field. This is achieved by splitting each field into individual 'beamlets', where a beamlet is the area representing a potential MLC opening (figure A.2). In one dimension this is set by the physical width of the MLC

leaf (fixed by MLC design), and in the other by the step increment of the leaf (which can be controlled).

IMRT can be used to either reduce normal tissue complications by more conformal shaping of the high dose region thereby improving quality of life, or to escalate the dose to the tumour, maintaining NTCP but potentially increasing tumour control.

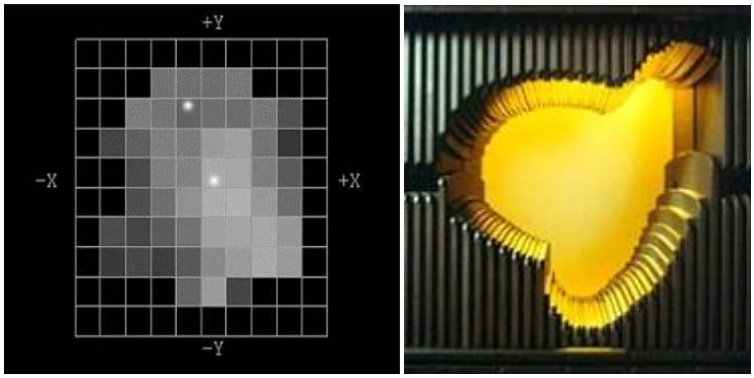

Figure A.2. (a) The beam can be broken up into individual beamlets, the intensity of each can be varied to obtain a more optimal dose distribution. (b) A multileaf collimator (MLC).

Optimisation

The task of the optimisation algorithm is to find to best combination of beam intensities to meet the dose *objectives* for the tumour whilst maintaining the dose *constraints* set for the organs at risk, usually set as DVH limits (see figure A.3).
All targets, organs at risk and sensitive structures must therefore be outlined. The IMRT prescription defines the limits, priorities, and goals for the optimization algorithm.

Numerous algorithms can be (and have been) used to perform this task. In simplistic terms the optimisation engine calculates a cost function, a single number describing the difference between the desired plan and the current plan. Then, during

each iteration, the intensity of each beamlet is altered to try and minimise this value until an optimum dose distribution is achieved. The stopping point is reached either when the dose objectives are met or the convergence criterion and/or a set number of iterations are reached.

As with any data reduction technique, this translation of treatment objectives into a single objective function results in significant loss of information about the dose distribution, so it is important to review the plan thoroughly. The plan with the lowest objective function may not necessarily be the best plan, and clinical judgement must be applied when reviewing dose distributions.

IMRT Prescription

IMRT Prescription

Structure	Type	Rank	Objective	Dose(Gy)	Volume(%)	Weight	Power	Status
RectumEd	OAR	2	Maximum	72.00	0	100	2.0	On
			Dose Volume	65.00	5	100	2.2	On
			Dose Volume	46.00	35	100	2.0	On
			Dose Volume	30.00	65	100	2.0	On
Bladder	OAR	3	Maximum	65.00	0	100	2.0	On
			Dose Volume	42.00	10	100	2.0	On
			Dose Volume	22.00	30	100	2.0	On
PTVcomb	Target	1	Maximum	75.50	0	100	2.2	On
			Goal	74.00	100		1.0	On
			Minimum	74.00	100	100	2.3	On

Figure A.3. A simple IMRT prescription for prostate IMRT (XiO TPS).

Segmentation

At the end of the optimisation process the TPS has an 'ideal' fluence map representing the relative intensities of the each beamlet which does not take into account any beam delivery constraints. A second step is generally required where the 'ideal' fluence map must be translated into a series of MLC segments using a leaf sequencing algorithm. This discretises the ideal fluence map (figure A.4) and converts

it into a series of control points specifying leaf positions as a function of MU delivery (figure A.5).

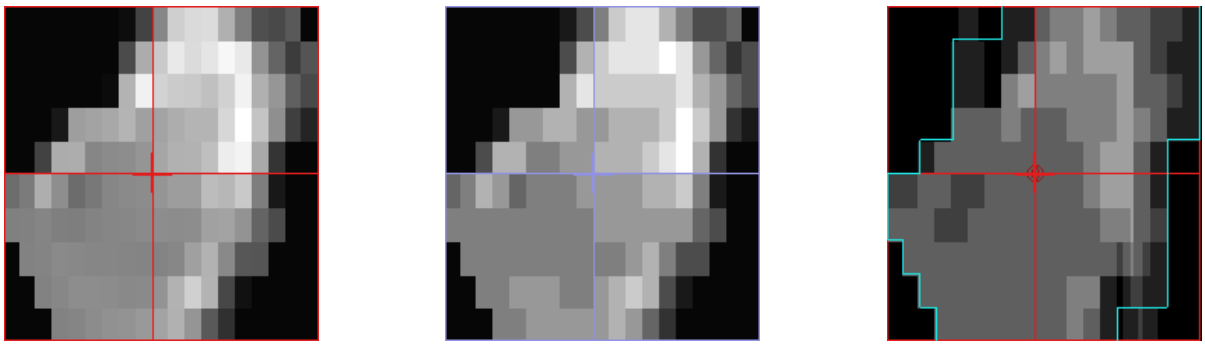

10 levels 5 levels Segmented

Figure A.4. In this XiO plan the 'ideal' fluence map needs to be converted into a discrete format by choosing a fixed number of intensity levels. With more levels the ideal map is reproduced more faithfully, but more segments are needed to deliver the plan.

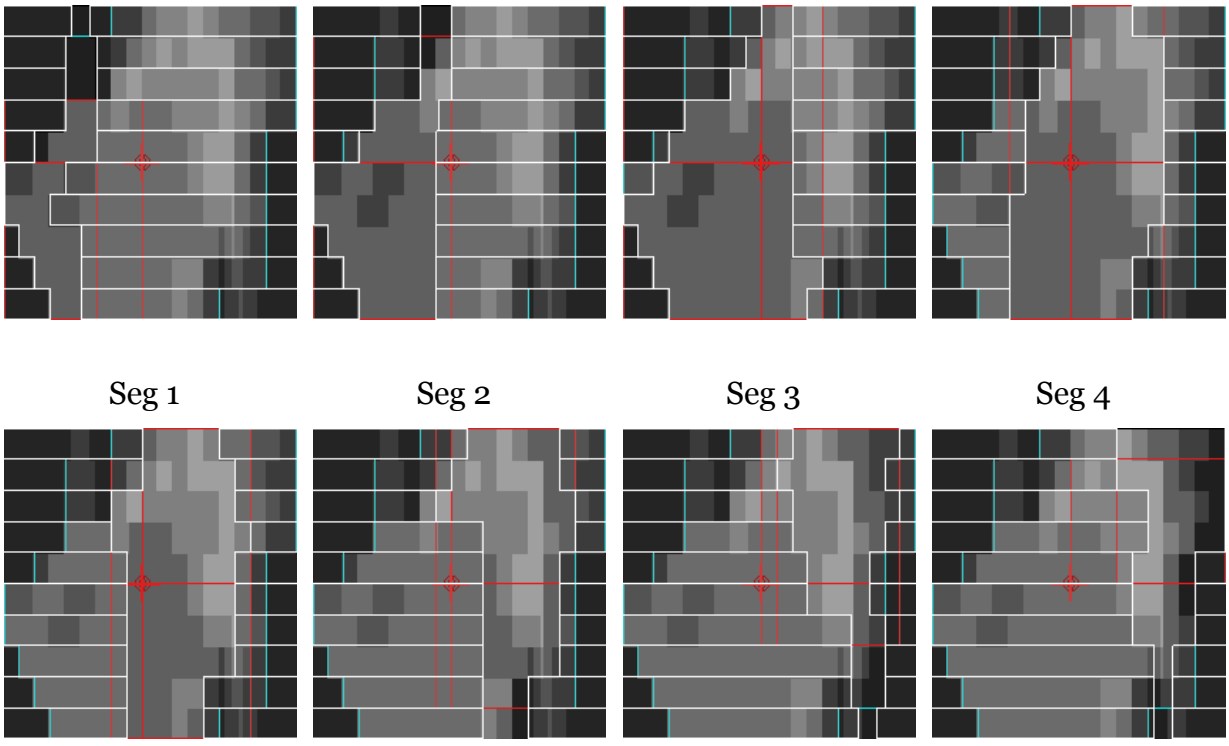

Seg 1 Seg 2 Seg 3 Seg 4

Seg 5 Seg 6 Seg 7 Seg 8

Figure A.5. The ideal fluence map is converted into a series of MLC shapes by the leaf sequencer. When superimposed on top of each other these beams will produce the segmented distribution.

The resulting superposition of MLC shapes may fail to reproduce the ideal fluence due to constraints on the shapes that can be made by the MLC (e.g. due to limits on over-travel distance, inter-digitation, leakage and scatter). Therefore, during this second stage the plan quality is often degraded. This can be reduced by decreasing the step size and increasing the number of intensity levels. The plan will have more segments and take longer to deliver, but will more closely resemble the optimised plan. The more complex the intensity distribution, the greater the deviation possible.

IMRT delivery techniques

IMRT can be delivered by a diverse range of delivery techniques (figure A.6), but the common feature is that they all try to control the dose distribution through the superposition of a large number of fields either from a number of fixed beam directions, or on one or multiple arcs.

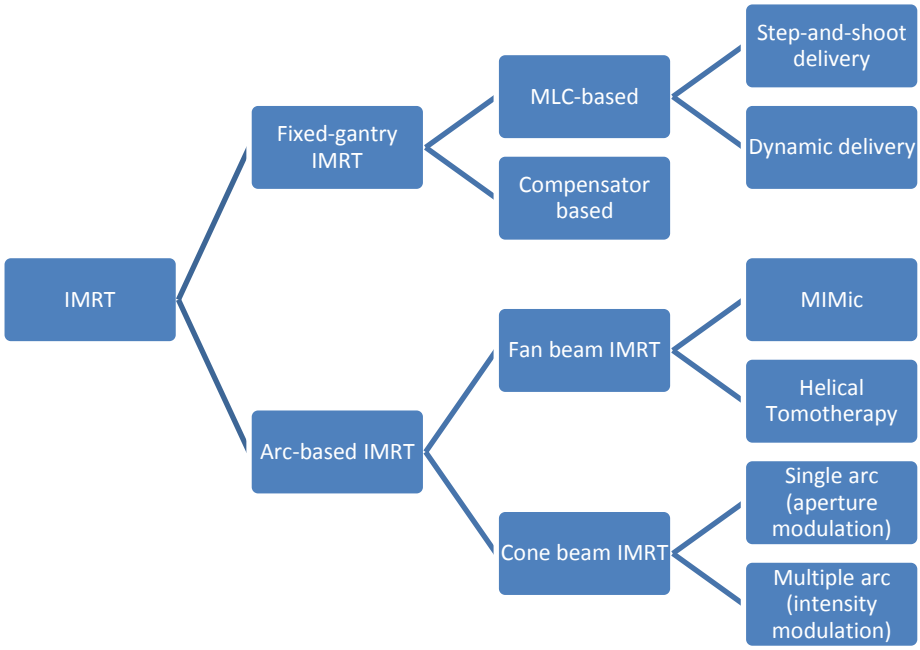

Figure A.6. Modified from Mundt (Intensity Modulated Radiation Therapy: A Clinical Perspective).

Throughout this thesis we are concerned with two aspects of inverse IMRT; that of step-and-shoot (MLC-based, fixed gantry angle), and VMAT (single or multiple arc-based cone beam IMRT).

In step-and-shoot IMRT the fluence is optimised at a set of fixed gantry angles. The fluence is then delivered by the superposition of a number of MLC shapes, one on top of the other. The beam is turned off whilst the MLCs are moving, and turned on again once the new shape has been formed. The gantry then rotates to the next angle and the process repeated.

VMAT (volumetric modulated arc therapy) is an advancement of the intensity-modulated arc therapy (IMAT) technique first proposed by Cedric Yu (Yu 1995). VMAT adds extra degrees of freedom to IMAT in that the gantry speed, dose rate and collimator angle, as well as MLC shape, can all be varied *during* delivery. Single or multiple arcs can be delivered depending on the complexity of the problem and the degree of modulation required.

IMRT is an inherently complex process, subject to a multitude of potential problems, some of which are discussed below. Several review and guidance documents have been published to assist departments in the complex processes of IMRT implementation (Ezzel *et al* 2003 & 2004, IPEM Report 96 2008, Purdy *et al* 2001, Van Esch *et al* 2002).

Problems/limitations of IMRT

Outlining

Dose placement is controlled by the optimisation algorithm which can only control dose in structures which it knows about. All targets and organs at risk must therefore

be outlined, which can be very time consuming, even when automatic outlining software is utilised.

Optimisation

All things being equal an IMRT plan should always produce a more homogeneous plan than uniform intensity beams from 3D conformal techniques, but in general this is not the case. The inhomogeneity occurs due to the overriding need to spare one or more critical organs, with the severity depending on the dose constraints and their proximity to the target.

Beam configuration can also have a significant effect on the plan quality. For fixed-beam IMRT beam angles are generally chosen so that the shortest path to irradiate the target, avoiding OARs, often placed in equi-angular steps, but the best distribution will be achieved by a large number of beam angles. Depending on the complexity of the plan the quality is seen to saturate above a certain number. If 7 to 9 beams are employed at evenly spaced gantry angles this is usually sufficient and beam angle optimisation does not add much to the plan. Stein *et al* found that this was most valuable for less than 6 beams (Stein 1997). Das *et al* (2003) showed that 3 to 5 beams optimised for beam angle gave similar results to a large number of beams evenly spaced. In general it is seen that 5 to 7 beams are sufficient for most plans with no beam angle optimisation.

In principle gantry angles can be optimised along with the beamlets but the computational time becomes excessive. Beam intensity profiles must be optimised for every test configuration because the influence of the gantry angles is not known until this beamlet optimisation is performed.

The use of VMAT technologies removes the need to decide on set gantry angles up-front. The start and stop positions for the delivery are specified and the algorithm

optimises the fluence delivery at each point on the gantry rotation. IMRT plans that are sensitive to number of beams and gantry angles used can benefit from this type of treatment.

Beam start-up

IMRT treatments delivered with step-and-shoot techniques tend to have a large number of segments, mostly with low MU (e.g. <10). For low MU delivery it is important for the beam to stabilise as quickly as possible after start-up as during start-up the beam energy, dose per MU and beam profiles can be unstable and vary from there intended characteristics. For VMAT delivery the quality of the delivery is also dependant on the rapid stabilisation of the beam as the gantry rotates.

Uncertainties in small field dosimetry

The doses associated with the small, off-axis, elongated fields associated with IMRT are difficult to predict. Most treatment planning systems have a limited ability to model changes in head scatter for complex situations, and variations in energy spectrum across the flattening filter and through treatment aids (such as the couch-top). This uncertainty requires the use of pre-treatment/patient-specific QA for IMRT plans.

Patient-specific QA

The intention of patient specific QA is to ensure that the correct dose and dose distribution are delivered to the patient. It is often difficult to determine if differences between measured and planned dose distributions are due to the TPS, data transfer, linac delivery, the measuring device or the analysis of the data. Detailed knowledge of each part is required to identify the cause of any discrepancies.

Patient specific QA is very time consuming and requires the use of specific equipment (figure A.7).

Leakage radiation

IMRT as an inefficient way to deliver dose, increasing MU demand by 2-3 times over conventional delivery. Leakage radiation scales directly with MU so out-of-field doses to the patient will increase. This raises the whole-body dose to the patient and may lead to increased demands on bunker shielding if IMRT is used for a significant proportion of treatments.

(a) 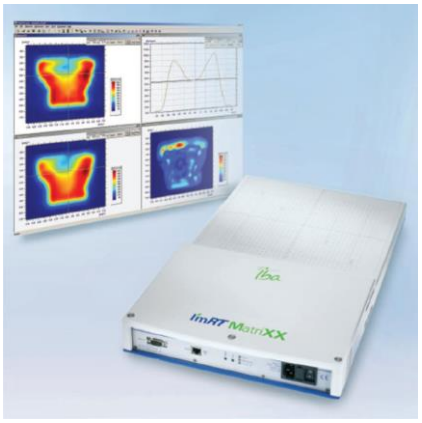

(b) 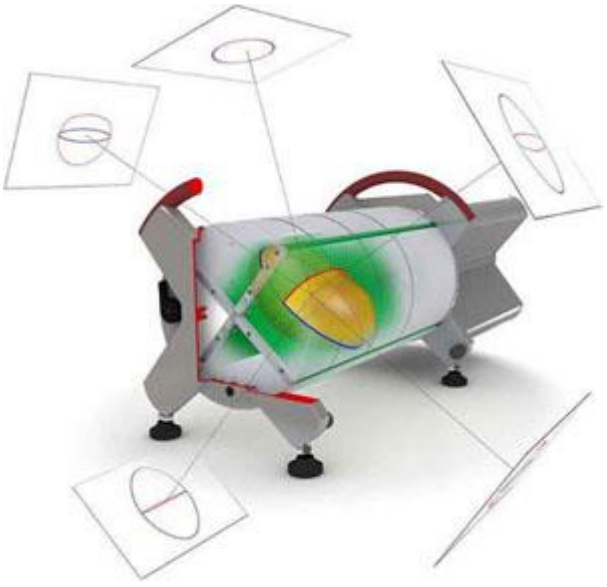

Figure A.7. Examples of equipment used for patient specific QA forIMRT. (a) The MatriXX (IBA, Germany) *and (b) Delta⁴* (ScandiDos, Uppsala, Sweden) *devices.*

APPENDIX B

DEFINITION OF PLANNING VOLUMES

Improvements and advances in radiotherapy must be measured by patient outcome in terms survival and quality of life, which relies heavily on the follow-up of patients. This in turn relies on the accurate prescribing, recording and reporting of radiotherapy doses. To do this it is necessary to have consistency in the way targets and organs are specified and to report these in a consistent way. The way in which tumours are outlined can vary, as do the prescription points, doses delivered and tolerance doses for organs. The sharing of data between different institutions and countries relies on this.

A dose difference as small as 5% may lead to a change in tumour response, or more likely, a change in normal tissue complication rate. This level of uncertainty in dose can easily be introduced by different reporting methods, and inadequate reporting can lead to the false interpretation of a study and its wrongful application.

ICRU volumes

The definition and delineation of treatment volumes has been defined by the International Commission on Radiation Units and Measurements (ICRU) and evolved with radiotherapy technology from Report 29 in 1978, through Report 50 (ICRU 1993) and a subsequent supplement to this, Report 62 (ICRU 1999) (figure B.1). These reports provide recommendations on the volumes and absorbed doses important to prescribing, recording and reporting radiotherapy treatments. These volumes are:

- Gross Tumour Volume (GTV)
- Clinical Target Volume (CTV)
- Planning Target Volume (PTV)
- Treated Volume
- Irradiated Volume
- Organ at Risk (OR or OAR)
- Planning Organ at Risk Volume (PRV)

Gross Tumour Volume (GTV)

The GTV represents the gross palpable or visible extent and location of the tumour. The extent can be determined by palpation or direct visualisation, or indirectly through different imaging modalities (CT, MRI etc), and may appear different depending on the examination technique used. If the tumour has been surgically removed before radiotherapy then no GTV can be defined.

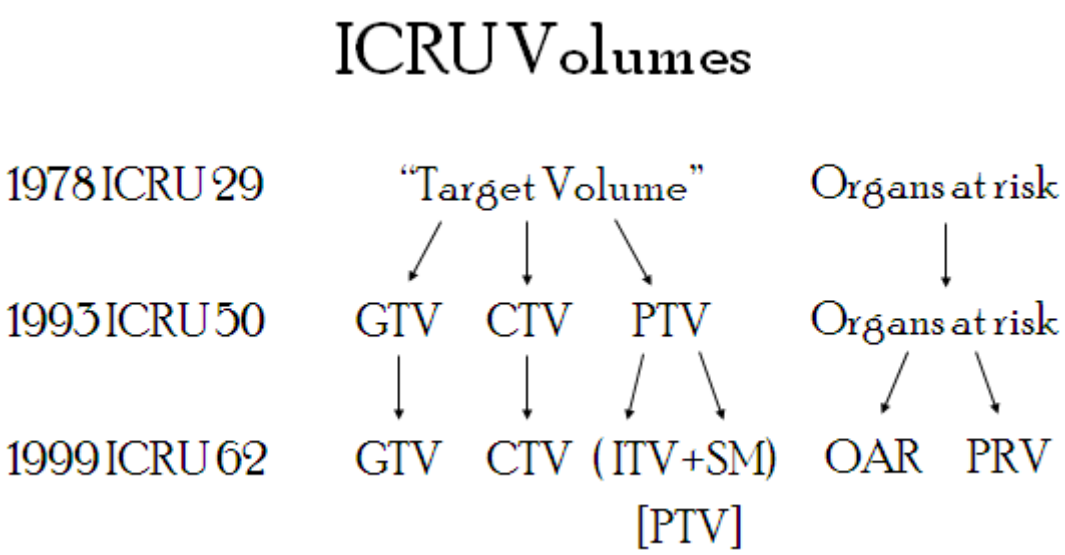

Figure B.1. Changes in the ICRU definition of volumes from report 29 to 62.

Clinical Target Volume (CTV)

Pathology studies of tumours removed surgically confirms that the GTV is generally surrounded by a region of 'normal' tissue, which may be invaded by *subclinical* microscopic extensions of the tumour. The CTV is an anatomical concept representing the volume of known or suspected tumour as it must be assumed that there may be cancer cells present even if they can't be detected.

If the cancer has spread to other regions of the body then there may be more than one CTV. Delineation therefore requires careful consideration of the capacity for local invasion to different regions and spread to the lymph nodes

The largest component of the GTV to CTV margin may be the delineation error in drawing the GTV. Consideration should be made for this in the margin used.

Internal Target Volume (ITV)

ICRU Report 62 recommends that an internal margin (IM) be added to the CTV to compensate for internal physiological movements and variations in the size, shape, and position of the CTV during treatment. The volume that includes the CTV with these margins is called the internal target volume (ITV) and therefore the ITV = CTV + IM.

Set-up Margin (SM)

To account for uncertainties in mechanical and human alignment a Set-up Margin (SM) is needed. These uncertainties depend on many factors, such as:

- variations in patient positioning,
- mechanical uncertainties of the equipment (e.g., sagging of gantry, collimators, and couch),
- dosimetric uncertainties,
- transfer errors from CT and simulator to the treatment unit,
- human factors.

Planning Target Volume (PTV)

The PTV is a geometrical concept to ensure prescribed dose is actually delivered to the CTV throughout the course of treatment and therefore consists of the Internal Margin (IM) and the Set-up Margin (SM). In practice the IM and SM are not added linearly but are combined together through the use of a 'margin recipe'.

These formulae are based on imaging studies identifying the random and systematic errors for a set treatment, and will be particular to each treatment centre.

The combination of each source of uncertainty, and therefore the margins required for each type of treatment can be calculated from population based studies. Many 'margin' formulae exist and the reader is referred to the publication 'Geometric Uncertainties in Radiotherapy' (BIR 2003) for further information.

Organs at Risk (OR/OAR)

Organs at Risk are normal tissues (e.g., spinal cord) whose radiation sensitivity may significantly influence the treatment planning process of prescribed dose. Knowledge about the sensitivity of normal tissues is derived mainly from clinical observations.

Planning Organ at Risk Volume (PRV)

As with the PTV, any movements of the Organ(s) at Risk during treatment, as well as uncertainties in the set-up during the whole treatment course, must be considered. The PRV is a geometrical concept used to ensure adequate OAR sparing will actually be achieved.

Note that a PTV and a PRV may overlap and a ranking needs to be established as to which takes priority, and the prescribed dose, or clinical intent altered to allow for this.

Treated Volume

The PTV should be enclosed by a minimum isodose surface which is adequate to treat the target. The volume enclosed by this isodose surface (usually 95%) is called the treated volume, and is generally larger than the planning target volume.

Irradiated Volume

The volume of tissue receiving a significant dose (e.g., ≥50% of the specified target dose) is called the irradiated volume. Again, this will depend on the treatment technique used, but will be larger than the treated volume. Figure B.2 illustrates the layering of these ICRU volumes.

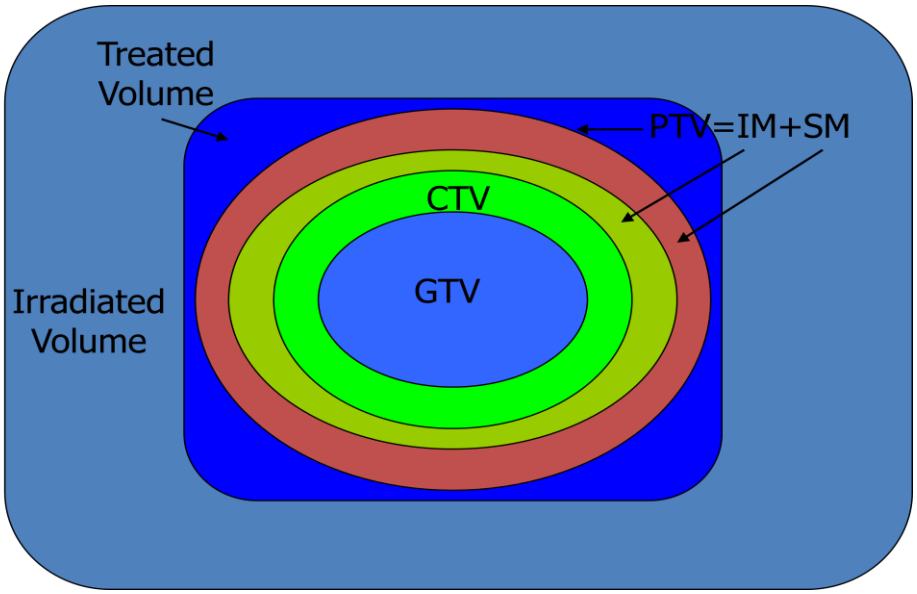

Figure B.2. ICRU volumes.

Dose Reporting

For simple plans it is adequate to report the dose the 'ICRU reference point'. This is a point within the plan that is:

- Clinically relevant and representative of the dose throughout the PTV
- Easy to define
- In a region where dose can be accurately determined

A suitable place would be within the central part of the tumour, ideally at the isocentre, and it is a basic requirement of ICRU to report the dose at the ICRU point and maximum and minimum doses to the PTV. The dose delivered to the tumour should be as uniform as possible, but kept within +7% and -5% of the prescribed dose.

ICRU Report 83 (ICRU 2010) extends these reports further to include the specific challenges of IMRT. In essence dose reporting should not to a fixed point, but to a volume because of the sharp dose gradients involved. The most stable way to prescribe the dose is the median dose ($D_{50\%}$), and maximum and minimum doses are reported at $D_{2\%}$ and $D_{98\%}$. The use of biological evaluation is also encouraged via the use of TCP, NTCP and EUD.

Reducing margins

A clear goal for radiotherapy is the reduction of treatment margins. In this way the volume of normal tissue irradiated can be minimised, resulting in fewer and less toxic complications. Improvements in imaging have led to the potential for more accurate target definition, but the accurate delineation of tumours is still of great concern. Outlining exercises performed on standardised cases have demonstrated the variation in the outlining of target volume both between hospitals and between professions (ICRU 50, ICRU 60, Weiss *et al* 2003). The standardisation of outlining is a critical step in reducing margins and is being tackled through training and participation in clinical trials etc.

Once the GTV and CTV are outlined, the radiation dose that can safely be delivered to the target is restricted by the damage caused to surrounding structures. If the PTV margin can be reduced then side effects can be minimised, or there is the possibility of dose escalation to improve tumour control (maintaining side effects).

The goal of IGRT is to improve the accuracy of the dose delivery by routinely imaging the patient in the treatment position during the course of treatment. By having a detailed knowledge of the actual position of the target and critical structures it is possible to reduce treatment margins, thereby reducing the amount of normal tissue irradiated. There are numerous approaches to IGRT which are beyond the scope of this report. Readers are referred to the publication 'On Target: ensuring geometric accuracy in radiotherapy' (RCR, 2008) for more information.

APPENDIX C

PUBLICATIONS

This article was published in the journal *Physics in Medicine and Biology* in 2008 and reports on the initial research performed to characterise the operation and dosimetric properties of an Elekta linear accelerator running without the flattening filter. This article forms the basis of most of chapter 2.

Cashmore J "The characterisation of unflattened photon beams from a 6MV linear accelerator". *Phys Med Biol.* **53,** 1933-1946, (2008).

IOP PUBLISHING PHYSICS IN MEDICINE AND BIOLOGY

Phys. Med. Biol. **53** (2008) 1933–1946 doi:10.1088/0031-9155/53/7/009

The characterization of unflattened photon beams from a 6 MV linear accelerator

Jason Cashmore

University Hospital Birmingham NHS Foundation Trust, UK

E-mail: jason.cashmore@uhb.nhs.uk

Received 3 December 2007, in final form 7 February 2008
Published 11 March 2008
Online at stacks.iop.org/PMB/53/1933

Abstract

Commissioning data have been measured for an Elekta Precise linear accelerator running at 6 MV without a flattening filter with the aim of studying the effects of flattening filter removal on machine operation and beam characterization. Modern radiotherapy practice now routinely relies on the use of fluence modifying techniques such as IMRT, i.e. the active production of non-flat beams. For these techniques the flattening filter should not be necessary. It is also possible that the increased intensity around the central axis associated with unflattened beams may be useful for conventional treatment planning by acting as a field-in-field or integrated boost technique. For this reason open and wedged field data are presented. Whilst problems exist in running the machine filter free clinically, this paper shows that in many ways the beam is actually more stable, exhibiting almost half the variation in field symmetry for changes in steering and bending currents. Dosimetric benefits are reported here which include a reduction in head scatter by approx. 70%, decreased penumbra (0.5 mm), lower dose outside of the field edge (11%) and a doubling in dose rate (2.3 times for open and 1.9 times for wedged fields). Measurements also show that reduced scatter also reduces leakage radiation by approx. 60%, significantly lowering whole body doses. The greatest benefit of filter-free use is perceived to be for IMRT where increased dose rate combined with reduced head scatter and leakage radiation should lead to improved dose calculation, giving simpler, faster and more accurate dose delivery with reduced dose to normal tissues.

1. Introduction

The flattening filter is regarded as an essential component of almost all linear accelerators, acting to produce a flat beam from the forward-peaked photon fluence produced at the target. However, despite their longstanding use in medical linear accelerators a number of problems

still remain. Monte Carlo studies have shown that the flattening filter is responsible for the majority of scatter produced in the treatment head (Petti *et al* 1983, Zhu and Bjarngard 1995) and is dependent on machine type and energy. Large amounts of head scatter make the complex, often elongated and off-axis fields shapes used in IMRT very difficult to calculate, limiting dose calculation accuracy and making this the subject of continuing research (Lam *et al* 1996, Hounsell and Wilkinson 1997, Jiang *et al* 2001, Zhu and Bjarngard 2003, Redpath 2005, Sikora *et al* 2007). Its presence also causes changes in beam quality away from the central axis necessitating the use of off-axis spectra and acts as the main source of electron contamination (which is also very difficult to model) (Nilsson 1985, Hounsell and Wilkinson 1999, Klein *et al* 2003). Mechanical positioning and electron beam steering are also crucial as any misalignments lead to asymmetries in the photon beam.

The problem with unflattened beams of course has always been the forward peak to the dose distribution. For IMRT however this should not be a problem as the actual beam shape can be taken into account in the segmentation process and therefore the filter should not be necessary at all. Also in many conventional planning situations, such as the head, neck and breast, a flat radiation field leads to radiation hotspots at the periphery of the target with the central portion of the beam left cold. In these cases a central axis boost is required, necessitating the use of field-in-field techniques or the addition of further beams from other directions. The forward peak associated with filter removal gives an inherent central axis boost, hence open *and* wedged beam characteristics have been measured with the aim of assessing any benefits to conventional treatment planning.

Flattening filter removal should greatly reduce the magnitude of head scatter and its variation with field size, simplifying these calculations and improving dose accuracy. Dose rate will be greatly increased and the x-ray spectrum should exhibit much less variation across the beam portal. All of these effects are potentially desirable properties for radiotherapy beams.

Previous studies have mainly focused on the use of Monte Carlo methods to study beam characteristics (Fu *et al* 2004, Titt *et al* 2006a, 2006b, Vassiliev *et al* 2006a, Mesbahi 2007), with the notable exceptions of Vassiliev *et al* (2006b), Ponisch *et al* (2006) and Zhu *et al* (2006) who have measured open beam properties for a Varian Clinac 21EX. The present study provides a thorough set of commissioning measurements for both open and wedged beams for an Elekta Precise linear accelerator with the focus on reduced head scatter for IMRT and beam shape (open and wedged) for conventional planning. The aim is not only to compare beam characteristics but to study the operation of the machine ready for clinical use and produce a functional beam model for unflattened beams for treatment plan comparisons.

2. Materials and methods

A low energy Elekta Precise linear accelerator fitted with a standard 80 leaf MLC producing a 6 MV photon (and 10 MeV electron) beam was used for measurements. The flattening filter is mounted at the secondary filter stage on a five-position rotatable carrier (carousel) in the head of the machine. Only two of these ports are used clinically in a low energy machine: one for the flattening filter and the other for the 10 MeV electron scatter foil, leaving three ports free. Within the machine's service mode it is a simple matter to rotate the filter out of the beam line leaving an open port. As well as utilizing an open port the additional unused ports were also used to house various thicknesses of copper and aluminium to study the effects of electron contamination on surface dose and machine operation.

A new, independent machine energy was created to run unflattened beams and kept inaccessible to the machine's 'clinical mode'. All energy-specific beam parameters pertaining

Table 1. Measurements made. Depth doses and profiles were measured with a Semiflex 0.125 cc chamber, scatter factors with a Farmer NE2571 chamber and build-up and surface doses with a NACP chamber in solid water.

Depth doses	Open/wedge	5, 10, 15, 20, 30 cm^2
Profiles	Open/wedge	15, 50, 100, 150, 200 mm depths
		For 5, 10, 15, 20, 30 cm^2
	Open diagonal	40 × 40 cm^2
Total scatter factors		3, 4, 5, 6, 7, 8, 9, 10, 12, 14, 16, 18, 20, 25, 30, 40 cm^2
Head scatter factors		3, 4, 5, 6, 7, 8, 9, 10, 12, 14, 16, 18, 20, 25, 30, 40 cm^2
Wedge factors		3, 4, 5, 6, 7, 8, 9, 10, 12, 14, 16, 18, 20, 25, 30 cm^2
Build-up	Open	5, 10, 15, 20 cm^2 at 0–17 mm depths
Surface dose	Open	3, 4, 5, 6, 7, 8, 9, 10, 12, 14, 16, 18, 20, 25, 30, 40 cm^2 at 3 mm depth
Leakage		50 cm and 100 cm from isocentre, patient plane
Dose rate	Open/wedge	10 × 10, d_{max} (15 mm)

to 6 MV were copied to this new energy and the gun servo, steering currents, beam hump and uniformity reset to allow the beam to run with all interlocks engaged.

Beam profiles and depth dose measurements were taken using a PTW MP3 Tandem watertank with Semiflex 0.125 cc chambers and running Mephysto 7.4 water phantom software. For scatter and wedge factor measurements a NE2571 Farmer chamber was used. Build-up measurements were made with a NACP parallel plate chamber.

A full set of commissioning data as recommended by CMS (2003) was measured along with surface and out-of-field doses to compare with concurrently measured 6 MV data (table 1).

Central axis depth dose measurements were measured for square fields from 5 × 5 to 30 × 30 cm^2 at 100 cm SSD for both open and wedged beams and profiles taken at five depths. A 40 × 40 cm^2 open field diagonal profile was also taken for beam modelling purposes. Penumbra measurements were made from films exposed at 100 cm SSD under 15 mm of solid water using Kodak X-Omat V film. Analysis was performed using a VIDAR scanner and ImageJ software (Rasband 2006).

3. Results

The beam essentially remains unaffected up until the point where it would normally strike the flattening filter; hence the vast majority of accelerator running parameters remain unchanged. Problems only start to arise when the beam reaches the ionization chamber; not only does this monitor the dose delivered but also acts to servo the radial and tangential steering currents (2R and 2T on Elekta machines) to maintain a symmetrical beam. The difference between the inner and outer plates (hump error) is also used to control the gun current and hence maintain beam energy. There are therefore three fundamental questions to ask of machine performance in removing the flattening filter:

(1) How does the increased dose rate/dose per pulse affect dosimetry?
(2) Can the gun servo be reset and still function to control the beam energy?
(3) Can the steering current servos be reset to allow operation around their new values?

3.1. Dosimetry

The first (and most obvious) consequence of taking out the flattening filter is the huge increase in observed dose rate. Running both beams at peak dose rate and taking measurements at d_{max}

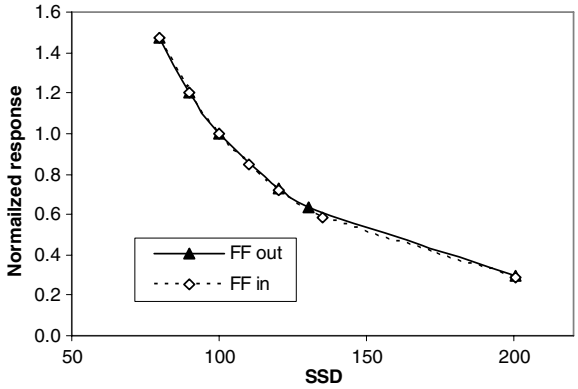

Figure 1. Dose-per-pulse dependence of a NE2571 Farmer type chamber.

(15 mm) with a Farmer chamber the dose rate is seen to rise by an average of 2.3 times for an open beam and by 1.9 times for a wedged beam. The lower value seen for the wedged beams is due to increased absorption (lower wedge transmission factor) in the physical wedge because of the change in energy spectrum. This increase in dose rate could clearly be a useful factor in many treatments (e.g. respiratory-gated breathing and stereotactic radiosurgery [SRS]) but the dose rate can always be lowered by dropping the pulse repetition frequency to regain normal dose rates if desired.

Repeat measurements under standard conditions confirm that the internal ion chambers respond well to the higher dose rate and that doses delivered are accurate ($<1\%$ error) down to 2 mu.

Figure 1 shows the dose-per-pulse dependence of a NE2571 Farmer chamber which is varied by changing the SSD, the curves are normalized at 100 cm SSD for a 10×10 cm^2 field. The dose-per-pulse will affect the response of the chamber, but the two curves overlie each other indicating that these corrections should hold even at these high dose rates. The characteristics of ionization chambers to pulsed radiation beams have been well reported (Derikum and Roos 1993, Bruggmoser *et al* 2007) but further work will be required to ascertain correction factors for these beams. In the current software version the machine cannot be calibrated to 1 mu = 1 cGy under standard conditions due to a software limitation on the range of 'dose reference' values.

3.2. Beam steering

Mechanical positioning of the flattening filter and accurate steering of the electron beam are crucial to flat beam production as any misalignment will lead to non-flat, asymmetrical beams. Starting from a symmetrical beam the 2R current (controlling symmetry in gun–target axis) was varied by ± 50 mA and bending fine (B_f) by ± 20 mA. Measurements with a Schuster BMS96 linear array (88 diodes with 5 mm spacing) demonstrate that for variations in beam steering and bending currents the unflattened beam exhibits almost half the variation in field asymmetry (ratio of absorbed dose at points ± 12 cm about the central axis) compared to the flattened beam (see table 2).

For flattened beams the dose either side see-saws about the central axis with the actual shape and magnitude of the shifts depend on a complex interaction of steering and bending currents that can be difficult to decouple (Karzmark *et al* 1993). For non-flattened beams,

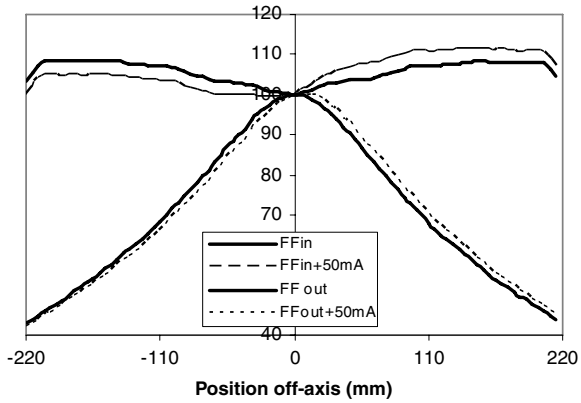

Figure 2. Profiles from a Schuster array demonstrating changes in beam symmetry for variations in 2R bending current of ±50 mA. For the flattened beam the asymmetry (ratio of absorbed doses ±12 cm from the central axis) amounts to 7.4% compared to 4.1% with the filter removed.

Table 2. Beam symmetry measurements recorded with a Schuster array. Values quoted are the percentage difference of readings ±12 cm off axis compared to the central axis value.

		FF in	FF out
2R	+50 mA	+7.3%	+3.8%
	−50 mA	−7.5%	−4.4%
Bf	+20 mA	+4.1%	+1.5%
	−20 mA	−6.5%	−2.4%

rather than altering the beam shape these variations simply act to shift the beam asymmetrically with the profile remaining the same relative shape (figure 2). In fact, the beam is so stable that the first interlock to be triggered when the steering currents are driven off is usually that for 'low dose rate' which is due to a loss of beam current as the beam is driven away from the target.

Small changes in energy and beam positioning during start-up are magnified by passing through the flattening filter. This can be a significant problem for IMRT where segments may be delivered with low numbers of monitor units (Sharpe *et al* 2000) and where the beam is unable to stabilize before the dose has been delivered. Delivered dose distributions could clearly be adversely affected by this. Since the flattening filter acts as an amplifier for any changes in beam steering and energy these problems are reduced with its removal. The Schuster array again was used to study beam start-up characteristics by integrating the dose over a low dose delivery. Whereas repeat measurements for a conventional beam show a 1.5% tilt in beam symmetry for a 5 mu beam (symmetry measured as defined previously), for the unflattened beam this is only 0.3%.

The flattening filter is an energy-sensitive component producing changes in beam profile as the beam energy varies. Elekta machines take advantage of this to servo the beam energy by monitoring the differences in the inner and outer plate signals (hump error) of the ionization chamber. Although the beam runs well under normal conditions the energy sensitivity with the filter out may not operate correctly under *all* circumstances and needs further study. In other accelerators the energy is regulated by other means (such as by controlling the voltage on the PFN to achieve maximum ion chamber current), so this would not be an issue.

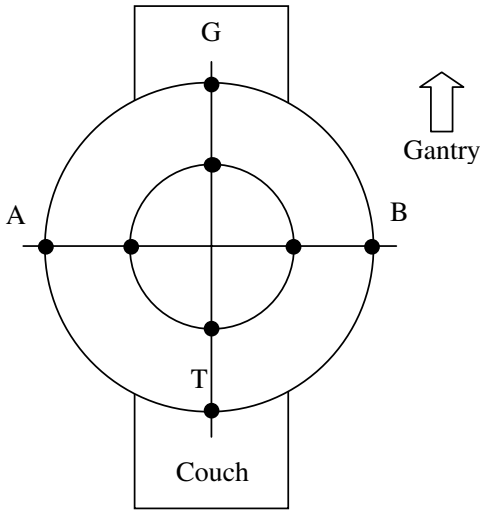

Figure 3. Specification of points used to measure patient plane leakage. The circles are of radii 50 cm and 100 cm. Readings at these points are taken with the collimators in the closed position and compared to a central axis reading for a 10 × 10 cm^2 field.

Table 3. Patient plane leakage measurements. G and T refer to movements towards the Gun and Target. A and B refer to movements left and right of centre when standing facing the gantry.

Leakage radiation (% of reference reading)			
Position	Filter in	Filter out	% Decrease
50 cm G	0.012	0.0068	42.2
50 cm T	0.005	0.0029	45.9
50 cm A	0.018	0.0079	55.4
50 cm B	0.019	0.0072	62.0
100 cm G	0.013	0.0054	58.5
100 cm T	0.011	0.0032	69.6
100 cm A	0.018	0.0079	55.4
100 cm B	0.025	0.0061	76.0
		Average decrease	58.1%

3.3. Leakage radiation

Patient plane leakage measurements were taken as recommended by the Elekta acceptance documents (Elekta 2005). A Farmer chamber (with 1.5 cm build-up cap) is placed at the cardinal angles at 50 and 100 cm from the isocentre (see figure 3). With the diaphragms closed the absorbed doses at these points are compared to a reference dose measured for a 10 × 10 cm^2 field at the isocentre. The leakage dose should not exceed 0.1% of the dose at the isocentre and this is easily achieved during normal use. For IMRT delivery, the number of monitor units required can be raised significantly compared to open beam delivery and hence leakage radiation will increase proportionally. Without the flattening filter the dose, on average, is 58% lower than those recorded for normal use (table 3).

Although the transmission factor through the MLC leaves and collimators remains essentially the same (ignoring any spectral changes) the new beam shape means that the

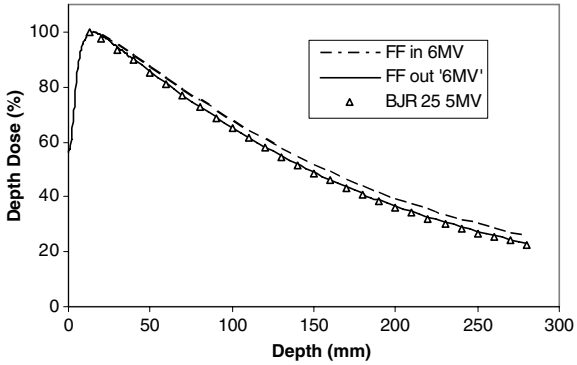

Figure 4. Depth doses for a 10 × 10 cm^2 field at 100 cm SSD. Lack of beam hardening is seen as an energy decrease to approx. 5 MV.

Table 4. Comparison of beam quality parameters.

Nominal energy (MV)	Beam description	PDD at 10 cm deep, D_{10} (%)	Depth of 80% dose, d_{80} (cm)	Depth of dose max. d_{max} (cm)	QI (TPR 20/10)
6	FF in	67.6	6.7	15	0.679
6	FF out	65.2	6.3	13.5	0.653
5	BJR 5 MV	65.0	6.2	12.5	0.646

photon fluence naturally falls off with distance from the central axis (falling to 50% at the beam edge). The magnitude of the leakage radiation through the collimators will scale directly with that of the photon fluence, so the dose outside the field edge (to normal tissues) will also be lower. This is a simple consequence of there being less primary radiation present at off-axis positions.

3.4. Depth doses

The flattening filter significantly hardens the radiation beam on the central axis but due to its physical shape the beam quality decreases with distance from the central axis. Production of contaminant electrons also affects depth doses beyond d_{max} but major effects are mainly seen in the surface region.

Central axis depth doses were measured at 100 cm SSD and normalized at a depth of 15 mm for open and wedged square field sizes from 5 × 5 to 40 × 40 cm^2 (30 × 30 cm^2 for wedge).

The filter attenuates the low-energy component of the spectrum increasing the apparent energy of the beam. With unflattened beams the addition of these soft x-rays to the beam spectrum lowers the observed energy and produces a beam with characteristics similar to a 5 MV beam (Jordan 1996) (figure 4). Table 4 shows comparisons for most of the commonly used beam specification parameters which also demonstrate a good match to 5 MV data. The flattening filter obviously hardens the beam appreciably but this drop in energy could easily be compensated for by adjusting accelerator parameters, if so desired. As yet there is very little published depth dose data for unflattened beams and none for Elekta accelerators or wedged beams, so if BJR25 were to be updated at some point it would be a good opportunity to include sample data.

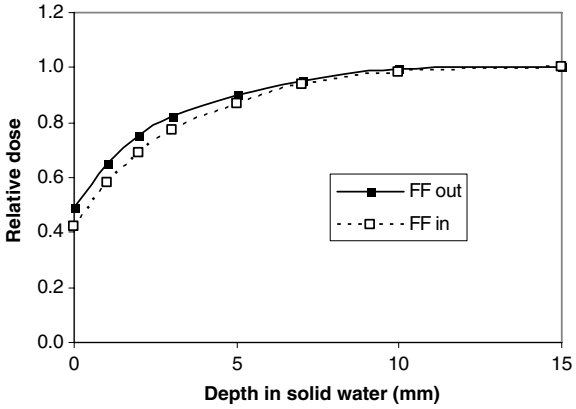

Figure 5. Build-up curves for a 10 × 10 cm^2 field measured in solid water. Filter-free beams show slightly increased surface dose compared to filtered beams at 6 MV.

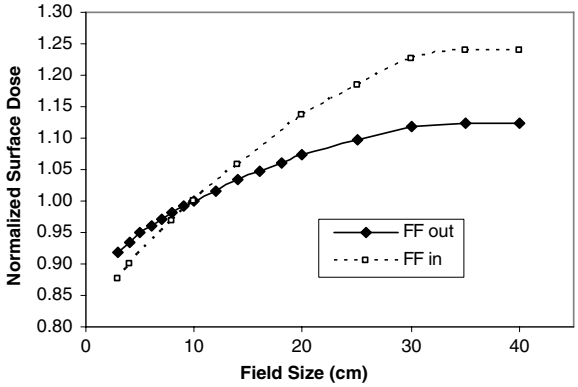

Figure 6. Variation of surface dose (at 3 mm depth) with equivalent square normalized to a 10 × 10 cm^2 field. Maximum to minimum ratio is 1.42 with the flattening filter in and 1.23 without, i.e. half the variation

3.5. Surface dose

Measurements in the build-up region show that there is a slight increase in surface dose with the flattening filter removed (figure 5). The reduced head scatter however produces appreciably less variation in dose near the surface (measured at 3 mm depth) with field size (figure 6) than is seen for flattened beams. Measurements were also performed with thin sheets of copper and aluminium (1.1 mm Al, 1.9 mm Cu, 1.9 mm Al) in place of the flattening filter with the hope of reducing surface dose, but no appreciable reduction is seen. During conventional use the contamination electrons produce a large position-dependent dose in the ion chamber servo plates which are then used to control the beam. With the filter removed the number of electrons reaching the ion chamber is so low that the signal at the servo plates is too low to operate the servos correctly. A certain amount of build-up is therefore necessary to boost these signals and the use of metal sheets demonstrates an increase in these signals and in the servo control of the beam, allowing the machine to run not just in service mode but with all interlocks engaged.

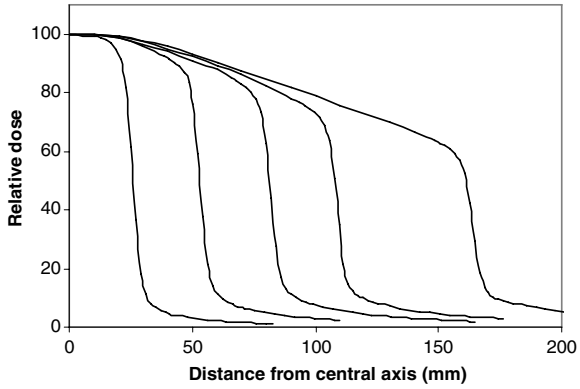

Figure 7. Lateral dose profiles of unflattened beams at a depth of 10 cm. Field sizes are 5, 10, 15, 20 and 30 cm^2.

Monte Carlo studies have demonstrated that the low-energy components of the beam spectrum are significantly enhanced (Tsechanski *et al* 2005, Mesbahi 2007) and these photons would be expected to deposit energy in the build-up region. The fact that depth dose curves are not altered significantly therefore indicates that the electron contamination in the beam must be lowered by a similar amount. This role reversal has a twofold benefit: firstly x-rays are much easier to model than electrons leading to possible improvements in the modelling of the build-up region and secondly these low kV photons will act to improve the contrast of portal images.

3.6. Profiles

Water tank scans show the forward-peaked nature of open beam profiles (figure 7). Small field scans show only minor differences in beam profile to those recorded normally as the flattening filter has very little effect over these dimensions; field sizes of 5 × 5 cm^2 and below show almost no change in profile. Larger field sizes show enhanced central axis dose with a rounding of the profiles; similar results have been shown for open beams with a Clinac 21EX (Vassiliev *et al* 2006b). Outside the treatment field the doses are lower for non-flattened beams due to the reduction in out-of-field scatter. This would effectively act to reduce the dose to surrounding normal tissues. At 90 cm SSD, 10 cm deep for a 10 × 10 cm^2 field, the dose 2 cm outside the field edge is reduced from 7.9% to 7.0% (11.3% relative change).

Beam profiles of the internal motorized wedge (nominal 60°) again show that there is a slightly faster drop-off in dose at the beam edge and lower dose outside of the field (figure 8). The wedge profiles are slightly convex rather than concave but importantly the overall effect of the wedge is retained. The wedge angle itself drops slightly from 56° to 53° for a 10 × 10 cm^2 field but these factors can easily be taken into account by the beam model.

3.7. Penumbra

The finite dimensions of ion chambers used for water tank measurements means that a blurring effect is added to recorded profiles and so any subtle changes in beam penumbra can be missed. Films were therefore used to assess beam penumbra (defined as the distance from 20% to 80% isodoses measured at 100 cm SSD at d_{max}). As expected, removal of the flattening filter produces a change in beam penumbra due to reduced extra-focal radiation, these effects

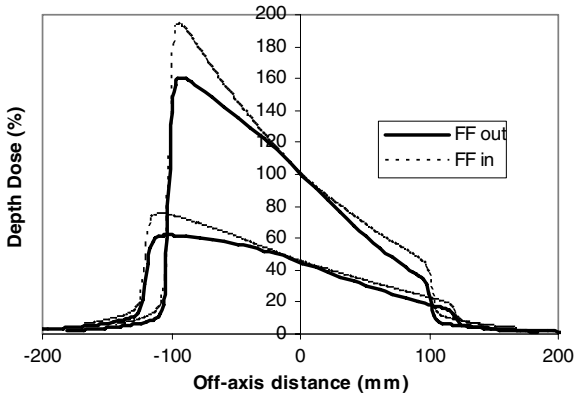

Figure 8. Comparison of measured wedge profiles for a 20 × 20 cm^2 field, normalized at d_{max}. Profile depths are at 15 and 100 mm.

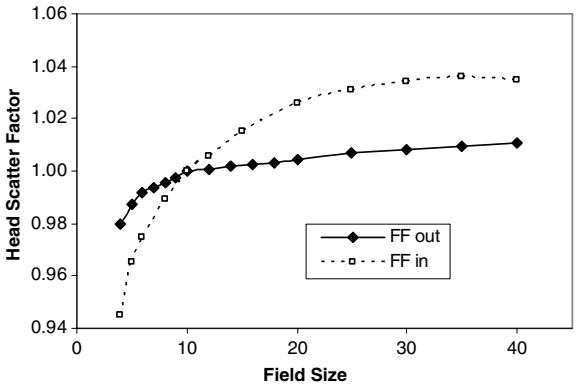

Figure 9. Head scatter measured using a perspex mini-phantom (normalized to a 10 × 10 cm^2 field).

however are of the order of 0.5 mm and although this is of course a good thing it will probably be of little practical advantage.

Obviously, as the field size increases the 80% point will lie some distance from the beam edge and another definition of penumbra is needed to make these values meaningful. The most likely definition involves redefining the position of the 100% reference point to be at the inflexion point of the curve rather than at the central axis.

3.8. Head scatter

Figure 9 shows head scatter measurements as a function of field size made using a perspex mini-phantom (90 cm SSD, 10 cm deep). A significant decrease is seen in the range of readings compared to the flattened field and a variation of only 3% is seen over the entire range 4 × 4 to 40 × 40 cm^2 compared to 9% with the filter in place. This is a reduction of approximately two thirds and matches well with other reported data (Zhu *et al* 2006). This has obvious consequences for beam dosimetry where errors in the calculation of head scatter lead to errors in monitor unit calculation, particularly in complicated off-axis (IMRT) situations.

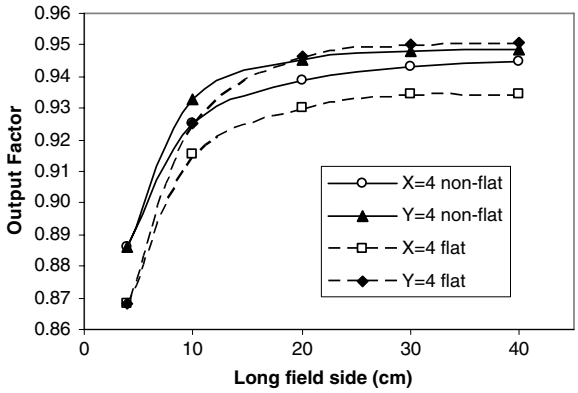

Figure 10. Collimator exchange effect. Output factor is plotted as a function of the long field side, keeping either the *X* or *Y* collimator fixed at 4 cm. Dotted lines are for conventional beam and solid lines for filter removed.

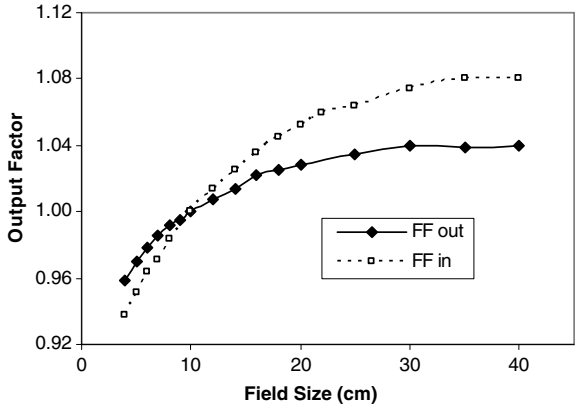

Figure 11. Variation of total scatter factor measured at 100 cm SSD, d_{max}, and normalized to a 10×10 cm^2 field.

One of the other major consequences of head scatter is the variation seen in machine output for rectangular fields depending on which jaw, upper or lower, defines the larger dimension. Measurements of this collimator exchange effect were made by sequentially fixing the *X* and *Y* jaws at 4 cm and varying the other jaw dimension from 4 to 40 cm. The magnitude of the effect is on average 1.6% for standard operation and 0.6% with the filter removed (figure 10). These figures reflect the two thirds reduction of head scatter observed in figure 9.

3.9. Total scatter

Total scatter factors measured at 100 cm SSD, d_{max}, also show a reduced range when plotted against equivalent square (see figure 11) with significant reduction at large field sizes. The difference in the two measured curves is due to the reduction of head scatter as the phantom scatter remains essentially the same and depends on the field dimensions at the surface.

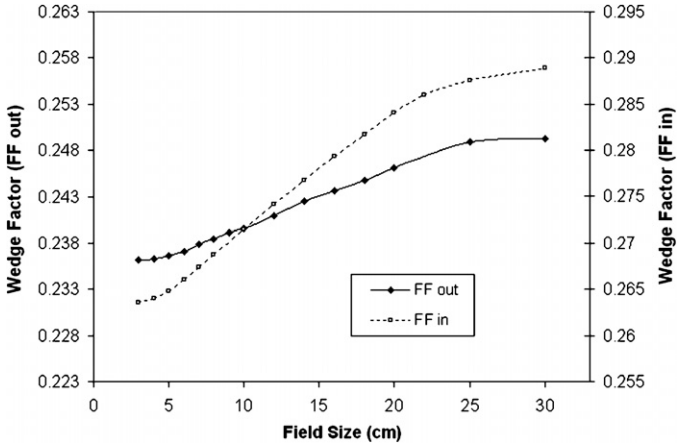

Figure 12. Wedge factors plotted on the same scale to compare variation with field size. The ratio of 30 × 30 to 4 × 4 readings is 1.098 with filter in and 1.055 filter out.

The ratio of 40 × 40 to 4 × 4 cm^2 readings is 1.15 for the flattened beam and 1.08 for the filterless beam, i.e. half the variation in total scatter factor. Similar results have been shown by Ponisch *et al* (2006).

3.10. Wedge factors

The softer spectrum and associated decrease in beam energy to approx. 5 MV lead to an increase in x-ray attenuation and hence to lower values of the wedge factor. Reduced head scatter also leads to less variation with field size; the ratio of 30 × 30 to 3 × 3 cm^2 readings for the flattened beam is 1.098 compared to 1.055 with the flattening filter out, i.e. half the relative range (figure 12). Again filter removal is seen to reduce the variation in field-size-dependent parameters.

4. Discussion and conclusions

Linear accelerator design has evolved around the need for flat radiation fields and a certain number of problems must be expected when the flattening filter is removed. Measurements reported here show that these problems, however, are fairly minimal and most likely to be resolved it seems with relatively simple software modifications since the vast majority of all machine running parameters remain unchanged. The only differences are observed at the ionization chamber where beam parameters such as flatness, symmetry and uniformity need to be reset, but this can be performed relatively easily and, with some build-up in place, the chamber servos operated well during the duration of the experiments. In fact, with the filter removed the beam symmetry is half as sensitive to changes in beam steering, retains a more consistent profile with these changes and is more stable during start-up irradiation.

To operate the machine clinically however it would be necessary to modify current IEC specifications (BS EN 60976 2001) which are based upon having square, flattened radiation fields. The standards are written to ensure the protection of the operator and patient and to define a number of parameters by which users can compare accelerator performance. With unflattened beams terms such as ‘flattened area’ are meaningless. Uniformity, flatness, symmetry, penumbra and field size definitions may need to be redefined for these beams.

The major benefit of filter removal is in the reduction of head scatter and leakage radiation, both of which cause significant problems in radiotherapy and come as a direct consequence of producing a flat beam, i.e., forcing a large proportion of the beam to interact in the flattening filter. Removal leads to a decrease in head scatter (potentially improving dose calculations) and to lower whole body doses (reducing the risk of secondary cancers). Reduced scatter also leads to a reduction in penumbra, dose outside of the field edge and gives less variation in field-size-dependent factors; again all useful properties.

The only major problem then is the actual beam shape. This should not be of much concern for IMRT since the intensity profile can easily be modulated by the MLCs to produce almost any profile necessary and the actual beam shape essentially becomes immaterial (within reason). The fundamental physics behind the IMRT optimization process remains the same; the modified beam profile is simply taken into account during the segmentation process. Reduced head scatter and increased dose rate should lead to simpler, faster and more accurate dose delivery with reduced dose to normal tissues.

The main application for unflattened beams is seen to be for IMRT but this should not be considered as a limitation for this technique. Small field profiles ($<6 \times 6$ cm^2) are almost unaffected so these can be used as normal. This is especially true of the very small fields used in stereotactic radiosurgery (SRS) where the flattening filter serves no useful purpose.

Further work will focus on treatment planning studies using larger conventional field sizes. Preliminary results using these larger fields show that the forward peak is actually very useful for treating areas such as the breast, where the use of flat radiation beams results in radiation hotspots at the extremes of the target region. Unflattened beams give an inherent boost to the centre of the breast to even out the dose over the entire region. Further, by mixing flattened and unflattened beams together a dose distribution can be formed anywhere between these two extremes and this can be tailored very simply and effectively to even out these dose gradients.

Acknowledgments

The majority of this work was carried out at University Hospital Coventry and Warwickshire. The author would like to thank Kevin Brown and Neil Harvey at Elekta for their assistance and for the provision of an additional energy licence for linear accelerator measurements.

References

Bruggmoser G, Saum R, Schmachtenberg A, Schmid F and Schüle E 2007 Determination of the recombination correction factor kS for some specific plane-parallel and cylindrical ionization chambers in pulsed photon and electron beams *Phys. Med. Biol.* **52** N35–50

BS EN 60976 2001 Medical electrical equipment—Medical electron accelerators—Functional performance characteristics

CMS XiO 2003 Beam Data Collection List DOC:9000-959-24H

Derikum K and Roos M 1993 Measurement of saturation correction factors of thimble-type ionization chambers in pulsed photon beams *Phys. Med. Biol* **38** 755–63

Elekta 2005 Customer Acceptance Tests Doc 4513 370 2065 04

Fu W, Dai J, Hu Y, Han D and Song Y 2004 Delivery time comparison for intensity-modulated radiation therapy with/without flattening filter: a planning study *Phys. Med. Biol* **49** 1535–47

Hounsell A R and Wilkinson J M 1997 Head scatter modelling for irregular field shaping and beam intensity modulation *Phys. Med. Biol* **42** 1737–49

Hounsell A R and Wilkinson J M 1999 Electron contamination and build-up doses in conformal radiotherapy fields *Phys. Med. Biol* **44** 43–55

Jiang S B, Boyer Al and Ma C 2001 Modelling the extra focal radiation and monitor chamber backscatter for photon beam dose calculation *Med. Phys* **18** 55–66

Jordan T J 1996 Central axis depth dose data for use in radiotherapy *Br. J. Radiol.* **(Suppl. 25)** 72

Karzmark C J, Nunan C S and Tanabe E 1993 *Medical Electron Accelerators* (New York: McGraw-Hill) p 127

Klein E E, Esthappan J and Li Z 2003 Surface and buildup dose characteristics for 6, 10, and 18 MV photons from an Elekta Precise linear accelerator *J. Appl. Clin. Med. Phys.* **4** 1–7

Lam K L, Muthuswamy M S and Tan Haken R K 1996 Flattening filter based empirical methods to parameterise the head scatter factor *Med. Phys.* **23** 343–52

Mesbahi A 2007 Dosimetric characteristics of unflattened 6 MV photon beams of a clinical linear accelerator: a Monte Carlo study *Appl. Radiat. Isot.* **65** 1029–36

Nilsson B 1985 Electron contamination from different materials in high energy photon beams *Phys. Med. Biol.* **30** 139–51

Petti P L, Goodman M S, Gabriel T A and Mohan R 1983 Investigation of buildup dose from electron contamination of clinical photon beams *Med. Phys* **10** 18–24

Ponisch F, Titt U, Vassiliev O N, Kry S F and Mohan R 2006 Properties of unflattened photon beams shaped by a multileaf collimator *Med. Phys* **33** 1738–46

Rasband W 2006 ImageJ 1.36b (USA: National Institutes of Health) http://rsb.info.nih.gov/ij

Redpath A T 2005 Modelling of output factors for conformal megavoltage x-ray beams *Br. J. Radiol.* **78** 612–22

Sharpe M B, Miller M B, Yan D and Wong J W 2000 Monitor unit settings for intensity modulated beams delivered using a step-and-shoot approach *Med. Phys* **27** 2719–25

Sikora M, Dohm O and Alber M 2007 A virtual photon source model of an Elekta linear accelerator with integrated mini MLC for Monte Carlo based IMRT dose calculation *Phys. Med. Biol.* **52** 4449–63

Titt U, Vassiliev O N, Ponisch F, Dong L, Liu H and Mohan R 2006a A flattening filter free photon treatment concept evaluation with Monte Carlo *Med. Phys* **33** 1595–602

Titt U, Vassiliev O N, Ponisch F, Kry S F and Mohan R 2006b Monte Carlo study of backscatter in a flattening filter free clinical accelerator *Med. Phys* **33** 3270–3

Tsechanski A, Krutman Y and Faermann S 2005 On the existence of low-energy photons (<150 keV) in the unflattened x-ray beam from an ordinary radiotherapeutic target in a medical linear accelerator *Phys. Med. Biol* **50** 5629–39

Vassiliev O N, Titt U, Kry S F, Ponisch F, Gillin M T and Mohan R 2006a Monte Carlo study of photon fields from a flattening filter-free clinical accelerator *Med. Phys.* **33** 820–7

Vassiliev O N, Titt U, Ponisch F, Kry S F, Mohan R and Gillin M T 2006b Dosimetric properties of photon beams from a flattening filter free clinical accelerator *Phys. Med. Biol.* **51** 1907–17

Zhu T C and Bjärngard B E 1995 The fraction of photons undergoing head scatter in x-ray beams *Phys. Med. Biol.* **40** 1127–34

Zhu T C and Bjärngard B E 2003 Head scatter off-axis for megavoltage x rays *Med. Phys.* **30** 533–43

Zhu X R, Kang Y and Gillin M T 2006 Measurements of in-air output ratios for a linear accelerator with and without the flattening filter *Med. Phys.* **33** 3723–33

APPENDIX D

PUBLICATIONS

This article was published in the *International Journal of Radiation Oncology Biology and Physics* in 2011 and details the out-of-field doses delivered in FFF mode, both under standard conditions and form IMRT delivery. This article forms the basis of most of chapter 7.

Cashmore J, Ramtohul M, Ford D "Lowering whole-body radiation doses in pediatric intensity-modulated radiotherapy through the use of unflattened photon beams" *Int. J. Radiat. Oncol. Biol. Phys.* **80** (4) 1220-1227, (2011).

Int. J. Radiation Oncology Biol. Phys., Vol. 80, No. 4, pp. 1220–1227, 2011

0360-3016/$ - see front matter

doi:10.1016/j.ijrobp.2010.10.002

PHYSICS CONTRIBUTION

LOWERING WHOLE-BODY RADIATION DOSES IN PEDIATRIC INTENSITY-MODULATED RADIOTHERAPY THROUGH THE USE OF UNFLATTENED PHOTON BEAMS

JASON CASHMORE, M.SC.,* MARK RAMTOHUL, PH.D.,* AND DAN FORD, F.R.C.R.†

*Radiotherapy Physics and †Cancer Centre, Hall-Edwards Radiotherapy Research Group, University Hospital Birmingham, Edgbaston, Birmingham, UK

Purpose: Intensity modulated radiotherapy (IMRT) has been linked with an increased risk of secondary cancer induction due to the extra leakage radiation associated with delivery of these techniques. Removal of the flattening filter offers a simple way of reducing head leakage, and it may be possible to generate equivalent IMRT plans and to deliver these on a standard linear accelerator operating in unflattened mode.
Methods and Materials: An Elekta Precise linear accelerator has been commissioned to operate in both conventional and unflattened modes (energy matched at 6 MV) and a direct comparison made between the treatment planning and delivery of pediatric intracranial treatments using both approaches. These plans have been evaluated and delivered to an anthropomorphic phantom.
Results: Plans generated in unflattened mode are clinically identical to those for conventional IMRT but can be delivered with greatly reduced leakage radiation. Measurements in an anthropomorphic phantom at clinically relevant positions including the thyroid, lung, ovaries, and testes show an average reduction in peripheral doses of 23.7%, 29.9%, 64.9%, and 70.0%, respectively, for identical plan delivery compared to conventional IMRT.
Conclusions: IMRT delivery in unflattened mode removes an unwanted and unnecessary source of scatter from the treatment head and lowers leakage doses by up to 70%, thereby reducing the risk of radiation-induced second cancers. Removal of the flattening filter is recommended for IMRT treatments. © 2011 Elsevier Inc.

Flattening filter, Pediatric, Intensity-modulated radiotherapy, Second cancers, Radiation-induced malignancies.

INTRODUCTION

Intensity-modulated radiotherapy (IMRT) is now a well-established technique used to concentrate dose into target region/s while sparing normal tissues, and is recognized as superior to three-dimensional (3D) conformal radiotherapy (CRT) in these respects. However, the increased number of beam directions used in IMRT compared with 3D-CRT means that a low-level "dose-bath" is given to a larger volume of normal tissues. Leakage radiation from the treatment head is also raised because IMRT delivery is wasteful of monitor units (MU), which can increase by a factor of 2 to 10 (typically 3–5) depending on the techniques and equipment used. Since leakage radiation is proportional to the number of MU delivered, IMRT is seen to increase whole-body doses to the patient.

Several authors have compared the delivery of 3D conformal plans against IMRT and reported that IMRT delivery may double the incidence of solid cancers in long-term survivors (1–5). The range of reported values varies considerably (1.2–8) because the MU demand for IMRT is largely dependent on both the software and the hardware used for planning and delivery, and also on the radiobiologic models used in each study.

Radiation-induced secondary cancers are not a serious concern until at least 5 years after treatment (6), with patients surviving longer than 10 years being most at risk. After successful treatment of the original disease, secondary cancers are diagnosed, on average, 15 years after treatment (7). A recent study (8) showed that of 115 pediatric patients diagnosed with secondary cancers after radiotherapy, 22% of the cancers were >5 cm from the planning target volume (PTV), and some were detected up to 1 m away. The peak frequency was seen to be in tissues receiving 2.5 Gy or less.

Reprint requests to: Jason Cashmore, M.Sc., Hall-Edwards Radiotherapy Research Group, Radiotherapy Physics, University Hospital Birmingham, Edgbaston, Birmingham, UK. Tel: (+44) 121-627-5826; Fax: (+44) 121-627-2386; E-mail: Jason.cashmore@uhb.nhs.uk

Supported in part by a grant from Elekta UK Ltd.

Conflict of interest: Jason Cashmore receives a grant from Elekta (Elekta Ltd, Crawley, UK) to study the properties of unflattened photon beams. The other authors report no conflict of interest.

Acknowledgments—The authors thank the staff at the Christie Hospital, Manchester, for the use of the pediatric phantom used in this study.

Received Jan 12, 2010, and in revised form Sept 23, 2010. Accepted for publication Oct 7, 2010.

With treatments becoming more successful and survival rates rising, the importance and incidence of second cancers will also increase and are likely to be of particular concern in children.

Peripheral doses are influenced by many factors and have been reported for a range of accelerators and beam energies (9–13). The dose to tissues close to the target site (within several centimeters) is dominated by internal scatter and head scatter (14) and is dependent on field size and energy.

At distances beyond the range of internal scatter, peripheral doses are dominated by head leakage and are therefore proportional to MU, so they are unavoidably higher for IMRT. Given that pediatric patients are also physically smaller, geometric factors play an important role. The distance from the field edge to any organ at risk (OAR) in a child (and also the depth from surface) will also be reduced, raising organ doses relative to comparable exposure in an adult.

One of the major sources of head scatter and leakage radiation in the treatment head is the flattening filter, and operation of an Elekta Precise linear accelerator without the flattener has been shown to reduce patient–plane leakage at 1 m by 58% at 6 MV (15). Other benefits are seen to include increased dose rate and improved beam stability. Several groups have investigated the treatment planning aspects of unflattened IMRT (16–18), and one author has investigated peripheral doses through Monte Carlo modeling (19), but to our knowledge, no direct

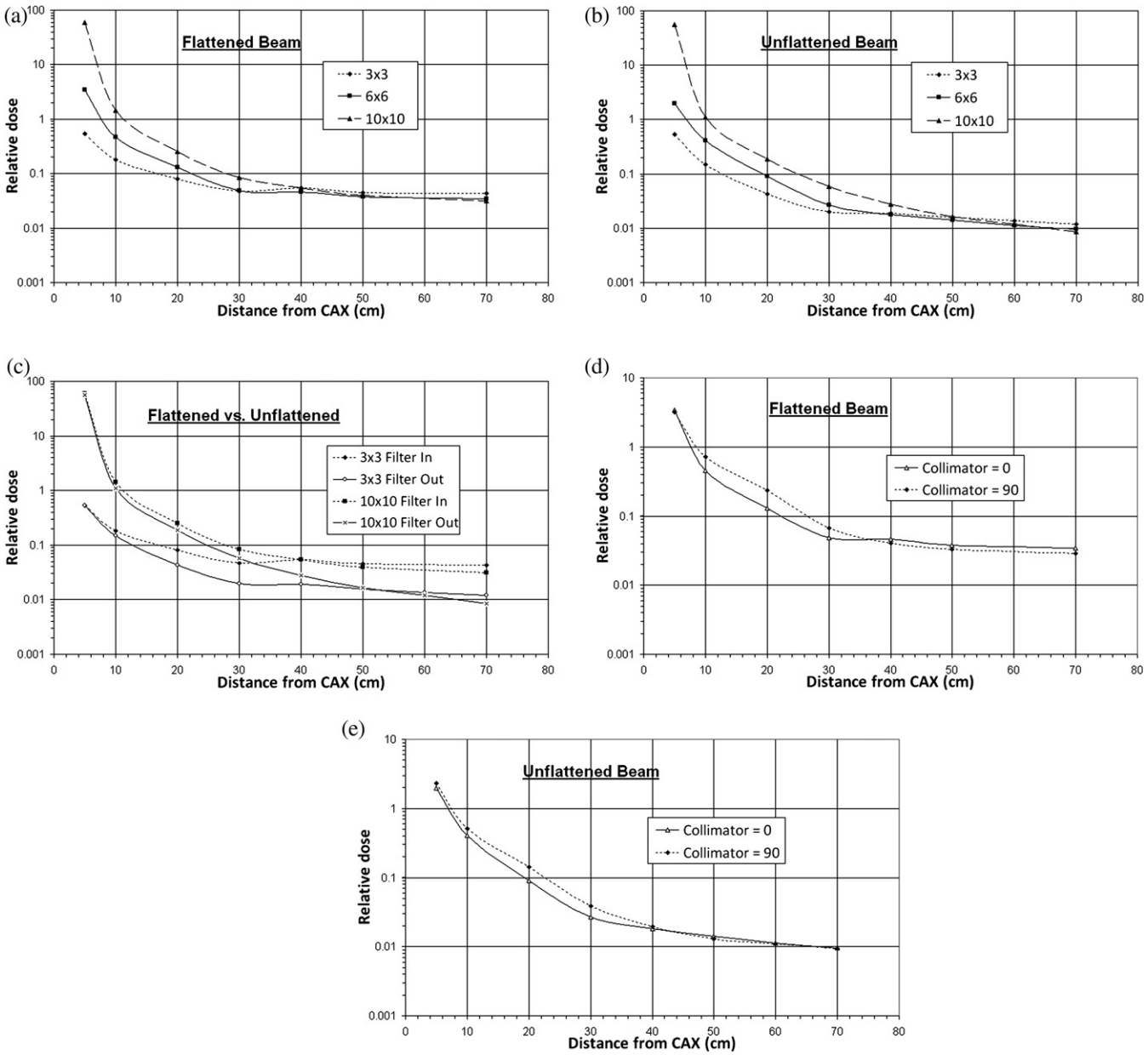

Fig. 1. Peripheral dose measurements as a function of distance from the central axis (CAX). Measurements are in water-equivalent material at a depth of 5 cm. (a) Flattening filter in, (b) flattening filter out for field sizes of 3×3, 6×6, and 10×10 cm^2. (c) Comparison between filter in and filter out for 3×3 and 6×6 cm^2 fields (10×10 cm^2 removed for clarity). Variation in dose for collimator rotations of 0° and 90°: (d) filter in, (e) with the filter out.

Table 1. Summary of dosimetric parameters used for plan evaluation

PTV coverage	
V_{90}	Volume of target (%) receiving 90% of prescribed dose
V_{95}	Volume of target (%) receiving 95% of prescribed dose
V_{100}	Volume of target (%) receiving 100% of prescribed dose
V_{107}	Volume of target (%) receiving 107% of prescribed dose
D_2	Dose to 2% of target volume
D_{98}	Dose to 98% of target volume
HI	Homogeneity index (D_2–D_{98}/Prescribed dose)*100
V_{PTV}	Volume of the planning target volume
CI	Conformity index volume of tissue $V_{NT\ 95}/V_{PTV}$
Normal tissue sparing	
V_{NT5}	Volume of tissue receiving 5% of prescribed dose
$V_{NT\ 95}$	Volume of tissue receiving 95% of prescribed dose

measurements have been reported between out-of-field doses for clinical delivery of comparative plans. If IMRT can be planned and delivered using a system with no flattening filter, then peripheral doses could be significantly reduced, lowering the incidence of secondary cancers.

This study aimed to investigate the potential of IMRT with unflattened photon beams by directly comparing the treatment planning and delivery of unflattened beam IMRT against the conventional IMRT standard. Since peripheral doses are so dependent on the software, hardware, and energy used, these have been kept constant (*i.e.,* the same planning system, plan quality, beam energy, and accelerator were used throughout).

METHODS AND MATERIALS

Linear accelerator

An Elekta Precise linear accelerator (Elekta Ltd, Crawley, UK) was commissioned at 6 MV with the flattening filter rotated out of the beam-line to operate in both conventional and unflattened (flattening filter-free) modes. Filter removal is straightforward because of its location on a rotating carousel, but the filter also produces secondary electrons that give an enhanced dose (and position-dependent information) to the ionization chamber to operate the steering servos. Without the filter, these signal levels drop and the servos no longer function correctly. A thin metal plate was therefore used to provide buildup into the chamber to restore these signals and allow the machine to function correctly.

Some material is also needed to remove contamination electrons (which do not provide position information but do increase surface dose) from the target/primary collimator, and to ensure that there is always some material between target and patient even in the event of target failure.

The flattening filter also acts as a beam hardener, removing low-energy x-rays from the beam spectrum, resulting in an unflattened 6-MV beam having depth dose characteristics similar to those of a 5-MV beam (15). For a Varian Clinac 21EX, this effect is greater, resulting in depth dose curves that resemble those of a 4-MV beam (20). When comparing plans, this change in energy may be an important factor, with any differences in plans or peripheral doses being due to this change in energy rather than to any inherent property of unflattened beams.

Critically in this work the beam energy was raised back to the appropriate energy by matching standard beam quality indices (D_{10} (67.5%) and QI/$TPR_{20/10}$ [0.675]) of the clinical beam.

Owing to the differential attenuation caused by the flattening filter, this match exists only on the central axis (CAX), but in this way any differences can be directly compared without excessive reference to beam energy.

As the dose rate is roughly doubled by filter removal for unflattened beam delivery. the pulse repetition frequency was lowered to maintain the same dose rate between delivery techniques. This removed any uncharacterized effects (such as chamber response, ion recombination) that might exist because of the delivery of IMRT at higher dose rates. Barring any small changes in MU and segmentation, the plans therefore took the same time to deliver in each case. Although the dose per pulse was approximately doubled by filter removal, the machine had been recalibrated so that 1 MU = 1 cGy under standard conditions ($10 \times 10\ cm^2$, 90 cm SSD, D_{max}), as for any other clinical beam.

Peripheral doses in a slab phantom

To establish a reference and provide baseline measurements, peripheral doses were measured for standard field sizes in a slab phantom consisting of tissue-equivalent material. Peripheral doses are

Table 2. Summary of doses (in Gy) recorded for planning target volume (PTV) coverage in each plan for flattening filter in (In) and filter out (Out) according to the evaluation parameters in Table 1

	Case1		Case2		Case3		Case4		Case5	
	In*	Out*	In	Out	In	Out	In	Out	In	Out
V_{90}	99.4	99.3	99.9	99.9	99.9	99.9	99.1	99	100	100
V_{95}	95.3	94.9	98.1	98.3	99.0	98.9	94.2	95.4	96.2	96.3
V_{100}	50.0	50.0	50.0	50.0	50.0	50.0	50	50	50	50
V_{107}	0.2	0.1	0.1	0.2	0.9	0.3	0.4	0.9	0	0
D_2	52.6	52.4	52.4	52.9	53.2	52.5	52.6	53.1	51.6	51.5
D_{98}	46.8	46.6	47.9	47.9	48.2	48.2	46.6	46.7	47.3	47.4
HI	11.5	11.5	8.9	9.9	9.9	8.5	11.9	12.7	8.5	8.1
V_{PTV}	420.5	420.5	497.8	497.8	309.9	309.9	441.6	441.6	60.3	60.3
CI	1.13	1.10	1.09	1.10	1.22	1.16	1.05	1.07	1.26	1.23
$V_{NT\ 5}$	1445.3	1433.9	939.1	934.3	1345.2	1313.2	1053.8	1038.1	1331.7	1321.8
$V_{NT\ 95}$	475.2	462.0	542.3	547.0	378.9	360.6	463.6	471.9	76.1	74

Volumes are expressed as a percentage, except the PTV volume which is in cc.

* 'In' refers to the flattening filter in position (*i.e.,* conventional intensity-modulated radiotherapy [IMRT]) and 'Out' refers to unflattened IMRT (flattening filter out).

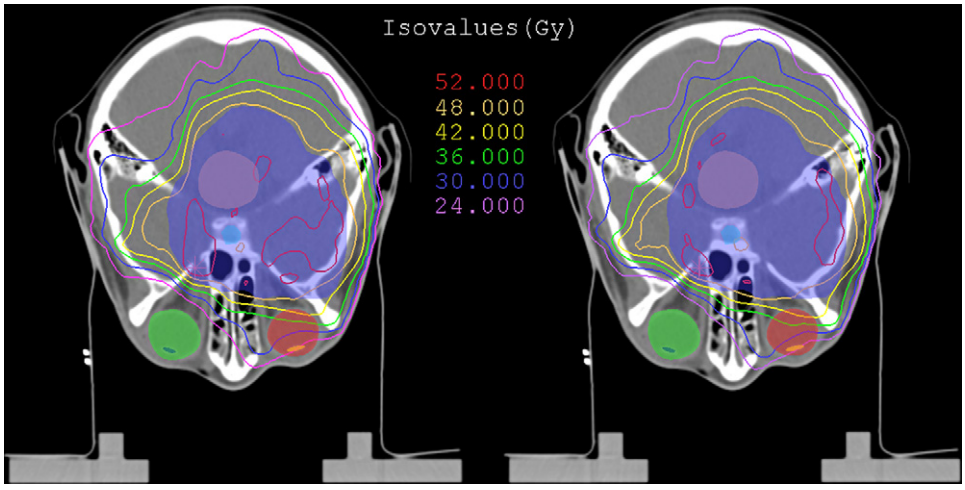

Fig. 2. Transverse slice through the center of the target region for Case 3 (an embryonal parameningeal rhabdomyosarcoma of the nasopharynx and skull base) showing dose distribution comparisons between each technique. Left, conventional intensity-modulated radiotherapy plan. Right, plan reoptimized with the flattening filter removed. The planning target volume is marked in blue, the pituitary in cyan, and the brainstem in brown. Isodoses lines are as marked.

relatively independent of measurement depth, and a depth of 5 cm was chosen as being representative for the cases studied.

Measurements were taken at regular intervals, from the CAX out to 70 cm away from the gantry, and recorded for a variety of field sizes and at collimator rotations of 0 and 90°, both with and without the filter. Readings were performed using a cylindrical ionization chamber (NE2571) and repeated with TLD-100 (Harshaw Chemical Company, Solon, OH) LiF thermoluminescent dosimeters (TLDs). For each position, 10 TLDs were used, and readings were normalized to the dose recorded for delivery under standard conditions (10×10, 90 cm SSD, D_{max}). These were then compared to the dose measured under the same conditions with the ionization chamber to characterize any differences in the energy response of the TLDs caused by the altered spectrum of scattered/leakage radiation.

Treatment planning system beam modeling

Commissioning data were measured and used to create a beam model within the XiO treatment planning system (Elekta CMS, XiO version 4.34.02). The basic machine parameters for the model (*e.g.,* machine limits) obviously remained the same, but a new beam spectrum, depth doses, and profiles along with total scatter ($S_{c,p}$) and phantom scatter (S_p) factors were required. In practice, total scatter and head scatter (S_c) were measured (and S_p calculated) because published S_p data are inaccurate for unflattened beams (21).

The XiO system uses two spectra for beam modeling to account for changes in beam quality across the flattening filter, one on the CAX and the other 7° off-axis. Although filter removal reduces the variation in beam spectrum across the beam, a small change still exists with the filter removed; however, it was seen that a single spectrum was sufficient to model the beam accurately, and a separate off-axis spectrum was not required. This reduced variation has also been shown experimentally by Georg *et al.* (22).

To remove any bias introduced by having a beam model for one technique "better" than another, all IMRT-specific beam data for both modes were measured concurrently using the same equipment and techniques. Both models were generated at the same time and to the same standard. For the final beam model, all differences between calculation and measurements were well within acceptable errors (±2%/2 mm).

IMRT treatment planning

Patient selection. For this study we retrospectively selected 5 pediatric patients recently treated for intracranial tumors with conventional 3D-CRT at our institution. Additional outlining was then performed by a consultant pediatric oncologist to enable IMRT planning for these patients. Intracranial tumors were chosen because they offered a challenge for the beam models involved and the opportunity to measure out-of-field doses over a large distance through the rest of the body.

Treatment plans were produced both with and without the flattening filter (10 plans in all). The number of beams and their gantry angles remained the same in each case (generally five equally spaced fields). Dose optimization priorities changed for each case, but the PTV was given priority unless a critical structure was compromised. In many cases, OARs were contained within the PTV, in which case care was taken to avoid dose hotspots occurring in these regions.

All plans received 50.4 Gy in 28 fractions prescribed to the mean of the PTV dose (*i.e.,* D_{V50} = 50.4 Gy). In each case, calculations were performed using the superposition algorithm, a step increment of 5 mm on the multileaf collimators (MLCs) and a 2-mm grid spacing.

For each IMRT case, a plan was produced first using the conventional IMRT beam model. Then, having found a set of dose

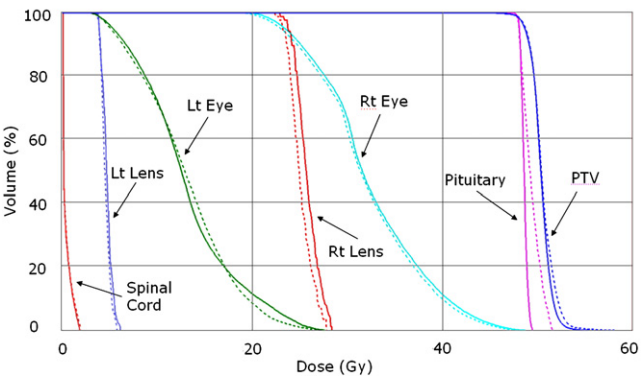

Fig. 3. Dose–volume histogram comparison between conventional (dotted lines) and unflattened (solid lines) plans for Case 5.

Table 3. Organ-at-risk doses (in Gy) for the 10 treatment plans (five cases)

	Case1		Case2		Case3		Case4		Case5	
OAR	In*	Out*	In	Out	In	Out	In	Out	In	Out
Lt eye†	34.3	33.6	13.3	13.1	32.0	32.4	36.9	36.6	3.7	3.4
Rt eye†	33.7	33.8	11.5	11.3	12.9	13.0	36.7	35.9	2.6	2.4
Lt lens	38.3	39.5	9.3	9.3	27.8	28.4	40.4	37.1	4.4	4.2
Rt lens	29.6	29.0	5.4	5.2	5.8	6.1	35.8	36.2	3.3	3.1
Optic chiasm	52.8	52.9	32.7	35.3	50.5	50.4	48.9	49.4	11.8	11.8
Brainstem	50.3	50.6	53.1	52.6	53.2	52.1	49.6	50.6	50.5	50.8
Spinal cord	2.9	2.7	49.8	49.7	2.0	1.8	49.6	48.6	0.6	0.5
Lt cochlea†	42.2	42.8	45.9	45.3	50.4	50.2	38.9	39.0	9.0	8.5
Rt cochlea†	44.6	43.5	45.8	47.7	31.5	33.6	48.8	48.5	8.1	7.6
Pituitary	51.8	51.6	53.6	52.6	51.6	49.5	50.0	51.3	14.9	15.3

* 'In' refers to the flattening filter in position (*i.e.,* conventional intensity-modulated radiotherapy [IMRT]) and 'Out' refers to unflattened IMRT (flattening filter out).

† All doses are the maximum point dose to that organ unless marked with a , in which case the mean dose is listed.

constraints to drive the optimizer to meet target and OAR limits, these same objectives were used to produce an optimized unflattened treatment plan. This process removed any interplanner or interplan bias from the evaluation. Plans were then evaluated according to standard dose indices to assess PTV coverage, homogeneity, and OAR sparing.

Verification measurements were performed by transferring the plan to a solid water phantom according to standard protocol. Absolute doses were measured at a depth of 5 cm using a 0.6-cm^3 cylindrical ionization chamber, and relative doses using a two-dimensional array (MatriXX, IBA Dosimetry), also at a depth of 5 cm.

Anthropomorphic phantom. Out-of-field doses are difficult to calculate with any degree of accuracy, and peripheral doses to OARs cannot be reliably or accurately predicted from large-field phantom studies (9). With an unflattened beam there may be significant changes in the number and shape of the beam segments required and the number of MU needed to deliver the prescribed dose. Scatter and leakage will also depend on the direction and energy of the scattered radiation, so they may be affected by the changes in beam spectrum. It is therefore important to measure these changes under representative conditions.

Phantom measurements yield dose measurements at the correct distance from the isocenter, at the correct depth and for clinically usable plans. For these reasons a commercially available anthropomorphic pediatric phantom (ATOM dosimetry model 706) (CIRS Inc., Norfolk, VA, USA) of a 10-year-old child was used to measure and compare peripheral doses for IMRT delivery.

The phantom consists of 25-mm-thick contiguous sections predrilled to hold TLDs. For each plan delivery, five LiF TLDs were placed at each of six points within the phantom corresponding to clinically relevant anatomic locations outside of the treated volume representing the thyroid, breast, lung, intestines, ovaries, and testes. Plans were delivered with the beam isocenter at the center of the head, and each plan was delivered three times to ensure that adequate dose levels were recorded by the TLDs

RESULTS

Peripheral doses in a slab phantom

As expected, peripheral doses were seen to decrease with distance from the field edge approximately exponentially, and to increase with increasing field size. In each case the readings generally started to converge beyond 40 cm from the CAX; however, doses measured with the filter removed dropped more quickly and to a lower level (Fig. 1).

For a 10 × 10 cm^2 field at 40 cm from CAX, the dose was only 50% that of the standard field, and at 70 cm from CAX, this fell to 38.5%. For a 3 × 3 cm^2 field the values were even lower: 34.7% and 27.8%, respectively. There was a significant drop in dose with the collimator rotation at 0° caused by the extra shielding (from the MLC carriage) within the treatment head, which was seen in both treatment modes with readings diverging at approximately 10 cm from the CAX and then reconverging at approximately 40 cm. At 20 cm this accounted for a 45% decrease in dose, and whenever possible IMRT plans are produced at collimator 0° to reduce this leakage dose.

Under the same delivery conditions, the TLDs showed significant differences compared to the ionization chamber readings, with the conventional beams under-responding, on average, by 7.5%, whereas the unflattened beams over-responded by almost 17%.

It is known that TLD-100 chips show variations in dose response at low energy, but they have been used previously to measure out-of-field doses (20). The differences observed between conventional and unflattened beams are most likely due to the changes in beam spectrum for scattered/leakage radiation between the two delivery modes. To account for these differences, the ratio between ionization chamber and TLD readings under the same conditions was taken, and these factors were used to correct measurements taken in the ATOM phantom.

IMRT plan evaluation

All 10 plans were assessed using standard evaluation criteria as shown in Table 1. Values are reported in Table 2 for each of the 10 plans created.

Figure 2 shows slices through the isocenter for Case 3 to illustrate the similarity of the plans. For all planned cases, the target coverage, homogeneity, and OAR doses both with and without the flattening filter were similar, with no one technique producing better plans than the other. This

Table 4. Segments and monitor units required to deliver identical plans by the two different delivery methods

Case	No. of fields	Conventional IMRT		Unflattened IMRT		Ratio of segments*	Ratio of MUs*
		Segments	MUs	Segments	MUs		
Case 1	5	89	18,146	89	19,186	1.000	1.057
Case 2	5	94	18,105	98	20,695	1.043	1.143
Case 3	5	85	17,928	76	17,767	0.894	0.991
Case 4	5	100	22,462	104	24,667	1.040	1.098
Case 5	5	57	10,924	59	11,310	1.035	1.035
Average						1.003 ± 0.063	1.067 ± 0.058

Abbreviations: IMRT = intensity-modulated radiotherapy; MUs = monitor units.
* Ratio is taken as unflattened/conventional IMRT.

can be seen diagrammatically in Fig. 3, which shows the dose–volume histogram for the two plans in Fig. 2. The correlation between plans for each case was tested, and differences were found to be statistically insignificant.

Table 3 lists the maximum point doses to the OARs for each case with and without the flattening filter. In many cases, OARs were within the PTV and so received unavoidably high doses.

Table 4 compares the number of segments and MU required to deliver the same dose distribution with the two techniques. Taking the ratio of (unflattened IMRT/conventional IMRT) for each of the five cases, the average for the number of segments required was 1.003 and the MU ratio was 1.067.

IMRT delivery quality assurance

The IMRT plans were delivered to a solid water phantom for standard IMRT quality assurance (QA) checks. IMRT is in routine use at our center, and all plans passed regular QA checks as set for clinical IMRT plans. Gamma index evaluation was performed using commercial software (OmniPro I'mRT v1.6, IBA dosimetry) with a criterion of 3%/3mm. The number of points with γ <1 should be greater than 95% in order for that beam to pass, and it can be seen from Fig. 4 that all beams from all plans passed this comfortably. Figure 4c shows that with the filter removed there was a trend toward greater consistency and a higher percentage of points passing the gamma evaluation than for

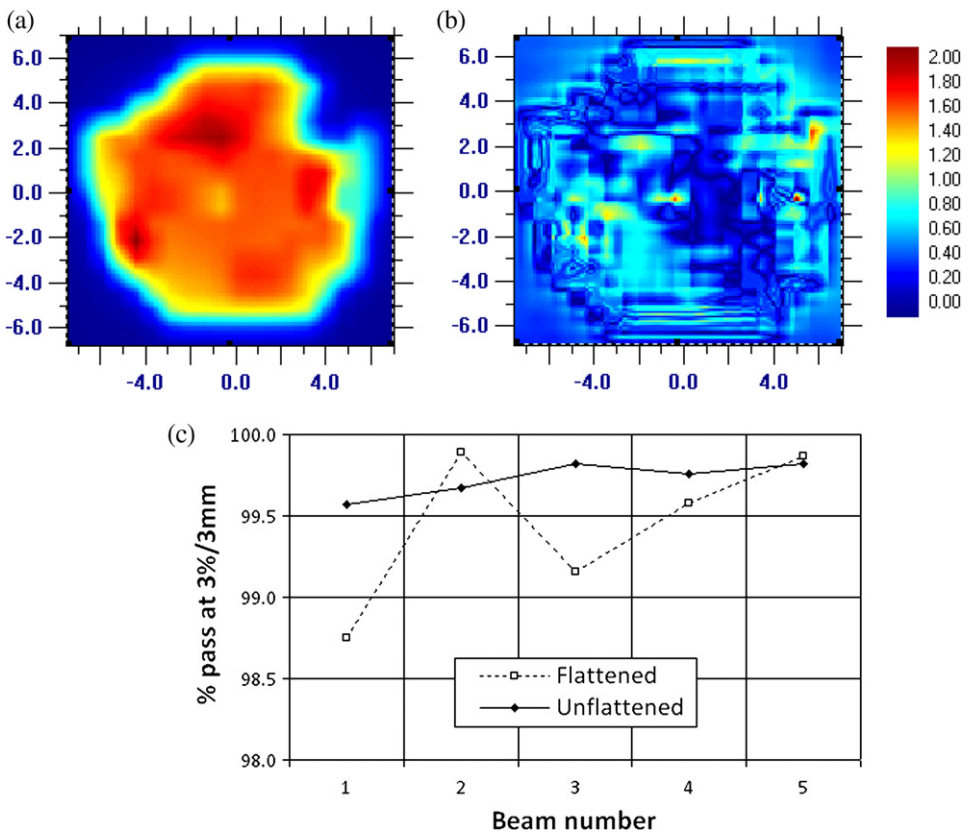

Fig. 4. Results from the intensity-modulated radiotherapy quality assurance analysis of Case 3. (a) typical fluence map (beam 1), (b) gamma analysis (3%/3 mm) two-dimensional array vs. treatment planning system, (c) plot of percentage of points passing evaluation for each beam.

Table 5. Summary of doses at specified points of interest for the five cases treated both with the flattening filter in (In) and out (Out)

		Case 1			Case 2			Case 5			
	Distance (mm)	In*	Out*	Ratio	In	Out	Ratio	In	Out	Ratio	Average Ratio
Head	0	100	100	1.00	100	100	1.00	100	100	1.00	1.00
Thyroid	100	1.730	1.288	0.745	2.256	1.778	0.778	0.755	0.570	0.755	0.763
Breast	200	0.202	0.167	0.825	0.248	0.195	0.784	0.010	0.078	0.781	0.797
Lung	250	0.159	0.112	0.701	0.189	0.132	0.701	0.082	0.057	0.700	0.701
Intestines	425	0.082	0.031	0.374	0.090	0.036	0.402	0.057	0.021	0.367	0.381
Ovaries	550	0.059	0.019	0.328	0.064	0.024	0.373	0.042	0.015	0.353	0.351
Testes	650	0.057	0.015	0.268	0.064	0.020	0.312	0.041	0.013	0.321	0.300

All doses are normalized to 100% at the beam isocenter (head), which is equal to 1.8 Gy (50.4 Gy/28#).
* In refers to the flattening filter in position (*i.e.,* conventional intensity-modulated radiotherapy [IMRT]), and Out refers to unflattened IMRT (flattening filter out). Distances are from the central axis (isocenter).

conventional delivery. This trend was observed for relative and absolute doses in all of the plans delivered.

Doses to distant organs

These measurements are summarized in Table 5 for each of the regions of interest and are shown graphically in Fig. 5. Even in regions close to the target volume, the doses are seen to be consistently lower for unflattened delivery. On average, the thyroid was only 5 cm from the field edge but still shows a 24% reduction in dose compared to the standard IMRT delivery.

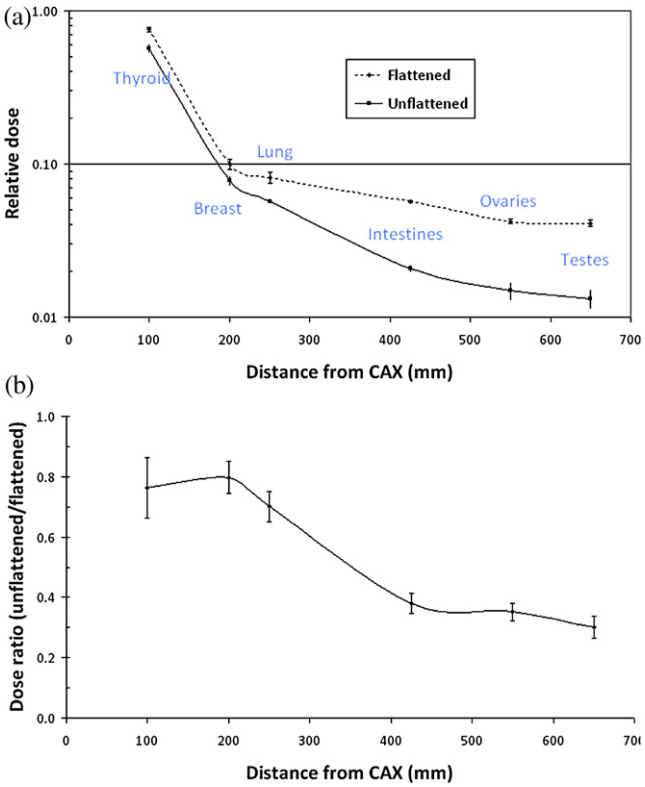

Fig. 5. Sample data from Case 5 illustrating the drop in peripheral dose for the unflattened beam delivery in the clinical intensity-modulated radiotherapy plans (a). (b) Plot of the average dose ratio (unflattened/flattened) for all of the plans delivered. CAX = central axis.

DISCUSSION

The XiO treatment planning system seems capable of both the modeling and the optimization of unflattened IMRT beams. The treatment plans produced are of the same quality as those for conventional IMRT, with virtually identical PTV coverage and OAR sparing, and this plan quality is maintained while retaining similar numbers of segments. There is a slight increase in the number of MU needed to deliver the same dose (6.7% for the cases studied), but this is an expected consequence of unflattened delivery because of the shape of the beam profile; delivering any dose *off-axis* will require the beam to be on for a longer period of time. Even taking this increase into account, the rise in MU required for unflattened delivery is modest compared to the reduction in leakage dose seen.

The risk of second cancer induction can be related back to these values and will scale with the ratio of absorbed doses. Taking a nominal distance of 50 cm to represent whole-body dose (13), the doses here are reduced on average by 64% for unflattened IMRT delivery, and obviously represent a significant reduction in risk from leakage radiation.

Under both standard and clinical conditions, out-of-field doses are seen to be lower at all positions relative to conventional delivery. In a recent Monte Carlo study by Kry *et al.* (23), however, unflattened beams were seen to increase the dose in the region from 3 to 15 cm from the field edge for IMRT delivery on a Varian accelerator. These differences may be due to variations in head design between the Elekta and Varian machines, or to the Varian accelerator having a slightly lower effective energy (4 MV). As the field size increases beyond the range used in this study, it is possible that there may be similar issues for larger PTVs and in adults, and further study is required to quantify this.

All IMRT plans passed regular patient-specific QA checks, and it was observed that with the filter removed there is a trend toward a higher pass rate with more points passing the gamma evaluation than for conventional delivery. Although these results are not conclusive, this may indicate an increase in calculational accuracy for unflattened beams, most probably caused by the reduction in head scatter; further work is under way at our institution to fully evaluate this.

Machines operating without a flattening filter are now commercially available, such as the TomoTherapy HI-ART (TomoTherapy, Inc., Madison, WI), CyberKnife (Accuray, Inc., Sunnyvale, CA), and TrueBeam (Varian Medical Systems, CA), indicating that in a "bottom-up" design the flattening filter is seen to be unnecessary for some treatments. Helical delivery systems, however, are inefficient in MU delivery because dose is delivered in a slice-by-slice fashion, so to deliver the same dose in clinical treatment plans requires 5 to 15 times as many MU (24). The TomoTherapy system has been designed with this in mind, with 23 cm of attenuation (tungsten jaws and MLC leaves), meaning that for static field delivery, leakage doses are reduced by 3 to 11 times compared to a conventional accelerator. When these factors are combined together, this results in similar, if not lower, leakage than for a conventional linac delivering IMRT (24).

Leakage may be reduced by increasing the shielding around the head, but this is both costly and cumbersome. Removal of the flattening filter is a relatively simple way of achieving the same effect on a conventional linac, and because the flattening filter doesn't actually seem to be required for IMRT, one can argue that it should be removed for IMRT treatments. A filter-free conventional linac could combine the best aspects of both delivery methods—a machine that has the inherent dose delivery efficiency of a linac combined with the reduction of scatter from flattening filter removal.

CONCLUSIONS

Flattening filter removal is not a complication but rather an exercise in simplification. Removal leads to a more stable beam with reduced head scatter and simplified beam modeling. These properties in turn may result in greater accuracy in dose predictions for IMRT, thereby helping to increase the accuracy of patient-specific QA.

Removal of the flattening filter for IMRT removes an unwanted and unnecessary source of scatter from the treatment head, significantly reducing whole-body radiation doses. If IMRT is to be used, then this risk must be balanced by an increase in local control and reduced toxicity. Any increase in whole-body dose must be justified for pediatric patients, who have the potential for such long-term survival, and as much as possible should be done to reduce these doses and lower the risk of cancer induction.

It is recommended that linac-based IMRT on conventional accelerators be performed without a flattening filter.

REFERENCES

1. Hall EJ, Wuu C. Radiation-induced second cancers: The impact of 3D-CRT and IMRT. *Int J Radiat Oncol Biol Phys* 2003;56:83–88.
2. Hall EJ. Intensity-modulated radiation therapy, protons, and the risk of second cancers. *Int J Radiat Oncol Biol Phys* 2006;65:1–7.
3. Kry SF, Salehpour M, Followill D, *et al*. The calculated risk of fatal secondary malignancies from intensity-modulated radiation therapy. *Int J Radiat Oncol Biol Phys* 2005;62:1195–1203.
4. Ruben JD, Davis S, Evans C, *et al*. The effect of intensity-modulated radiotherapy on radiation-induced second malignancies. *Int J Radiat Oncol Biol Phys* 2008;70:1530–1536.
5. Verellen D, Vanhavere F. Risk assessment of radiation-induced malignancies based on whole-body dose equivalent estimates for IMRT in the head and neck region. *Radiother Oncol* 1999;53:83–88.
6. NCRP Report No. 115, Risk Estimates for Radiation Protection National Council on Radiation Protection and Measurements. Bethesda, MD: NCRP; 1993.
7. Bassal M, Mertens AC, Taylor L, *et al*. Risk of selected subsequent carcinomas in survivors of childhood cancer: A report from the Childhood Cancer Survivor Study. *J Clin Oncol* 2006;24:476–483.
8. Diallo ID, Haddy N, Adiadi E, *et al*. Frequency distribution of second solid cancer locations in relation to the irradiated volume among 115 patients treated for childhood cancer. *Int J Radiat Oncol Biol Phys* 2009;74:876–883.
9. Followill D, Geis P, Boyer A. Estimates of whole-body dose equivalent produced by beam intensity modulated conformal therapy. *Int J Radiat Oncol Biol Phys* 1997;38:667–672.
10. Klein EE, Maserang B, Wood R, *et al*. Peripheral doses from pediatric IMRT. *Med Phys* 2006;33:2525–2531.
11. Mansur DB, Klein EE, Maserang BP. Measured peripheral dose in pediatric radiation therapy: A comparison of intensity-modulated and conformal techniques. *Radiother Oncol* 2007;82:179–184.
12. van der Giessen PH. Calculation and measurement of the dose at points outside the primary beam for photon energies of 6, 10 and 23 MV. *Int J Radiat Oncol Biol Phys* 1994;30:1239–1346.
13. Xu George X, Bednarz B, Paganetti H. A review of dosimetry studies on external-beam radiation treatment with respect to second cancer induction. *Phys Med Biol* 2008;53:R193–R241.
14. Lillicrap SC, Morgan HM, Shakeshaft JT. X-ray leakage during radiotherapy. *Br J Radiol* 2000;73:793–794.
15. Cashmore J. The characterisation of unflattened photon beams from a 6MV linear accelerator. *Phys Med Biol* 2008;53:1933–1946.
16. Cashmore J. Flattening filter free radiotherapy: 9th Biennial Meeting on Physics and Radiation Technology for Clinical Radiotherapy. *Radiother Oncol* 2007;84:S100.
17. Stathekis S, Esquivel C, Gutierrez A, *et al*. Treatment planning and delivery of IMRT using 6 and 18MV photon beams without a flattening filter. *Appl Radiat Isot* 2009;67:1629–1637.
18. Vassiliev ON, Kry SF, Kuban DA, *et al*. Treatment planning study of prostate cancer intensity modulated radiotherapy with a Varian Clinac operated without a flattening filter. *Int J Radiat Oncol Biol Phys* 2007;68:1567–1571.
19. Kry SF, Price M, Followill D, *et al*. The use of LiF (TLD-100) as an out-of-field dosimeter. *J Appl Clin Med Phys* 2007;8:169–175.
20. Vassiliev ON, Titt U, Pönisch F, *et al*. Dosimetric properties of photon beams from a flattening filter free clinical accelerator. *Phys Med Biol* 2006;51:1907–1917.
21. Kragl G, Wetterstedt S, Knäusl B, *et al*. Dosimetric characteristics of 6 and 10MV unflattened photon beams. *Radiother Oncol* 2009;93:141–146.
22. Georg D, Kragl G, Wetterstedt S, *et al*. Photon beam quality variations of a flattening filter free linear accelerator. *Med Phys* 2009;37:49–53.
23. Kry SF, Vassiliev ON, Mohan R. Out-of-field photon dose following removal of the flattening filter from a medical accelerator. *Phys Med Biol* 2010;55:2155–2166.
24. Ramsey CR, Seibert R, Mahan SL, *et al*. Out-of-field dosimetry measurements for a helical TomoTherapy system. *J Appl Clin Med Phys* 2006;7:1–11.

APPENDIX E

PUBLICATIONS

This article was published in the journal *Medical Physics* in 2012 and reports on the implementation and validation of FFF beams within the Monaco treatment planning system. This article forms the basis for large sections of chapter 4.

Cashmore J, Golubev S, Dumont JL *et al* "Validation of a virtual source model for Monte Carlo dose calculations of a flattening filter free linac" *Med.Phys.* **39** (6) 3262-3269, (2012).

Validation of a virtual source model for Monte Carlo dose calculations of a flattening filter free linac

Jason Cashmore[a)]
Hall-Edwards Radiotherapy Research Group, University Hospital Birmingham NHS Foundation Trust, United Kingdom, B15 2TH

Sergey Golubev and Jose Luis Dumont
Elekta CMS Software, St. Louis, Missouri 63043

Marcin Sikora
Department of Oncology and Medical Physics, Haukeland University Hospital, Bergen 5021, Norway

Markus Alber
Section for Biomedical Physics, University Hospital for Radiation Oncology, Hoppe-Seyler-Str 3, 72076, Tübingen, Germany

Mark Ramtohul
Hall-Edwards Radiotherapy Research Group, University Hospital Birmingham NHS Foundation Trust, United Kingdom, B15 2TH

(Received 17 August 2011; revised 9 March 2012; accepted for publication 10 April 2012; published 22 May 2012)

Purpose: A linac delivering intensity-modulated radiotherapy (IMRT) can benefit from a flattening filter free (FFF) design which offers higher dose rates and reduced accelerator head scatter than for conventional (flattened) delivery. This reduction in scatter simplifies beam modeling, and combining a Monte Carlo dose engine with a FFF accelerator could potentially increase dose calculation accuracy. The objective of this work was to model a FFF machine using an adapted version of a previously published virtual source model (VSM) for Monte Carlo calculations and to verify its accuracy.
Methods: An Elekta Synergy linear accelerator operating at 6 MV has been modified to enable irradiation both with and without the flattening filter (FF). The VSM has been incorporated into a commercially available treatment planning system (Monaco™ v 3.1) as VSM 1.6. Dosimetric data were measured to commission the treatment planning system (TPS) and the VSM adapted to account for the lack of angular differential absorption and general beam hardening. The model was then tested using standard water phantom measurements and also by creating IMRT plans for a range of clinical cases.
Results: The results show that the VSM implementation handles the FFF beams very well, with an uncertainty between measurement and calculation of $<1\%$ which is comparable to conventional flattened beams. All IMRT beams passed standard quality assurance tests with $>95\%$ of all points passing gamma analysis ($\gamma < 1$) using a 3%/3 mm tolerance.
Conclusions: The virtual source model for flattened beams was successfully adapted to a flattening filter free beam production. Water phantom and patient specific QA measurements show excellent results, and comparisons of IMRT plans generated in conventional and FFF mode are underway to assess dosimetric uncertainties and possible improvements in dose calculation and delivery. [http://dx.doi.org/10.1118/1.4709601]

Key words: Monte Carlo, flattening filter free, unflattened, virtual source model

I. INTRODUCTION

Therapeutic photon beams are generated by stopping a narrow electron beam in a metal target. These bremsstrahlung x-rays have a relatively constant angular energy spectrum, but a strongly forward peaked energy fluence which becomes more peaked as the initial electron energy increases. This translates into a triangular shaped beam profile.

To provide a more uniform fluence distribution, it is customary to insert a conical flattening filter (FF) of a high-Z material into the beam. The primary function of the filter is to provide a "nominally" flat radiation beam (e.g., at 10 cm depth), but in doing this, the filter causes negative side-effects such as

- changes in the spectrum due to differential photon absorption
- the need for the introduction of "horns" in the particle fluence to compensate for this angular variation of the spectrum
- a reduction in dose rate
- the creation of a significant source of extrafocal scattered radiation.

Such uniform beams can be advantageous for conventional treatments, but in practice, although a beam can be within flatness specification under uniform conditions (e.g., 10 cm depth in a homogeneous phantom with a flat surface), it may be significantly skewed taking into account realistic treatment geometries with inhomogeneities, body surface curvature, and treatment at depths other than the reference depth. Flattening filters have been regarded as an integral part of linear accelerators since their first medical use in the 1950s, but for beams with modulated intensity, an initially "flat" radiation distribution should not be necessary, and removing the filter will remove these disadvantages.

Several studies have reported flattening filter free (FFF) characteristics for Elekta,[1–3] and Varian[4–6] accelerators via direct measurement, Monte Carlo (MC) simulation, and by multisource modeling.[7] These studies demonstrate that filter free operation results in reduced leakage, higher dose rates, and simplified beam modeling. Further studies have also demonstrated that these properties result in significant reductions in doses to organs outside of the treated volume for equivalent delivery of intensity-modulated radiotherapy (IMRT) and SBRT plans on a prototype FFF Elekta linac.[8,9]

In theory, FF removal could increase the dosimetric confidence in a plan due to reductions in off-axis beam softening and by virtue of having less scattered photons and contamination electrons in the beam. The accuracy of the beam model could therefore be improved since we are reducing the uncertainty in these components. Coupling this with a Monte Carlo dose calculation algorithm could eventually lead to more accurate dose prediction compared to standard techniques.

The objective of this work was to model a FFF machine using an adapted version of a previously published virtual source model (VSM)[10–12] for Monte Carlo calculations and to test this implementation against standard phantom measurements and for delivery of clinically relevant IMRT plans. Effort has been concentrated on a prototype 6 MV FFF beam from an Elekta Synergy linear accelerator. This is a research unit that does not operate in clinical mode. Although the eventual aim is to demonstrate a difference in calculation accuracy between FFF and conventional beams, the aim of this work is to demonstrate the adaptability of the VSM for FFF MC dose calculations.

II. MATERIALS AND METHODS

II.A. VSM—Source densities and particle fluence distribution

For MC simulations, a beam can be described by the phase space parameters (position, direction of motion, and energy) of the constituent photons and electrons. It is possible to generate these parameters analytically in a phase space plane in front of the patient and use MC transport for particles passing through the patient. A virtual source model allows for efficient generation of particle parameters and can be commissioned for conventional linear accelerators with semiautomatic modeling tools. The VSM-based MC computes dose in the following way:

(1) Source type, energy, position, and direction of particles are sampled from the VSM. The required number of particles is generated on the fly in an arbitrary plane above the collimators to achieve a predefined level of statistical noise in the patient.
(2) The particles are transported through collimators or transmission probability filters,[12] e.g., in the multileaf collimator (MLC) plane.
(3) The dose deposited in the patient is calculated using the XVMC code.[13,14]

The VSM treats particles coming from different parts of the accelerator as if they were coming from three different virtual sources. These sources are the primary photon source, the secondary photon source, and the electron contamination source, with relative contributions P_{pri}, P_{sec}, and P_{econ}, respectively. The primary source is defined in the plane of the electron beam target where primary photons originate from interactions within the target. The secondary source models all of the photons that result from interactions occurring in places other than the target. The positions of the secondary source and the electron contamination source are free parameters which are set according to the machine geometry. The secondary source is located at the base of the primary collimator and the electron contamination source at the base of the FF (or the build-up plate).

It is assumed that each of the sources has a Gaussian shape with standard deviations σ_{pri}, $\sigma_{\mathrm{sec}}(E)$, and $\sigma_{\mathrm{econ}}(E)$ for primary photon distribution, energy-dependent secondary photon distribution, and energy-dependent electron contribution, respectively, according to the following expressions:

$$\sigma_{\mathrm{sec}}(E) = \Sigma_{\mathrm{sec}}\left(\frac{E}{E_0}\right)^{-0.34} \quad \text{if E} \geq 0.511 \text{ MeV}, \tag{1}$$

$$\sigma_{\mathrm{sec}}(E) = \Sigma_{\mathrm{sec}}\left(\frac{0.511}{E_0}\right)^{-0.34} \quad \text{if E} < 0.511 \text{ MeV}, \tag{2}$$

where E = particle energy, $E_0 = 1$ MeV, and Σ_{sec} = free parameter, the base data standard deviation of the secondary source, and

$$\sigma_{\mathrm{econ}}(E) = \Sigma_{\mathrm{econ}}(E/E_0)^{-0.18}, \tag{3}$$

where Σ_{econ} = free parameter, the base data standard deviation of the electron source.

Upon generation of a photon in the source location, the particle fluence in a phase space plane that is located above the collimators is initially flat. The particle weight is altered depending on the angle between its direction and the central axis (CAX) according to a tabulated profile. While it is possible to measure the energy fluence in air with a small detector fitted with a build-up cap, it proves more robust to measure a cross-profile in a water tank at the dose maximum (D_{max}) and determine the table by forming the ratio of the measurement to a simulation with a pristine, flat energy fluence.

II.B. VSM—Energy spectra

The primary photon spectrum (S_{pri}) on the central axis before the flattening filter is described by

$$S_{\text{pri}}(E) = \omega_0 \quad \text{if} \quad E_{\text{bin}} \le E < E_{\min}, \tag{4}$$

$$S_{\text{pri}}(E) = \left(\frac{E}{E_{\max}}\right)^{-b_{\text{pri}}} - 1 \text{ if } E \ge E_{\min}, \tag{5}$$

where E = photon energy (MeV), $E_{\min}$ and $E_{\max}$ are minimum and maximum photon energies.

For $E_{\min}$, a fixed value of 0.5 MeV is used. ω_0 = low energy bin parameter. b_{pri} = free parameter.

In the implementation of this VSM for flattened beams, this primary spectrum is attenuated with an appropriate, radially dependent filter function.[11]

The secondary photon spectrum $S_{\text{sec}}(E)$ describes the secondary photons on the CAX after the flattening filter.

$$S_{\text{sec}}(E) = \omega_S \quad \text{if } E_{\text{bin}} \le E < E_{\min}, \tag{6}$$

$$S_{\text{sec}}(E) = e^{-b_{\text{sec}}E} - e^{-b_{\text{sec}}E_{\max}} \quad \text{if } E \ge E_{\min}, \tag{7}$$

where E_{bin}, ω_S = low energy bin parameters and b_{sec} = free parameter.

The off-axis energy softening is approximated by using two parameters (δb_{pri} and δb_{sec}) which define the relative change of the primary and secondary spectra with respect to the tangent of angle to the CAX [tan(ν)] at the scoring plane

$$b_{\text{pri}}(\nu) = b_{\text{pri}} + \delta b_{\text{pri}} \tan(\nu), \tag{8}$$

$$b_{\text{sec}}(\nu) = b_{\text{sec}} + \delta b_{\text{sec}} \tan(\nu). \tag{9}$$

The energy spectrum of the contaminating electrons is approximated by an exponential function

$$S_{\text{con}}(E) = N_e \exp\left(-\frac{E}{\langle E_e \rangle}\right), \tag{10}$$

where N_e = normalization factor and $\langle E_e \rangle$ = mean electron energy.

The VSM is defined by fixed and open parameters. Fixed parameters are derived from a BEAMnrc simulation of the treatment head which is performed only for a given accelerator type. Open parameters are fitted in the polyenergetic kernel superposition commissioning routine for each individual linac.[13] The free parameters of the VSM are derived from basic beam data measurements performed in water and by minimizing the differences between calculated and measured data.

For the purpose of verifying the dose calculation accuracy of this model, the Monaco™ treatment planning system (TPS) (Elekta CMS software, St. Louis, MO) was used (version 3.1), which incorporates a commercial implementation of this model (VSM v.1.6).

II.C. FFF accelerator and beam properties

An Elekta Precise linear accelerator has been modified to enable irradiation both with and without the FF. In practice, the filter cannot simply be removed but needs to be replaced by a thin metal "enhancer" plate in the same position as the FF. This plate generates electrons which provide build-up dose to the ionization chamber to give sufficient signal to the servo plates so they, in turn, can operate properly to control the beam quality and steering.[8] Several materials and thicknesses of materials have been used in previous studies and these have recently been reviewed by Georg *et al.*[15] This prototype Elekta unit uses a 2 mm stainless steel plate which provides sufficient dose to the chamber without adding significantly to scatter. The differential attenuation of this plate can be neglected; in contrast, the overall rather large filter effect of the FF removes photons below about 1 MV almost completely on the CAX, and decreasingly toward the field edge. Dosimetric data for a linac operating with this combination of plate and energy have not been reported in the literature. These differences are briefly summarized below.

II.C.1. Depth dose slope

Without the beam hardening effect of the filter, the depth dose (DD) beyond $D_{\max}$ for unflattened beams are close to those of flattened 5 MV beams. For the machine used in this work, the beam energy has been raised back to 6 MV on the central axis by matching the quality index $\text{QI/TPR}_{20/10}$ (0.675) to the clinical 6 MV (flattened) beam.

II.C.2. Surface dose

Filter removal leads to an increase in the number of low energy x-rays (softer beam spectrum) which acts to increase the surface dose. Counterbalancing this is a reduction in electron contamination, especially at high electron energies. Measurements and MC simulations in the build-up region of unflattened beams indicate that, at 6 MV, this leads to a slight overall decrease in the surface dose. The variation with field size is also reduced for these beams compared to standard flattened beams (by approximately half).

II.C.3. Dose maximum

The softer spectrum moves $D_{\max}$ closer to the surface, whereas a lower contribution from photon scatter and electron contamination moves $D_{\max}$ deeper. Both effects almost cancel out in practice.

II.C.4. Lateral profiles

Without angular-dependent differential attenuation, there is a relatively small off-axis softening for FFF beams. Low spectral variation across the field (beam quality) results in less variation in the shape of lateral profiles with depth. Reduced head scatter (Sc) also results in lower doses outside of the field, which also falls off faster with distance. Small field sizes are relatively unaffected by filter removal, but beyond approximately 10×10 cm^2, the triangular shape of beam profiles is apparent, and photon fluence starts to decrease.

II.C.5. Head scatter

The FF is known to be the main component contributing to variation of head scatter in the treatment head. These

variations must be accurately modeled if dose calculations are to be correctly performed. The head scatter factor is seen to vary by 3% between field sizes of 3×3 and 40×40 cm^2 with the FFF machine compared to 9% for the standard 6 MV beam. The collimator exchange effect is also reduced by filter removal.[1]

II.C.6. Dose rate

The FF is composed of several centimeters of high Z materials, and one of the most immediate consequences of filter removal is the increase in dose rate. Measurements on the central axis indicate an increase in dose rate by a factor of 1.7 to 800 MU per min. Dose rates of 1200 MU per min are expected in the clinical version. If high dose rates are not required, the linac can simply run at a lower rate by changing the pulse repetition frequency (PRF). These gains in dose rate are effectively due to an increase in the dose per pulse, so regardless of PRF/dose rate, the ion recombination factors needed for accurate dosimetry should be investigated.

II.D. Model commissioning

Measurements for beam modeling included depth dose curves and profiles for various field sizes measured in a water phantom (Blue Phantom2, IBA Dosimetry, Germany). Measurements were performed at SSD = 100 cm with suitable detectors [CC01, CC13 IBA Dosimetry, NE2577 Nuclear Enterprises Ltd. (now QADOS, UK)]. Monaco is used clinically in our department with conventional flattened beams and the data set and equipment used for FFF measurements matched those originally used to commission this beam energy. In this way, the FFF and FF data can be said to be of the same standard and can be directly compared against one another.

The measurement set consisted of the following:

- Depth dose curves for field sizes: 2, 3, 5, 10, 15, 20, 30, and 40 cm^2.
- In-plane and cross-plane profiles for field sizes: 2, 3, 5, 10, 15, 20, and 30 cm^2 at depths of 1.5, 5, 10, and 20 cm.
- Diagonal profiles for the largest field size: 40×40 cm^2.
- Output factors for square fields: 2, 3, 5, 10, 20, 30, and 40 cm^2 at 10 cm depth.

The unique feature of the VSM is that it represents the primary photon spectrum before it reaches the flattening filter. Therefore, turning off the flattening filter correction corresponds to physically removing the flattening filter from the accelerator head. The procedure for modeling the FFF machine is very similar to modeling a standard machine and as a starting point a previously created model of the FF linear accelerator from the same vendor was used. The model parameters were modified as follows:

(1) The radially dependent, differential attenuation of the FF in the conventional model was turned off. Further variations in off-axis spectrum were kept constant [Eq. (8)].
(2) The relative contribution from primary photons P_{pri} was increased.
(3) $E_{\max}$ was increased along with b_{pri} to provide a better agreement of the depth dose, especially in the $D_{\max}$ region. This accounts for the retuning of the machine to produce a typical 6 MV quality index.
(4) The secondary source Gaussian sigma was made wider by a factor of $\sim$2 due to the fact that in the absence of the flattening filter, the primary collimator contributes most of the scatter.
(5) To correct the fluence profile for FFF beams, the tabulated parameters for radial energy fluence variation were adjusted to the diagonal cross-profiles at $D_{\max}$.

The results of the VSM phase space reconstruction are independent of the dose calculation engine used; therefore, it can be coupled with other MC dose engines. MC simulation and treatment planning were performed in the Monaco TPS using a water phantom of size $50 \times 50 \times 35$ cm^3. The voxel size was set at 2 mm for the smallest 2×2 cm^2 field and 3 mm for the rest of the fields with statistical uncertainties set to 0.5%.

II.E. Treatment planning

In order to expose the FFF model to a range of conditions and test the beam model and the accuracy of the dose calculation (and delivery), a series of treatments with increasing complexity and treatment volume were planned. These sites consisted of skull base, esophagus, prostate, and head and neck cases.

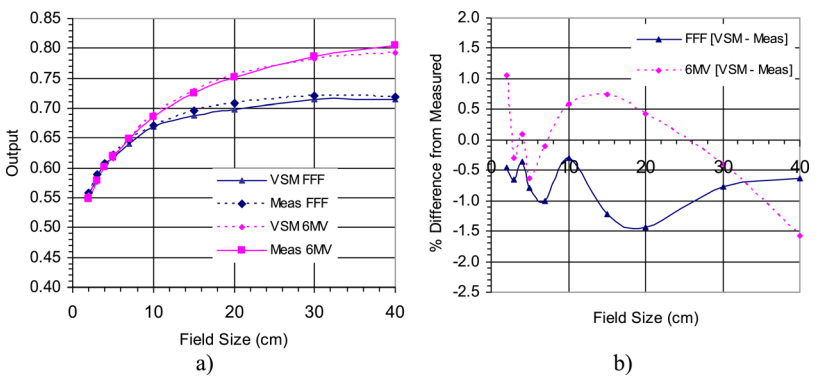

FIG. 1. (a) Absolute output factors as a function of field size for FFF and conventional 6 MV beams as predicted by the TPS compared to measurement. (b) Difference in output factors, calculated minus measured.

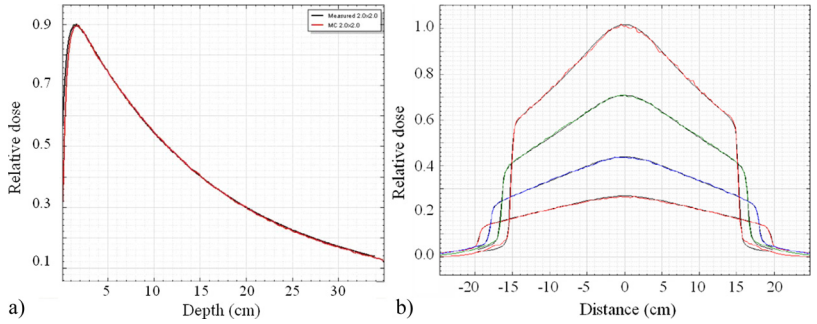

FIG. 2. Sample beam data: (a) PDD curve for 2×2 cm^2 field, (b) cross-profiles for a 30×30 cm^2 field for the FFF model.

To test the model under the extreme influence of the unflattened beams, the isocenter for the prostate and head and neck plans were placed asymmetrically so that large parts of the fields were exposed to the off-axis region of the beam.

For each plan, a set of constraints were found to give the optimal distribution. The plans were then reoptimized using the FFF beam model and adapted as necessary to fulfill the dose constraints.

These beams were then recalculated on a phantom (2%, 2 mm) for delivery to a Delta^{4PT} (ScandiDos, Inc., Sweden) IMRT verification device. All deliveries were made with the gantry at 0° to remove any influence from the treatment couch.

III. RESULTS

III.A. Water phantom data verification

Figure 1(a) shows a plot of output factor variation with field size for FFF and conventional beams, and Fig. 1(b) the difference in calculated relative output factor curve against measurement. These are absolute values as predicted by the planning system and not scaled to measured data. The absolute outputs can be predicted within 1.5% of measurements over the entire range of field sizes.

Figure 2(a) shows a sample DD curve for a 2×2 cm^2 field size and Fig. 2(b) shows profiles at depths of D_{max}, 5, 10, and 20 cm for a 30×30 cm^2 field. Figure 3 shows, for various depths and fields sizes, the percentage difference between measured and calculated depth dose curves. The spread in values is approximately 1.5% (+0.5 to −1.0) in both cases indicating that the beam model is of similar quality for both FFF [Fig. 3(a)] and conventional [Fig. 3(b)] beams, and within the measurement uncertainty for these fields. Figure 4 shows comparisons of FFF beam profile measurements against TPS predictions for field sizes from 2×2 to 30×30 cm^2 with their respective 1D γ-analysis for acceptance criteria of 2%/2 mm. It can be seen that all points had $\gamma < 0.8$. For set criteria of 1%/1 mm, 93% of all points had $\gamma < 1$.

III.B. Treatment plans

As the volume of the tumor (treatment length) and complexity of the plan increase, there is a tendency to see an underdosage in regions far from the central axis, which is seen as a sloping shoulder on the DVH curve. It is possible to compensate for this by further penalizing cold spots within the tumor, and in the Monaco TPS, this can be achieved by increasing the cell sensitivity (α) of the tumor or adding a quadratic underdose penalty. This acts to maintain plan quality but brings about an increase in both the number of segments and monitor units needed to deliver the plan. It

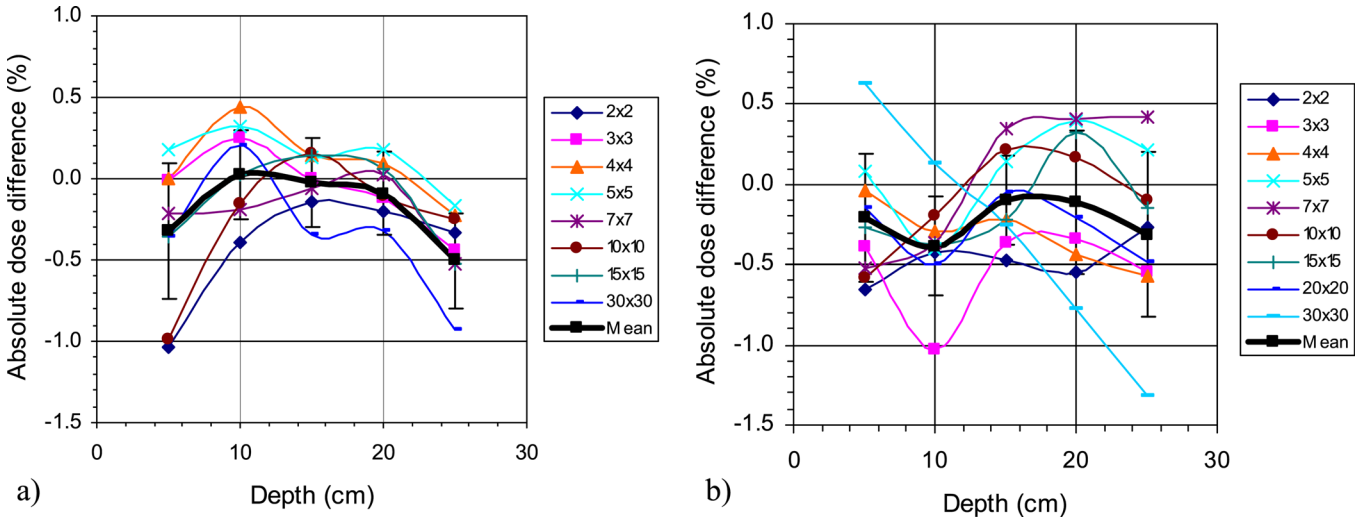

FIG. 3. Absolute dose difference between measured and calculated depth doses curves (100 cm source-surface distance) for the field sizes indicated for (a) FFF and (b) FF beams. Monte Carlo variance is set at 0.5%.

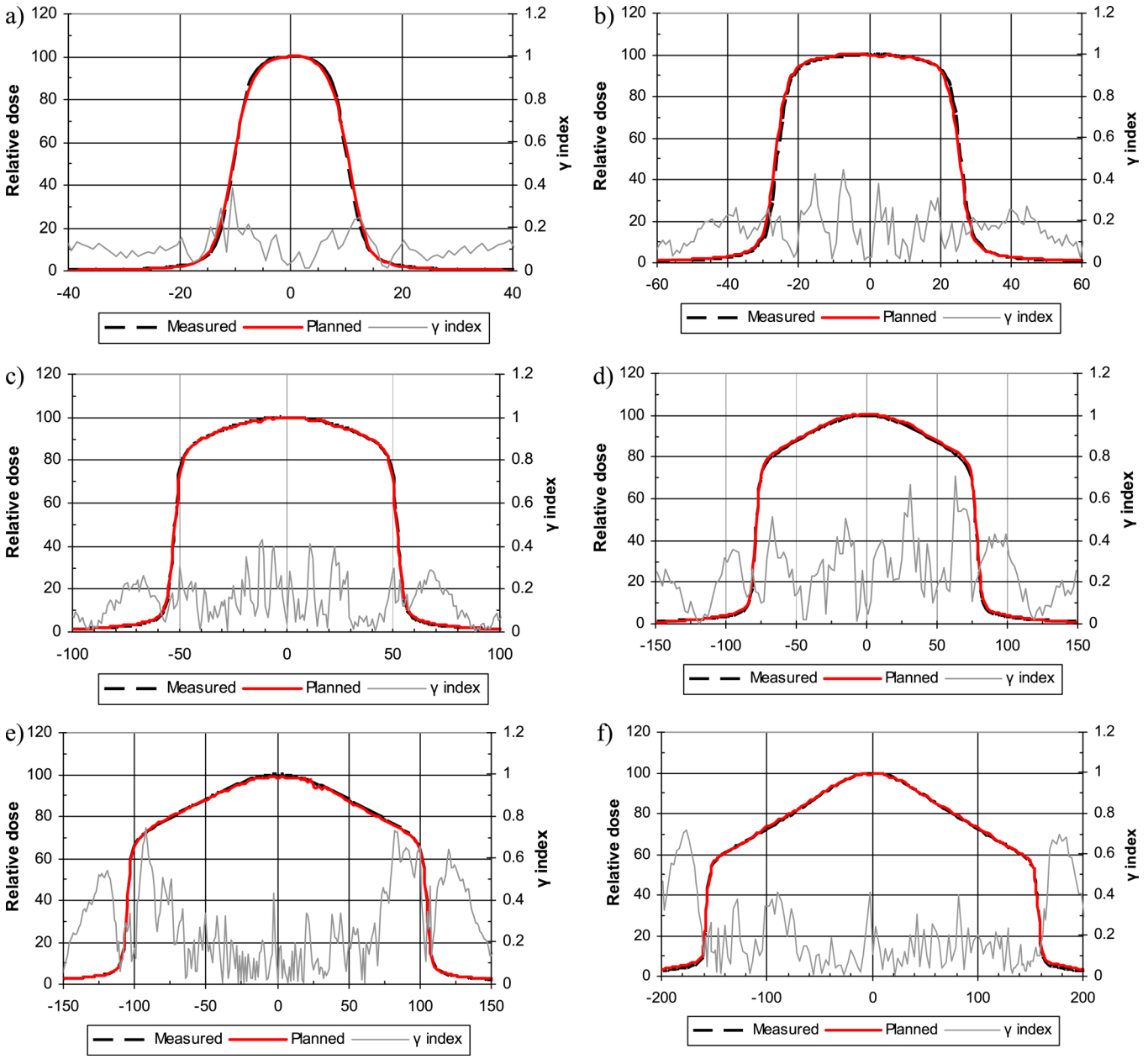

FIG. 4. Comparison of calculated vs measured beam profiles for sample field sizes of (a) 2×2 cm^2, (b) 5×5 cm^2, (c) 10×10 cm^2, (d) 15×15 cm^2, (e) 20×20 cm^2, and (f) 30×30 cm^2 at 100 cm SSD and a depth of 5 cm. Criteria for gamma analysis are 2%/2 mm.

can be seen from Table I that as the treatment volume and plan complexity increase there is a corresponding increase in the number of segments and MU needed to deliver the FFF plans. Figure 5 shows a color-wash dose distribution on sagittal and coronal CT slices through the tumor for a head and neck FFF IMRT plan. The dose volume histogram indicates that the plans are equivalent in terms of both PTV coverage and organ at risk sparing.

TABLE I. Number of segments and monitor units needed for each treatment plan and the relative increase in each necessary to deliver the FFF plans.

		Segments			Monitor units		
	PTV volume (cm^3)	6 MV	FFF	% Difference	6 MV	FFF	% Difference
Skull base	23.2	20	21	+5.0	416	446	+7.2
Esophagus	555.4	64	67	+4.7	785	931	+18.6
Prostate	804.5	66	68	+3.0	828	951	+14.9
Head and neck	918.7	168	183	+8.9	1343	1682	+25.2

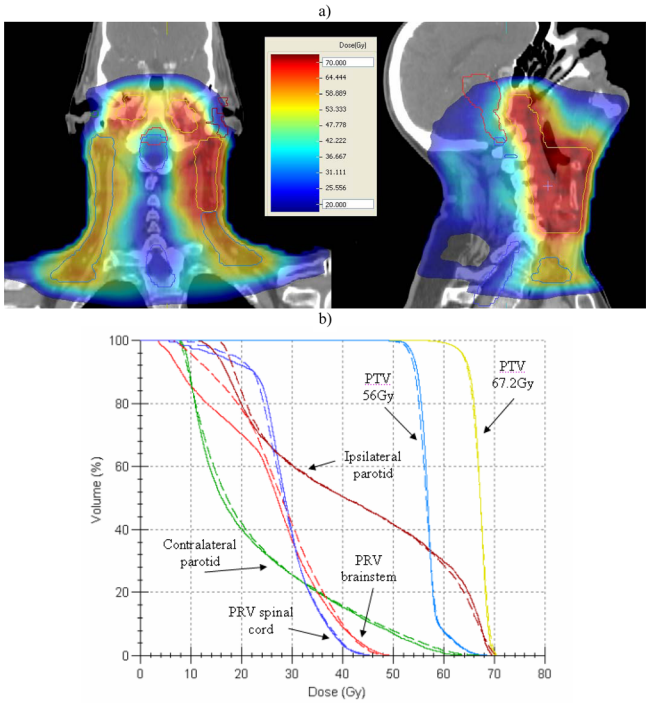

FIG. 5. Beam setup for IMRT planning of a head and neck case showing sagittal and coronal color-wash maps (a) and dose volume histogram (b). The FFF beam is displayed as the dotted line, 6 MV solid.

III.C. Verification of IMRT beams

Table II shows the absolute dose differences and statistics for the gamma analysis of the sample plans analyzed at both 3%/3 mm and 2%/2 mm acceptance criteria. It can be seen that as the volume of tumor and the complexity of the plan increase the pass rate begins to fall (as expected), but all plans pass the standard IMRT acceptance criteria of 95% of points <1 using a 3%/3 mm tolerance.

IV. DICSUSSION AND CONCLUSION

Removal of the flattening filter invalidates the assumption of energy fluence and phantom scatter homogeneity in the incident beam so a TPS must be able to model an arbitrary shape of the energy fluence. It is therefore important to be able to handle the incident particle fluence by means of a sufficiently general calculation algorithm.

The virtual source model for flattened beams was successfully adapted to a flattening filter free beam production by particle fluence warping with tabulated parameters and modifying the energy spectrum to account for the lack of angular differential absorption and general beam hardening. Since the VSM was initially derived from studies of phase spaces created by BEAMnrc,[16] it captures the salient features of the various sources of radiation in a linear accelerator without overly limiting assumptions, and thereby provides enough latitude to model flattening filter removal.

Beam modeling of the 6 MV FFF beam within Monaco is seen to be as accurate as that used clinically. Depth dose predictions are generally within 0.5% for the FFF beam, with only a few outliers up to 1% which is more consistent than for the conventional beam model. 1D gamma analysis of beam profiles for selected criteria (2%/2 mm) also show an excellent

TABLE II. Gamma analysis and absolute dose difference of individual beams for the IMRT plans. Percentage of points passing gamma analysis ($\gamma < 1$) at 3%/3 mm and 2%/2 mm for the individual beams of each plan.

		Gamma analysis 3%/3 mm		Gamma analysis 2%/2 mm		Absolute dose difference (%)	
Treatment site	Beam	6 MV	FFF	6 MV	FFF	6 MV	FFF
Skull base	1	100.0	100.0	99.5	100.0	−0.8	0.2
	2	99.8	100.0	93.5	92.4	−0.2	0.5
	3	100.0	99.8	90.6	89.4	−0.9	−0.1
	4	99.8	99.3	92.9	92.3	−0.1	0.0
	5	99.8	100.0	92.4	91.2	−0.6	0.1
Esophagus	1	100.0	99.0	98.3	89.9	0.6	1.2
	2	100.0	99.8	99.1	95.9	0.0	1.0
	3	100.0	100.0	100.0	99.8	−0.1	0.3
	4	100.0	100.0	100.0	99.1	−0.7	0.5
	5	100.0	99.8	98.8	97.2	0.2	1.0
Prostate + nodes	1	99.4	97.2	93.5	86.2	0.8	1.4
	2	99.8	100.0	97.6	98.4	0.2	0.7
	3	100.0	99.8	97.7	92.8	0.1	0.9
	4	100.0	100.0	98.8	98.8	0.0	0.7
	5	100.0	99.9	98.0	94.9	0.0	0.6
Head and neck	1	97.7	98.3	87.8	84.8	0.9	1.4
	2	100.0	98.8	97.6	94.6	0.4	1.1
	3	99.7	99.5	97.5	94.3	0.3	1.1
	4	99.5	100.0	95.7	96.9	0.3	0.9
	5	99.4	99.2	92.0	84.0	0.4	1.2
	6	99.1	98.3	94.4	87.6	0.6	1.3
	7	99.7	99.8	97.5	95.8	0.3	0.9

agreement. This matches well with commissioning results reported by Hrbacek *et al.*[17] and Kragl *et al.*[18] for FFF beams from Varian and Elekta linacs, respectively. Any differences between prediction and measurement where γ exceeded 1 occurred mainly within the out-of-field regions of the beam profiles and only for the larger ($>15 \times 15$ cm^2) field sizes.

It has been observed that as the field sizes needed for planning increase then so do the number of MU required to deliver these plans; this is a natural consequence of the FFF beam profile since it will require longer beam on times to deliver doses off-axis. The complexity of the plan is also seen to increase the number of segments required to treat the FFF plans compared to the conventional IMRT plans if plan quality is to be maintained. This may be more specifically related to the fact that segmentation algorithms used are optimized for flattened rather than unflattened beam profiles. Commercial planning systems do not currently consider the nonflat beam profile during optimization.

The optimization of nonuniform beam profiles has been discussed by Kim *et al.*[19] who reported that segment numbers required for FFF beams can be significantly reduced once this is taken into account in the optimization process. Such an addition is likely to reduce the number of segments required to deliver modulated FFF plans.

In general, the clinical implementation of this filter free design into a commercially available treatment planning system (Monaco) shows excellent results. Commissioning of the model can be performed by the same set of standard water phantom data as for the flattened beam models. These measurements need not be overly sophisticated and hence help to avoid errors in the commissioning process.

All beams for the planning exercises passed the defined acceptance criteria used for standard IMRT patient specific quality assurance tests. Once the test criteria are tightened to 2%/2 mm, slight differences can be seen between the flattened and FFF deliveries, with the conventional beams generally receiving slightly higher pass rates. There may be several reasons for this including the increased number of segments delivered and also the fact that the linac is still a prototype (nonclinical) release. Once the Elekta FFF linac is released for clinical use with fully optimized hardware and dosimetry, these tests should be repeated to assess any possible improvements in dose calculation and delivery.

ACKNOWLEDGMENTS

The author would like to thank Kevin Brown from Elekta Crawley for assistance in setting up the FFF mode and to James Satterthwaite for helpful discussion and comments concerning the paper. Many thanks also to Rick Sims for discussions around Monaco planning and beam verification. Jason Cashmore holds a research contract with Elekta UK Ltd. to study the properties of unflattened photon beams. Sergey Golubev and Jose Luis Dumont work for Elekta CMS Software. Markus Alber works as a consultant for Elekta CMS Software.

[a]Electronic mail: jason.cashmore@uhb.nhs.uk

[1]J. Cashmore, "The characterization of unflattened photon beams from 6 MV linear accelerator," Phys. Med. Biol. **53**, 1933–1946 (2008).
[2]G. Kragl *et al.*, "Dosimetric characteristics of 6 and 10 MV unflattened photon beams," Radiother. Oncol. **93**, 141–146 (2009).
[3]M. Dalaryd *et al.*, "A Monte Carlo study of a flattening filter-free linear accelerator verified with measurements," Phys. Med. Biol. **55**, 7333–7344 (2010).
[4]O. Vassiliev, U. Titt, S. F. Kry, and F. Ponisch, "Monte Carlo study of photon fields from flattening filter-free clinical accelerator," Med. Phys. **33**(4), 820–827 (2006).
[5]O. Vassiliev *et al.*, "Dosimetric properties of photon beams from a flattening filter free clinical accelerator," Phys. Med. Biol. **51**, 1907–1917 (2006).
[6]U. Titt *et al.*, "A flattening filter free photon treatment concept evaluation with Monte Carlo," Med. Phys. **33**(6), 1595–1602 (2006).
[7]W Cho *et al.*, "Multisource modeling of flattening filter free (FFF) beam and the optimization of model parameters," Med. Phys. **38**(4), 1931–1942 (2011).
[8]J. Cashmore, M. Ramtohul, and D. Ford, "Lowering whole-body radiation doses in pediatric intensity-modulated radiotherapy through the use of unflattened photon beams," Int. J. Radiat. Oncol., Biol., Phys., **80**(4), 1220–1227 (2011).
[9]G. Kragl *et al.*, "Flattening filter free beams in SBRT and IMRT: Dosimetric assessment of peripheral doses," Z. Med. Phys. **21**(2), 91–101 (2011).
[10]M. Sikora, O. Dohm, and M. Alber, "A virtual source model of an Elekta linear accelerator with integrated mini MLC for Monte Carlo based IMRT dose calculation," Phys. Med. Biol. **52**, 4459–4463 (2007).
[11]M. Sikora and M. Alber, "A virtual source model of electron contamination of a therapeutic photon beam," Phys. Med. Biol. **54**(24), 7329–7344 (2009).
[12]M. Sikora, "Virtual source modelling of photon beams for Monte Carlo based radiation therapy treatment planning," Ph.D. dissertation, University of Bergen, Norway, 2011.
[13]M. Fippel, "Fast Monte Carlo dose calculation for photon beams based on the VMC electron algorithm," Med. Phys. **26**, 867–878 (1999).
[14]J. Kawrakow and M. Fippel, "Investigation of variance reduction techniques for Monte Carlo calculation using XVMC," Phys. Med. Biol. **45**, 2163–2183 (2000).
[15]D. Georg, T. Knoos, and B. McClean, "Current status and perspective of flattening filter free photon beams," Med. Phys. **38**(3), 1280–1293 (2011).
[16]D. W. O. Rogers *et al.*, "BEAM: A Monte Carlo code to simulate radiotherapy treatment units," Med. Phys. **22**, 503–524 (1995).
[17]J. Hrbacek, S Lang, and S. Klock, "Commissioning of photon beams of a flattening filter-free linear accelerator and the accuracy of beam modeling using an anisotropic analytical algorithm," Int. J. Radiat. Oncol., Biol., Phys. **80**(4), 1228–1237 (2011).
[18]G. Kragl, D. Albrich, and D. Georg, "Radiation therapy with unflattened photon beams: Dosimetric accuracy of advanced dose calculation algorithms," Radiother. Oncol. **100**, 417–423 (2011).
[19]T. Kim *et al.*, "Inverse planning for IMRT with nonuniform beam profiles using total-variation regularization (TVR)," Med. Phys. **38**(1), 57–66 (2010).

APPENDIX F

PUBLICATIONS

This article has been submitted for publication in the journal *Physics in Medicine and Biology* and reports on surface dose measurements for FFF beams under a range of clinical treatment conditions. This article forms the basis of most of chapter 3.

Cashmore J "Surface dose variations in 6 and 10MV flattening filter free (FFF) photon beams" (2013).

Surface dose variations in 6 and 10MV flattening filter free (FFF) photon beams

Jason Cashmore
Hall-Edwards Radiotherapy Research Group, University Hospital Birmingham NHS Foundation Trust, United Kingdom, B15 2TH.
E-mail: jason.cashmore@uhb.nhs.uk

Purpose: As the use of linear accelerators operating in flattening filter free (FFF) modes becomes more wide-spread it is important to have an understanding of the surface doses delivered to patients with these beams. Flattening filter removal alters the beam quality and relative contributions of low energy x-rays and contamination electrons in the beam. Having dosimetric data to describe the surface dose and buildup regions under a range of conditions for FFF beams is important if clinical decisions are to be made.
Methods: An Elekta Synergy linac with standard MLCi head has been commissioned to run at 6MV and 10MV running with the flattening filter in or out. In this linac the 6MV FFF beam has been energy-matched to the clinical beam on the central axis (D_{10}). The 10MV beam energy has not been adjusted. The flattening filter in both cases is replaced by a thin (2mm) stainless steel plate. A thin window parallel plate chamber has been used to measure a comprehensive set of surface dose data in these beams for variations in field size and SSD, and for the presence of attenuators (wedge, shadow tray and treatment couch).
Results: Surface doses are generally higher for small field sizes and lower for large field sizes with a cross-over at 15x15cm^2 at 6MV and 25x25cm^2 at 10MV. This trend is also seen in the presence of the wedge, shadow tray and treatment couch. Only small differences (<0.5%) are seen between the beams on varying SSD. At both 6 and 10MV the filter free beams show far less variation with field size than conventional beams.
Conclusions: By removing the flattening filter a source of contamination electrons is exchanged for a source of low energy photons (as these are no longer attenuated). In practice these two components almost balance out.
No significant effects on surface dose are expected by the introduction of FFF delivery.

Keywords: skin dose, filter free, unflattened, surface dose

I. Introduction

It is well known that megavoltage (MV) photon beams provide a skin-sparing effect, but the actual magnitude of this can depend on a number of treatment parameters. Changes in field size, source-to-surface distance (SSD) and beam energy all cause changes in surface dose. In particular the introduction of materials into the beam line such as shadow trays and patient support devices can cause large increases in dose to the skin. At the same time it is also important that doses to targets close to the surface (such as for head & neck and breast treatments) are accurately known so that under-dosage does not occur.
Doses received by the basal skin layer can result in a range of problems from minor (such as erythema/epilation) to serious (desquamation/necrosis) depending on the doses received. A full knowledge and understanding of these doses is therefore necessary if clinical decisions are to be

made, and these effects have been studied by a number of authors [1-4] for conventional 'flattened' beams.
Until recently the flattening filter was generally considered to be a standard component in C-arm linear accelerators, but with the introduction of the TrueBeam (Varian Medical Systems, Palo Alto, CA) and Versa HD (Elekta AB, Stockholm, Sweden) accelerators the clinical use and literature surrounding FFF radiotherapy is increasing. Unflattened photon beams offer the possibility of increased dose rate and reduced scatter/leakage radiation and have been shown to be unnecessary for the production and delivery of IMRT and small field treatments [5-9].
Several authors have reported surface dose variations with field size in FFF beams [10-13], but data for changes in SSD, tray, wedge, couch etc. are unavailable. With this in mind measurements of surface doses for FFF beams are required to assess any potential changes in dose that may damage the skin.
The purpose of this investigation was to evaluate and compare trends in surface dose for 6 and 10 MV flattened and FFF beams under conditions routinely experienced in radiotherapy treatments. These conditions were for:

- variations in field sizes (square fields, sizes 3x3 to 40x40 cm^2);
- variation in source-surface-distance (SSD) (55 to 140cm);
- the presence of
  - motorized wedge (0–60°);
  - blocking tray
  - carbon fiber couch

II. Background

II. A. Skin doses

Skin doses arise from a combination of effects and will depend on the magnitude and relative contributions from contamination electrons, low-energy photons and backscattered radiation. Contamination electrons in particular can give rise to significant doses in the skin and will be influenced by several factors including head design, beam energy, SSD, field size or introduction of materials into the beam close to the patient. Skin dose can therefore vary significantly from one setup to another and can be a limiting factor in some treatments [1].
Since the flattening filter is responsible for the majority of contamination electrons reaching the patient surface [14] its removal is therefore likely to *reduce* this contribution. However, the filter also acts as a beam hardener, removing low-energy photons from the spectrum. With the filter removed the low-energy component is allowed to pass through to the patient and act to *increase* the surface dose.
The use of motorized wedges and perspex shadow trays (blocking trays) in conjunction with filter removal could also change these characteristics significantly. Since conventional planning with unflattened beams has been shown to be of use [15, 16] data has also been measured for the motorized wedge and shadow tray. Dose measured under different conditions (wedge, SSD, tray etc.) can also be a good indicator of the relative levels of dose from low energy photons and from contamination electrons (although no attempt has been made to separate these two components here).

II. B. Dose measurement

In the buildup region of high energy photon beams electronic equilibrium does not exist, therefore percentage depth ionization (PDI) and percentage depth dose (PDD) are not equal. Under these conditions electronic fluence perturbations in the air-sensitive volume of the cavity cause ionization chambers to exhibit an 'over-response', and determining PDD from PDI measurements is difficult. This will occur for measurements carried out in the dose build-up region (and in the transition zones between different media), with a magnitude depending on the geometrical characteristics of the chamber. The over-response will be greatest at the surface and decrease as dose maximum (d_{max}) is approached, and electronic equilibrium restored.
In these circumstances it is generally accepted that extrapolation chambers provide the most accurate means of measurement. These chambers, however, are unavailable in most departments and are also very time consuming to use, therefore parallel plate chambers are routinely used to measure surface and buildup doses, and corrections must be applied to convert ionization to dose. The over-response of the chamber has been shown to be mainly due to electron in-scattering from the side walls, which is determined by the width of the guard ring [17, 18]. Perturbation factors will therefore depend on the dimensions of the chamber.
Several methods have been introduced to correct for the perturbation effects seen when using parallel plate chambers in the build-up region of high-energy photon beams. These are based either on correction based methods from extrapolation chamber measurements, or by direct derivation of individual perturbation factors.
In the first method the chamber reading is corrected by a subtractive factor that depends on the beam energy, chamber geometry and depth of measurement [17-20]. These factors are essentially independent of field size but increase with decreasing energy.
In the second method perturbation factors are derived explicitly. For parallel-plate chambers the PDD at depth *d* can be expressed as

$$PDD(d) = PDI(d)\frac{\left[\left(\frac{\bar{L}}{\rho}\right)_{air}^{med} P_{fl} P_{wall} P_{cel}\right]_{d}}{\left[\left(\frac{\bar{L}}{\rho}\right)_{air}^{med} P_{fl} P_{wall} P_{cel}\right]_{d_{max}}} \qquad [1]$$

Where $\left(\overline{L_\Delta}/\rho\right)_{air}^{med}$ is the mean restricted collision stopping power from medium to air and P_{fl}, P_{wall} and P_{cel} are perturbation factors for the fluence, wall and central electrode respectively. When $d>d_{max}$ these factors do not change and can be considered as invariant and the dose ratio is then equal to the ionization ratio (PDD = PDI) [21]. In the buildup region however, perturbations in the electron fluence cause these chambers to over-respond so that PDI>PDD. Since perturbation factors are known to have a strong dependence on chamber design, depth of measurement and beam energy, P_{fl}, P_{wall}, P_{cel} and $\left(\overline{L_\Delta}/\rho\right)_{air}^{med}$ must be independently evaluated.
Recent studies have shown that the product $P_{fl}P_{wall}P_{cel}$ changes by less than 1% from the surface to d_{max} [22, 23] and that $\left(\overline{L_\Delta}/\rho\right)_{air}^{med}$ changes by less than 4% for beams up to 18MV. The maximum deviation occurs at the phantom surface and will be less than 5%, reducing to 0% at d_{max}.
For certain ion chambers and beam energies some of these factors have been evaluated (e.g. Ref 24). The presence of beam modifiers such as the wedge can change the photon beam spectrum

appreciably, so removal of the flattening filter and associated changes in the beam spectrum are therefore likely to cause significant changes to this. For FFF beams in general these are unknown and an independent set of over-response factors would be required for more accurate prediction. For these reasons the effective point of measurement method as described McEwen *et al.* [23] was employed to calculate dose in the buildup region, accepting limitations.

III. Materials and methods

III. A. Linear accelerator

An Elekta Synergy linear accelerator (Elekta AB, Stockholm, Sweden) with a standard 80 leaf MLCi head has been used for measurements. The linac is fitted with a motorized wedge (nominal 60° wedge angle) and an iBEAM evo carbon fiber couchtop, both of which were assessed.
The flattening filter is replaced with a 2mm stainless steel plate that is used to shield out contamination electrons from the primary collimator, and to provide build-up into the ionization chamber. Without this plate the signals in the chamber are too low to accurately control the beam energy and steering servos.
Removing the flattening filter changes the energy spectrum of the beam since lower energy photons are no longer removed from the beam. This results in unflattened beam having 'softer' beam spectra than their beam hardened counterparts. The 6MV beam can be energy matched to the conventional beam by adjusting the beam running parameters. In this way the depth doses at 10cm depth, $TPR_{20/10}$ QI/$TPR_{20/10}$ [0.675] for a 10x10cm^2 field are the same. FF removal also affects the variation in the energy spectrum across the beam (making it much more uniform) but energy matching across the beam is not possible. In contrast, and in following with other work [12, 25] the 10MV beam has not been adjusted. The $TPR_{20/10}$ for the 10MV and 10MV FFF beams are 0.737 and 0.716, respectively.

III. B. Experimental setup

Measurements were taken in a phantom composed of 30x30cm^2 WT1 Solid Water slabs (Radiation Physics, St Bartholomew's Hospital, London) of varying thickness, with 15 cm of backscatter material to ensure full phantom scatter conditions. Further sheets of Solid water were added to take readings in the buildup region (maintaining SSD) (FIG 1a). Doses were measured with an NACP-02 (Scanditronix, IBA Dosimetry) parallel plate ionization chamber. The NACP chamber has a 'coin-shaped' sensitive volume with a diameter of 10mm, a height of 2mm and a guard ring of 3mm in width [26]. In the literature a guard ring of at least 5mm is recommended for measuring skin doses [18], but both Carl [1] and McEwen [23] have investigated its use and found it to be suitable.
The chamber was embedded in the phantom such that the entrance window of the chamber was flush with the surface with the central axis perpendicular to this. The doses at depth were measured by adding layers of phantom material while maintaining the SSD at 100cm to the top of the phantom (FIG 1a). The effective point of measurement itself was taken as the inside of the entrance window which, for the NACP-02 chamber (with a composite window of 0.1 mm Mylar and 0.5 mm graphite) is equivalent to 1 mm of water. Surface dose measurements therefore represent a measurement depth of 1mm, and all results are plotted relative to the dose measured at d_{max} (15mm 6MV, 22mm 10MV) for the same field size.
Surface dose readings are therefore reported as relative surface dose (RSD) where:

$$RSD = d_{surface} / d_{\max}$$

Buildup curves through the carbon fiber couch we measured according to the setup shown in FIG 1b, with the gantry rotated to 180° to deliver radiation through the couch. Couch transmission factors were measured using a Farmer type chamber (NE2577 Nuclear Enterprises Ltd. (now QADOS, UK)) set at isocentre within 10cm of WT1 (FIG 1c). Couch factors are expressed as the ratio of the posterior to anterior electrometer readings.
Polarity corrections in x-ray beams are generally small, but can become significant for parallel plate chambers, especially in the buildup region [27]. It is expected that the largest differences will occur at the surface, and that this will reduce as d_{max} is approached. To estimate polarity effects buildup curves were measured at ±200V over the buildup region, representing the full range of contamination conditions at 6 and 10 MV.

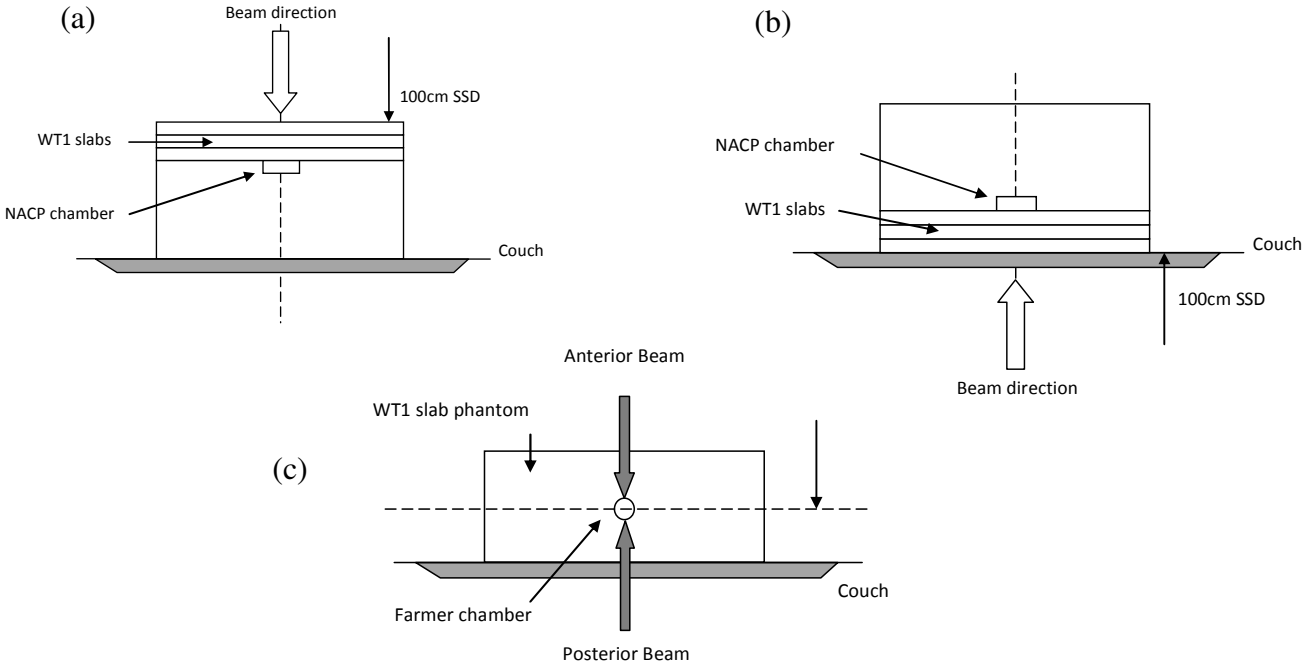

FIG 1. Experimental setup for (a) surface dose and buildup, (b) surface dose and buildup through the couch, (c) couch transmission factors.

IV. Results

IV. A. Bias effects

Surface doses were measured at positive and negative polarity (±200V) under representative high and low conditions (surface and d_{max}). Figure 2 shows these buildup curves for both 6 and 10MV FFF beams (for a 10x10cm^2 field), and the ratio of these readings (+ve/-ve) vs. depth.
As expected, the correction becomes larger as the measurement point moves closer to the surface and was found to differ by <1.3% (1.3% at 6MV, 1.1% at 10MV) and fall to unity at d_{max}. This was considered to be of small enough magnitude to disregard as the main purpose of this paper is to compare surface doses and evaluate trends. Readings were therefore taken at -200V only for the remainder of the study.

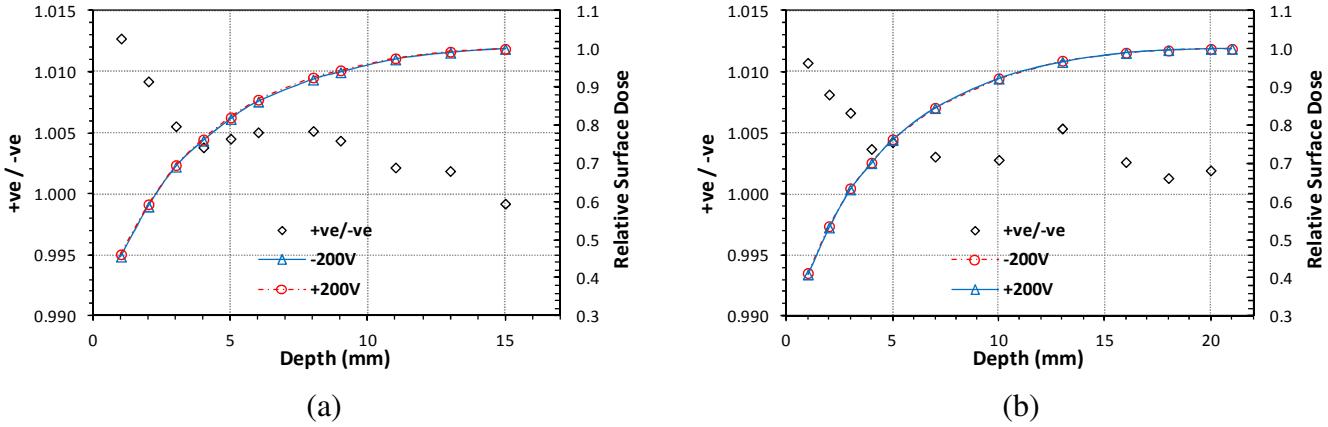

FIG 2. Fractional surface dose as a function of depth for +ve and –ve polarization voltages for (a) 6MV and (b) 10MV photons. The +ve/-ve ratio shows the increasing disequilibrium towards the surface.

IV. B. Field size variation

Surface doses are seen to increase fairly linearly with increasing field size, albeit at a shallower incline for FFF beams than for the conventional. At 6MV the unflattened beam shows a slight increase in RSD at smaller field sizes (+3.4% at 3x3cm^2) and decrease at larger (-7.1% at 40x40cm^2) with equivalency at 15x15cm^2.

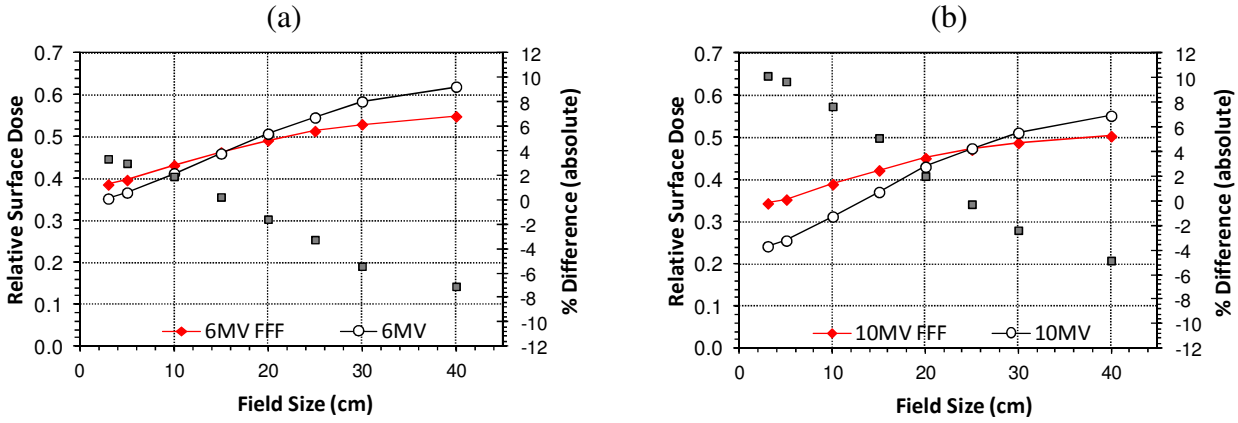

FIG 3. Variation of surface dose with field size for Flattened and FFF beams for jaw settings of 3x3 to 40x40cm^2. (a) 6MV and (b) 10MV.

At 10MV there is again far less variation in the RSD with field size for the FFF beams, but the conventional beam generally exhibits lower surface doses. At small field sizes the unmatched 10MV FFF shows an increase of 10% in absolute terms over the conventional 10MV beam; in contrast, the largest field size the FFF beam then shows a 5% decrease. The surface doses are equivalent for a field size of 25x25cm^2.

For the 6MV beam there is a variation in RSD of 26.7% (absolute) in changing from a 3x3 to 40x40cm^2 field (0.353 to 0.620) compared to 16.2% (0.387 to 0.549) for the FFF equivalent. At 10MV these values are 31.0% for 10MV (0.242 to 0.552) and 16.0% for 10MVFFF (0.344 to 0.504). The variation of surface dose with FS is very similar for the 6 and 10MV FFF beams showing only minor differences with field size (0.44%cm^{-1} FFF at 6MV and 0.43%cm^{-1} at 10MV. For conventional operation these gradients are 0.72%cm^{-1} at 6MV and 0.84%cm^{-1} at 10MV.

IV. C. Wedge

The skin dose for wedged field increases as field size is increased in a similar manner to the skin dose for open fields.
With the wedge in place surface doses at both 6 and 10MV are seen to be generally lower for FFF beams. This is true at all field sizes for 6MV (FIG 4a) and those beyond 12x12cm for 10MV (FIG 4b). The slope of the curves is also much shallower for the unflattened beams. This is demonstrated clearly in FIG 4c where wedge only data is plotted for each beam.

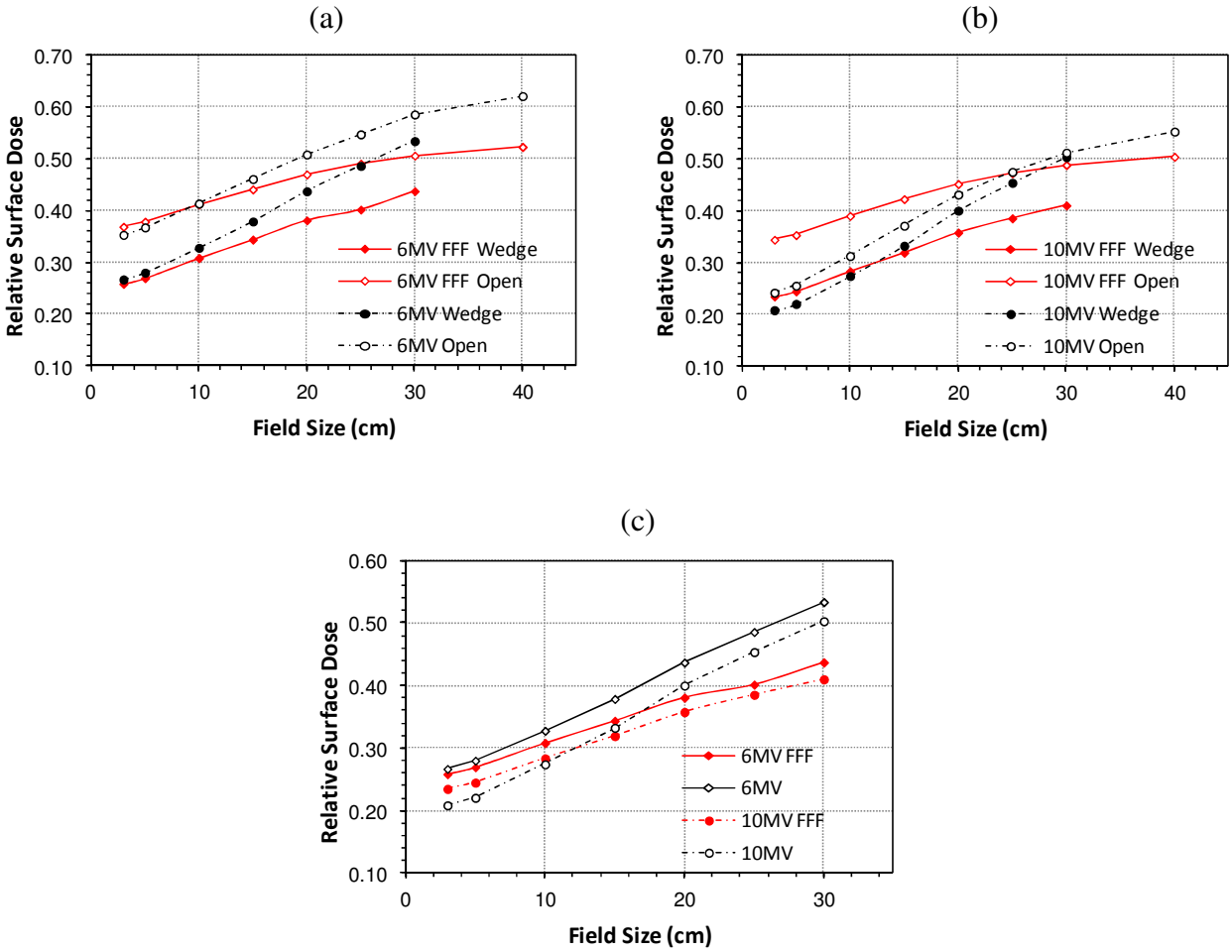

FIG 4. Variation of RSD with field size for wedged beams. (a) 6MV FFF and conventional open and wedged beams, (b) variation at 10MV, (c) wedge only data for 6 and 10MV.

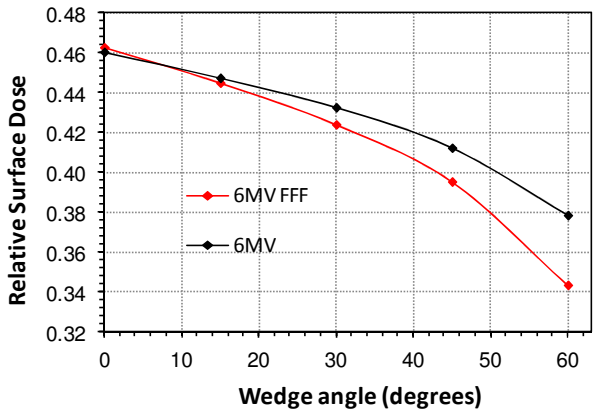

FIG 5. RSD variation with wedge angle for motorized wedge, 6MV. Field size is 15x15cm^2.

The gradient of these lines is 0.66%cm^{-1} vs. 0.99%cm^{-1} at 6MV and 0.65%cm^{-1} and 1.09%cm^{-1} at 10MV, again demonstrating much less variation with field size for filter free.
Skin doses for wedge angles of 15°, 30°, 45°, and 60° were also measured for the motorized wedge at 6MV only (figure 5). Since the wedge is shown to reduce RSD the greatest difference is observed when the field is fully wedged.

IV. D. SSD variation

At 6MV there is little difference between the FFF and conventional beams, except near the treatment head where the FFF beams show a reduction in surface dose of up to 5%. Increasing the beam energy to 10MV shows the typical reduction in surface dose. The FFF beam again shows reduced doses at the shortest SSD's, but this quickly reverses with the conventional 10MV beams exhibiting a marked reduction in dose beyond 60cm SSD.
RSD is very stable between 90 and 140cm SSD then shows a sharp rise for measurements closer to the treatment head. Again, there is a reduction seen in the variation in FFF beams than for conventional beams.
SSD variations were also investigated with the wedge in place. At both 6 and 10MV a larger dose difference is seen between FFF wedge and open data than is seen for the conventional beams. The highest RSD is seen for 10MV FFF beams, and lowest for the 10MV wedge. A 10% reduction in RSD is seen for 10MV FFF compared to only 4% for 10MV. At 6MV these figure are 11% vs. 7%.

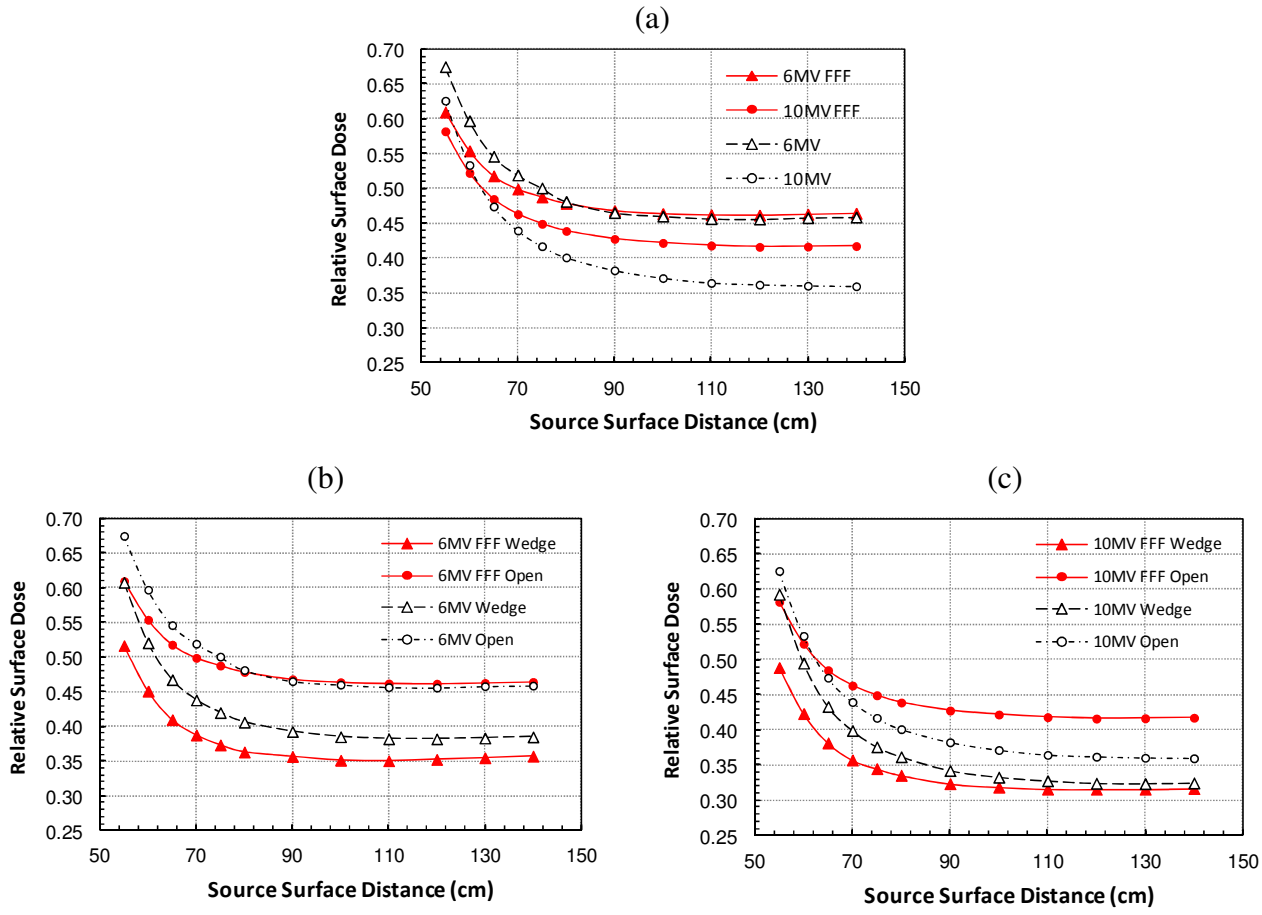

FIG 6. Effect of changes in source to surface distance on surface dose for 6MV and 10MV beams for open and wedged beams (15x15cm^2).

IV. E. Shadow tray

Inevitably the insertion of an acrylic shadow tray (10mm thick acrylic [polymethyl methacrylate]) into the beam causes an increase in the observed surface dose. At 6MV the smallest field sizes exhibit very similar readings, but these rapidly diverge as field size increases with the FFF beam having a much shallower slope. For a 40x40cm^2 field the difference rises to 12% for the FFF beam. For the 10MV beams the slope is once again much shallower for the FFF energy. There is a switch over from higher to lower surface doses at around 20x20cm^2 with doses being approximately 10% higher for 3x3cm^2 and 15% lower for 40x40cm^2.

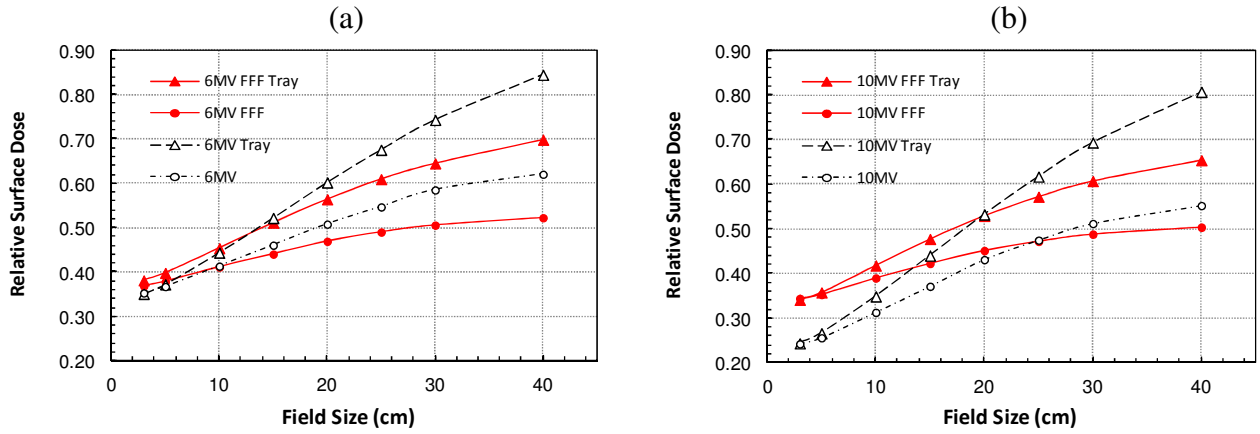

FIG 7. Variation of RSD when passing through Perspex shadow tray for (a) 6MV and (b) 10MV.

At 10MV a reduced variation with field size is again prevalent with a gradient reduction for FFF. The slope of FFF curves is calculated to be 0.85%cm^{-1} FFF vs. 1.33%cm^{-1} at 6MV and 0.85%cm^{-1} vs. 1.52%cm^{-1} at 10MV.

IV. F. Carbon fiber couch

FIG 8 (a, b) show the buildup characteristics when passing through the couch. The curves for both 6 and 10MV show very little difference between FFF and conventional beams. At 6MV there is a slight decease for FFF (~3%) at the surface, but nothing large enough to be of clinical significance. As the field size is varied from 5x5 to 40x40cm^2 the difference is slightly exaggerated (up to 6%) (FIG 8 c, d).
Couch transmission factors follow a similar pattern between FFF and conventional energies with the FFF beams showing a greater factor at both energies, 0.976 vs. 0.982 for 6MV and 0.982 vs. 0.988 for 10MV.

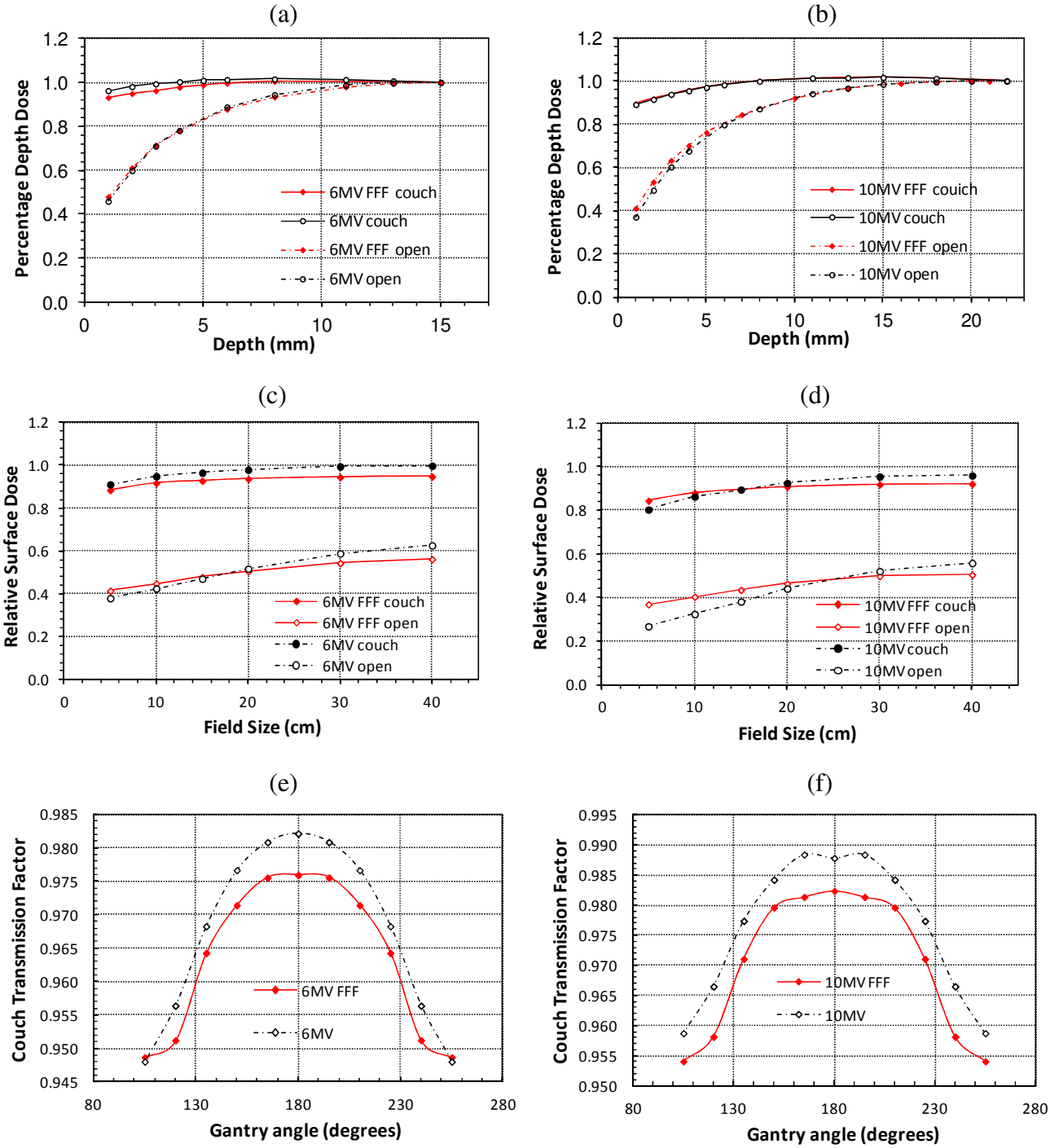

FIG 8. Buildup curves for (a) 6MV and (b) 10MVwith and without the treatment couch intersecting the beam. Relative surface dose vs. field size for (c) 6MV and (d) 10MV. Couch transmission factors vs. gantry angle (e, f).

The variation of couch transmission factor with changing gantry angle and with field size are shown in figures 8e and 8f.

V. Discussion & Conclusions

By passing through the flattening filter conventional beams exhibit a hardened beam spectrum so tend to contain a low amount of low-energy x-rays which will lead to lower surface doses, but high amounts of contamination electrons, raising surface doses. FFF beams on the other hand contain larger amounts of low-energy photons since these are no longer filtered out by the flattening filter, but lower amounts of contamination electrons, reversing the situation seen in the conventional filtered beam. In practice it seems that these effects almost cancel each other out so that the overall magnitude of surface doses from FFF beams are not too dissimilar to those seen in the original beams.

The increase in surface dose with increasing field size is a well known effect and it is electron contamination that gives rise to most of this variation [28], so the overriding effect of filter removal is a reduction in the variation of surface doses with field size. Here, the reduction in electron contamination means that the FFF beams show much less variation with changes in field size compared to filtered beams. In general surface doses in FFF are higher for small field sizes and lower for larger field sizes with the cross-over at 15x15cm^2 for 6MV and at 25x25cm^2 for 10MV. Kragl [12] observed a similar variation in surface dose with field size for an energy-matched Elekta linac (42.3% at 5x5cm^2, 56.5% at 30x30cm^2 compared to 39.7% and 53.1% seen here). These readings are 2-3% higher than those seen in this study but can be explained by the use of a 6mm Cu plate in earlier versions of the filter plate, instead of a 2mm stainless steel as in final configuration. Kragl also reported data for a non energy-matched Elekta linac at 6MV reporting surface doses of 47.1% at 5x5cm^2 and 61.6% at 30x30cm^2, and increase of approx. 5% over operation in the energy matched linac. In the un-matched machine the average energy is reduced to around 5MV by filter removal so this increase in surface doses (by approx. 5%) can be explained by the change in beam quality.

A similar situation is seen for the Varian TrueBeam accelerator where the beam energy is not adjusted and FFF doses are seen to be higher at all field sizes for both 6 and 10MV compared to operation with the filter in place [10, 13]. Surface doses are strongly dependent on beam energy, so by altering the beam energy to match, maintaining $TPR_{20/10}$ on the central axis, surface doses can be reduced.

Materials in the path of the beam can both generate electrons and absorb them from further upstream. Since it is relatively thin and of low-Z material the tray generates more electrons than it stops, and these pass through to reach the patient, raising skin doses. As the field size increases more electrons are emitted from the shadow tray, therefore higher doses are expected for larger field sizes compared to open fields.

Fontenla *et al* [29] showed an increase in the skin dose of approximately 16% when a tray was added into a 25x25cm^2 field at 6 MV. Our data shows an increase of 13% for the conventional beams and 9.5% for the 6MV FFF. At 10MV these figures are 14.2 and 10% respectively.

Electrons generated by the shadow tray are likely to be similar in both beams indicating that the initial contamination from upstream must be higher in the conventional beam.

The wedge is of sufficient thickness to absorb all of the contamination electrons rising from the head of the linac [30], but surface doses will be influenced by electrons generated within the wedge. These are produced in a thin layer close to the exit surface, equivalent in thickness to the range of the secondary electrons.

Regardless of beam energy the presence of the wedge is seen to reduce surface doses, by up to 10% for larger field sizes. Compared to conventional fields the FFF beams again show a reduction in RSD across all field sizes with the slope of the curve being much shallower for FFF operation, and filter removal is seen to have a much larger effect on the 10MV FFF beam than the 10MV (10% at 10MV FFF compared to 4% for 10MV). Considering the blocking tray, wedged fields and open

fields together the overall reduction in the slope of the curves with field size is seen to be reduced by 36.1% at 6MV and 44.4% at 10MV.
Considering the variation of RSD with SSD at 6MV it seems that this remains very stable at SSD's beyond 90cm. At shorter SSD's there is a significant rise in surface dose for both beams, but to a greater extent for the conventional 6MV. This again indicates the presence of greater number of contamination electrons in the filtered beam, which are gradually absorbed by the air column as SSD increases. At 10MV the surface dose is generally higher for the FFF beams at all but the shortest SSD's, but the variation is much reduced for FFF operation. Again an approximate 10% reduction in RSD is seen on filter removal at both beam energies with the wedge in place, and this is consistent across all SSD's.
Increasing the beam energy is known to reduce surface dose so even though 10MV FFF doses are seen to be slightly higher than for standard 10MV operation, they are still lower than those seen at 6MV. At 10MV differences in surface dose may be due to the lower effective energy of the beam compared to the standard as in this study the 10MV FFF beam has not been energy matched. The small variation seen between 6MV FFF and 10MV FFF over a range of conditions indicates that a change in beam energy to match the 10MV might have little overall effect.
Several authors have studied the effects of carbon fiber couchtops on surface dose (e.g. Refs 31-33). The proximity of the patient to the couch means that the skin sparing effect is almost completely lost and surface doses increase to 85-95% of that seen at d_{max}, and for FFF beams a similar pattern is observed. At 6MV a very slight reduction in %DD is seen for FFF operation, and at 10MV the buildup curves are almost identical. The variation of RSD with field size is again seen to be reduced for FFF use being universally lower for 6MV over all field sizes, and lower at 10MV beyond 15x15cm^2.
Since the unflattened beams contain more low-energy photons than conventional beams the transmission factor of the couch is greater for both FFF energies (by approx. 0.5%), showing a similar variation with gantry angle to that observed for normal use.
Removal of the flattening filter has been shown to have many benefits over conventionally filtered beams for the delivery of treatments techniques such as (but not limited to) SRT, SBRT and IMRT. The present study indicates that the surface doses from these beams are very similar to those experienced for conventional flattened beams, and are therefore unlikely to cause concern in a clinical setting. However, as variations in electron contamination with SSD, or from the introduction of wedges, trays and couches are not taken into account in most treatment planning systems [28], it is possible that the use of FFF beams may help to reduce the uncertainty of dose calculations in the buildup region.

Declaration

The author holds a research contract with Elekta UK Ltd to study FFF beams.

References

1. J. Carl and A. Vestergaard, "Skin damage probabilities using fixation materials in high-energy photon beams," *Radiother. Oncol*. **55**, 191-198 (2000).
2. A. Lamb and S. Blake, "Investigation and modelling of the surface dose from linear accelerator produced 6 and 10MV photon beams," *Phys. Med. Biol.* **43,** 1133-1146 (1997).

3. S. Kim, C.R. Liu, T.C. Zhu and J.R. Palta, "Photon beam skin analyses for different clinical setups," *Med. Phys.* **25**(6), 860-866 (1998).
4. E.I. Parsai, D. Shvydka, D. Pearson *et al*, "Surface and build-up region dose analysis for clinical radiotherapy photon beams," *Appl. Radiat Isot. **66** 1438-1442 (2008).*
5. M. Scorsetti, F. Alongi, S. Castiglioni *et al,* "Feasibility and early clinical assessment of flattening filter free (FFF) based stereotactic body radiotherapy (SBRT) treatments," *Radiat Oncol.* **6**:113 (2011).
6. O.N. Vassiliev, S.F. Kry, D.A Kuban *et al,* "Treatment planning study of prostate cancer intensity modulated radiotherapy with a Varian Clinac operated without a flattening filter," *Int. J. Radiat. Oncol. Biol. Phys* **68**(5), 1567-1571 (2007).
7. J. Cashmore, S. Golubev, J.L. Dumont *et al,* "Validation of a virtual source model for Monte Carlo dose calculations of a flattening filter free linac," *Med. Phys.* **39**(6), 3262-3269 (2012).
8. S. Stathekis, C. Esquivel, A. Gutierrez *et al,* "Treatment planning and delivery of IMRT using 6 and 18MV photon beams without a flattening filter," *Appl. Radiat Isot.* **67**(9), 1629-1637 (2009).
9. G.G. Zhang, L. Ku, T.J. Dilling *et al,* "Volumetric modulated arc planning for lung stereotactic body radiotherapy using conventional and unflattened photon beams: a dosimetric comparison with 3D technique," *Radiat Oncol.* **6**:152 (2011).
10. O.N. Vassiliev, U. Titt, F. Pönisch *et al,* "Dosimetric properties of photon beams from a flattening filter free clinical accelerator," *Phys. Med. Biol.* **51,** 1907–1917 (2006).
11. J. Cashmore, "The characterisation of unflattened photon beams from a 6MV linear accelerator," *Phys Med Biol.* **53**(7)**,** 1933-1946 (2008).
12. G. Kragl, S. af Wetterstedt, B. Knäusl *et al,* "Dosimetric characteristics of 6 and 10MV unflattened photon beams," *Radiother. Oncol*. **93**(1), 141-146 (2009).
13. Y. Wang, M.K. Khan, J.Y. Ting *et al*, "Surface Dose Investigation of the Flattening Filter-Free Photon Beams," *Int. J. Radiat. Oncol. Biol. Phys.* **83**(2), E281-E285 (2012).
14. B. Nilsson and A. Brahme, "Electron contamination from photon beam collimators," *Radiother. Oncol.* **5**(3), 235-244 (1986).
15. J. Cashmore, "Flattening filter free radiotherapy," 9th Biennial Meeting on Physics and Radiation Technology for Clinical Radiotherapy *Radiother. Oncol. **84**, S100 (2007).*
16. S. Stevens, K.E. Rosser, J.I Bedford, "A 4 MV flattening filter-free beam: commissioning and application to conformal therapy and volumetric modulated arc therapy," *Phys. Med. Biol.* **56**, 3809-3824 (2011).
17. B. Nilsson, A. Montelius, "Fluence perturbation in photon beams under nonequilibrium conditions," *Med. Phys.* **13**(2), 191-5 (1986).
18. B.J. Gerbi, F.M. Khan, "Measurement of dose in the build-up region using fixed-separation plane-parallel ionization chambers," *Med. Phys.* **17**(1), 17-26 (1990).
19. D.E. Velkley, D.J. Manson, J.A. Purdy, G.D. Oliver, "Build-up region of megavoltage photon radiation sources," *Med. Phys.* **2**, 14-24 (1975).
20. J.A. Rawlinson, D. Arlen, D. Newcombe, "Design of parallel plate ion chambers for build-up measurements in megavoltage photon beams," *Med. Phys.* **19**(3), 641-8 (1992).
21. W. Abdel-Rahman, J.P. Seutjens, F. Verhaegen et al, "Validation of Monte Carlo calculated surface doses for megavoltage photon beams," *Med. Phys.* 32(1), 286-298 (2005).

22. L.H. Gerig, M. Niedbala, B.J. Nyiri, “Dose perturbations by two carbon fiber treatment couches and the ability of a commercial treatment planning system to predict these effects,” *Med. Phys.* **37**(1), 322-328 (2009).
23. M.R. McEwen, I. Kawrakow, C.K. Ross, “The effective point of measurement of ionization chambers and the build-up anomaly in MV x-ray beams,” *Med. Phys.* **35**(3), 950-958 (2008).
24. D.E. Mellenberg, “Dose behind various immobilization and beam modifying devices,” *Int. J. Radiat. Oncol. Biol. Phys.* **32**(4), 1193-1197 (1995).
25. D. Georg, G. Kragl, S. af Wetterstedt *et al*, “Photon beam quality variations of a flattening filter free linear accelerator,” *Med. Phys. **37**(1), 49-53 (2010).*
26. Nordic Association of Medical Physics. Electron beams with mean energies at the phantom surface below 15 MeV. Supplement to the recommendations by the Nordic Association of Clinical Physics (NACP) 1980. *Acta Radiol. Oncol.* **20**(6), 401-15 (1981).
27. B.J. Gerbi, F.M. Khan, “The polarity effect for commercially available plane-parallel ionization chambers,” *Med. Phys.* **14**(2), 210-5 (1987).
28. A. Lopez Medina, A. Teijeiro, J. Garcia *et al,* “Characterization of electron contamination in megavoltage photon beams,” *Med. Phys.* **32**(5), 1281-1292 (2005).
29. D.P. Fontenla, J.J. Napoli, M. Hunt *et al*, “Effects of beam modifiers and immobilization devices on the dose in the build-up region,” *Int. J. Radiat. Oncol. Biol. Phys*. **30**(1), 211-219 (1994).
30. B.M. Rao, S.G. Prasad, K. Parthasaradhi *et al,* “Investigations on the near surface dose for three 10-MV x-ray beam accelerators with emphasis on the reduction of electron contamination,” *Med. Phys.* **15**(2), 246-249 (1988).
31. D.W. Smith, D. Christophides, C. Dean *et al*, “Dosimetric characterisation of the iBEAM evo carbon fiber couch for radiotherapy,” *Med. Phys.* **37**(7) 3595-3606 (2010).
32. S. McCormack, J. Diffey, A. Morgen, “The effect of gantry angle on megavoltage photon beam attenuation by a carbon fiber couch insert,” *Med. Phys.* **32**(2), 483-487 (2005).
33. T.P. Meydanci, G. Kemikler,” Effect of a carbon fiber tabletop on the surface dose and attenuation for high-energy photon beams,” *Radiat. Med.* **26**(9), 539-544 (2008).

APPENDIX G

PRESENTATIONS OF WORK

- CMS TPS User Group Meeting, Hull Oct 2006
- ESTRO26, Barcelona - Sep 13th 2007
- Christie Hospital, Manchester - Oct 4th 2007
- Royal Marsden Hospital, Surrey - Oct 18th 2007
- Elekta, Crawley - Nov 15th 2007
- BIR, London - Radiotherapy Treatment Accuracy - Jun 24th 2008
- IPEM, Bath, Biennial Radiotherapy Meeting - Sept 2nd 2008
- UCLH, London - 7th Nov 2008
- PROS, Montreal – 2009
- Elekta/CMS TPS User Group Meeting – Leicester 2009
- ESTRO, London - EPID Imaging with FFF – 2010
- ESTRO, London - FFF SRS Poster - 2010
- Hall-Edwards Research Meeting – Birmingham 2010
- BIR Improving Treatment Accuracy – London 2010

- Elekta – Crawley Oct 2010
- Elekta/CMS User Group Meeting – Croatia 2010
- ESTRO, Barcelona - FFF Surface Poster, 2010
- ESTRO, Barcelona - FFF Dose Survey Poster, 2010
- ESTRO, Barcelona - FFF AutoCAL Poster, 2010
- Elekta User Group Meeting, London May 2011
- Elekta Aus/NZ TPS Meeting - Sydney Sept 2011

APPENDIX H

POSTER PRESENTATIONS

During the course of this work 4 posters were prepared on different aspects of FFF research, either by the author or under supervision of the author.

"*Surface dose characterisation of 6 and 10MV unflattened photon beams*", Cashmore J. ESTRO (2010).

"*EPID based calibration of MLC leaves for a filter free linac*", Ramtohul M and Cashmore J, ESTRO (2010).

"*Dose survey for a flattened and unflattened photon beams*", Phillips J, George L, Ramtohul M, Jennings A, Cashmore J, ESTRO (2010).

"*Stereotactic radiosurgery with unflattened photon beams*", Heyes G, Cashmore J. ESTRO (2011).

SURFACE DOSE CHARACTERISTICS OF 6 & 10MV UNFLATTENED PHOTON BEAMS

University Hospitals Birmingham NHS
NHS Foundation Trust

Jason Cashmore, Hall-Edwards Radiotherapy Research Group, University Hospital Birmingham, UK jason.cashmore@uhb.nhs.uk

Introduction

Linear accelerators operating in flattening-filter-free (FFF, or unflattened) modes are becoming more widely used. The changing beam spectrum and relative amounts of low-energy photon and electrons make it important to have an understanding of changes in surface doses in this mode, especially if clinical decisions are to be made. Trends in surface dose for 6 and 10 MV flattened and unflattened beams are reported for a range of clinically relevant parameters.

Method

An Elekta Precise linac has been commissioned to run at 6MV and 10MV with the flattening filter in or out. The 6MV beam has been matched to the clinical beam on the central axis ($TPR_{20/10}$). The 10MV beam energy has not been adjusted. The flattening filter is replaced by a thin metal filter to provide sufficient build-up into the ionisation chamber. A thin window parallel plate chamber (NACP-02) has been used to measure data in the buildup region (corrected for polarity and recombination).

Skin Doses

Skin doses arise from a combination of effects and will depend on the magnitude and relative contributions from contamination electrons, low-energy photons and backscatter. Contamination electrons in particular can give rise to significant doses in the skin and will be influenced by several factors including head design, reduced SSD, increased field size or introduction of material into the beam close to the patient. Skin dose can therefore vary significantly from one setup to another and can be a limiting factor in some treatments. The flattening filter simultaneously acts as a source of contamination electrons and as a beam hardener, removing low-energy photons from the spectrum. Its removal could therefore affect this greatly. The use of motorised wedges and Perspex shadow trays in conjunction with filter removal will also change these characteristics and will depend on their relative contributions.

Results

	Field Size	Source Surface Distance	Wedge	Shadow Tray
6 MV	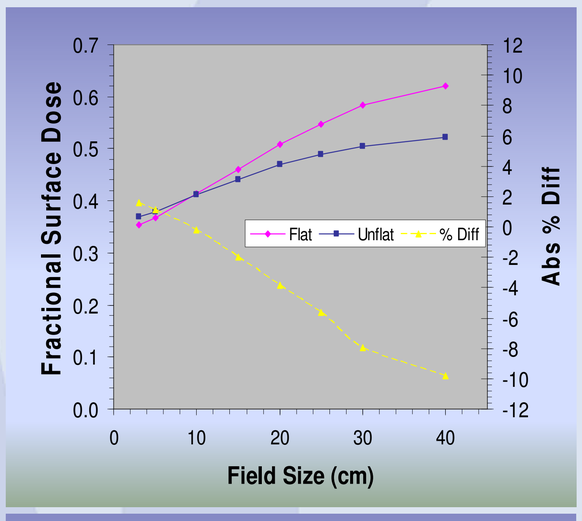	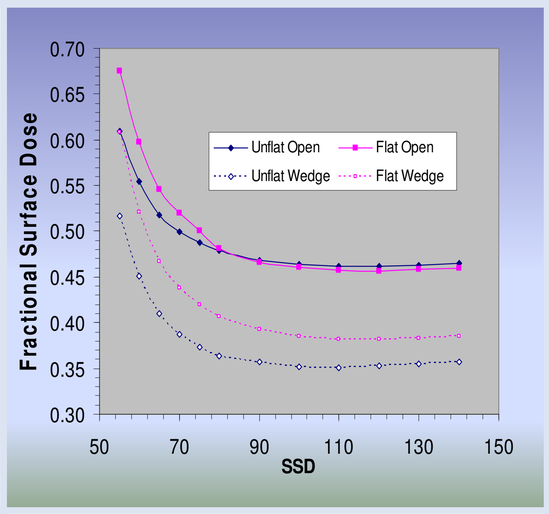	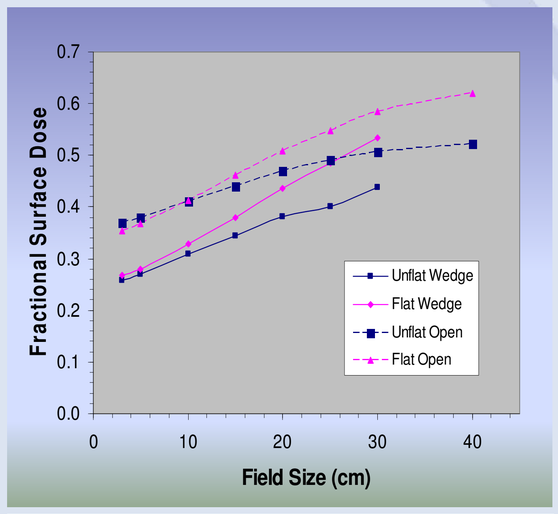	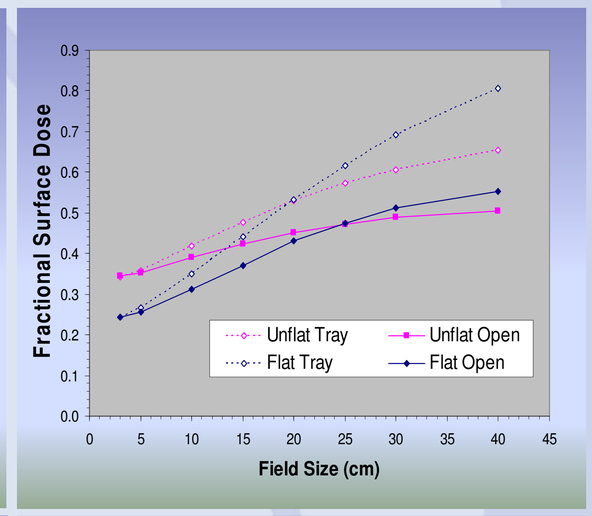
10 MV	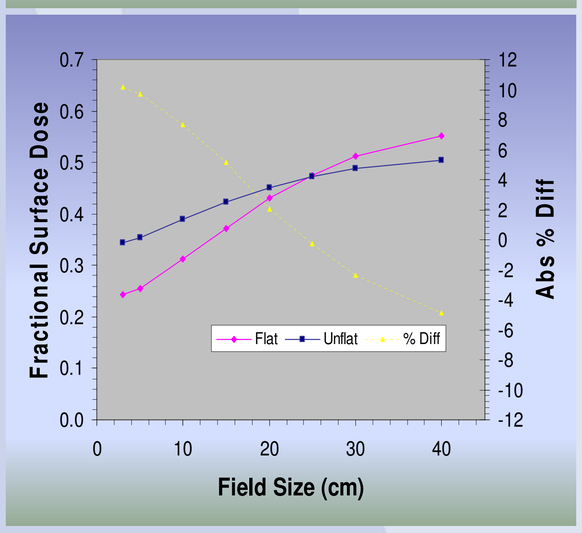	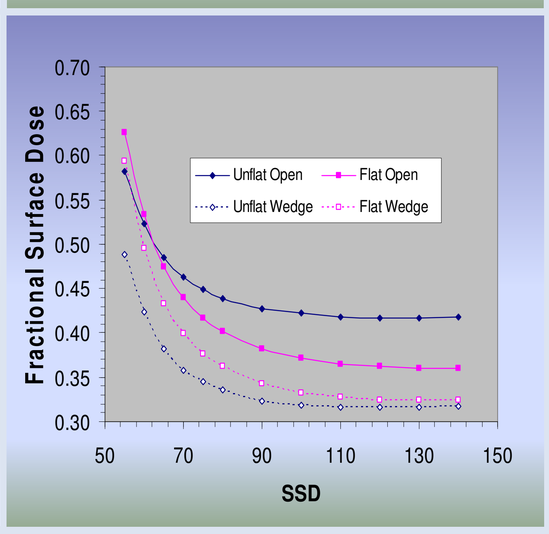	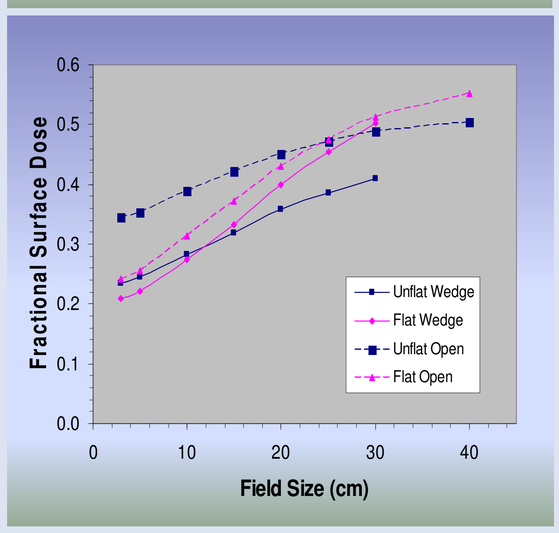	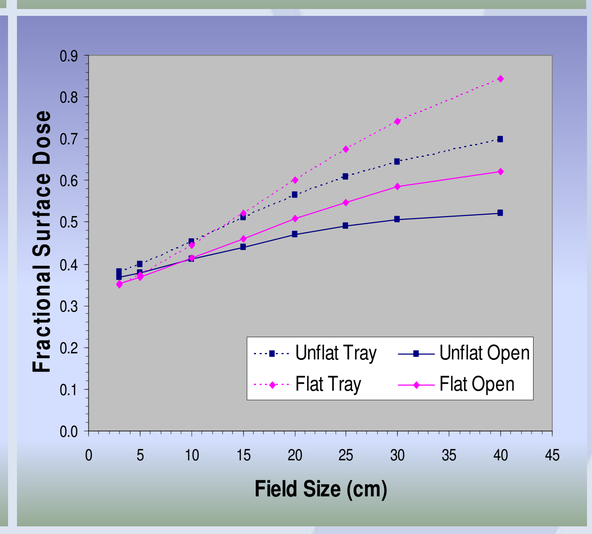

At 6MV surface dose measurements (measured as fractional surface dose relative to D_{max} [FSD]) are universally lower for unflattened beams (by up to 10% for fields >30cm). This is repeated in the presence of the wedge, shadow tray and treatment couch. Only small differences (<0.5%) are seen on varying SSD. For the 10MV beam the situation is more complicated with a cross-over in dose at mid to large field sizes. At this energy FSDs are generally higher (up to 10%) for the unflattened beam at smaller field sizes (<30cm open, <10cm wedged).

Conclusions

By removing the flattening filter a source of contamination electrons is swapped for a source of low energy photons (as these are no longer attenuated). In practice these two components almost balance out. At both 6 and 10MV the filter free beams show far less variation in surface doses than conventional beams. No significant effects on surface dose are expected by the introduction of flattening filter free delivery at 6MV.

Cashmore J, THE CHARACTERISATION OF UNFLATTENED PHOTON BEAMS FROM A 6MV LINEAR ACCELERATOR. *Phys Med Biol* **53**:1933-1946, 2008.

Cashmore J, Ramtohul M, Ford D, LOWERING WHOLE-BODY RADIATION DOSES IN PEDIATRIC INTENSITY-MODULATED RADIOTHERAPY THROUGH THE USE OF UNFLATTENED PHOTON BEAMS. *Int. J. Rad. Onc. Biol. Phys.* 2010. In press

Acknowledgments

Many thanks to staff at Elekta UK Ltd. for their continued support of this work.

EPID Based Calibration of MLC Leaves For a Filter Free Linac

Queen Elizabeth Hospital Birmingham
Part of University Hospitals Birmingham NHS Foundation Trust

Mark Ramtohul[1] and Jason Cashmore[1]

[1]Hall-Edwards Radiotherapy Research Group, University Hospitals Birmingham, U.K.
Correspondence: mark.ramtohul@uhb.nhs.uk

Purpose

Accurate calibration of the field defining jaws and MLCs is essential for the delivery of photon beams in radiotherapy, especially for IMRT. Standard software packages are available to perform these calibrations using images captured by the EPID. There is an increasing use of flattening filter free machines for IMRT delivery, and with the changes in beam profile and transmission for these beams it is essential that calibration procedures for un-flattened beams are developed to provide an equivalent calibration.

Methods

Actual beam calibration of EPID:

Calibrate panel with flattened beam. → Use ACAL to perform calibration. → Switch to un-flattened linac calibration keeping original MLC calibration. → Calibrate panel with un-flattened beam. → Use ACAL to perform calibration.

Even gain calibration of EPID:

Calibrate panel with flattened beam and 10 cm solid water at 90SSD. → Use ACAL to perform calibration. → Switch to un-flattened linac calibration keeping original MLC calibration. → Use ACAL to perform calibration.

Equipment:
- Elekta Precise linac.
- 6MV flattened and un-flattened energy matched beam
- IViewGT EPID
- AutoCal software V2.0 (Scanditronix Wellhofer)

Edge Detection:
- Local maximum uses a percentage of the greatest value on a profile to define the field edge.
- Steepest gradient uses second differential to determine the field edge.

Item Part Values (IPVs):
- 7 IPV ≈ 1mm.

Results

Field sizes:

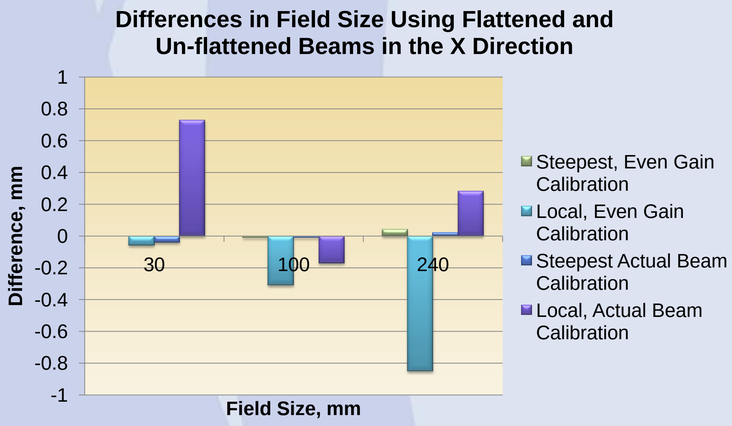

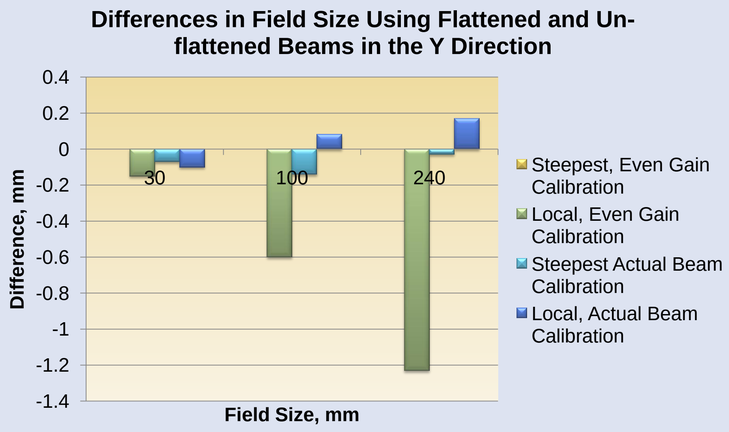

Field sizes agree well when using flattened and un-flattened beams with either even gain or actual beam calibrations. A worst case difference of 1.2 mm was found for a 240mm field size. Steepest gradient edge detection produced the least differences.

MLC minor offsets and gains:

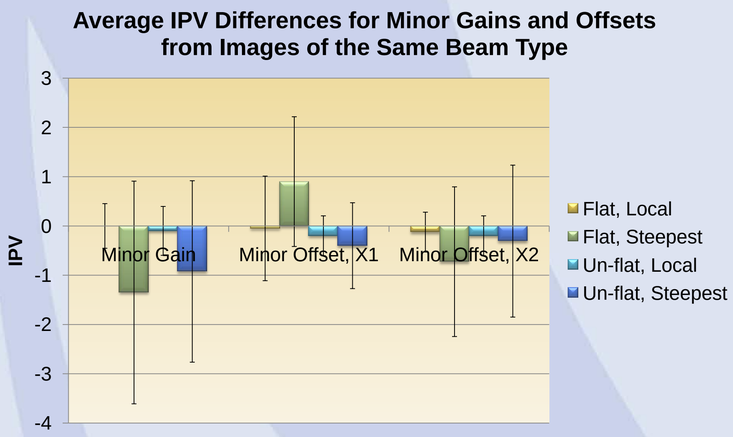

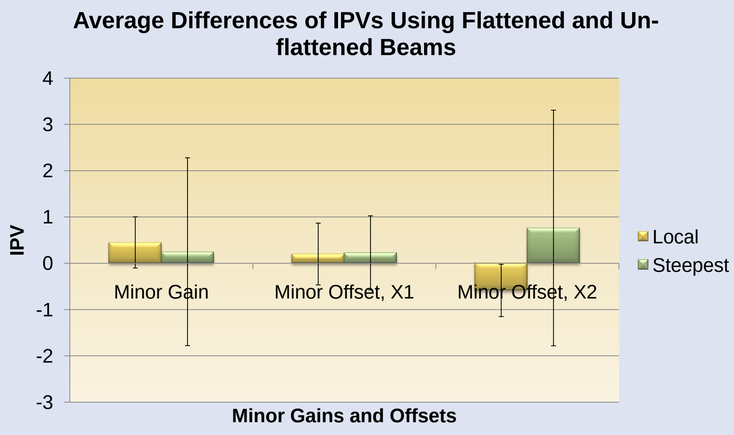

Comparisons of consecutive analyses of minor gains and offsets using an even gain calibration produce consistent results with differences averaging about 0 IPV within errors. Calibrations produced by flattened and un-flattened beams are also consistent. Local maximum edge detection produces the most consistent results.

Conclusions

The AutoCal calibration software provides an accurate method for calibrating both the jaws and MLCs for a filter free Elekta Precise linac. The EPID calibration effects the MLC calibration obtained, however as the gradients of the penumbra are much sharper than the gradients across the beam, the effects are small. By choosing appropriate measures to find the field edges, a single MLC calibration suitable for both flat and un-flat beams is possible.

Acknowledgements

The authors would like to thank Elekta for providing support with this project.

Dose survey for flattened and unflattened photon beams

J. Phillips, L. George, M. Ramtohul, J. Cashmore and A. Jennings
Jim.phillips@uhb.nhs.uk

Hall-Edwards Research Group, University Hospital Birmingham NHS Foundation Trust

Queen Elizabeth Hospital Birmingham
Part of University Hospitals Birmingham NHS Foundation Trust

Introduction and methods

Medical accelerators utilising a flattening filter free (FFF) design can offer significant advantages over those operating in a conventional 'flattened' mode, such as increased dose rate. Due to changes in the beam spectrum, beam profile, and levels of scatter radiation originating from the treatment head, dose rates and cumulative doses measured inside and outside of the treatment vault will be altered. Previous studies [1] have indicated that FFF IMRT significantly reduces whole-body doses to patients. In addition, FFF IMRT is expected to allow for reductions in shielding requirements or in occupational exposures.

Measurements in 40x40cm open field

An Elekta Precise linear accelerator has been modified to operate in conventional and unflattened modes (6MV mode matched in terms of depth dose and quality index; in 10MV operation, the unflattened beam is unmodified, and thus has a lower average energy than the clinical beam). Instantaneous dose rates were measured outside a linac bunker at 6MV and 10MV for flattened and unflattened beams, using a standard compensated GM tube. Field sizes from 40x40cm to 2x2cm were used; only the 40x40cm fields delivered a measurable dose rate. FFF dose rates were normalised to the clinical dose rate for the same MV to make the results directly comparable.

Measurements using a 6MV IMRT plan

Cumulative doses were measured for delivery of a 6MV head and neck IMRT plan (67.2Gy equivalent) at several points inside and outside the bunker using calibrated Harshaw lithium fluoride TLD-100s. For both plans, all fractions were delivered consecutively with a 20cm thick solid water phantom positioned in the beam to simulate clinical attenuation conditions.

Instantaneous dose rates and cumulative doses

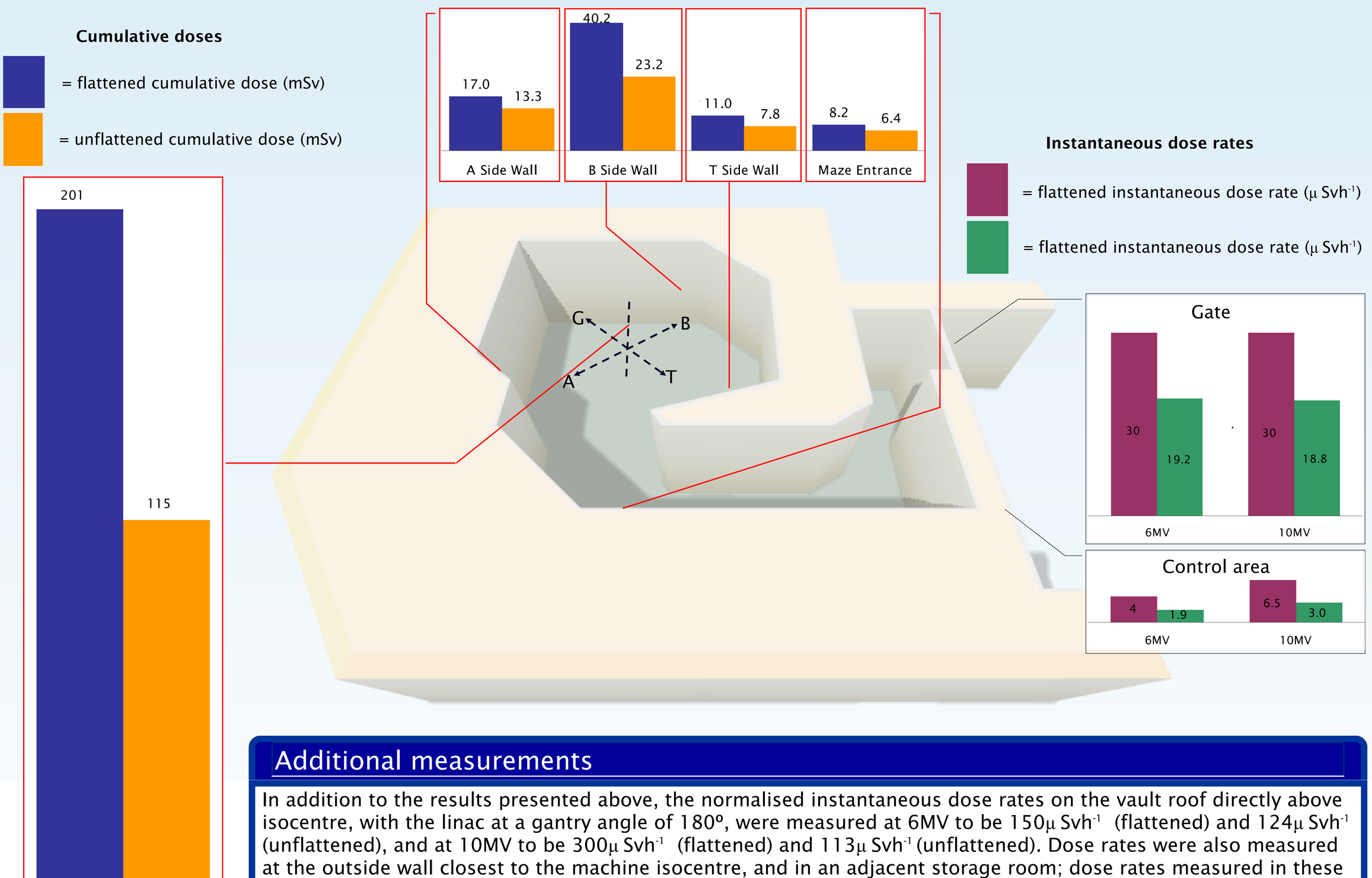

Additional measurements

In addition to the results presented above, the normalised instantaneous dose rates on the vault roof directly above isocentre, with the linac at a gantry angle of 180º, were measured at 6MV to be 150μ Svh^{-1} (flattened) and 124μ Svh^{-1} (unflattened), and at 10MV to be 300μ Svh^{-1} (flattened) and 113μ Svh^{-1} (unflattened). Dose rates were also measured at the outside wall closest to the machine isocentre, and in an adjacent storage room; dose rates measured in these locations were found to be indistinguishable from background.

Cumulative doses were also measured at the gate, the edge of the controlled area, in an adjacent store room, on the roof directly above the isocentre, and on an outside wall; these doses were found to be similar to background levels.

Conclusions and discussion

All measurable external dose rates for large fields were found to be lower in the unflattened case; in particular unflattened dose rates at both MV settings in the control area were half the flattened values.

Cumulative dose measurements using TLDs were lower for FFF operation at the edges of the treatment vault and in the maze for equivalent head-and-neck IMRT plans; this is despite the FFF plan requiring 33% more monitor units to deliver than the conventional IMRT plan.

For beams of similar dose rate FFF beams produce both lower instantaneous and cumulative dose rates, leading to potential savings in shielding requirements or occupational exposure.

However, if the higher dose rates achievable with FFF beams were to be used clinically, instantaneous dose rates would increase, which might reduce the savings predicted here.

[1] Lowering Whole-Body Radiation Doses in Pediatric Intensity-Modulated Radiotherapy Through the Use of Unflattened Photon Beams, Jason Cashmore, Mark Ramtohul and Dan Ford, *Int. J. Rad. Onc. Biol. Phys.*, 17 December 2010

Queen Elizabeth Hospital Birmingham
Part of University Hospitals Birmingham NHS Foundation Trust

Stereotactic Radiosurgery with Unflattened Photon Beams

Geoff Heyes and Jason Cashmore
Hall Edwards Radiotherapy Research Group
Queen Elizabeth Hospital Birmingham, United Kingdom.

Stereotactic radiosurgery (SRS) treatments are defined by single fraction, high dose treatments with sharp dose fall-off. The flattening filter serves no useful purpose for these small fields and its removal simultaneously reduces leakage radiation and increases dose rate. Benefits to the patient may include tighter beam penumbra and lower out-of-field doses.

Method

Small field dosimetry data has been measured for an Elekta Precise linear accelerator adapted to run at 6MV either with or without the flattening filter fitted. Six BrainLab conical collimators (10, 12.5, 15, 17.5, 20 and 22.5mm diameter) have been commissioned in both modes and data entered into the BrainScan (v 5.31) SRS treatment planning system.

Profiles and depth doses were measured with a CC01 chamber in a BluePhantom2 watertank (iBA dosimetry) at 92.5cm SSD. Clinical SRS plans for a number of intracranial patients have been re-calculated using the unflattened beam, and compared to plans achievable with the flattening filter in place.

Results

Field sizes (FWHM) are unaffected for the Unflattened (UF) beams, but exhibit a sharper beam penumbra (80-20%) with a reduction of up to 0.5mm and lower dose outside of the field (**graph below right**).

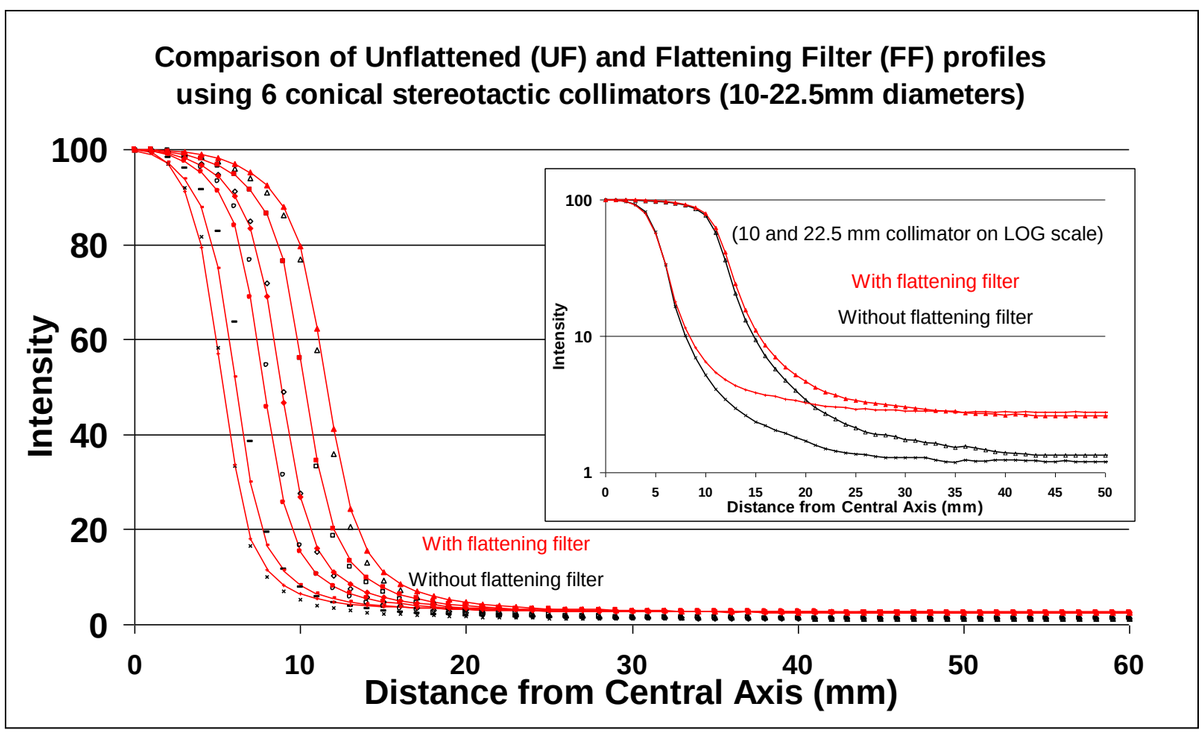

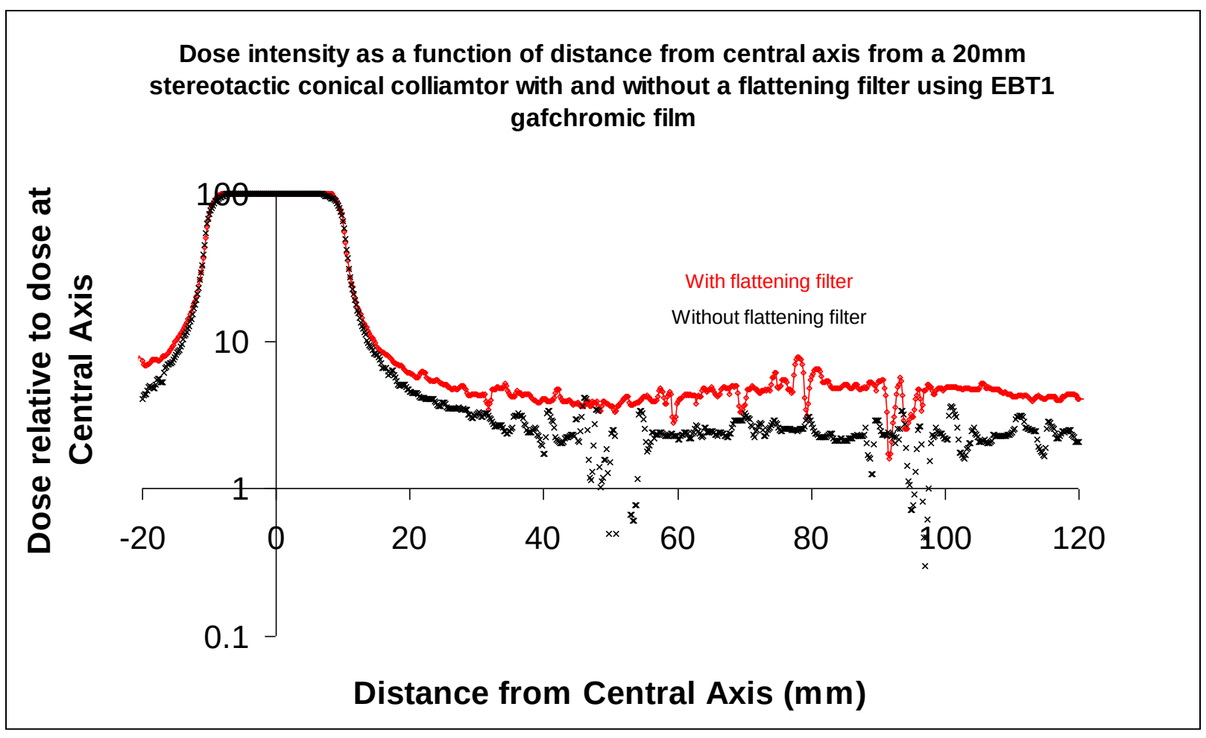

Treatment Plans

Doses measured at 25mm from the central axis were lower for the unflattened beam than for the flattened beam for all the collimators (**graph above left**), due to the reduction in the linac head leakage observed when the flattening filter is removed. This reduction in the dose outside the central axis provides normal tissue sparing. The effect of normal tissue sparing is magnified for stereotactic radiosurgery over conventional radiotherapy due to the fact that the stereotactic plan involves multiple small field arced (typically 100 degree) beams, each with a high number of monitor units.

Plans have been produced for 3 intracranial cases. Each case was planned with conventional beams then recalculated with the unflattened beam model. The plan opposite (Acoustic neuroma, **chart, right**) required 2 isocentres to cover the PTV, one using 4 arcs and a 20mm collimator, the second 3 arcs with a 10mm collimator, each arc covering 100 degrees. The dose to the lesion, brainstem and normal brain have been assessed.

The dose volume histogram to the lesion remains unchanged, however tissue sparing was seen for brainstem and normal brain. The most significant differences were observed for the low isodoses. For a prescribed dose of 12Gy, the V10 for normal brain and brainstem were reduced by nearly 60% and 10% respectively by using the unflattened beam model. (**table, below**).

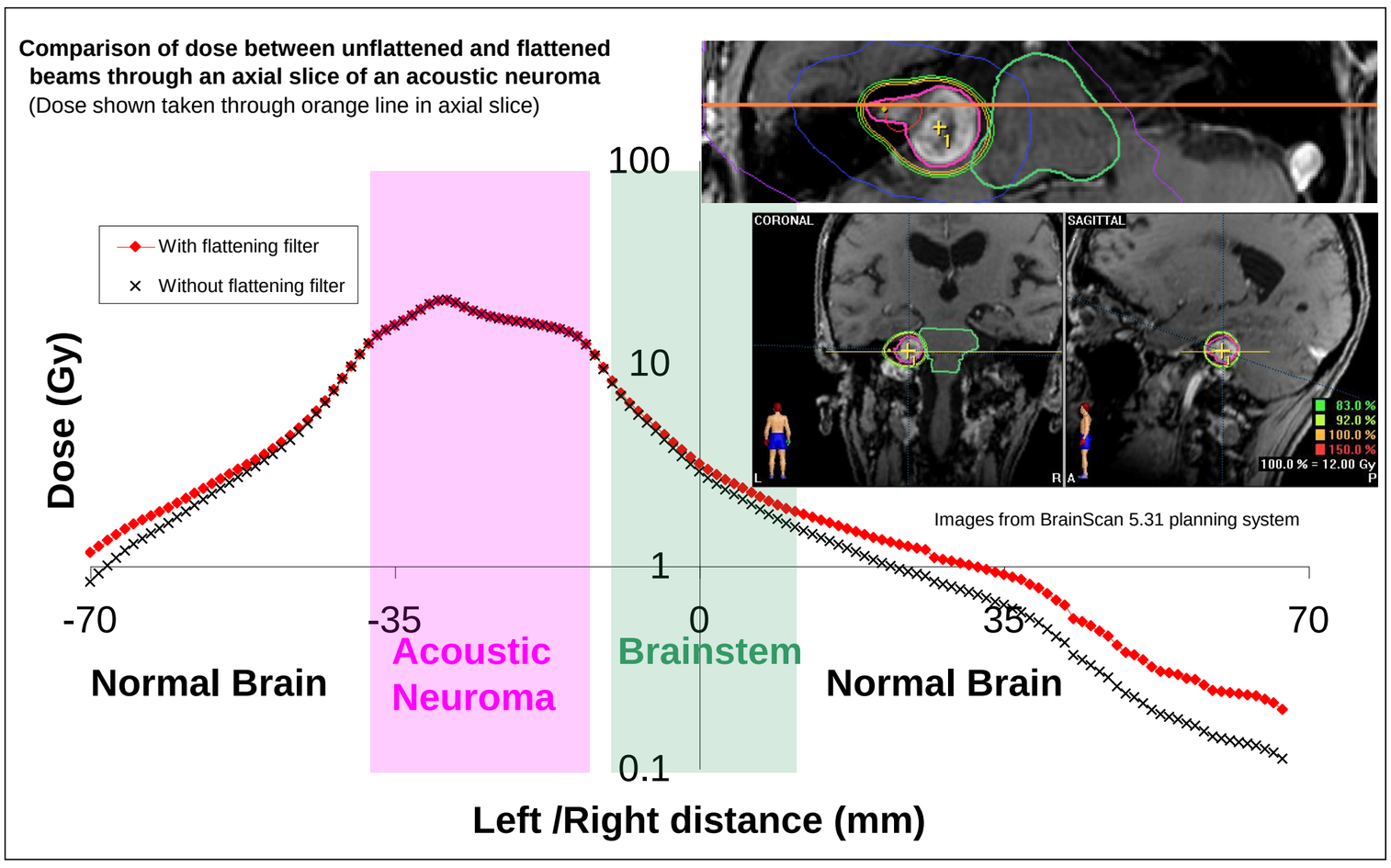

		V10 (cc)	V20 (cc)	V50 (cc)	V100 (cc)
Normal tissue	Unflattened beam	249.3	61.9	11.7	2.9
	With Flattening Filter	396.6	80.5	12.6	3.0
(3005.6cc)	**% Reduction using UF**	**-59.1**	**-30.1**	**-7.7**	**-3.8**
Lesion	Unflattened beam	2.4	2.4	2.4	2.4
(2.42cc)	With Flattening Filter	2.4	2.4	2.4	2.4
	% Reduction using UF	0.0	0.0	0.0	0.0
Brainstem	Unflattened beam	12.5	7.5	1.7	0.2
(14.31cc)	With Flattening Filter	13.6	8.7	1.8	0.2
	% Reduction using UF	-8.7	-15.7	-8.5	0.0

Conclusions

Removal of the flattening filter removes an unnecessary source of scattered radiation from the linac head. Identical lesion coverage can be achieved but with greater critical and normal tissue sparing. At large (50 cm) distances from the treatment field, leakage doses are reduced by up to 50%. Whist this will reduce the extracranial dose to a patient, we have shown intracranial dose sparing can also be achieved. It is therefore recommended that stereotactic radiosurgery without the flattening filter in place should be developed clinically.

This work has been partially funded by Elekta UK ltd.